



**Fakultät für Medizin**

**I. Medizinische Klinik**

# **Combining hiPSC and CRISPR/ Cas9 technologies for studying cardiac disease and development**

**Lisa K. Dreizehnter**

Vollständiger Abdruck der von der Fakultät für Medizin der Technischen Universität München zur Erlangung des akademischen Grades eines

**Doctor of Philosophy (Ph.D.)**

genehmigten Dissertation.

**Vorsitzender:** Prof. Dr. Jürgen Ruland

**Betreuer:** Prof. Dr. Karl-Ludwig Laugwitz

**Prüfer der Dissertation:**

1. Prof. Dr. Alessandra Moretti
2. Prof. Dr. Dr. Stefan Engelhardt

Die Dissertation wurde am 07.11.2016 bei der Fakultät für Medizin der Technischen Universität München eingereicht und durch die Fakultät für Medizin am 24.02.2017 angenommen.



## Abstract

Reprogramming of somatic cells into human induced pluripotent stem cells (hiPSCs) by expression of a defined set of transcription factors allows patient- specific generation of hiPSC lines. By differentiation of patient hiPSCs into cardiomyocytes (CMs) *in vitro*, disease mechanisms and pathogenic pathways can be investigated. Two varying heterozygous *de novo* point mutations on the *CALMI* gene were previously identified as long QT syndrome (LQTS)- causing mutations by whole genome sequencing of two patients<sup>1</sup>. hiPSC lines were generated of patient's skin fibroblasts, characterized and differentiated into patient- specific CMs. hiPSC- CMs of one patient were further analysed. Electrophysiological examinations confirmed (AP) prolongation. Incomplete Ca<sup>2+</sup>- dependent inactivation (CDI) of Ca<sub>v</sub>1.2 channels was identified as underlying cause of the mutation-induced electrical abnormalities

The newly discovered genome- editing technology CRISPR/ Cas9 represents a highly versatile and efficient tool for disease modelling applications, among many other applications. Correction of LQTS- causing *CALMI* mutations, as well as knock- out of the *CALMI* gene have been attempted in the patients' hiPSCs. Genome- editing was successfully performed in parallel experiments, by knocking- out the *MEIS1* gene in a healthy control (ctr) hiPSC line on both alleles. The full *MEIS1* knock- out was confirmed on transcriptional and on protein level. Effects of *MEIS1* knock- out on human cardiogenesis *in vitro* was assessed.

## Zusammenfassung

Das Reprogrammieren somatischer Zellen in humane, induzierte, pluripotente Stammzellen (hiPSCs), durch Expression einer bestimmten Kombination von Transkriptionsfaktoren, ermöglicht die Generierung von Patienten- spezifischen hiPSC Linien. Durch die *in vitro* Differenzierung von Patienten hiPSCs zu Kardiomyozyten können Krankheitsbilder und pathogene Signalwege untersucht werden. Zwei unterschiedliche heterozygote *de novo* Punktmutationen im *CALMI* Gen wurden zuvor als Grund für Langes QT Syndrom (LQTS) anhand von Sequenzierungen des gesamten Genoms in zwei Patienten identifiziert <sup>1</sup>. hiPSC Linien wurden aus Hautzellen der Patienten generiert, charakterisiert und zu Patienten- spezifischen Kardiomyozyten differenziert. hiPSC- Kardiomyozyten einer der beiden Patienten wurden tiefgründiger analysiert. Elektrophysiologische Untersuchungen bestätigten ein verlängertes Aktionspotenzial. Eine unvollständige Ca<sup>2+</sup>- abhängige Inaktivierung des Ca<sub>v</sub>1.2- Kanals wurde als Grund für die mutationsbedingten elektronischen Abnormitäten identifiziert.

Die neu entdeckte CRISPR/ Cas9 genome- editing Technologie ist ein vielseitig einsetzbares und effizientes Werkzeug, unter anderem im Bereich des disease- modelling. Es wurde versucht, die LQTS- verursachende *CALMI* Mutation in Patienten hiPSC zu korrigieren und das *CALMI* Gen durch Knock- out auszuschalten. Parallel dazu wurde erfolgreich das *MEIS1* Gen auf beiden Allelen in einer gesunden Kontroll- hiPSC Linie durch genome- editing ausgeschaltet. Der totale knock- out von *MEIS1* wurde auf transkriptioneller und proteinbiologischer Ebene bestätigt. Die Auswirkungen des *MEIS1* knock- outs auf humane Kardiogenese wurden untersucht.

# Table of Contents

I.	Introduction .....	6
1.1	Stem Cells .....	6
1.2	Human induced pluripotent stem cells (hiPSCs).....	7
1.2.1	hiPSC generation.....	7
1.2.2	Applications of hiPSCs .....	8
1.2.3	Genome- editing in hiPSCs.....	11
1.3	Calmodulin (CaM) .....	19
1.3.1	Structure, expression and importance .....	19
1.3.2	CaM mutations and associated diseases.....	20
1.3.3	LQTS.....	21
II.	Hypothesis and aims of the project .....	23
2.1	Patient- specific disease modelling of <i>CALMI</i> mutations .....	23
2.2	Analysis of the role of <i>MEIS1</i> in human cardiogenesis <i>in vitro</i> .....	23
III.	Material and methods.....	24
3.1	Patients and ctr cell lines .....	24
3.2	Cell culture methods.....	24
3.2.1	Cell culture material and media .....	24
3.2.2	hiPSC generation.....	26
3.2.3	hiPSC culturing methods.....	26
3.2.4	Differentiation of hiPSCs into CMs.....	29
3.2.5	Dissociation of CMs.....	30
3.2.6	Lentivirus production and transfection of hiPSCs .....	31
3.2.7	Transduction of hiPSCs.....	32
3.2.8	Selection of hiPSCs.....	34
3.3	Molecular biology methods.....	35
3.3.1	qRT PCR and RT PCR.....	35
3.3.2	PluriTest analysis .....	39
3.3.3	Protein extraction and WB analysis .....	39
3.3.4	FRET- Camui CR construct cloning.....	41
3.3.5	Homologous recombination .....	42
3.3.6	CRISPR/Cas9.....	46
3.3.7	Colony screening.....	51
3.3.8	Cleavage detection and TIDE analysis .....	54
3.4	Imaging techniques .....	55
3.4.1	Colourimetric detection.....	55
3.4.2	Fluorescent detection .....	55
3.5	Electrophysiological measurements.....	57
3.6	List of Oligonucleotides .....	60

IV.	Results.....	66
4.1	Generation and characterization of hiPSCs from patients carrying <i>CALMI</i> mutations.....	66
4.1.1	Generation of <i>CALMI</i> - hiPSCs by reprogramming of patient dermal fibroblasts.....	66
4.1.2	Genetic characterization of generated hiPSC lines.....	69
4.1.3	Evaluation of pluripotency of generated lines.....	72
4.2	Differentiation of <i>CALMI</i> - hiPSCs into CMs.....	78
4.3	Evaluation <i>CALMI</i> - CM phenotype.....	79
4.3.1	<i>CaMKII</i> activity measurements.....	81
4.3.2	Analysis of electrophysiological phenotype.....	82
4.4	Genome- editing of the <i>CALMI</i> locus.....	91
4.4.1	<i>CALMI</i> genomic locus targeting by homologous recombination.....	92
4.4.2	Genome- editing in <i>CALMI</i> - hiPSCs using CRISPR/ Cas9.....	95
4.4.2.1	<i>CALMI</i> mutation correction.....	95
4.4.2.2	Generation of <i>CALMI</i> knock- out line.....	108
4.4.2.3	TIDE analysis.....	111
4.5	Genome- editing of the <i>MEIS1</i> locus.....	113
4.5.1	Generating <i>MEIS1</i> knock- out line.....	113
4.5.2	Investigating the role of <i>MEIS1</i> during human cardiogenesis <i>in vitro</i> .....	126
V.	Discussion.....	131
5.1	Importance of disease modelling in <i>CALMI</i> - hiPSC lines.....	131
5.1.1	Optimal control lines: knock- out and correction of the mutated allele.....	133
5.1.2	Off- target analysis.....	136
5.1.3	New CRISPR versions.....	137
5.2	Applications of CRISPR/ Cas9 to investigate genes of cardiogenesis <i>in vitro</i> .....	138
5.2.1	The role of <i>MEIS1</i> in cardiogenesis.....	139
5.2.2	Effects of <i>MEIS1</i> knock- out on hiPSC cardiac differentiation.....	140
5.2.3	Multiple and conditional gene targeting as analysis tool for cardiogenesis.....	142
5.3	Future outlook of CRISPR/ Cas9.....	144
VI.	References.....	147
VII.	Appendix.....	161
7.1	List of Abbreviations.....	161
7.2	List of figures and tables.....	162
7.3	Plasmid maps.....	165
7.4	List of publications.....	167
VIII.	Acknowledgements.....	168

# I. Introduction

## 1.1 Stem Cells

Stem cells are defined as primitive cells, that can give rise to identical stem cells, as well as into at least one type of differentiated or specialised cell. Naturally occurring, there are two types of stem cells in the human organism, human embryonic stem cells (hESCs) and adult stem cells (ASCs)<sup>2</sup>. Embryonic stem cells are derived from the inner cell mass of human blastocysts during *in vitro* fertilization 5 days after fertilization of the oocyte<sup>3</sup>. Their main feature is pluripotency, a term used to describe the ability to give rise to all tissues found in adult humans. hESCs are however not able to form a complete new individual, since they are unable to give rise to e.g. the placenta. This feature distinguishes them from totipotent cells found in fertilized oocytes and cells resulting from the first cell divisions afterwards<sup>2</sup>. Shambloott and colleagues were among the first researchers in 1998 to cultivate hESCs and starting to characterize them *in vitro*<sup>4</sup>. The great value of hESC culture for future *in vitro* studies was comprehended and classical characterization procedures for pluripotency and the capability of these stem cells to differentiate into cells of all three germ layers were established<sup>4</sup>. Pluripotency was shown *in vitro* by alkaline phosphatase positivity, expression of the immunological markers SSEA-1, -3, -4, TRA-1-60, and TRA-1-81, a normal karyotype and ability to differentiate into mesodermal, endodermal and ectodermal cell lineages<sup>4</sup>.

ASCs have been found in brain, skeletal muscle, bone marrow and umbilical cord blood. They are generally believed to be responsible for tissue regeneration after injury and are remaining in a quiescent state unless activated<sup>5-7</sup>. At first believed to have a limited differentiation capacity into cells of the organ where they reside, more recent research highlights a multipotent phenotype of ASCs<sup>8-10</sup>. They represent a multipotent alternative for ethological controversial hESC research and have gained more attention over the last years<sup>11-13</sup>.

## 1.2 Human induced pluripotent stem cells (hiPSCs)

### 1.2.1 hiPSC generation

hESC research raises many ethical and legal issues since it requires derivation of cells from blastocysts or embryos<sup>14</sup>. Derivation of patient- specific ESCs for disease modelling is difficult<sup>15</sup>. The discovery by Takahashi and Yamanaka in 2006, that somatic cells can be induced to become pluripotent stem cells, known as induced pluripotent stem cells (iPSCs), revolutionised stem cell research and led the path to a new level of disease modelling<sup>15</sup>. One year after the first report on mouse iPSC generation by ectopic overexpression of a defined set of transcription factors in mouse fibroblasts<sup>16</sup>, Yamanaka and Takahashi reported the generation of human iPSCs (hiPSCs) by transfection of adult fibroblasts with the same set of transcription factors<sup>15</sup>. Adult human dermal fibroblasts were transduced with retroviruses containing OCT3/4, SOX2, KLF4, and c-MYC and cultured on proliferation- deficient mouse embryonic fibroblasts (MEFs). Thorough characterizations showed expression of ESC marker genes OCT3/4, SOX2, NANOG, GDF3, REX1, FGF4, ESG1, DPPA2, DPPA4, and hTERT by qRT PCR at levels similar to those of hESCs. Expression of ESC specific surface antigens SSEA-3, SSEA-4, TRA-1-60, TRA-1-81 and TRA-2-49/6E was demonstrated. Embryonic body (EB) formation proved the capacity of the cells to differentiate into endodermal, ectodermal and mesodermal lineages<sup>15</sup>. Reprogramming human cells was a ground breaking discovery and opened up a completely new field of research in disease modelling, drug discovery, therapy and many more<sup>17</sup>. Shinya Yamanaka received 2012 the Nobel Prize in Physiology and Medicine for his work<sup>18</sup>.

Initial disadvantages of using integrating retrovirus was soon abolished by establishment of refined reprogramming protocols using non- integrative Sendai virus or mRNA (messenger ribonucleic acid) for the delivery of the 4 Yamanaka factors<sup>17</sup>. Today, patient-specific hiPSC generation by Sendai reprogramming is a highly valued tool and the basis for many research areas<sup>19</sup>. hiPSCs generation has been constantly improved over the years and generation of pluripotent cells is possible from many somatic cell sources, including Keratinocytes, Fibroblasts or blood T- cells. Delivery methods of reprogramming factors range from retroviral to protein delivery into cells<sup>20</sup>. Fewer and different factors necessary for reprogramming have been identified and reprogramming efficiencies can be positively influenced by epigenetic regulation<sup>18</sup>.

### 1.2.2 Applications of hiPSCs

hiPSCs can be differentiated into many somatic cell types. Protocols are available to generate cardiac myocytes, smooth muscle cells, neurons, hepatocytes, endothelial cells, hematopoietic cells and others<sup>17</sup>. The fields of applications of hiPSCs are numerous, ranging from disease modelling, *in vitro* embryogenesis studies, drug screenings, up to tissue replacement in regenerative medicine. Figure 1 describes generation of hiPSCs, their differentiated target cells and applications in disease modelling, drug discovery and preclinical trials. Somatic cells are derived from patients and reprogrammed by e.g. transfection with Sendai virus or retrovirus expressing the 4 Yamanaka factors OCT4, SOX2, KLF4 and c-MYC. Derived patient-specific pluripotent hiPSCs can be differentiated by various protocols into specialized cells. For example, by forming EBs and spontaneous differentiation protocols, cardiomyocytic differentiation can be induced. Derived specialized cells can potentially be reintroduced into the patient for cell therapy. Differentiated cells are a platform for *in vitro* disease modelling by which pathogenic molecular mechanisms are deciphered. These cells are also a valuable tool to perform drug screenings and identify target pathways. Together with toxicity tests performed on those cells, new drugs can be developed and tested preclinically. This represents an important stage for better safety of new developed drugs and effects can be directly tested in patient-specific affected cell types.

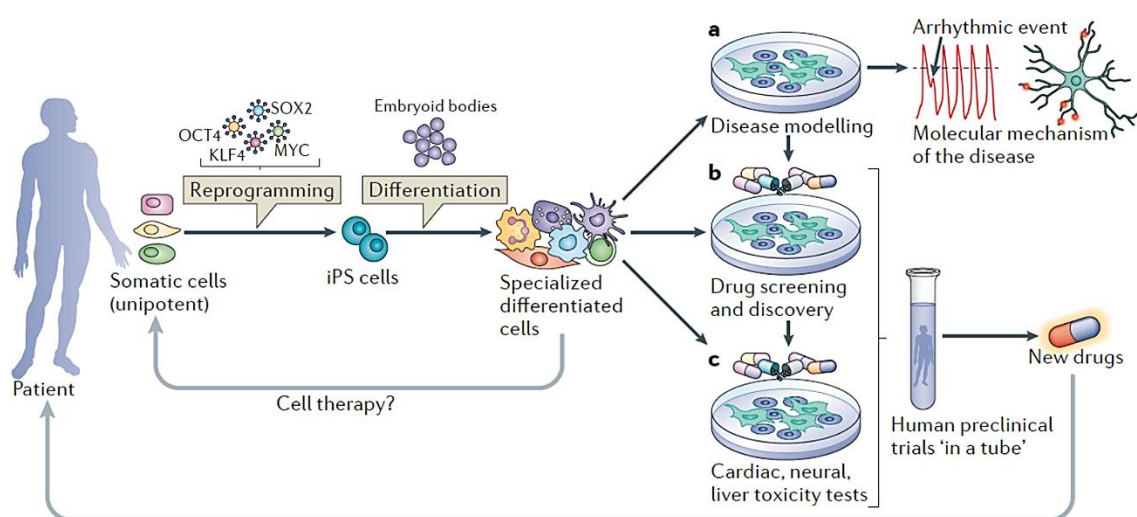


Figure 1: Generation of hiPSCs, their differentiated cells and applications.

Somatic cells taken from a patient are reprogrammed into hiPSCs using the four Yamanaka factors. hiPSCs are differentiated *in vitro* using different protocols to derive specialized cells. (a) hiPSCs are used for disease modelling and researching the molecular mechanism and cause of disease, e.g. arrhythmic events in CMs or neurogenic differentiation defects. (b) hiPSC-derived cells are used for drug screenings and identification of target pathways. (c) Toxicity tests are performed on hiPSC-derived cells as human preclinical trials as early stage of drug discovery process. Figure adapted from Bellin et al.<sup>17</sup>.

### *Disease modelling using hiPSCs*

Derivation of patient- specific hiPSCs and further differentiation of those cells enables researchers to investigate disease phenotypes in affected tissues that are usually difficult to acquire from patients. Due to the self- renewing capacity of hiPSCs, tissue resources are theoretically unlimited. Especially research of cardiac and neuronal diseases has profited from the hiPSC technology. Molecular pathways can be studied and linked to observed phenotypic effects in the diseased cell types. By understanding deranged pathways, patient- and disease- specific treatment options can be chosen and tested on the diseased cells before bringing it to clinical application. Monogenetic disorders that show a high penetrance and arise early during development are ideal to study in hiPSC disease models. Complex genetic disorders can also be modelled using hiPSCs, but are more challenging <sup>21</sup>. Even epigenetic disorders were successfully modelled using hiPSCs <sup>22</sup>. It has been shown that hiPSC- derived differentiated cells recapitulate the disease phenotype *in vitro* and even reflect the severity of disease <sup>23</sup>.

Especially cardiac and neurological disorders have been examined by using the hiPSC technology. Cardiac disorders like LQTS <sup>24-26</sup>, Brugada syndrome <sup>27</sup>, Timothy Syndrome <sup>28</sup>, LEOPARD syndrome <sup>29</sup> or catecholaminergic- proarrhythmic- ventricular- tachycardia (CPVT) <sup>30,31</sup> have been examined *in vitro* on hiPSC- derived CMs. CMs reflect disease phenotypes in electrophysiological experiments, corresponding to phenotypic effects measured in patient's electrocardiograms. Signalling pathways can be studied in depth and compared between healthy and diseased hiPSC- derived CMs. Structural abnormalities have been shown due to protein expression and distribution deficits, like Titin in hiPSC- CMs of a patient with dilated cardiomyopathy <sup>32</sup>.

hiPSCs can be differentiated into a variety of neuronal cell types. Modelled disorders of the nervous system have been shown for familial dysautonomia <sup>33</sup>, Rett syndrome <sup>34</sup>, Parkinson's disease <sup>35</sup>, Schizophrenia <sup>36</sup>. Defects in differentiation, migration change, in protein levels and stress susceptibility were identified in different neurological disease models which contributed greatly towards a better understanding of the corresponding diseases. Interestingly, correlations between psychiatric disorders and genetic and neuronal pathologies have been discovered for the first time, as for schizophrenia <sup>36</sup>.

### *Drug screening using hiPSCs*

The hiPSC technology provides a high potential platform to screen and develop for new drugs. Many other commonly used model organisms do not resemble human physiology and cellular pathways and are therefore only limited suitable. Especially disease phenotypes and underlying altered pathways can differ significantly between organisms or are not possible to mimic at all. If a certain disease has been already characterized in hiPSC based *in vitro* models and pathogenic pathways are known, a defined set of candidate drugs can be investigated and resulting effects immediately assessed. Many drugs have been proven useful to ameliorate disease phenotypes in patient-specific hiPSCs. Examples, just to name a few, include Dantolene for Wolfram Syndrome<sup>37</sup> or CPVT<sup>30</sup>, CHIR-99021 against bipolar disorder<sup>38</sup>, and Propranolol for LQT1<sup>24</sup>. This so-called candidate drug approach can be considered a major contribution towards personalised medicine<sup>21</sup>. Already established therapies can be re-validated and tailored towards patient-specific needs. On the contrary, high-throughput screenings (HTS) of small molecule libraries can be used to find novel therapeutic compounds in a cost-effective model of human disease physiology<sup>39</sup>. Scientists have also used a combined approach, by first screening large libraries with HTS and subsequently screening a selected panel of compounds on specialised cells<sup>40</sup>.

### *Regenerative cell therapy using hiPSCs*

Application of hiPSCs in regenerative medicine is of high interest in the scientific community. However, several safety concerns have to be addressed before using hiPSC-based cell therapy. Abnormalities acquired in hiPSCs during generation and culture on the genetic and epigenetic level have to be ruled out<sup>41,42</sup>. Tumorigenicity and immunogenicity of hiPSCs are highly relevant safety concerns that need to be clarified as well. The formation of unintended tissue, either malignant or benign, might be caused due to heterogeneity of introduced cell populations. Cells might also de-differentiate and cause formations of neoplasts. Several strategies have been developed to monitor tumorigenicity<sup>43-47</sup>. Cellular rejection and immune response need to be inhibited to guarantee engrafted cell survival. Autologous hiPSCs were shown to not cause immunologic rejection, but are a very cost- and time-consuming source of tissue compared to cells and tissues from allogenic banks<sup>48</sup>. First clinical and preclinical studies were performed to treat macular degeneration<sup>49</sup>, ischemic cardiomyopathies<sup>50</sup>, spinal cord injuries<sup>51</sup>, or Parkinson's

disease<sup>52</sup> using hiPSCs or hiPSC- derived cells. Above mentioned challenges hinder progress and translation of cell therapy into the clinic. Regenerative cell therapy with hiPSCs holds great potential. Future progress and insights on safety will bring regenerative medicine with hiPSCs to further clinical studies and applications.

### 1.2.3 Genome- editing in hiPSCs

The efficient and precise genome- editing technology further complements hiPSC technology for multiple research and therapeutic applications. By correcting precisely gene mutations in disease hiPSCs back into their wt sequence, isogenic control hiPSCs can be generated. Isogenic ctr lines of patient hiPSCs provide the optimal ctr for disease modeling within the same genomic background. By introducing point mutations or even a number of mutations in healthy ctr lines, pathogenic pathways and resulting disease phenotypes can be researched. Precise genome editing can shed light on embryogenesis and involvement on genes in pathways.

Gene- targeting approaches in hiPSCs, compared to their mouse counterparts, represent a more challenging task. Genome- editing in hiPSCs requires single- cell culturing of hiPSCs, a culturing state in which sensible hiPSCs are not easily kept. Their low transfection frequency is another challenge to overcome to make genome- editing a feasible tool. The addition of ROCK inhibitor to culturing media to prevent apoptosis, as well as usage of the mild EDTA- based splitting solution improved hiPSC single- cell culture<sup>53</sup>. Different strategies have been developed and tested so far to manipulate hiPSCs genetically<sup>54</sup>. In the following chapters, the most frequently used and promising genome- editing strategies are being focused on.

#### *Targeting vector approach*

The targeting vector approach makes use of the DNA recombination function of eukaryotic cells. Homologous recombination (HR) is usually performed within genomic regions of high similarity, by breaking and re-joining DNA segments, to maintain genome integrity and to generate genetic diversity<sup>55</sup>. Initial gene targeting vector design consisted of one long (5- 10kb) and one short (1-4kb) homology arm, as well as an antibiotic selection cassette for positive selection<sup>56</sup>. The antibiotic selection cassette is usually driven by a ubiquitous PGK promotor and flanked by *loxP* sites, that allow for later excision by a *Cre*- recombinase after integration of the target vector sequence. This antibiotic selection step proved to be necessary due to the low frequency of targeting events. HR efficiencies

in hiPSCs have been improved by using adeno and adeno- associated viruses (AAV) for targeting vector transfer <sup>57,58</sup> and bacterial artificial chromosomes (BAC), allowing for design of longer homology arms <sup>59</sup>. This approach represented the first method to create isogenic ctr lines for hiPSC disease modelling, by correcting or inserting specific mutations. A few research groups so far managed to correct disease- causing mutations in patient- derived hiPSCs using this targeting strategy <sup>60,61</sup>. Precise DNA sequences can be knocked- in or knocked- out, or gene mutations can be corrected, depending on the target vector design.

### *Homologous- directed repair (HDR) by HR*

HR is dependent on the local chromatin structure, as well as the cell undergoing the transit phase between the S- and G2 phase of the cell cycle <sup>62</sup>. DSB by HR is one of the two major DNA repair mechanisms of eukaryotic cells. DSB- induced HR has recently been employed for different gene- targeting strategies. DSBs can cause mutations and cell death if not repaired <sup>63</sup>. Depending on the phase of the cell cycle and type of DSB, the cells initiates specific repair pathways. While NHEJ is more prone to introducing small insertions or deletions (indel) during repair, HDR is very correct, but depends on a template DNA for repair. The use of a designed homologous sequence as repair template can be exploited to insert alternative sequences in the cells' DNA. Figure 2 describes the two DSB repair mechanisms of eukaryotic cells. Genome- editing tools like TALENs or CRISPR/ Cas9 (clustered regularly interspaced short palindromic repeats, CRISPR- associated genes) enzymatically provoke DSBs for DSB- mediated HDR.

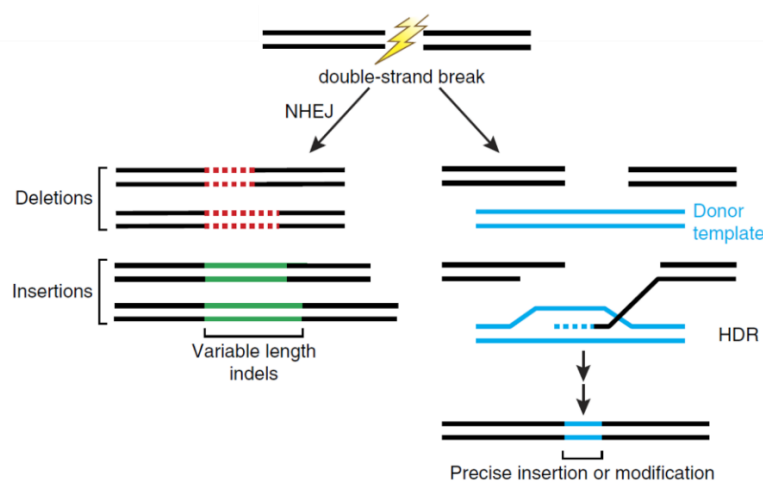


Figure 2: Cellular repair mechanism pathways induced by double strand breaks.

Double strand breaks are either repaired by NHEJ, likely resulting in deletions or insertions, or by HDR. HDR uses a donor template for copying the missing sequence and integrating the copy into the damaged region. Figure adapted from Sander and Joung <sup>64</sup>.

### *TALENs and CRISPR/ Cas9*

A powerful approach to introduce site-specific DSBs in the DNA is the use of custom-engineered nucleases, such as TALENs or CRISPRs.

Transcription activator- like effector nucleases (TALENs) consist of a *FokI* cleavage domain fused to DNA- binding domains of the TALE protein. TALENs are designed by linking together 33- 35 amino acid (aa) repeat domains, each recognising a single base pair. TALE repeats can be combined and linked together to recognise specific DNA sequences. The endonuclease domain *FokI* induces DSBs adjacent to the TALEs' homology region in the genomic DNA sequence. Following the induction of a DSB at a specific genomic locus, HDR- mediated custom alterations can be provoked <sup>65</sup>. This nuclease-mediated genome- editing technique disclosed a new dimension of genetic analysis and disease modelling. Downsides of this technique are the sensitivity to CpG methylation of the endonuclease, complex protocols to assemble the TALE domains and difficult delivery of TALEN constructs together with donor DNA constructs due to their size <sup>66</sup>.

The Cas endonuclease protein was originally discovered in bacteria as an acquired immune system against foreign DNA <sup>67</sup>. The CRISPR- Cas mechanism incorporates alien DNA or RNA into CRISPR repeat cassettes and transcribes them into pre- CRISPR RNA (pre- crRNA). pre- crRNA is being processed to crRNA, and forms a complex with the Cas protein. The Cas- crRNA complex binds complementary pathogenic DNA and the endonuclease cleaves and silences the pathogenic DNA sequence-specifically. CRISPR/ Cas systems can be grouped into 2 classes, with class 1 representing the evolutionary ancestral system and the class 2 system having evolved from class 1 <sup>68</sup>. The most commonly employed CRISPR/ Cas system for gene editing research is the class 2, type 2 CRISPR/ Cas9 system from *Streptococcus pyogenes* (SpCas9). This SpCRISPR/ Cas9 system consists of the Cas9 nuclease, the crRNA sequence encoding the target sequence and a trans- activating crRNA (tracrRNA), required for processing the crRNA into functional units. Each crRNA consists of a 20 nucleotide (nt) sequence. In the target genome, the corresponding 20- nt sequence needs to be flanked by a NGG protospacer adjacent motive (PAM) to be recognised as invading DNA sequence. The SpCas9 nuclease will induce a blunt DSB 3 base pairs (bps) upstream (5') of the PAM. The high potential of this system was soon exploited and protocols and plasmids were made available by pioneering researchers. Human codon- optimised and nuclear localization sequence- flanked Cas9 expressing plasmids are commercially available. By selecting a suitable 20- nt target

sequence and cloning this sequence into a gRNA cloning vector, a sequence- specific crRNA fused to a tracrRNA will express the active and sequence- specific single- guide RNA (sgRNA) <sup>69</sup>. DSBs are being induced at the point of interest in the target genome and custom alterations by HDR- mediated cellular repair response are promoted. The ease- of use and cloning steps required to create custom CRISPR/ Cas9 plasmids, multiple options to deliver the plasmids and high targeting efficiency proves this technique a new genome- editing tool with very high potential.

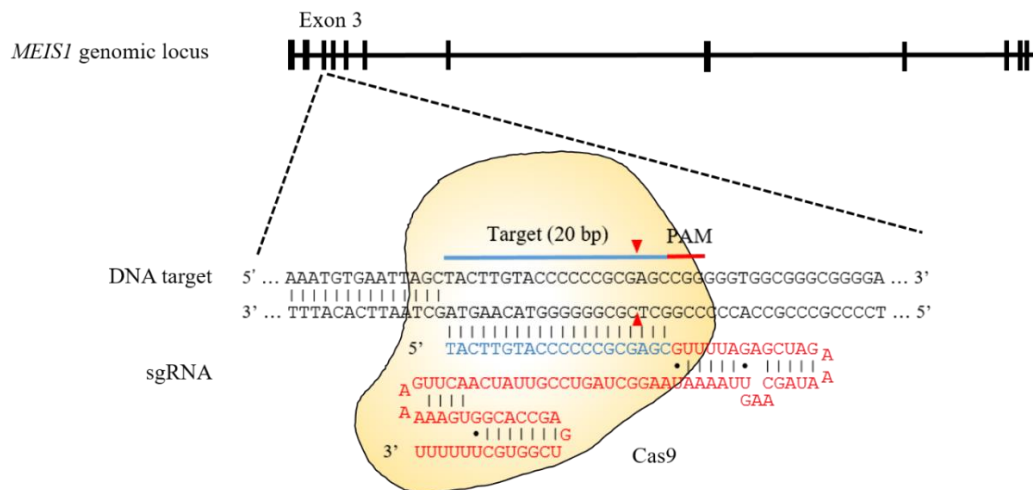


Figure 3: Schematic of the Cas9-sgRNA complex.

The SpCas9 protein (yellow) is targeted to the genomic locus (shown here for the *MEIS1* locus) by the 20-nt sgRNA. Sequence- specific crRNA is written in blue, sgRNA scaffold depicted in red. The genomic target sequence is indicated by the blue bar, red part highlights 5'-NGG PAM motive. The Cas9 endonuclease produces a blunt DSB 3 bps upstream of the PAM. Figure adapted from Ran *et al.* <sup>69</sup>.

### CRISPR/ Cas9 variants

Cas9 possesses the nuclease domains HNH and RuvC to cleave DSBs. By exchanging one aspartate to alanine in the RuvC domain, the endonuclease activity is altered to only nick one strand of the double strand target DNA <sup>70</sup>. This Cas9 nickase mutant was developed to increase HDR efficiency, since this repair pathway is privileged in repairing single strand breaks. The frequency of unwanted indel formations from off- target cleavage is potentially decreased <sup>69</sup>. Two specifically placed gRNAs can further be used to provoke DSBs with a higher target precision and less off- target events. Cas9 mutants completely lacking nuclease activity are employed to recruit fluorescent protein labels, chromatin modifying enzymes or transcriptional modulators <sup>69</sup>. Other SpCas9 variants have been engineered by mutating key residues, rendering the endonuclease specific to altered PAMs, like the VRQR- Cas9 or VRER- Cas9. HF- Cas9 and eCas9 variants of SpCas9

became more sequence specific by mutating specific residues <sup>71</sup>. Cas9 orthologues originating from other organisms can be exploited as well, but are not as efficient as SpCas9 <sup>72</sup>.

#### *Gene knock- out, genome- editing and gene knock- in*

Depending on the type of gene editing one wants to perform in the target cells, different gRNA design strategies, Cas9 variants and the use of template DNA are being chosen. Knocking- out a gene of interest can for example give insights on gene function, downstream pathways or impact of mutations within the genomic background of a patient. By targeting CRISPR/ Cas9 towards a sequence located within the first exons of the gene and without providing the cell a template DNA for HDR repair, NHEJ is likely to be chosen as repair mechanism for the created DSB. NHEJ is an erroneous repair mechanism, often leading to insertions, deletions or duplication of small fragments at the site of DSB <sup>69</sup>. Faulty repair of the target sequence can lead to frameshifts, producing with high probability a stop codon further downstream in the sequence. Incorrect mRNA sequences are often already degraded by the cell before translation, or resulting proteins are non-functional and being degraded.

Gene- editing using CRISPR/ Cas9 requires the co- delivery of a template sequence together with the plasmids encoding the endonuclease and the gRNA. The most commonly used template DNA to induce HDR and precise gene alterations is single- strand oligodeoxynucleotides (ssODN). Best HDR efficiencies following DSB have been reported with ssODNs ranging between 90 and 120 bp length <sup>73,74</sup>. These shorter oligos are suitable for introducing smaller nt changes, however, if reporter genes or larger genomic sequences are to be integrated, template DNA is provided as plasmid <sup>75</sup>.

Knocking- in larger stretches of foreign DNA, like reporter constructs or antibiotic resistance cassettes, requires the use of targeting vectors or long double- stranded DNA sequences with homology arms, as described before for the target vector approach. Some research groups successfully generated reporter hiPSC lines <sup>76-78</sup>. However, targeting rates of HDR- based strategies like gene- editing by ssODNs and gene knock- ins in human cells have been reported to be low <sup>79</sup>, due to the intrinsic inefficiency of HDR in human cells. Precise gene- editing is found to be especially inefficient in hiPSCs and has been estimated to be as low as  $1 \times 10^{-5}$ , without pre- selection <sup>78</sup>.

### *Importance of CRISPR/ Cas9 in disease modelling*

The easy cloning and handling of CRISPR/ Cas9 plasmids, as well as the straight- forward requirements for gRNA design, promoted this newly discovered gene editing method fast into many researcher's toolboxes. Disease modelling relies on the introduction of the faulty gene in other modelling organisms or specific correction of mutations. CRISPR/ Cas9 is theoretically able to target every gene in every organism, as long as target sequences meet PAM sequence criteria. Delivery options of plasmids encoding the enzyme and the gRNAs are ranging from plasmid transfection to transduction by AAV. Researchers are working on other delivery options, like lipofection of Cas protein. Genome- editing by CRISPR/ Cas9 is an efficient and scarless editing method, no residues will be left in the sequence after editing. Other genome- editing methods, like TALEN or classical homologous recombination by target vector recombineering are much costlier in terms of time and money. The latter will also leave "foreign DNA" in the edited sequence. CRISPR/ Cas9 for disease modelling is applicable in all known model organisms, however especially useful in *in vivo* mice models and *in vitro* cell culture disease modelling.

The CRISPR/ Cas9 genome- editing tool enables to precisely alter single nts, an important aspect for disease modelling. Effects of point mutations can be investigated by either correcting a point mutation suspected to cause a disease phenotype, or by inserting point mutations into healthy backgrounds. Multi- genetic disorders can also be investigated by introducing more than one alteration into the genome. CRISPR/ Cas9 allows for multiplex- editing by using several gRNA target sequences at the same time. Due to the small size of gRNAs, several gRNA sequences can be encoded on a single vector. Only minimal cytotoxicity has been reported when multiplexing gRNAs <sup>80</sup>.

By combining the hiPSC technology with the CRISPR/ Cas9 genome- editing tool, a new era of disease modelling has begun. For monogenic and multigenic disease, genotype- phenotype correlations can be explored in detail by correcting mutations in patient- derived hiPSCs and further differentiating them into the affected specialized cell. Correcting the mutation in disease hiPSC lines provides the optimal ctr while remaining in the same isogenic disease background. Inserting disease- associated mutations in a healthy ctr background further elucidates effects of these mutations. Corrected hiPSC- derived specialized cells and mutated ctr cells furthermore provide a highly potent platform for drug screening approaches in a personalized medicine setting. However, it has to be emphasized, that applying genome- editing by CRISPR/ Cas9 to hiPSCs remains challenging,

due to the fragile nature of hiPSC and low HDR efficiency. A well- grounded technical expertise and high hiPSC quality is necessary, followed by arduous screenings of targeted clones to obtain genetically modified cells. Only several research groups have successfully applied CRISPR/ Cas9 in hiPSCs for disease modelling by correcting point mutations in patient- derived hiPSCs or inserting disease causing mutations into healthy ctr backgrounds <sup>81-83</sup>.

#### 1.2.4 Differentiation of hiPSCs into the cardiac lineage

hiPSCs can be induced to differentiate into cells of all three embryonic germ layers *in vitro*. Differentiation protocols recapitulate the embryonic development of the cell type of interest. hiPSC- derived CMs are a valuable tool to investigate embryonic heart development and as human cardiac model. Research studies on electrophysiology, molecular pathways, protein biochemistry, drug development and disease models can be performed. By generating hiPSC- derived CMs from patients suffering from cardiac disease, pathological mechanisms can be studied directly in the affected cell type without the need to perform invasive procedures on the patient. Several protocols have been established so far to induce cardiac differentiation in hiPSCs. Formation of CMs in hiPSCs is believed to follow the same signalling pathways as in embryonic cardiomyogenesis <sup>84</sup>. Different protocols have been established that drive cardiac differentiation by adding specific small molecules and growth factors in a defined order to the culture. Other protocols aggregate hiPSCs to EBs to induce spontaneous *in vitro* cardiogenesis. Efficiencies of differentiation protocols can vary within cell lines and are most likely dependent on cell quality, culturing conditions and quality of supplements. Protocols are being constantly improved and companies offer commercially available cardiac differentiation kits. While kits for cardiac differentiation reach very high efficiencies of beating CMs in a monolayer, they only promote cardiac lineage development and suppress differentiation into cells of other tissues. Depending on the research question, it can be important to promote cardiogenesis within a cell population resembling human embryonic development, supporting spontaneous differentiation protocols with EB formation <sup>85</sup>.

### *Key genes in cardiac development*

The human heart is one of the first organs to develop during embryogenesis<sup>86</sup>. During embryonic development, the three germ layers endoderm, ectoderm and mesoderm are formed shortly after gastrulation. Mesoderm formation is greatly influenced by NODAL, BRY and WNT3<sup>87</sup>. The mesodermal germ layer is giving rise to cardiac progenitor cells, that later form the heart. Cardiac precursor cells start migrating out of the primitive streak due to MESP1 signaling<sup>88</sup>. Two major cardiac progenitor populations give rise to the future heart, the first heart field (FHF) and the second heart field (SHF). Progenitor cells of the FHF will give rise to the left ventricle and minor parts of the atria and conduction system. The SHF forms the right ventricle, outflow tract and atria. HCN4 is considered a marker for FHF<sup>89</sup>, whereas ISL1 marks the SHF cardiac progenitor cells. ISL1<sup>+</sup> cardiac progenitors are multipotent, play a major role in SHF development and can give rise to CMs, endothelial cells and smooth muscle cells<sup>90</sup>. The secondary master regulators NKX2.5 and GATA4 are being expressed in FHF and SHF and further drive myocardial differentiation. FHF cells continue to form the cardiac chambers and trabeculation in the ventricles, influenced by NKX2.5, TBX5, MYOCD, GJA5 and NPPA expression. NKX2.5, GATA4, ISL1, MEF2C, FOXH1, TBX1 and others play important roles in further differentiation of the SHF into the right ventricle, outflow tract and atria<sup>91</sup>.

### *Knock- out of key genes in cardiac development*

Knock- out studies in mice are a valuable tool to identify genes and their roles during cardiogenesis. The major role of ISL1<sup>+</sup> cardiac progenitor cells in SHF was identified by phenotypic effects in *Isl1*<sup>-/-</sup> mice<sup>92</sup>. Homozygous *Nkx2.5* knock- out mice show defects in heart looping, indicating the importance of this transcription factor in ventricular cardiac development. Downstream signaling of Nkx2.5 to MLC2V has also been identified with this model<sup>93</sup>. Our current understanding of cardiac development is based on knock-out studies in mice and other model organisms. However, using mice as model organisms for cardiac development has its limitations. Embryogenesis in mice is faster than in humans and morphological differences are present<sup>94</sup>. The iPSC technology and cardiac differentiation of hiPSCs represents a great new human model system. By manipulating cardiac genes, using state- of the art genome- editing techniques, and observing consequences in hiPSC- derived CMs, new insights in human cardiogenesis can be achieved.

### *MEIS1 in cardiac development*

*MEIS1* is a transcription factor of the HOX gene family. It possesses a TALE (three aa loop extension) homeodomain to interact with other genomic regions<sup>95</sup>. It has been previously identified to activate oncogenic genes, cause cellular hyper proliferation in myeloid leukemia cells and to be involved in hematopoiesis<sup>96</sup>. Wamstadt and colleagues identified Meis1 as a key regulator of cardiac development in mouse cardiac precursor cells. Meis1 and Gata4 were shown to co- activate cardiac enhancers in luciferase assays<sup>97</sup>. *Meis1* knock- out in mice results in hematopoietic defects and embryonic lethality, as well abnormalities in eye, brain, lung and heart during embryogenesis<sup>98,99</sup>. Post- natal, *Meis1* knock- out studies in mice revealed its role in cell cycle arrest in CMs<sup>100</sup>. All present data and insights are based on mouse studies. A study performed on human embryonic stem cells (hESC)- derived CMs identified MEIS2 as regulator of cardiac development based on Chromatin Immunoprecipitation followed by next- generation sequencing (ChIP- Seq). The role of *MEIS1* in human cardiac development remains to be elucidated.

## 1.3 Calmodulin (CaM)

### 1.3.1 Structure, expression and importance

CaM is a 148 aa protein important for Calcium ( $\text{Ca}^{2+}$ ) sensing in cells. The relatively small  $\alpha$ - helical protein possesses N- and C- terminal lobes, which contain EF- hand motifs that can bind 2  $\text{Ca}^{2+}$  ions each. The N- and C- terminal lobes display different  $\text{Ca}^{2+}$ - binding affinities.  $\text{Ca}^{2+}$  binding induces a conformational change of the protein, influencing binding characteristics to other targets. 3 independent genes located on different chromosomes encoding for identical CaM proteins highlight the importance of this signalling molecule. At least 8 mRNAs are transcribed from these 3 *CALM* genes, utilizing different polyadenylation signals. CaM is highly conserved within all vertebrate species, further supporting its pivotal role<sup>101</sup>. CaM is phosphorylated *in vivo* by different kinases. Depending on phosphorylation status,  $\text{Ca}^{2+}$ - free (ApoCaM) or  $\text{Ca}^{2+}$ - bound state, the protein is influencing and binding a great number of different binding partners<sup>102</sup>. CaM is expressed in all eukaryotic cells and is involved in  $\text{Ca}^{2+}$  transport, contraction of cells, cell

metabolism, gene expression, proliferation and others<sup>103</sup>. Identified targets of CaM- regulated proteins range from Cabin 1, a transcriptional regulator in Thymocytes, to dendritic Ca<sup>2+</sup> signalling protein Striatin, and EGF receptors, among many others<sup>104</sup>.

CaM plays a central role in the cardiac contraction cycle. CaM interacts with Ca<sub>v</sub>1.2 channels, influencing both inactivation and facilitation of L-type calcium channels<sup>105</sup>. CaM binding to the K<sub>v</sub>7.1 channel is needed for cardiac I<sub>ks</sub> channel formation and Ca<sup>2+</sup>- sensitive mediation of I<sub>ks</sub> current<sup>106</sup>. CaM decreases the open probability of RyR2 channels in CMs, essentially influencing SR Ca<sup>2+</sup> release<sup>107</sup>. Ca- CaM activates the Calcium- CaM-dependent kinase II (CaMKII), resulting in a phosphorylation of the kinase. The activated CaMKII in turn phosphorylates Ca- channels, slowing its inactivation and promoting I<sub>Ca</sub> facilitation<sup>103</sup>. Additionally, it is believed that CaM might act on gene expression and excitation- transcription coupling<sup>103</sup>. The indispensable role of CaM in cardiac cells, as well as in other cells is indisputable.

### 1.3.2 CaM mutations and associated diseases

During recent years, CaM mutations on all three genes have been identified to cause LQTS, CPVT, or both in patients. The pathogenic CaM variants provoke autosomal dominant syndromes at an early age, often leading to cardiac arrhythmia and sudden cardiac death<sup>108</sup>. To date, at least 12 *CALM* mutations have been described to be associated with LQTS, CPVT or idiopathic fibrillation, most of them being classified as *de novo* mutations<sup>109</sup>. In defiance of the broad function of CaM in eukaryotic cells, mutation carriers rarely display disease phenotypes other than arrhythmogenic symptoms<sup>110</sup>. CPVT- associated CaM mutations are linked to aberrant regulation of the RyR2 channel<sup>110-113</sup>. During CM contraction, RyR2 channels mediate Ca<sup>2+</sup> release of the SR. CaM binds to RyR2 receptors in the cell and facilitates the termination of Ca<sup>2+</sup> release. Aberrant regulation of mutated CaM evokes arrhythmogenic Ca<sup>2+</sup> disturbances, spontaneous Ca<sup>2+</sup> waves and increased spark activities, causing a CPVT phenotype<sup>110,113</sup>. *CALM* mutations manifesting a LQTS phenotype have been characterized so far in heterologous systems or by overexpression of the mutated CaM in mouse CMs<sup>1,114-116</sup>. CaM is pre- bound to L- type Ca<sup>2+</sup> channels, where it reacts to local Ca<sup>2+</sup> influx and cytosolic Ca<sup>2+</sup> levels. Ca<sup>2+</sup>- bound CaM undergoes conformational changes and promotes rapid inactivation of the Ca<sub>v</sub>1.2 channel Ca<sup>2+</sup> current. The reduced Ca<sup>2+</sup> affinity of mutated CaM impairs this process, consequences are a prolongation of AP and subsequently cardiac arrhythmias<sup>115</sup>.

## 1.3.3 LQTS

*LQTS and causing mutations*

LQTS is a cardiac arrhythmia affecting approximately 1/ 2000 people of the general population. It is the leading cause for sudden cardiac death (SCD) within the young population <sup>117</sup>. Hallmarks of the syndrome include a prolonged QT interval (QTc >480 ms) on the electrocardiogram (ECG), delayed repolarisation of the ventricular myocardium, T wave alterations, susceptibility to torsade de pointes (TdP), seizures and sudden cardiac death <sup>118</sup>. LQTS is usually inherited as an autosomal- dominant trait, *de novo* mutations account for approximately 5- 10% of the symptom <sup>119</sup>. The three major causative genes of LQTS are *KCNQ1*, *KCNH2* and *SCN5A*, namely LQT1- 3. However, there are up to date 15 associated genes recognised to cause LQTS. A complete list of genes is shown in Table 1: List of genes associated with LQTS

CaM- mediated LQTS was first reported in 2013 in infants carrying mutations in *CALM1* and *CALM2*, discovered by whole exome sequencing <sup>1</sup>.

<i>LQTS type</i>	<i>Gene</i>	<i>Protein</i>	<i>Current</i>
<i>Romano–Ward syndrome</i>			
LQT1	<i>KCNQ1</i>	Kv7.1	$I_{Ks} \downarrow$
LQT2	<i>KCNH2</i>	KV11.1	$I_{Kr} \downarrow$
LQT3	<i>SCN5A</i>	Nav1.5	$I_{Na} \uparrow$
LQT4	<i>Ankyrin-B</i>	Ankyrin	Na <sup>+</sup> /K <sup>+</sup> ATPase and so on
LQT5	<i>KCNE1</i>	MinK	$I_{Ks} \downarrow$
LQT6	<i>KCNE2</i>	MiRP1	$I_{Kr} \downarrow$
LQT7	<i>KCNJ2</i>	Kir2.1	$I_{K1} \downarrow$
LQT8	<i>CACNA1C</i>	CaV1.2	$I_{Ca-L} \uparrow$
LQT9	<i>CAV3</i>	Caveolin3	$I_{Na} \uparrow$
LQT10	<i>SCN4B</i>	SCN $\beta$ 4subunit	$I_{Na} \uparrow$
LQT11	<i>AKAP-9</i>	Yotiao	$I_{ks} \downarrow$
LQT12	<i>SNTA1</i>	Syntrophin- $\alpha$ 1	$I_{Na} \downarrow$
LQT13	<i>KCNJ5</i>	Kir3.4	$I_{KACH} \downarrow$
LQT14	<i>CALM1</i>	Calmodulin1	Disorder of calcium signaling
LQT15	<i>CALM2</i>	Calmodulin2	
<i>Jervell and Lange–Nielsen syndrome</i>			
JLN1	<i>KCNQ1</i>	Kv7.1	$I_{Ks} \downarrow$
JLN2	<i>KCNE1</i>	MinK	$I_{Ks} \downarrow$

Table 1: List of genes associated with LQTS

List of LQTS with corresponding affected genes, proteins and resulting changes in ion currents or pathways. Adapted from Nakano and Shimizu <sup>120</sup>.

### *LQTS modelling in hiPSC- CMs*

*In vitro* cell culture overexpression models and transgenic animals contributed greatly to our understanding of cardiac diseases. The LQTS phenotype was recapitulated in various animal and heterologous expression models<sup>121,122</sup>. However, these models only partially mirror the molecular and cellular disease phenotypes due to differences in heart physiology, as well as gene and protein expression profiles between species<sup>123</sup>. Patient-derived hiPSCs provide the opportunity to have principally unlimited access to diseased ventricular, atrial and nodal CMs, carrying all the disease-relevant genetic alterations. Disease models of LQTS have been successfully generated and patient-specific hiPSC-CMs recapitulate the disease phenotype *in vitro*. Prolonged APs in atrial and ventricular cells have been measured, and defects in ion currents and channel activations could be shown in several models reported<sup>25,124-126</sup>. Moreover, the system has proven valuable to test drugs and cytotoxic effects preclinical on patient-specific hiPSC-derived CMs. Treatment options were assessed on these CMs and effects on pro-arrhythmic compounds could be shown<sup>23,30,124,127</sup>.

Limitations of modelling LQTS with hiPSC-derived CMs include the level of CM maturity obtained resembling an embryonic state rather than an adult CM state. A fetal-like phenotype of hiPSC-derived CMs has been shown on the gene expression level, as well as on morphological level in LQTS-patient hiPSC-CMs<sup>30</sup>. Those CMs present in addition with less negative resting membrane potentials, AP amplitudes are smaller, as well as the upstroke velocity compared to adult CMs<sup>128</sup>. However, current limitations to LQTS disease modelling and modelling of other cardiac diseases using hiPSC-derived CMs will most likely be overcome by future technical advances.

## II. Hypothesis and aims of the project

### 2.1 Patient- specific disease modelling of *CALMI* mutations

Patient- specific hiPSCs are produced and further differentiated into CMs. Electrophysiological examination of hiPSC- derived CMs display the reported LQTS phenotype *in vitro*. Pathogenic mechanisms in CMs can be further examined by electrophysiological and molecular investigations. Disturbed pathways in the affected CMs are identified, and treatment options can be analysed by preclinical *in vitro* testing of drugs. Correction of the LQTS causative point mutations in the *CALMI* gene in patient- derived hiPSCs, using the CRISPR/ Cas9 technology, abolishes the disease phenotype in derived CMs. Knocking- out of the mutated *CALMI* gene in patient hiPSCs will also cause the derived CMs to return to a healthy phenotype, since no more mutated CaM protein is translated. Other *CALM* transcripts will be upregulated to compensate the lack of CaM protein in the cells.

### 2.2 Analysis of the role of *MEIS1* in human cardiogenesis *in vitro*

MEIS1 is an important transcriptional co- activator during cardiogenesis and embryonic development. By knocking- out the *MEIS1* gene in healthy ctr hiPSCs, derived CMs are disturbed in differentiation and proliferation. Transcriptomic effects on other cardiogenic genes in the *MEIS1*- KO line shed light on the range of influence of MEIS1 during cardiac development.

### III. Material and methods

#### 3.1 Patients and ctr cell lines

Somatic skin fibroblasts of 2 unrelated probands were obtained from Lia Crotti and colleagues, as described in their publication <sup>1</sup>. hiPSC lines were generated from fibroblasts, as described in chapter 3.2.2. hiPSC line of patient with *de novo* mutation at protein position D130G (coding region position c.A389G) of the *CALM1* gene was named *CALM1*-D130G, generated hiPSC line of patient with *de novo* mutation at protein position F142L (coding region position c.C426G) of the *CALM1* gene was named *CALM1*-F142L.

The unrelated ctr hiPSC line C6 was used, generated from an adult Caucasian healthy female of 60 years of age, as described before in publications by Gramlich and colleagues <sup>32</sup>. The ctr C6 hiPSC line was generated from somatic skin fibroblasts, using the Sendai Virus reprogramming method. As a second unrelated healthy ctr, the HAK ctr hiPSC line was used. HAK was generated from a healthy, 30 years old male of Afro-American origin from keratinocytes using the Sendai Virus reprogramming method.

#### 3.2 Cell culture methods

##### 3.2.1 Cell culture material and media

3.5 cm and 6 cm cell culture dishes were purchased from Falcon (Cat No. 353001 and Cat No. 353004), 10 cm cell culture dishes and 96- well plates were purchased from Nunclon (Cat No. 150350 and Cat No. 161093). 15 cm cell culture dishes are acquired from Greiner Cellstar (Cat No. 639160). 50 ml and 15 ml Falcon tubes are from Greiner Cellstar (Cat No. 227261 and Cat No. 188271).

##### *List of media and supplements*

- Fibroblast growth medium: DMEM/F-12 (Invitrogen, Cat No. 21331-046), 10% FBS (Invitrogen, Cat No. 16141-079), 2 mM L- Glutamine (Invitrogen, Cat No. 25030-081), 100 µm MEM Non- essential Amino Acids (Invitrogen, Cat No. 11140-050), 1x Penicillin/Streptomycin (Invitrogen, Cat No.15140-122)

- MEF medium: DMEM/F-12, 10% FBS, 2 mM L- Glutamine, 100  $\mu$ M MEM Non- essential Amino Acids, 1 mM Sodium Pyruvate (Invitrogen, Cat No. 11360-070), 1x Penicillin/Streptomycin, 0.1 mM  $\beta$ - Mercaptoethanol (Invitrogen, Cat No. 31350-010)
- Melton EB2: DMEM/F-12, 2% FBS, 2 mM L- Glutamine, 100  $\mu$ M MEM Non- essential Amino Acids, 1x Penicillin/Streptomycin, 0.1 mM  $\beta$ - Mercaptoethanol
- Melton EB20: DMEM/F-12, 20% FBS, 2 mM L- Glutamine, 100  $\mu$ M MEM Non- essential Amino Acids, 1x Penicillin/Streptomycin, 0.1 mM  $\beta$ - Mercaptoethanol
- hiPS medium: DMEM/F-12, 20% KSR (Invitrogen, Cat No. 10828-028), 2 mM L- Glutamine, 100  $\mu$ M MEM Non- essential Amino Acids, 1x Penicillin/Streptomycin, 0.1 mM  $\beta$ - Mercaptoethanol
- 2x hiPS freezing medium: 20% hiPS medium, 60% FBS, 20% DMSO (Invitrogen, Cat No. D12345)
- E8 Medium: E8 basal medium (Invitrogen, Cat No. A1517001) supplemented with its E8 supplement, 0.5x Penicillin/Streptomycin
- 1x iPS feeder- free freezing medium: mFreSR (StemCell Technologies, Cat No. 05854)
- 1x iPS single- cell freezing medium: 35% DMEM/F-12, 5% DMSO, 10% Ethylene Glycol (Sigma Aldrich, Cat No. 324558), 50% FBS
- HEK medium: DMEM/F-12, 10% FBS, 2 mM L- Glutamine, 1 mM Sodium Pyruvate, 2 mM L- Glutamine, 1x Penicillin/Streptomycin
- Colony Screening buffer: 300  $\mu$ l 1 M Tris (Sigma Aldrich, Cat No. 1185-53-1) pH 8.0, 60  $\mu$ l 0.5 M EDTA (Invitrogen, Cat No. AM9260G), 1.5 ml 1 M KCl (Sigma Aldrich, Cat No. 7447-40-7), 60  $\mu$ l 1 M MgCl<sub>2</sub> (Sigma Aldrich, Cat No. M8266), 28 ml purified H<sub>2</sub>O, filter sterilized; 200  $\mu$ g/ml RNase A (Quiagen, Cat No. 19101), 670  $\mu$ g/ml Proteinase K (Sigma, P2308) both added freshly
- Dissociation Buffer: PBS<sup>-/-</sup> (Invitrogen, 14190-250), 2.5 mg/ml Trypsin (Invitrogen, Cat No. 2158203), 1 mg/ml Collagenase IV (Cell Systems, LOT 43K14405A), 20% KSR, and 1 mM CaCl<sub>2</sub> (Sigma Aldrich, Cat No. 10043-52-4)
- Single- cell iPS freezing medium: 35% DMEM/F-12, 5% DMSO, 10% Ethylene Glycol (Sigma Aldrich, Cat No. 107-21-1), 50% FBS, sterile filtered
- EDTA single- cell splitting solution: 500 ml PBS<sup>-/-</sup>, 0.9 g NaCl (Sigma Aldrich, 7647-14-5), 500  $\mu$ l 0.5 M EDTA, filter sterilized

### 3.2.2 hiPSC generation

The CytoTune reprogramming Kit from Thermo Fisher Scientific with Lot number 47720 was used for fibroblast reprogramming. hiPSC generation was performed according to the CytoTune User Manual. Human primary skin fibroblasts (PSF) were obtained from patients by skin biopsy. PSF were cultured on 0.1% gelatine- coated (Sigma, Cat No. G1393) cell culture dishes in fibroblast growth medium for one passage. On the day of transduction, cells reached a density of  $5 \times 10^5$  cells/ well. Before transduction, each CytoTune Sendai Virus (SeV) component (hOct3/4, hSOx2, hKlf4 and hc- Myc) was combined in 1 ml fibroblast medium, corresponding to  $3 \times 10^6$  cell infection units/ ml (CIU) each. Fibroblast medium was aspirated from PSF plate and cells were transduced with CytoTune Sendai virus (SeV) mix at an MOI of 3. The virus mix was left on the cells for 24h and plate was incubated at 37 °C and 5% CO<sub>2</sub> in a cell culture incubator (Thermo Scientific, HERA cell 150i). After 24h, medium was replaced with fresh fibroblast medium and subsequently changed every other day for 6 days. 6 days after transduction, new 10 cm cell culture dishes were first coated with 0.1% gelatine and then pre- seeded with MEF feeder cells at a density of  $2.5 \times 10^6$  cells per 10 cm dish. The following day, the transduced plate was washed twice with PBS<sup>-/-</sup> and incubated with 0.3 ml 0.05% Trypsin (Invitrogen, Cat No. 25300-096) at room temperature. Detaching cells were collected in excess fibroblast medium and spun at 200x g for 4min (Hettich centrifuge Rotina 420R). The supernatant was aspirated and the cell pellet was carefully resuspended and counted using a hemocytometer.  $5 \times 10^4$  cells were plated per 10 cm dish and incubated overnight as described before. Remaining cells were used for RNA extraction. 24h after plating cells onto MEF feeder plates, medium was switched to hiPS cell medium and changed every 24h. hiPSC colonies emerged and were picked after 2- 3 weeks.

### 3.2.3 hiPSC culturing methods

#### *hiPSC culture on MEF feeders and manual splitting*

hiPSC were cultured on MEF feeder coated cell culture plates in hiPS medium as described before in the publication of Moretti and colleagues<sup>24</sup>, unless stated otherwise. In general, MEF feeder plates were prepared 24h before usage. MEF cells were plated on gelatine- coated cell culture plates in MEF medium at a density of  $4.5 \times 10^4$  cells/cm<sup>2</sup>. MEF plates were washed once with DMEM/F-12 before hiPS medium supplemented with

10  $\mu$ M ROCK Inhibitor (Merck Millipore, Cat No. SMCM075) and 10 ng/ml bFGF (Invitrogen, Cat No. PHG0264) was added. Medium was changed every 24h on hiPSC plates and plates were kept in a cell culture incubator at 37 °C and 5% CO<sub>2</sub>. hiPSCs were manually passaged every 5- 7 days. 1h before cell splitting, 10  $\mu$ M ROCK Inhibitor was given to the hiPSC plates. For manual passaging, hiPSC plates were placed under a light microscope (Olympus CKX31) with 4x magnification (UPlanFL N 4x). Using a 12 mm syringe (Braun Omnican 40, Cat No. 9161627), approximately 8 colonies of 2.5 mm diameter were cut into a squared pattern. In total, around 30 rhombus- shaped pieces were transferred into one 3.5 cm MEF feeder coated cell culture dish. Media was changed to hiPS medium supplemented with 10 ng/ml bFGF 24h after splitting.

To freeze hiPSCs grown on feeders, plates were first washed once with DMEM/F-12. 0.5 ml dissociation buffer was dispersed per 3.5 cm plate and plate was incubated for 5min at 37 °C. Using a P1000 pipette, colonies were washed off carefully with pre- warmed hiPS medium without detaching the feeder layer. Colonies were collected in a 15 ml falcon tube in excess warmed hiPS medium. Tubes were centrifuged at 200x g for 5min and supernatant was discarded. 60- 80 colonies per 3.5 cm dish were frozen in 1 ml 1x hiPS freezing medium by dilution of freezing medium 1:1 with hiPS medium. Mix was transferred carefully into CryoTube Vials (Thermo Scientific, Cat No. 377224), tubes were placed in a freezing container (Sigma Aldrich, Cat No. C1562-1EA) and placed at -80 °C for at least 24h before transferred to long term storage in liquid nitrogen.

#### *Feeder- free hiPSC culture*

Feeder- free hiPSC culture was executed in Essential 8 medium supplemented with 0.5x Pen/Strep. Plates were pre- coated with Geltrex (Invitrogen, Cat No. A1413302) according to manufacturer's protocols. Before colonies were split, plates were placed under a light microscope with 5x magnification. Differentiated areas of hiPSC colonies were scratched away manually before passaging, using a 10  $\mu$ l sterile pipette tip. hiPSC plates were washed twice with DMEM/F-12 and incubated for 6min at 37 °C with 1x Dispase (Stem Cell Technologies, Cat No. 07913). After incubation, Dispase was discarded and plates were washed carefully with DMEM/F-12. Using a 13 mm cell scraper (TTP, Cat No. 99002), colonies were scraped off the surface in 1 ml DMEM/F-12, collected and passed through a 40  $\mu$ m cell strainer (Corning, Cat No. 352340). Cell strainer was flipped upside down and remaining pieces of hiPSCs attached to the strainer were washed out and collected in a 50 ml falcon tube using an appropriate volume of fresh E8 medium.

Cell solution was transferred carefully to Geltrex- coated plates and incubated for 24h in E8 medium supplemented with 10  $\mu$ M Thiazovivin (Sigma Aldrich, Cat No. SML1045). Cells were passaged every 4- 7 days at a 1:4 or 1:6 ratio and medium was changed every 24h.

To freeze hiPSCs grown in feeder- free conditions, plates were washed once with DMEM/F-12 and incubated with 0.5 ml 1x Dispase at 37 °C for 6min. After incubation, Dispase was discarded and plates were washed carefully again with DMEM/F-12. Using a 13 mm cell scraper, colonies were scraped off the surface, collected in pre- warmed hiPS medium and spun down at 200x g for 5min. Supernatant was discarded and cell pellet was carefully resuspended in 1 ml mFreSR (Stemcell Technologies, Cat No. 05854) per 3.5 cm cell culture plate. Cell suspension was transferred to CryoTubes, placed in a freezing container at -80 °C for 24h and then transferred to liquid nitrogen long term storage.

#### *Single- cell adaptation and single- cell culture of hiPSCs on feeders*

hiPSC colonies were cut manually by placing the plate under a light microscope and cutting the colonies using a syringe. For the first passage of adaptation, rhombus- shaped pieces were cut as small as possible, putting more pressure on the syringe when cutting. Media was changed and using a P1000 pipette, rhombus- shaped pieces were lifted off and collected on a fresh plate in hiPS medium supplemented with 10  $\mu$ M ROCK inhibitor. Medium was changed daily. After approximately 4 days, cell clumps were passaged using TrypLE Express (Invitrogen, Cat No. 1755751). Medium was aspirated and plates were washed once with DMEM/F-12. 1 ml TrypLE was incubated per 3.5 cm plate for 5min at 37 °C and enzymatic reaction was stopped by adding serum- containing medium in excess. Cells were collected and centrifuged at 200x g for 5min. Supernatant was discarded and cells were re- plated at a 1:1 or 1:2 ratio on fresh feeder- coated cell culture plates in hiPS medium supplemented with 10  $\mu$ M ROCK Inhibitor. Cells were subsequently passaged once or twice per week with TrypLE at a 1:1.5 or 1:2 ratio. After 3- 4 passages cells were considered single- cell adapted and were split at a 1:3 ratio every 3- 4 days. Single- cell adapted cells were frozen and thawed at a 1:1 ratio in single- cell hiPS freezing medium (composition, see 3.2.1)

*Feeder-free single-cell adaptation and single-cell culture of hiPSCs*

hiPSCs adapted to feeder-free growth in E8 medium on Geltrex substrate were split using EDTA splitting solution. hiPSC plates growing as colonies were washed twice with EDTA solution. As a first single-cell adaptation step, 1 ml EDTA was added per 3.5 cm plate and incubated for 5 min at RT. EDTA solution was aspirated carefully and 1 ml E8 medium was added boldly with a P1000 pipette to the plate, causing the colonies to dislodge and break up in bigger pieces. Pieces were transferred carefully without further pipetting into new Geltrex plates at a 1:2 ratio in E8 medium supplemented with 10  $\mu$ M Thiazovivin. 24 h after splitting, medium was changed to regular E8 medium. Medium was changed every 24 h subsequently. After 2-3 days, before plate reached 70% confluency and pieces started forming round colonies, EDTA splitting was performed again. EDTA solution was incubated on the plates for 7 min at RT. Cell solution was distributed on new plates in a 1:3 or 1:4 ratio in E8 medium with Thiazovivin. 24 h later medium was exchanged again to regular E8 medium and single-cell adapted hiPSC plates were split again after 2-3 days. Over the time course of several passages, single-cell adapted cells were split higher with every passage, in an up to 1:10 ratio. Before plates reached 90% confluency, they were passaged to prevent colony growth and differentiation.

To freeze single-cell adapted hiPSCs, plates were first washed twice with EDTA splitting solution. 1 ml EDTA solution was incubated on cells for 7 min at RT per 3.5 cm plate. Subsequently, EDTA was discarded and detaching cells were collected in excess E8 medium. Cell solution was spun down at 200x g for 5 min, supernatant was discarded and cell pellet was reconstituted in 1 ml 1x single-cell freezing medium per 3.5 cm cell dish. Cell suspension was transferred to CryoTubes, placed in a freezing container at -80 °C for 24 h and then transferred to liquid nitrogen long term storage.

### 3.2.4 Differentiation of hiPSCs into CMs

For generation of hiPSC-derived CM, hiPSC colonies were formed first into embryonic bodies (EB). hiPSC cell plates were washed once with DMEM/F-12 before 1 ml dissociation buffer was added per 3.5 cm plate. Plate with dissociation buffer was then incubated for 10 min at 37 °C. Dissociated hiPSC pieces were carefully flushed off the feeder plate with hiPS medium. Cell pieces were collected in excess hiPS medium and spun down at 1200 rpm for 5 min. Supernatant was removed carefully and the remaining cell pellet was collected in MEF-conditioned medium supplemented with 10  $\mu$ M ROCK Inhibitor and

10 ng/ml bFGF. Dissociated hiPSC pieces were maintained on MEF- conditioned medium on polyhema- coated (Sigma, Cat No. P3932) cell culture plates for 3 days without medium change. Medium was changed to EB20 supplemented freshly with 50 µg/ml L-Ascorbic Acid (Sigma, Cat No. A5960) on days 3 and 5, by first carefully collecting old medium together with floating EBs in a 15 ml falcon tube. Floating EB tubes were left at RT until sedimented. Medium was then aspirated carefully and floating EBs were collected in fresh EB20 medium supplemented with Ascorbic Acid in an appropriate volume. EB suspension was incubated in the same polyhema- coated plates until day 7 of differentiation. On differentiation day 7, floating EBs were collected and plated on gelatine-coated 4- well cell culture plates (Thermo Scientific, Cat No. 176740) at a density of around 10 EBs/ well in EB20 medium supplemented with Ascorbic Acid. Medium was changed every 2 days with fresh EB20 with Ascorbic Acid. Beating forci were observed from day 10 on. 21 days after differentiation, medium was changed to EB2 medium and beating CM loci were excised using a 12 mm syringe. Excised loci were placed in 4- well cell culture plates in EB2 medium. Medium was subsequently changed every 7 days on explant plates.

Cardiac differentiations of HAK hiPSCs and *MEIS1*- KO hiPSCs for Western Blot (WB) and qRT PCR analysis was induced, using the PSC CM Differentiation Kit (Thermo Fisher Scientific, Cat. No. A2921201) according to manufacturer's guidelines. In general, hiPSCs were previously adapted to single- cell growth and seeded on Geltrex in E8 medium into 12- well cell culture plates. Induction of differentiation was performed on 80% confluent wells. Beating loci were observed from day 7 of induction onwards.

### 3.2.5 Dissociation of CMs

24h before explant dissociation, cell culture plates were coated with fibronectin. Fibronectin (Sigma, Cat No. F1141) was diluted 1:100 in 1x PBS<sup>Ca2+/Mg2+</sup> (Invitrogen, Cat No. 14080-048) and added to the plates. Plates were incubated at 4 °C overnight before use. Around 10 beating CM explants were collected per 1.5 ml tube and washed twice with 500 µl pre- warmed 1x HBSS (Invitrogen, Cat No. 24020-117). Washed loci were equilibrated in 250 µl HBSS supplemented with 1.5 mg/ml Collagenase type II. After sedimentation of loci to the bottom of the tube, supernatant was carefully removed and explants were incubated with fresh HBSS/Collagenase solution for 1h at 37 °C in a shaking

thermomixer (Eppendorf, Thermomixer compact) at 750 rpm. CM- containing supernatant was collected in a 15 ml tube containing 5 ml pre- warmed EB20 medium. Tube with CM- solution was kept in a cell culture incubator at 37 °C. Remaining explants were dissociated for another 30min in 250 µl HBSS/ Collagenase solution as described before and supernatant was collected subsequently. This step was repeated up to two more times until remaining CM clumps were broken up. Finally remaining clumps were incubated in 250 µl Accumax (Millipore, Cat No. 1500700180) for 10min at 37 °C in the shaking thermomixer and pipetted carefully if necessary until completely separated. Collected cell solution was then centrifuged at 200x g for 5min. Supernatant was aspirated and pellet was suspended in the required volume of EB2 medium. CMs were plated as single cells on plates pre- coated with fibronectin and medium was changed to fresh EB2 the day after dissociating and subsequently every 3- 4 days.

### 3.2.6 Lentivirus production and transfection of hiPSCs

#### *Lentivirus production*

HEK293 cells (Laboratory stock) of passage 4 were thawed in 10 cm cell culture plates in HEK medium and split in a 1:3 to 1:4 ratio in different cell numbers. Plates that reached 70- 75% confluency on the next day were chosen for transfection. Transfection was performed with FuGENE HD Transfection Reagent (Promega, Cat No. E2311). FuGENE transfection complexes were prepared with the following components per 10 cm cell plate to be transfected: 500 µl OptiMEM (Invitrogen, Cat No. 1912191), 7.5 µg pRRL.sin-18 transfer vector plasmid, 4.875 µg CMVΔR8.74 packaging plasmid, 2.625 µg VGV.G envelope plasmid, 45 µl FuGENE HD. Components were mixed gently and incubated at RT for 15- 30min. Mix was subsequently added dropwise to the HEK293 cell plates and distributed carefully by rocking the plates back and forth. Plates were incubated over night at 37 °C in a cell incubator (5% CO<sub>2</sub>). The following day, 4 ml of fresh HEK medium was added on top of the old medium and incubated for another 24h. 48h post- transfection, virus- containing supernatant was collected and centrifuged at 3000 rpm for 15min and 4 °C. Virus- containing supernatant was then aliquoted in 0.5 ml aliquots and frozen at -80 °C.

### *Transfection of hiPSCs*

To transfect hiPSCs with CRISPR/ Cas9 constructs, the TransIT-2020 Transfection Reagent (Mirus, Cat No. MIR 5404) was used. 24h previous transfection,  $1.25 \times 10^6$  single-cell adapted hiPSCs were plated on a 3.5 cm Geltrex- coated cell culture dish. Plates reached approximately 80% confluency by the next day. 3- 4h before transfection, medium on cell culture dish was replaced with fresh culture medium. Before transfection, transfection reagent was warmed up to RT. 250  $\mu$ l OptiMEM (Invitrogen, Cat No. 1912191) was gently mixed with 3  $\mu$ g Cas9 plasmid or 1.5  $\mu$ g plasmid and 1.5  $\mu$ g ssODN and 9  $\mu$ l transfection reagent and mix was incubated for 30min at RT. TransIT/ DNA mix was added dropwise to the plate and carefully distributed by rocking the plate cross- wise. Plate was incubated for 24h to 48h in a cell culture incubator. Cells were then used for analysis by FACS, cleavage detection analysis or antibiotic selection.

### 3.2.7 Transduction of hiPSCs

#### *Electroporation*

A Gene Pulser Xcell Electroporation System from Biorad was used for electroporation of hiPSCs, together with 4 mm electroporation cuvettes (PeqLab, Cat No. 712030(LE)). Cells used for electroporation were cultured on MEF feeder plates and adapted to single-cell growth for at least 8 passages. 1- 2 days before the electroporation, cells were dissociated with 1x TrypLE Express for 5min at 37 °C and plated on BD Matrigel hESC-qualified Matrix (BD, Cat No. 354277) coated 10 cm cell culture plates in MEF- conditioned medium. 3- 4x 10 cm hiPSC plates were prepared per electroporation experiment. Cells were grown on Matrigel until 80% confluent. 3- 4h before electroporation, cells were treated with 5  $\mu$ M ROCK inhibitor. PBS<sup>-/-</sup> and electroporation cuvettes were placed on ice. Cells were dissociated with TrypLE, counted in a Neubauer Zählkammer and spun down in ice- cold PBS<sup>-/-</sup>. Per electroporation, 15  $\mu$ g Cas9- encoding plasmid and 15  $\mu$ g gRNA plasmid, or 30  $\mu$ g Cas9 all-in one plasmid were suspended with 30  $\mu$ g ssODN in a total volume of 200  $\mu$ l ice- cold PBS<sup>-/-</sup>.  $10 \times 10^6$  cells were dissolved in 500  $\mu$ l ice- cold PBS<sup>-/-</sup> and carefully blended with the DNA mix. The 800  $\mu$ l cell/DNA mixture was filled into one ice- cold 4 mm electroporation cuvette and incubated on ice for 5min. The outside of the cuvette was subsequently dried off thoroughly and placed in the electroporator. Cells were transformed with the following settings: exponential decay pulses, 250 V and 500  $\mu$ F. The time constant determined by the machine was noted after the pulse as an

indicator of quality of electroporation. Best results are expected at time constants between 10 and 14 ms. After the pulse, cells were collected in 10 ml pre-warmed hiPS medium and pelleted for 5min at 200x g. Obtained pellet was suspended carefully in pre-warmed conditioned media supplemented with 10 ng/ml bFGF and 5  $\mu$ M ROCK inhibitor and plated on a 15 cm Matrigel-coated cell culture dish. The day after the electroporation, media was replaced with new MEF-conditioned media supplemented with 10 ng/ml bFGF. 96-well cell culture feeder plates or 3.5 cm feeder plates were prepared for recovery after fluorescence-activated cell sorting (FACS sorting).

### *Nucleofection*

hiPSCs were cultured in feeder-free conditions in E8 medium, as described before, and adapted to single-cell growth for at least 4 passages. E8-conditioned medium was collected from hiPSC plates every 24h and sterile filtered. Nucleofection was performed using the Human Stem Cell Nucleofector Kit 2 (Lonza, Cat No. VPH-5022) and the Amaxa 2D Nucleofector. Cells were treated with 10  $\mu$ M ROCK inhibitor 1-2h before nucleofection. Plates were washed once with DMEM/F-12 and incubated with 0.5 ml Accutase (GE Healthcare, Cat No. L11-007) for 5min at 37 °C. Cells were collected and 0.8x 10<sup>6</sup> cells were used per nucleofection. Correlating volume of cell solution for 0.8x 10<sup>6</sup> cells was spun down at 200x g for 5min and supernatant was discarded carefully. Nucleofection solution was prepared, by adding 18  $\mu$ l Supplement 1 to 82  $\mu$ l Human Stem Cell Nucleofector Solution 2 per round of nucleofection. Solution mix was incubated for 5min at 37 °C. Cell pellet was resuspended carefully with 100  $\mu$ l nucleofection suspension mix and transferred to a nucleofector cuvette. 5  $\mu$ g total DNA was added into cell suspension in the cuvette. Suspension/DNA mix was mixed by swirling the cuvette gently and tapping it 3 times on the hood surface. Cuvette was inserted into the Amaxa 2D Nucleofector and program B-016 was set and executed. Nucleofected cells were retrieved in 500  $\mu$ l pre-warmed conditioned E8 medium supplemented with 10  $\mu$ M ROCK inhibitor and 10 ng/ml bFGF in a sterile 1.5 ml tube. Cells were incubated at 37 °C for 10min. Geltrex-coated 4-well cell culture plates were equipped and pre-incubated with 0.8 ml E8 medium per well, with the E8 medium composed of 50% fresh and 50% conditioned E8, supplemented with 10  $\mu$ M Thiazovivin and 10 ng/ml bFGF. Cell suspension was transferred dropwise into 2 wells of the prepared 4-well cell culture plates and incubated for 24h at 37 °C. 24h after nucleofection, medium was replaced and antibiotic selection of successfully nucleoporated cells with puromycin was started.

### 3.2.8 Selection of hiPSCs

#### *FACS sorting*

This method describes cell sorting of green fluorescent protein (GFP) expressing cells after electroporation with GFP- encoded Cas9 plasmids. hiPSCs were cultured as single cells on MEF- feeder plates and electroporated as described before. 24- 48h after electroporation, cells were dissociated from MEF- feeder plates by incubation with TrypLE for 5min at 37 °C. Cells were spun down for 5min at 200x g and obtained cell pellet was carefully resuspended in 500 µl PBS<sup>-/-</sup> supplemented with 2% FBS. Cells were dissociated into single cells by passing through a 35 µm cell strainer cap (Filcons, Cat No. 03033S) and kept on ice until sorted. Cell sorting was performed in collaboration with the Flow Cytometry FACS Unit of the Technical University München. For deposition of single cells into MEF- feeder coated 96- well plates, the MoFloII Legacy (BeckmanCoulter) machine was used. Single- cell sorting was performed at 10000 eps (events per second) at a single 0.5 sort mode and 60 psi through a 70 µm nozzle. In case of sorting cells into collection tubes, the Aria FACS machine (BeckmanCoulter) was used. Sorting speed was at 20000 eps. In general, cell populations were first gated for forward scatter (FS) and Pulse Width on a linear scale to exclude cell aggregates and cell debris from the analysis. As a second gate, forward and sideward scatter was gated. GFP was excited with a 488 nm laser and detected in the FL1 channel with a 530/40 bandpass filter. Dead hiPSCs reflect exciting laser light visible in the PE channel, therefore gates were set to exclude those cells. Autofluorescence was measured by excitation at 561 nm in Aria and 488 nm in MoFlo II. Emission was detected at 550 and 582.15 longpass and bandpass filter. GFP positive cells at a fluorescent intensity of 102 on the logarithmic scale were chosen to be collected and plated in either 96- well feeder plates as single cell per well or up to 10000 per 3.5 cm feeder cell culture plate. Cells were recovered from FACS sorting on MEF- feeder coated cell culture plates in culture media consisting of 50% fresh hiPS medium and 50% MEF- conditioned medium, supplemented with 20 ng/ml bFGF and 5 µM ROCK inhibitor. 4 days after sorting, wells were supplemented on top with fresh hiPS medium containing 30 ng/ml bFGF. Once colonies started to appear, medium was changed every other day to fresh hiPS medium supplemented with 10 ng/ml bFGF. After 9- 12 days post sorting, colonies reached the size of approximately 2 mm and were split into new MEF- feeder coated cell culture plates and screened for successful genomic alterations, as described in chapter 3.3.7.

### *Puromycin selection*

Puromycin tolerance of cell lines to be nucleofected with pSpCas9(BB)-2A-Puro (PX459) V2.0 plasmid was examined beforehand by performing puromycin kill- curves. Single- cell adapted hiPSCs were plated in multiple wells of Geltrex- coated 24- well plates (Nunc, Cat No.150687) in E8 medium and cultured until 80% confluent. Puromycin was purchased as powder from Calbiochem (Cat No. 540411) and dissolved in sterile H<sub>2</sub>O at a concentration of 50 µg/ml. Puromycin solution was aliquoted and stored at -20 °C. Puromycin was added to E8 medium without Pen/Strep at various concentrations and added to the wells for up to 4 days. Medium was exchanged every 24h. Antibiotic concentrations were tested on wells in duplicates and 2 wells without the addition of antibiotics was included as negative ctr. Optimal puromycin concentration was considered the concentration that killed 90% of cells after 48h and all the cells after 3 days of selection. The patient hiPSC line with mutation F142L was positively selected at 0.2 µg/ml after 3 days, the ctr hiPSC line HAK at 0.35 µg/ml puromycin.

24h after nucleofection, E8 medium was replaced with fresh medium without Pen/Strep and supplemented with the appropriate concentration of puromycin. Medium was exchanged every 24h and cells were observed carefully. Selection process was stopped after 24 to 48h, depending on the amount of viable cells left. Once approximately 90% of cells were eliminated, medium was exchanged to regular E8 medium and subsequently exchanged every 24h. After approximately 7 days post- selection, hiPSC colonies were grown to sufficient size to be separated into separate wells of a Geltrex- coated 4- well plate in E8 medium. While separation, pieces of colonies were isolated for colony screening, as described in chapter 3.3.7.

## 3.3 Molecular biology methods

### 3.3.1 qRT PCR and RT PCR

#### *qRT PCR for pluripotency of generated hiPSC lines*

Pluripotency of generated hiPSC lines were assessed by measuring transcription levels of endogenous pluripotency marker genes. For qRT PCR analysis, total RNA was first extracted using the Absolutely RNA Nanoprep Kit (Agilent, Cat No. 400753), Absolutely

RNA Microprep Kit (Agilent, Cat No. 400805) or Absolutely RNA Miniprep Kit (Agilent, Cat No. 400805), according to manufacturer's protocols. Uninfected primary skin fibroblasts from 6 cm cell culture dishes were lysed with 700  $\mu$ l Lysis Buffer per cell line. Confluent 6 cm cell culture dishes of hiPSC lines passage 2 were lysed as well in 700  $\mu$ l Lysis Buffer and total RNA was extracted with the Absolutely RNA Miniprep Kit. Total RNA was eluted in 30  $\mu$ l pre-warmed Elution Buffer. RNA concentration was estimated with a Nanodrop 1000 Spectrophotometer (Thermo Fisher Scientific). Up to 1  $\mu$ g of RNA was added to the Reverse Transcriptase PCR (RT PCR) to generate copy DNA (cDNA). RT PCR reaction was performed with reagents from the High Capacity cDNA Reverse Transcription Kit (Applied Biosystems, Cat No. 4368813), according to the product manual. Maximum 1  $\mu$ g of total RNA was given as input to the master mix. Reaction was performed in a Thermocycler DNA Engine PCR machine (Peltier Thermal Cycler, Bio-rad).

Produced cDNA was diluted 1:3 with sterile H<sub>2</sub>O and immediately used for further qRT PCR analysis or stored at -20 °C. qRT PCR reactions were performed with reagents from the Power SYBR Green PCR Master Mix (Applied Biotechnologies, Cat No. 4367659). Primer pairs of endogenous genes associated with pluripotency chosen were *c-MYC*, *KLF4*, *OCT3/4*, *SOX2*, *NANOG*, *REX1* and *TDGF1*, as previously described in the publication of Moretti and colleagues<sup>129</sup>. Primer sequences are listed under 3.6.

The following master mix was set up per reaction:

Reagent	Volume [ $\mu$ l]
2x Power SYBR Green PCR Master Mix	5
Forward Primer [10 $\mu$ M]	0.3
Reverse Primer [10 $\mu$ M]	0.3
cDNA Template	1
Sterile H <sub>2</sub> O	3.4
total	10

Table 2: qRT PCR Reaction master mix

Gene expression was assessed with a 7500 Fast Real- Time PCR machine (Applied Biosystems) and the following program:

Cycle	Time [min]	Temp [°C]	
1	00:20	50	40 x
2	10:00	95	
3	00:15	95	
4	01:00	60	
5	00:15	95	
6	01:00	60	
7	00:30	95	
8	00:15	60	

Table 3: qRT PCR program

Gene expression values were estimated relative to corresponding primary skin fibroblasts and normalised to *GAPDH*. Primer sequences are listed under 3.6.

#### *qRT PCR of embryonic germ layer specific lineage markers*

To assess the capability of generated hiPSC lines to differentiate into cells of all three embryonic germ layers, qRT PCR analysis on marker genes representing the three embryonic germ layers was performed on EBs day 21 of differentiation. For each biological replicate, a 4- well plate of plated EBs per cell line was lysed in 600  $\mu$ l Lysis Buffer and total RNA was extracted using the Absolutely RNA Miniprep Kit. Total RNA was eluted in 30  $\mu$ l pre- warmed Elution Buffer. Up to 1  $\mu$ g of RNA was transcribed into cDNA. cDNA was diluted 1:3 with sterile H<sub>2</sub>O and Power SYBR Green Master Mix was applied as described before. Primer pairs corresponding to the endodermal genes *PDX1*, *SOX7*, and *AFP*, the mesodermal genes *CD31*, *DES*, *ACTA2*, *SCL*, *MYL2* and *CDH5* and the ectodermal genes *KRT14*, *NCAM1*, *TH*, and *GABRR2* were used as qRT PCR targets, as described previously in the publication of Moretti and colleagues<sup>129</sup>. Primer sequences

are listed under 3.6. Expression values were calculated relative to corresponding undifferentiated hiPSC clones and normalised to *GAPDH*.

#### *qRT PCR analysis of CM explants*

To elucidate transcription expression levels of different genes in hiPSC generated CM, total RNA was extracted from explanted beating loci of 2.5 months age. In general, around 30 explants were used for total RNA extractions using the Absolutely RNA Nanoprep Kit (Agilent, Cat No. 400753) per sample. Total RNA extractions were performed according to manufacturer's guidelines. Samples were eluted in 10  $\mu$ l 60 °C pre-warmed Elution Buffer and RNA concentration was estimated by Nano Drop measurement. cDNA synthesis was performed as described before. qRT PCR Primer pairs for each transcript of the three *CALM* genes were designed according to standard Oligonucleotide design guidelines. The sequences can be found under 3.6. Expression values were calculated relative to corresponding *GAPDH* values and normalised to the average of all *GAPDH* values.

qRT PCR analysis was also performed on a selection of cardiac ion channel genes and binding partners of CaM. Target genes selected were *PMCA1*, *PMCA2*, *PMCA3*, *PMCA4*, *SLC8A1*, *SERCA*, *CACNA1C*, *PLN*, *cTNT* and *RYR2*. Sequences of oligonucleotides are listed under 3.6. Here, total RNA was extracted and further processed for qRT PCR analysis from 2.5 months old explanted beating loci. Expression values were calculated relative to corresponding *GAPDH* values and normalised to *cTNT* values.

#### *RT PCR of Sendai transgenes*

To show the presence of delivered Sendai transgenes of infected fibroblasts and to prove the absence of those transgenes in uninfected fibroblasts, total RNA was extracted from infected and uninfected fibroblasts per cell line. 1  $\mu$ g of total RNA was transcribed to cDNA. The PCR was conducted with the FIREPol DNA Polymerase (Solis Biodyne, Cat No. 01-01-1000) according to manufacturer's manual. 25 ng/ $\mu$ l cDNA was used as DNA input. The master mix with Primer Sets *c-MYC* and *SOX2* was supplemented with Solution S, due to amplification of GC- rich DNA templates. Primer Sets *SOX2*, *KLF4* and *OCT3/4* use the same reverse Primer. Primer sequences are listed in 3.6.

The following PCR program was performed:

Cycle	Time [min]	Temp [°C]	
1	05:00	95	34 x
2	00:30	95	
3	00:30	55	
4	00:30	72	
5	05:00	72	
6	∞	4	

Table 4: Sendai RT PCR program

PCR product was loaded on a 1.5% EtBr- Agarose Gel together with a 2- log DNA ladder (New England Biolabs, Cat No. N3200S). Gel was run for 30min at 240 V. Separated bands were made visible and documented with a UV- light documentation system from Biovision 3000WL (PeqLab).

### 3.3.2 PluriTest analysis

To further assess level of pluripotency of generated hiPSC lines, total RNA was extracted on selected clones using the Absolutely RNA Microprep Kit. To perform whole genome microarray analysis, RNA was hybridized on Illumina HT12v4 microarrays. The raw microarray data were analysed with the PluriTest algorithm, according to Muller *et al.*<sup>130</sup>. This assay was performed by Dr. Parrotta at Magna Græcia University, Catanzaro, Italy.

### 3.3.3 Protein extraction and WB analysis

#### *Protein sample preparation*

Expressed protein levels of *MEIS1* in ctr and *MEIS1*- KO cell lines were measured by WB analysis. 80% confluent 3.5 cm *MEIS1*- KO hiPSCs and HAK ctr hiPSCs were induced to cardiac differentiation for 48h. Cell lysis buffer was prepared freshly by adding 1x Complete Mini EDTA- free Protease Inhibitor Cocktail (Roche, Cat No. 11836170001) to 300 µl cold RIPA buffer (Sigma Aldrich, Cat No. R0278) per 3.5 cm well placed on ice. Dishes were incubated on ice with lysis buffer for 20min and cells were collected in 1.5 ml tubes and spun in at 14000 rpm for 15min at 4 °C. Supernatant was collected in fresh tubes and shock- frozen in liquid nitrogen for storage at –80 °C or immediately used for protein concentration determination.

Protein concentration was determined by colourimetric detection using the BCA Protein Assay Kit (Pierce, Cat No. 23227) according to the corresponding manual and a 550 nm ELISA reader (Dynatech MR5000). 5  $\mu$ l protein extract was mixed with 200  $\mu$ l BCA substrate in a 96- well plate alongside with a standard BSA curve ranging from 0 mg/ml up to 2 mg/ml. Plate was incubated at 37 °C for approximately 20min. Values read by the ELISA machine were used for calculating protein concentrations of samples according to the protein standard reference curve. Protein extracts were denatured by boiling for 5min at 95 °C in 4x sample buffer (200 mM Tris- HCl pH 6.8, 4 mM EDTA, 40% glycerol (Sigma Aldrich, Cat No. G2025), 4%  $\beta$ -Mercaptoethanol, 0.1 mg/ml bromphenol blue (Sigma Aldrich, Cat No. B0126)) and stored at -80 °C until further analysis.

### *SDS electrophoresis*

To separate proteins by size, SDS- PAGE gels were prepared, following standard guidelines. To prepare 2x 10% resolving gels in a Mini Protean II System (BioRad, Cat No. 1658003EDU) gel cast, 7.9 ml sterile H<sub>2</sub>O, 6.7 ml 30% Bis- Acrylamide (Biorad, Cat No. 161-0156), 5 ml Tri- HCl pH 8.8, 200  $\mu$ l 10% SDS (Sigma Aldrich, Cat No. L4509), 200  $\mu$ l 10% APS (Sigma Aldrich, Cat No. A3678) and 8  $\mu$ l TEMED (Sigma Aldrich, T9281). 5% stacking gels were added on top of the resolving gels by mixing 5.5 ml sterile H<sub>2</sub>O, 1 ml Tris- HCl pH 6.8, 1.3 ml Bis- Acrylamide, 80  $\mu$ l 10% SDS, 80  $\mu$ l 10% APS and 8  $\mu$ l TEMED. Gels were fixed in the according Mini Protean II gel running tanks filled with 1 x running buffer (diluted from 10x running buffer in sterile H<sub>2</sub>O: 30.3 g Tris, 144 g glycine, 10 g SDS in 1 l sterile H<sub>2</sub>O) and proteins were separated for 1 h at 150 V.

### *WB*

After separating proteins by SDS- PAGE, protein bands were transferred on Hybond ECL nitrocellulose membrane (Amersham, Cat No. RPN 203E) in a wet blotting chamber (Mini Protean System II blotting module from BioRad) in 1x blotting buffer (diluted from 10x blotting buffer in sterile H<sub>2</sub>O: 30.2 g Tris, 144 glycine in 1 l sterile H<sub>2</sub>O, adding 20% MeOH to final volume). Proteins were transferred for 90min at 100 V and at 4 °C. Blotted membranes were washed once in sterile H<sub>2</sub>O and stained in Ponceau S for 2min. After further washing with TBST, blocking of membrane pieces was performed for 1h at RT in either 5% skim milk in TBST or 5% BSA in TBST. Membranes were incubated with primary antibody in 5% skim milk/TBST or 5% BSA/TBST accordingly, overnight at 4° C. For detecting Meis1 protein, the Anti-Meis1 antibody from abcam #ab19867 was used at a concentration of 1:1000 in skim milk, and the anti- Meis1 antibody from Abnova

#H00004211-A01, at a concentration of 1:1000 in skim milk. As a loading ctr, HSP90 antibody (Cell signalling, Cat No. 4874) was used at a working concentration of 1:1000 in BSA. Following primary antibody incubation, membranes were washed 3x for 5min in TBST and secondary antibodies were incubated for 1h at RT. The following secondary antibodies, conjugated with horseradish peroxidase were used: Anti- goat IgG (Donkey, Cat No. 705035147), Anti- mouse IgG (Donkey, Cat No. 715035151), Anti- rabbit IgG (Goat, Cat No. 111035144), all from Jackson Laboratory. After incubation with secondary antibodies, the membrane strips were washed 3x for 5min with TBST and incubated for 1min with WB Detection Reagent (GE Healthcare, Cat No. RPN2232). Membranes were exposed to film (Amersham Hyperfilm ECL, Cat No. 28906837). Films were developed in a WB developing machine and scanned to subsequently quantify the expression of bands on the PC with ImageJ software.

#### 3.3.4 FRET- Camui CR construct cloning

The plasmid pcDNA3-Camui-CR was purchased from Addgene (plasmid number 40256). In order to deliver the FRET construct into hiPSC- derived CMs by Lentivirus, the open reading frames (ORFs) 1 and 2, encoding the FRET protein, were cloned into a lentiviral transfer vector. The lentiviral transfer vector pRRL.sin-18.PPT.PGK.MCS.IRES.GFP.pre (laboratory stock) was used as a cloning backbone. The IRES.GFP encoding sequence was cut out of pRRL.sin-18.PPT.PGK.MCS.IRES.GFP.pre. ORF1 and 2 were cut out of pcDNA3-Camui-CR plasmid and ligated into the backbone of pRRL.sin-18.PPT.PGK.MCS.pre.

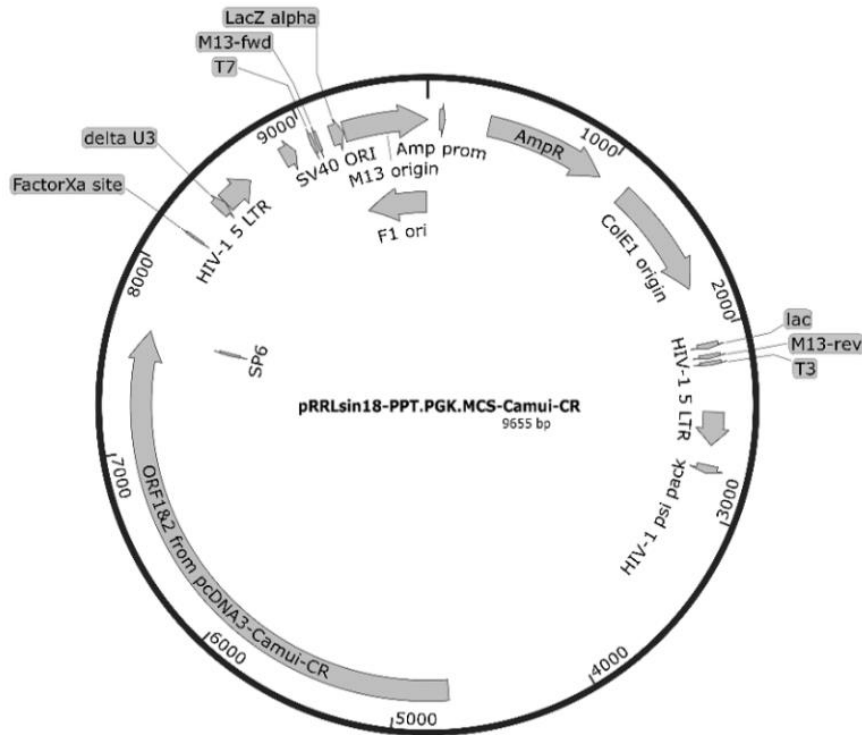


Figure 4: Map of pRRL.sin-18.PPT.PGK.MCS.Camui-CR.pre.

The open reading frames ORF1 and 2 of the Addgene plasmid pcDNA3-Camui-CR were cut out by enzymes SacI and NheI and cloned into the pRRL.sin-18.PPT.PGK.MCS.pre lentiviral transfer vector. Plasmid map shows a selection of restriction enzyme cutting sites. For complete map, see Appendix (7.3).

### 3.3.5 Homologous recombination

#### *Targeting vector cloning*

One approach to correct the patient's mutations in hiPSCs in vitro is by classical homologous recombination. Exon 5 and 6 of *CALMI* was targeted by homologous recombination, using the BAC recombineering system. Cloning steps were performed according to guidelines from Dr. Bellin (Leids Universitair Medisch Centrum) and under supervision of Dr. Pane (AstraZeneka Goteborg). Detailed cloning steps used as guideline can be found on the website of Gene Bridges ([www.genebridges.org](http://www.genebridges.org)). 3 BAC clones were obtained from Empire Genomics, covering the genomic sequences from exon 5 and 6 of the human *CALMI* gene. BAC clones ordered were RP11-471B22 (genomic region 8986901-90047968), RP11-257P13 (genomic region 89909676-90094755) and RP11-99C24 (genomic region 89927463-90094722). Exon 5 and 6 of all three BAC clones were checked for unwanted mutations by Sanger sequencing. Primers are listed under 3.6. BAC clone RP11-471B22 was chosen. As a first step, the neomycin resistance cassette loxP-Pgk-

gb3-Neo-loxP, named NeoR, was cloned into intron 5 of *CALMI* BAC. The plasmid containing the NeoR cassette was kindly provided by Dr. Bellin and used later as a sequence template to clone into intron 5. Bacteria starter cultures were grown from the NeoR plasmid. Intron 5 of the BAC clone was sequenced using primers listed under 3.6. 70 nts long oligos were ordered, designed to anneal to 50 nts of the intronic region of intron 5, followed by 20 nts complementary to the 5' end of the neo cassette. Complementary 70 nts oligos were ordered to reverse complement the 50 nts of intronic region of the *CALMI* gene, followed by 20 nts of the 3' end of the neo cassette sequence. Sequences of these oligos are listed under 3.6. A standard Taq polymerase PCR reaction was performed with the 70 nts oligonucleotides as forward and reverse primer and the bacterial culture containing the NeoR plasmid as DNA template. Annealing temperature was set to 62 °C for 30sec, elongation cycle at 68 °C for 2min. Denaturation, annealing and elongation steps were repeated for 25 cycles. 1.5 kb PCR product was cleaned up by QIAquick PCR Purification, eluted in TE buffer and stored at -20 °C for later use.

The pRedET recombination vector (pSc101-BAD-gbA-tet) obtained from Gene Bridges was amplified by standard bacterial culture and purified. ET vector was first introduced into BAC- containing *E.coli* to render the BAC more prone to perform recombineering. All steps were performed according to the Gene Bridges protocol. BAC containing *E.coli* culture were grown until an OD<sub>600</sub> of approx. 0.4 was reached in 4 tubes containing each 10 ml LB/chloramphenicol. Cells were collected and electroporated with 50 ng Red/ET plasmid in 200 µl 10% glycerol. Electroporation settings were 1.8 kV, 25 µF, 200 Ω resistance, in a 1 mm electroporation cuvette (PeqLab, Cat No. 712010(LE)). Cells were recovered in 1 ml LB without antibiotics, let grown for 30min and plated on Tet/Kana plates over night at 30 °C. Colonies were picked and stocks made. Next, overnight cultures of obtained *E.coli* containing BAC and Red/ET plasmids were grown at 30 °C and collected at an OD<sub>600</sub> of approx. 0.2 in 4 tubes of 10 ml LB/Chloramp/Tet. 0.4% of 10% L-arabinose (Sigma- Aldrich, Cat No. A3256) was added to cultures to induce recombinase expression. When an OD<sub>600</sub> of approx. 0.4 was reached, cells were harvested and electroporated with 500 ng of the NeoR PCR product described in the previous paragraph. The same electroporation settings as before were used. Bacteria were recovered in 1 ml LB, incubated for 2h at 37 °C and streaked on agar plates without Tet. Plates were incubated over night at 37 °C and picked colonies were amplified in starter cultures. Isolated DNA from a selection of clones was sequenced using inNeoF and inNeoR2 primers (sequences listed under 3.6). Clone with inserted Neo cassette within intronic region was

amplified, BAC containing the Neo insert was extracted and stored at -20 °C in sterile H<sub>2</sub>O.

Subsequently, the partial BAC containing exon 5 and 6 and inserted Neo cassette was inserted into the minimal vector. The minimal vector was obtained from Gene Bridges. As a preliminary step, the Red/ET vector was again delivered to E.coli containing the BAC/Neo construct, as described before. Once the E.coli with BAC/Neo construct were successfully electroporated, the minimal vector was delivered by electroporation. Bacteria were first grown until an OD<sub>600</sub> of approx. 0.2, then recombination was induced by incubation with 10% L- arabinose. At an OD<sub>600</sub> of 0.4, bacteria were collected by centrifugation, washed with chilled glycerol and divided into 20 µl of bacterial cells per 10 ml of LB. Cell solution was mixed with 100 ng of minimal vector and electroporated with above mentioned settings. Cells were then recovered in 1 ml LB without antibiotics and subsequently streaked out on agar plates containing ampicillin. 24h later, colonies were picked, DNA was isolated and clones were analysed with Sanger sequencing using the Primer set 2 nd-step-rec forward and reverse (sequences see under 3.6). Clone showing the correct sequence of targeting vector, containing homology arms spanning exon 5 and 6 and Neo resistance selection cassette, was amplified in E.coli and DNA was extracted and stored at 4 °C until further use.

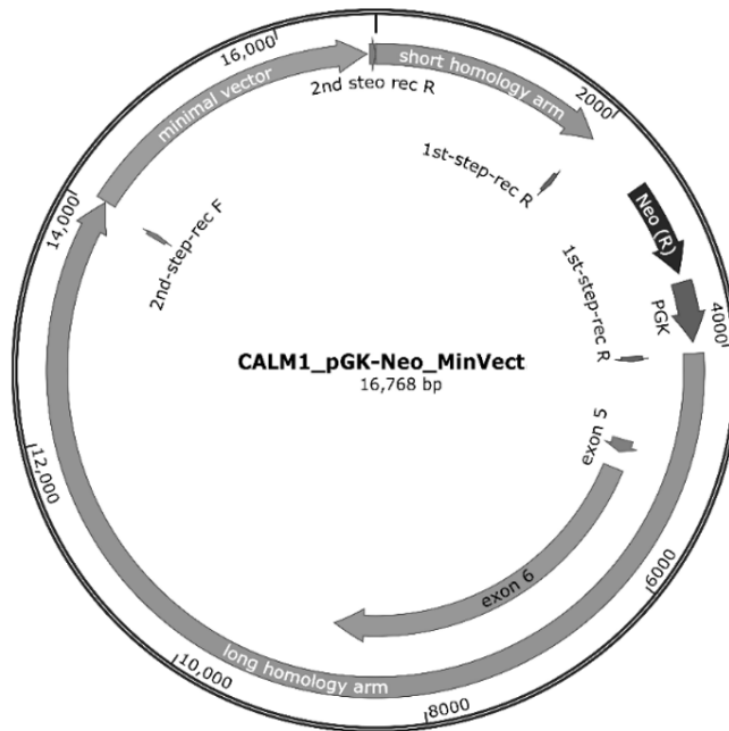


Figure 5: Map of *CALM1*-pGK-Neo-MinimalVector construct.

Minimal vector construct for correction of *CALM* point mutations by homologous recombination. For complete map, see Appendix (7.3).

#### *Delivering of targeting construct*

Correction of *CALM1* point mutation by classical homologous recombination in patient's hiPSCs was performed using the construct described in 3.3.5 and single-cell adapted hiPSCs on Geltrex in E8 medium or on neomycin-resistant MEF feeder cells in hiPS medium. The protocol "Generation of Human Embryonic Stem Cell Reporter Knock-In Lines by Homologous Recombination" from Davis *et al.* was used as guideline<sup>131</sup>. Prior to electroporation, the targeting vector was linearized by incubation with restriction endonucleases. 430  $\mu$ g of the vector were digested in 10x BSA, 10x restriction digestion buffer 4 (New England Biolabs, Cat No. B7004S), 1000 Units NotI HiFi restriction enzyme (New England Biolabs, Cat No. R3189M) and sterile H<sub>2</sub>O in a total volume of 230  $\mu$ l. Reaction mixture was incubated at 37 °C overnight and subsequently heat inactivated at 65 °C for 20min. A small amount of digested plasmid was loaded on a 0.9% Agarose Gel to test for complete linearization before proceeding with precipitation and electroporation. DNA was precipitated by adding 30  $\mu$ l NaAc (3 M, pH 7.4) and 270  $\mu$ l 100% EtOH to the vector in a total volume of 600  $\mu$ l with sterile H<sub>2</sub>O. Samples was mixed, incubated at -20 °C for 30min and spun at maximum speed at 4 °C for 20min. Precipitate was then washed with 700  $\mu$ l 70% EtOH and spun again for 5min before discarding the

supernatant and air-drying the pellet. Linearized Vector was resuspended in 80  $\mu$ l of sterile TE by shaking at 37 °C. Concentration was estimated by Nano Drop from a 1:2 dilution with TE.

Delivery of the linearized plasmid was performed by electroporation. 20  $\mu$ g linearized vector was electroporated on  $10 \times 10^6$  cells. Electroporation was performed at 250 V and 500  $\mu$ F and cells were recovered and distributed on 5x 6 cm cell culture plates pre-seeded with neomycin-resistant MEFs or on Geltrex plates in pre-conditioned medium supplemented with 10  $\mu$ M ROCK inhibitor or 10  $\mu$ M Thiazovivin and 10 ng/ml bFGF. Two days after electroporation, medium was changed to normal hiPS or E8 medium. 4 days after electroporation, antibiotic selection was started by adding 50  $\mu$ g/ml G418 (Life Technologies, Cat No. 11811-023) to hiPS medium without Pen/Strep, or E8 medium without Pen/Strep. Selection was executed for 7 days, with medium change every 24h. Four days into selection, MEF-coated dishes were supplemented with fresh neomycin-resistant MEFs at  $1 \times 10^4$  MEFs/cm<sup>2</sup>. 12 days after electroporation, emerged colonies were picked and screened, as described in chapter 3.3.7.

### 3.3.6 CRISPR/Cas9

#### *CRISPR/ Cas9 correction construct cloning*

To correct the single point mutations in patient's hiPSCs by HDR, the Cas9 protein encoding constructs pCas9\_GFP (Addgene, #44719) and pCas9D10A\_GFP (Addgene, #44720) were purchased. The plasmids were kindly deposited by Kiran Musunuru's Lab. pCas9D10A\_GFP translates into the Cas9 (D10A) mutant Nickase, which is causing single strand DNA breaks as compared to Cas9 translated from Addgene's pCas9\_GFP plasmid, causing DNA double strand breaks (DSB). Both plasmids co-express GFP, connected with a 2A linker motive for optimal co-expression levels. Transcription is driven by a CAG promoter, optimised for expression in hiPSCs. These plasmids are delivered each together with a gRNA expression vector into the hiPSC by either electroporation or nucleoporation.

Later experiments were mainly performed with Cas9 nuclease plasmids. Following methods and results are therefore focussed on Cas9 nuclease.

*gRNA design and gRNA vector cloning*

The gRNA cloning vector #41824 (Addgene), deposited by George Church, was used as the gRNA empty backbone. In order to guide the Cas9 protein sequence- specific to the point of mutation, gRNA sequences were identified, using the online CRISPR design tool (crispr.mit.edu). CRISPR design criteria and experimental setup were chosen according to the stembook protocol by Peters and colleagues<sup>132</sup>. Expressed Cas9 protein and gRNA sequence form a dimer in the nucleus. CRISPR/ Cas9 binding sites were chosen to comply to the sequence G(N)<sub>19</sub>NGG. CRISPR design was executed to perform the DSB as proximal as possible to the site of point mutation. For each patient, one gRNA sequence with least off- target hit score and highest targeting score was chosen to be cloned into the gRNA cloning vector. The targeting score for each guide sequence is determined by subtracting the sum of off- target hit scores in the target genome from 100% on- target activity. Off- target hit scores are computed by total number of mismatches, mismatch absolute position in regard to the PAM site and mean pairwise distance between the calculated mismatches. Only exonic off- targets were considered. More details on the underlying logarithms can be found on the stated website.

The following gRNA sequences were chosen per target mutation:

gRNA name	Score	On target locus	Off- targets	gRNA sequence
F142L corr gRNA	24	chr14:+ 90808976	27	TATATTTGTCTTTTCAGAAT
D130G corr gRNA	82	chr14:+90870836	11	GACGGACAAGTCAACTATGA

Table 5: gRNA sequences for mutation correction approach

Cloning steps to insert gRNA sequences into the gRNA cloning vector were performed in dependence to the gRNA Synthesis Protocol deposited by George Church on the Addgenes' website. Single strand oligonucleotides were ordered from Sigma Aldrich at a synthesis scale of 0.025  $\mu$ mole and HPLC purification. 100 bp oligonucleotides were designed to incorporate the gRNA target sequence as follows:

Forward Oligo: 5' TTTCTTGGCTTTATATATCTTGTGGAAAGGACGAAACACC  
G(N)<sub>19</sub> gtttagagctagaaatagcaagttaaataaggctagtc 3'

Reverse Oligo: 5' gactagccttatttaacttgctatttctagctctaaaac (N)<sub>19</sub>C  
GGTGTTTCGTCCTTTCCACAAGATATATAAAGCCAAGAAA 3'

If the chosen 20 nt gRNA sequence did not start with a guanine (G), an additional G was included before the gRNA targeting sequence to improve annealing capacity. This was the case for the gRNA design for the F142L correction gRNA plasmid. Exact sequences of 100 nt oligonucleotides of the gRNAs can be found in the Primer List (chapter 3.6).

Forward and reverse 100 nt oligonucleotides were resuspended in annealing buffer at a final concentration of 100  $\mu$ M. Annealing buffer was prepared from 39.12 ml sterile H<sub>2</sub>O, 400  $\mu$ l 1 M Tris pH 7.5, 80  $\mu$ l 0.5 M EDTA, 400  $\mu$ l 5 M NaCl and filter sterilized before use. Equal amounts of both oligonucleotides were added to a 1.5 ml tube and incubated at 90 °C for 3min. Tube was then placed at room temperature for at least 45min until cooled below 30 °C. gRNA cloning vector was linearized by incubation at 37 °C for 1h with the restriction enzyme AflII (New England Biolabs, Cat No. R0520S) in NEB buffer 2 supplemented with BSA (New England Biolabs, Cat No. B002S). Annealed 100 nt oligonucleotides and linearized gRNA cloning vector were ligated using the Gibson Assembly Kit (New England Biolabs, Cat No. E5510S). Linearized vector and annealed gRNA inserts were incubated at a 1:5 ratio in 2x Gibson Assembly Master Mix. Total volume was filled up to 20  $\mu$ l with sterile H<sub>2</sub>O and mix was incubated in a thermomixer at 50 °C for 15min. 2  $\mu$ l of assembly reaction were transformed into competent cells, according to standard laboratory protocols. Bacteria were dispersed onto kanamycin-containing agar plates and emerging colonies were picked after 24h incubation at 37 °C. Starter cultures were grown per picked bacterial colony and plasmid DNA was extracted using a standard miniprep kit. A selection of plasmid DNA clones was sequenced to confirm the correct insertion of gRNA into the cloning backbone using the T7 forward sequencing primer (see chapter 3.6). After confirmation of correct product, an endotoxin-free maxiprep was prepared and plasmid was stored in TE buffer at -20 °C until further usage.

#### *CRISPR/ Cas9 all-in one construct cloning*

In order to having to deliver only one plasmid into hiPSCs for CRISPR/ Cas9 experiments, the sequence-specific gRNAs per patient were cloned in frame into the pCas9\_GFP (Addgene, #44719) and pCas9D10A\_GFP (Addgene, #44720). As a first step, the AflII restriction enzyme cutting sites were eliminated in the Cas9-coding sequence. The Cas9 open reading frames were cut out of the original Addgene plasmid using BamHI and XhoI (New England Biolabs, Cat No. R0136S and R0146S) and the excised 1538 bp piece was used in the mutagenesis reaction. The other resulting piece of

7733 bp was cleaned up and stored at 4 °C for later use. Mutagenesis reaction was performed according to manufacturer's guidelines, using the QuickChange II Site-directed Mutagenesis Kit (Agilent Technologies, Cat No. 200521). The piece excised earlier was cloned into the pBluescript- SK(+) (laboratory stock). Transformation was performed and DNA was extracted subsequently. A first round of mutagenesis was performed to remove one AflII restriction enzyme cutting site by exchanging one nt in a silent manner. Oligonucleotide sequences are listed under 3.6. PCR reaction was then transformed into competent bacteria and DNA was extracted by miniprep from 5 picked bacterial colonies. Sequences were confirmed by Sanger sequencing with T3 and T7 standard sequencing primer (see List of Primers, 3.6). One clone was chosen to perform the second round of mutagenesis, using another set of mutagenesis primers, as listed under 3.6. Mutated DNA was transformed once more into competent bacteria, amplified, extracted by miniprep. Mutated Cas9 ORF was ligated back into the Cas9 plasmid backbones.

In order to clone the gRNA sequences into the mutated Cas9 plasmids, plasmids were linearized with MluI (New England Biolabs, Cat No. R0198S) blunted and subsequently digested with SpeI restriction enzyme (New England Biolabs, Cat No. R0133S). The gRNA cloning vector was also digested with SpeI and EcoRV (New England Biolabs, Cat No. R0195S). This piece encodes the gRNA scaffold sequence in frame with the U6 promoter sequence for gRNA expression and was further ligated into the linearized mutated Cas9 plasmids. Transformations into competent bacteria were followed by miniprep to extract amplified DNA. The resulting plasmids were analysed for correct ligation by restriction digestion. Correct plasmids were amplified, endotoxin-free extracted and stored in TE buffer at 4 °C. Genome-editing experiments were mostly performed with the Cas9 nuclease plasmid.

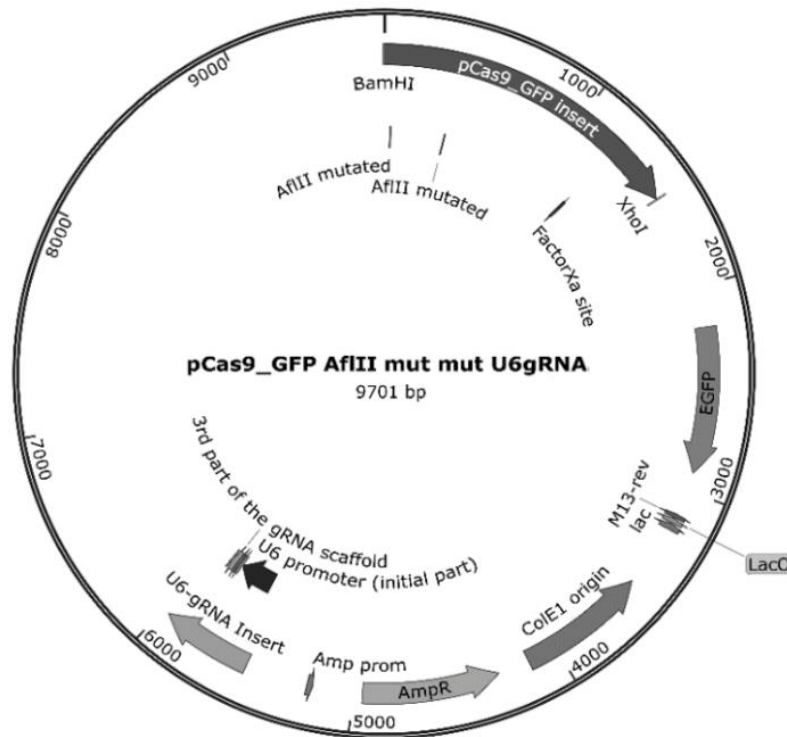


Figure 6: Map of pCas9\_GFP-AflII<sup>mut/mut</sup>-U6-gRNA.

The U6- gRNA ORF was cloned into pCas9\_GFP and pCas9D10A\_GFP. AflII restriction enzyme recognition sites were mutated to allow for later sequence- specific cloning of gRNA sequences. For complete map, see Appendix (7.3).

These above described cloning steps were performed in parallel with Addgene's pCas9\_GFP (Addgene, #44719) and pCas9D10A\_GFP (Addgene, #44720) plasmids. To further clone mutation- specific gRNA sequences into the Cas9 all-in one plasmids, a Gibson Assembly cloning protocol was followed. Patient- specific gRNA oligonucleotides were annealed in annealing buffer at 100  $\mu$ M. pCas9\_GFP-AflII<sup>mut/mut</sup>-U6-gRNA plasmid was linearized using AflII restriction enzyme and gRNA sequences were ligated into the plasmid as described before, using the Gibson Assembly Kit and protocol. Plasmid was transformed into competent bacteria, amplified and DNA was extracted by miniprep. After sequence confirmation by Sanger sequencing, plasmid was amplified at maxiprep scale and stored at 4 °C in TE buffer.

#### *ssODN template oligo design*

To introduce a desired sequence into the genome by HDR, a ssODN was designed and co- delivered into the hiPSCs with the Cas9 and gRNA encoding plasmids. ssODNs were designed to be 200 bp long, with the sequence matching the antisense strand. The non-

homologous nts were located near the centre of the ssODN sequence. In addition, a restriction enzyme cutting site was incorporated into the ssODN design by exchanging a synonymous nt from the original sequence. Importantly, this exchange of nts did not change the aa sequence of the resulting protein. Incorporation of a restriction cutting site allows for fast screening of clones for HDR. 120 bp ssODNs were purchased by Sigma Aldrich as PAGE purified oligos at 0.05  $\mu$ mole synthesis scale. ssODN sequences can be found in the Primer List (3.6).

#### *CRISPR/Cas9 knock- out construct cloning*

To elucidate the effect of *CALMI* mutations and effects of CaM knockouts in hiPSCs and their derived CMs, insertions or deletions in early exons of the *CALMI* gene were inserted. These indels are very likely to disturb the ORF of the gene, causing a knock- out or aberrant protein. The *CALMI* knock- out approach was pursued with the Cas9 encoding plasmid pSpCas9(BB)-2A-Puro (PX459) V2.0 (Addgene, #62988), carrying a puromycin resistance cassette, therefore rendering the cells resistant to puromycin in a transient manner. The pSpCas9(BB)-2A-Puro (PX459) V2.0 plasmid was also used for the *MEISI* knock- out approach. gRNA oligo design and cloning steps for these plasmids are described here as general procedures, regardless of target sequence. gRNA oligo sequences ordered for each target gene are listed in detail under 3.6. This plasmid already encodes the gRNA scaffold and was deposited by Feng Zhang. 19 nt gRNA inserts were ordered as 100  $\mu$ M oligonucleotide to conform the following guidelines:

Forward Oligo: 5' CACCCg(N)<sub>19</sub>

Reverse Oligo: 5' AAAC(N)<sub>19</sub>c

Cloning steps were performed according to the publication of Ran and colleagues<sup>69</sup>.

#### 3.3.7 Colony screening

In order to find genome edited clones in a time efficient manner, a colony screening protocol was established. Depending on the targeted genomic locus and the cell line used for the experiments, different sets of primers were used in the PCR reaction. The colony screening procedures and PCR program were identical for all targets.

Colony screening buffer was supplemented freshly with 200  $\mu$ g/ml RNase A (Qiagen, Cat No. 158922) and 670  $\mu$ g/ml Proteinase K (Sigma, Cat No. P2308). 30  $\mu$ l lysis buffer

was transferred into each tube of a 0.2 ml 8- strip PCR tube (Simport, Cat No. 2013082) and placed on ice. Colonies that were big enough to be separated after puromycin selection, neomycin selection or colonies that have grown to sufficient size after FACS sorting were carefully cut into pieces using a syringe, as described before. Between 1 and 3 pieces of the colony were separated per clone and taken up in 3  $\mu$ l by a P10 pipette. Pieces were carefully transferred into the tube containing lysis buffer. This was performed for each clone separate and with new P10 pipette tips each to exclude cross- contaminations. PCR tubes with cell solution were spun down quickly and incubated at 60 °C for 3h followed by 90 °C for 2min. Lysate was stored at 4 °C for next day usage or kept on ice for immediate prosecution. 4  $\mu$ l of cell lysate was added as input in the colony PCR reaction mix. The Platinum Taq High Fidelity polymerase (Invitrogen, Cat No. 1930962) and its appendant 10x High Fidelity PCR buffer was used in this PCR reaction.

Reagent	Volume [ $\mu$ l]
10x High Fidelity PCR Buffer	2.5
MgSO <sub>4</sub> [50 mM]	1
dNTPs [10 mM]	0.5
Forward Primer [10 $\mu$ M]	0.5
Reverse Primer [10 $\mu$ M]	0.5
Platinum <i>Taq</i> DNA High Fidelity Polymerase [5 U/ $\mu$ l]	0.1
Cell lysis solution	4
Sterile H <sub>2</sub> O	15.9
total	25

Table 6: Colony PCR master mix

A PCR primer pair was designed to amplify a 1025 bp genomic region around the *CALMI*- D130G and -F142L loci. Primers are named RA\_CRISPR\_F and RA\_CRISPR\_R. For each target sequence, positive ctr primer pairs were designed. They amplify a genomic DNA stretch within the *CALMI* gene containing an enzyme digestion site for EcoRV and XmnI. Primer pairs are named PosCtrD130G and PosCtrF142L, listed under 3.6. The primer pairs to amplify the region for *CALMI* knock- out clones were named GeneArt\_Calm\_seq\_F and GeneArt\_Calm\_seq\_R. Primer pairs spanning the region of exon 3 of the *MEIS1* gene to screen for knock- outs were named GeneArt\_MEISKOguide1+4\_F and GeneArtMEISKO\_guide1+4\_R. Primers used for colony

screening of targeted clones by homologous recombination were named ColScrShortFw and ColScrNeoRev. Full sequences of all primer pairs are listed under 3.6.

The following colony PCR program was performed:

Cycle	Time [min]	Temp [°C]	
1	02:00	94	} 35 x
2	00:15	94	
3	00:30	61.1	
4	01:00	68	
5	05:00	68	
6	∞	4	

Table 7: Colony PCR program

To screen clones targeted with the pCas9\_GFP and pCas9D10A\_GFP plasmids and an ssODN template for correction of point mutations, a restriction enzyme digestion step was followed after the colony PCR. An EcoRV restriction site was incorporated into the ssODN for the D130G correction and an s site was integrated in the ssODN used for F142L mutation correction. 5 µl of the colony PCR sample was diluted 1:1 with sterile H<sub>2</sub>O. PCR samples were estimated at 4 ng/µl and an enzymatic digestion reaction volume of 20 µl with appropriate volume enzyme digestion buffer and amount of enzyme was executed according to standard laboratory protocols. Enzymes and appendant reaction buffers were obtained from New England Biolabs (XmnI, Cat No. R0194S). After incubation at 37 °C for 1h, sample was supplemented with 1x loading dye (laboratory stock) and sample was loaded on a 1.5% Agarose Gel. DNA bands were separated for 30min at 240V in parallel with a 2 -log DNA Ladder (New England Biolabs, Cat No. N3200) and bands were visualized and documented with a UV- light documentation system.

Clones retrieved after nucleofection with knock- out CRISPR/Cas9 constructs were screened by Sanger sequencing. For each sample, the 25 µl PCR output was filled up to 100 µl with sterile H<sub>2</sub>O and DNA was purified using the QIAquick PCR Purification Kit (Qiagen, Cat No. 28104). DNA was eluted in 30 µl elution buffer supplied by the kit and concentration was measured by Nanodrop. 80 ng DNA was sent to Eurofins MWG Operon for sequencing. Sequencing primer used for *CALMI* knock- out screening were named Calm\_KO\_seq\_F, primer for knock- out screening at the *MEIS1* locus were named GeneArtMEISKO\_guide1+4\_F. Clones recovered after electroporation with the homologous recombination vector were screened by PCR as described above. Primer pairs de-

signed are annealing only in the genome after homologous recombination occurred, giving no product in clones negative for homologous recombination. After the PCR, product was loaded on a 1.5% Agarose gel, run at 150 V for 30min and bands were visualised as described before and analysed for the correct band at 2 kb size. Positive screened clones were further cultured for several passages and DNA was extracted to analyse the genome by Sanger sequencing.

### 3.3.8 Cleavage detection and TIDE analysis

#### *Cleavage detection analysis*

The GeneArt Genomic Cleavage Detection Kit (Thermo Fisher Scientific, Cat No. A24372) was used to assess the efficiency of designed gRNAs for locus specific cleavage and to determine the efficiency of cloned all-in one constructs compared to the 2 plasmids strategy. Primers designed to amplify the locus being investigated can be found in the List of Primers (3.6). For cleavage detection analysis, transfection of 80% confluent hiP-SCs plates with the plasmids and gRNAs to be investigated were performed, as described in 0. Cells were collected 24h after transfection and lysed according to the manufacturer's guidelines. Cleavage Detection analysis was performed according to the manufacturer's guidelines.

#### *TIDE analysis*

Colonies analysed by Sanger sequencing that showed genomic aberrations compared to wild-type (wt) ctr sequences were analysed further with the online accessible sequence decomposition tool TIDE. The tool is available online as free web tool in a restricted version at [www.tide.nki.nl](http://www.tide.nki.nl) and was developed by scientists from the Netherlands Cancer Institute. Sequencing files in the .ab1 format were uploaded together with a wt ctr sequence and the 20 nt gRNA sequence used for the gene editing experiment. Default settings of TIDE were applied to calculate the editing efficiency in a quantitative manner, as well as to determine the prevailing indels of the targeted sequence. The left boundary of the alignment window was set to 100 bp, the right boundary was set automatically at -10 bp from the break site. The decomposition window was set from 15 bp downstream of the break site to 15 bp before the end of the shortest sequence read. The indel size range was set to 10 bp and p-value threshold was set to  $p < 0.001$ . Analysed knock-out clones showing the highest targeting efficiency and indels causing most likely a premature stop

codon in the coding sequence were further propagated and analysed for downstream effects.

### 3.4 Imaging techniques

#### 3.4.1 Colourimetric detection

##### *Alkaline phosphatase detection in hiPSCs*

Direct alkaline phosphatase activity was analysed on hiPSC clones as an early measure of pluripotency. hiPSC plates were washed once with PBS<sup>Ca<sup>2+</sup>/Mg<sup>2+</sup></sup> for 3min and fixed in 3.7% (vol/vol) formaldehyde (Sigma Aldrich, Cat No. F8775) in PBS<sup>Ca<sup>2+</sup>/Mg<sup>2+</sup></sup> for 5min at RT. Plates were then washed again 3 times with PBS<sup>Ca<sup>2+</sup>/Mg<sup>2+</sup></sup> for 3min each and washed subsequently once with distilled water. 200 µl NBT/BCIP alkaline phosphatase blue stock solution (Roche, Cat No. 11681451001) was diluted in 10 ml reagent buffer (0.1 M Tris-HCl pH 9.5, 0.1 M NaCl, and 0.05 M MgCl<sub>2</sub>) and incubated on plates for 10-15min at RT. Reaction was stopped by removing reagent and washing plates 3 times with PBS<sup>Ca<sup>2+</sup>/Mg<sup>2+</sup></sup>. Microscopy was performed using imaging systems (DMI6000-AF6000), filter cubes and software from Leica microsystems. Level and evenly distribution of blue staining was used as a measure of pluripotency state of clones.

#### 3.4.2 Fluorescent detection

##### *Immunofluorescent staining of hiPSCs and hiPSC- CMs*

hiPSC plates and dissociated hiPSC- derived CMs were washed once with PBS<sup>Ca<sup>2+</sup>/Mg<sup>2+</sup></sup> for 3min before fixation. Fixation of cells was performed with 3.7% (vol/vol) formaldehyde in PBS<sup>Ca<sup>2+</sup>/Mg<sup>2+</sup></sup> for 15min at RT. Plates were washed 3x with PBS<sup>Ca<sup>2+</sup>/Mg<sup>2+</sup></sup> for 5min. Following washing, cells were permeabilised and blocked in 0.1% Triton X-100 (Sigma Aldrich, Cat No. 93443) with 10% goat serum (Invitrogen, Cat No. PCN5000) in PBS<sup>Ca<sup>2+</sup>/Mg<sup>2+</sup></sup> for 1h at 37 °C. 1- 10 µg/ml primary antibody was incubated for 1- 2h at 37 °C or overnight at 4 °C in 0.1% Triton with 1% goat serum in PBS<sup>Ca<sup>2+</sup>/Mg<sup>2+</sup></sup>. For pluripotency staining, the following primary antibodies were used: human Nanog (rabbit polyclonal, Abcam, Cat No. ab21624, 1:500), TRA1-81-Alexa-Fluor-488-conjugated (mouse monoclonal, BD Pharmingen, Cat No. 560174, 1:20). For CM staining cardiac troponin T (cTNT) (mouse monoclonal clone 13-11, Thermo Scientific, Cat No. MS-295, 1:300) and

$\alpha$ -actinin (mouse monoclonal clone EA-53, Sigma-Aldrich, Cat No. A7811, 1:300) were used. For Sendai virus staining, anti- Sendai virus (rabbit polyclonal, MBL, Cat No. MBL-PD029, 1:1000) was used. After primary antibody incubation, plates were washed 5x for 3min with PBS  $Ca^{2+}/Mg^{2+}$  supplemented with 0.1% Triton. Secondary antibodies were suspended in 0.1% Triton with 1% goat serum in PBS  $Ca^{2+}/Mg^{2+}$  and incubated for 1h at 37 °C. The following secondary antibodies were used specific to appropriate species: Alexa-Fluor-488, -594 and -647 (Life Technologies, 1:500). Cell Nuclei were detected with 1  $\mu$ g/ml Hoechst 33258 (Invitrogen, Cat No. H3569). Following secondary antibody incubation, samples were washed 5x for 3min with 0.1% Triton in PBS  $Ca^{2+}/Mg^{2+}$  and samples were mounted with Dako fluorescence mounting medium (Dako, Cat No. S3023) for preservation. Samples were left in the dark at RT to dry for 24h and kept at 4 °C for short-term storage. Microscopy was performed using imaging systems (DMI6000-AF6000), filter cubes and software from Leica microsystems.

#### *EdU and cTNT FACS staining*

To measure percentage of cells in mixed cell populations that are CMs and proliferative, a co-staining of differentiated cells for cTNT and EdU was performed. The minimum of cells used per sample was 1 well of a 12- well plate. To detect proliferation in cells, 10 mM EdU solution was added to wells for 24h before cells were harvested and lysed for cTNT staining and fixation. The Click-iT EdU Alexa Fluor 488 Flow Cytometry Assay Kit (Invitrogen, Cat No. C10425). After incubation with EdU, cells were harvested using Collagenase solution (see 3.2.5) for 3x 15min at 37 °C and collected. Samples were washed once with 3 mL of 1% BSA, centrifuged at 300 rcf for 5min and supernatant was discarded. Pellets were resuspended in 100  $\mu$ l of Fixative D and incubated for 15min at RT in the dark. Samples were washed afterwards with 1% BSA solution and afterwards resuspended in 100  $\mu$ l Washing and Fixative Solution E. Incubation was performed for 15min at RT. Click iT Reaction cocktail was prepared according to the manual and 500  $\mu$ l was added per sample. Solution was then mixed for 30min at RT on a shaker protected from light. Samples were subsequently washed again with 3 ml washing reagent and blocked in 10% FBS in 0.1% Saponin/ PBS  $Ca^{2+}/Mg^{2+}$  solution for 1h at RT. Primary cTNT antibody (mouse monoclonal clone 13-11, Thermo Scientific, Cat No. MS-295, 1:300) was diluted 1:500 in 1% FBS in 0.1% Saponin/ PBS  $Ca^{2+}/Mg^{2+}$  solution and incubated at RT for 1h. Samples were washed once more and incubation with anti- mouse secondary antibody Alexa-Fluor -647 (Life Technologies, 1:500) was performed on RT for 1h. Cells

were washed subsequently with 0.1% Saponin/ PBS  $\text{Ca}^{2+}/\text{Mg}^{2+}$  solution and pellet was re-suspended in 150  $\mu\text{l}$  0.1% Saponin/ PBS  $\text{Ca}^{2+}/\text{Mg}^{2+}$  solution and filtered by adding an additional 150  $\mu\text{l}$  of solution. Samples were analysed in a Flow Cytometer machine from Beckman Coulter according to standard FACS protocols and analysed using the Kaluza Flow Cytometry Analysis software.

#### *CaMKII activity measurement*

In order to see differences in *CaMKII* activation status between hiPSC- derived CMs from patient and ctr cell lines, 2.5 months old CM explants were infected with lentivirus delivering the FRET- based biosensor Camui- CR. CMs were dissociated and 1- 1.5 explants per well were distributed in a 384- well assay microplate (Corning, Cat No. 3712) pre-coated with fibronectin, in EB2 medium. For infecting, virus- solution and EB2 media were mixed in a 1:1 ratio and supplemented with 8  $\mu\text{g}$  polybrene (Polybrene Hexadimethrine Bromide, Sigma, Cat No. H9268). 80  $\mu\text{l}$  infection solution was added per well and incubated overnight (37 °C, 5%  $\text{CO}_2$ ). 24h after infection, 20  $\mu\text{l}$  fresh EB2 media was added to the wells. 2 days after infection, medium was changed to fresh 100  $\mu\text{l}$  EB2 per well. On day 5, 100  $\mu\text{l}$  fresh clear EB2 media (made from DMEM/F-12 without phenol red, Invitrogen, Cat No. 21041-025) was added per well. Measuring of FRET activity was performed from day 7 until day 9 of infection with medium change every 48h. FRET activity measurement was recorded with an epifluorescence microscope equipped with an image splitter (Optosplit II, Cairn Re-search, Faversham, UK) in the emission pathway. A dual band excitation filter for 425-500 nm and 550-575 nm was combined with a dichroic mirror for 500-550 nm and 600-680 nm wavelength as filter sets. The Optosplit device used has a bandpass of 520/28 nm, a beam splitter of 568 nm and a bandpass of 630/75 nm. Recordings were made with a Zyla-V sCMOS camera (Andor, Belfast, UK). The RFP to GFP fluorescence ratio was calculated after correcting for background signals.

### 3.5 Electrophysiological measurements

Electrophysiological measurements on *CALMI* patient CMs were performed by M. Rochetti and colleagues at the Dipartimento di Biotecnologie e Bioscienze at the Università degli Studi di Milano – Bicocca. Electrophysiological methods are outlined in short and can be found elaborately described in the appurtenant publication <sup>133</sup>.

*I<sub>CaL</sub> biophysical measurements*

CMs derived from hiPSC of patients carrying mutations in the *CALM1* gene were voltage-clamped in whole-cell configuration to measure  $I_{CaL}$  and  $I_{BaL}$ . Measurements were performed at RT and according to standard protocols. TTX (Tocris, Cat No. 1078) was used at a concentration of 10  $\mu$ M to prevent falsification of measurements by  $Ca^{2+}$  ions flowing through  $Na^+$  channels. For  $I_{BaL}$  measurements,  $Ba^{2+}$  was used at some concentrations, replacing  $Ca^{2+}$  ions. Measurements were obtained with a MultiClamp 700B amplifier and a Digidata 1440A (both Molecular Devices). A pClamp 10.4 filter (Molecular Devices) at 2 kHz was used for filtering.  $I_{CaL}$  I/V relations were obtained and steady-state activation curves were derived by measuring the peak current at 30 ms at different test potentials. Steady-state inactivation curves at 2 s voltage steps from -50 to 0 mV and by normalizing to the maximal current. Half activation and inactivation and slope were determined by Boltzmann equation to estimate activation and inactivation curves.  $I_{CaLw}$  was calculated by the overlap of area under activation and inactivation curve and quantified.

CDI was estimated by measuring remaining currents at r100 and r300 for  $Ca^{2+}$  and  $Ba^{2+}$  at equimolar concentrations. CDF was evaluated by increasing the pacing from 0.05 Hz to 1 Hz abruptly. Conventional paired pulse ctr was used for measuring the time course of recovery from inactivation of  $I_{CaL}$ . Current amplitudes were normalized to  $C_m$  to calibrate for variations in cell size. Rat adult CMs were used as positive ctr for CDF measurements as previously described<sup>134</sup>.

*Electrical activity measurements*

Field potentials (FP) were recorded with a 256-electrode MEA (Multi Channel Systems) from spontaneously beating clusters. MEA chambers were previously coated with Matrigel and clusters were plated in EB2 medium. Data was analysed with MC Rack, MC Data Tool (Multi Channel Systems) and pClamp suite (Molecular Devices). FPD was measured as a means of electrocardiographic interval, according to standard protocols. FPDc were calculated by Bazett's correction. APs were recorded at rates of 0.5 to 3 Hz in whole-cell clamped CMs and with standard Tyrode's solution at 36 °C. To circumvent non-physiological APs due to low expressed  $I_{K1}$  in hiPSC-CM, a human  $I_{K1}$  numerical dynamic clamp model was used. The  $I_{K1}$  model was applied using the Real-Time eXperiment Interface v1.0 (RTXI) with the Ubuntu 10.04 LTS software and an A/D converter (BNC-2120, National Instruments, Austin, TX, USA). AP rate-dependency was analysed under DC and native conditions.

### *Twitch measurements*

A Video Edge detection System paired to a Multiclamp 700B Amplifier and Digidata 1440A was used for recording spontaneous contractions on beating clusters.

### *Intracellular Ca<sup>2+</sup> measurements*

Experiments were performed by Dr. Rochetti and her colleagues in collaboration<sup>133</sup>. Tyrode's solution was composed of 2 mM 4-AP and 1 mM BaCl<sub>2</sub>. Pipette solutions consisted of 110 mM K-aspartate, 23 mM KCl, 3 mM MgCl<sub>2</sub>, 0.2 mM CaCl<sub>2</sub>, 5 mM HEPES-KOH, 0.5 mM EGTA-KOH, 5 mM ATP Na<sup>+</sup>-salt, 5 mM phosphocreatine Na<sup>+</sup> salt and 0.4 mM GTP Na<sup>+</sup> salt at pH 7.3. Intracellular Ca<sup>2+</sup> measurements were performed under physiological conditions. Fluo-4 AM (Life Technologies, Cat No. F14201) at a concentration of 10 μM was loaded into CM for Ca<sup>2+</sup> and measured after 1h incubation of Fluo-4 AM at RT. Prior to measuring, CM were washed for 10min for de-esterification. Excitation was performed at 488 nm and emission was measured at 535 nm with a band-pass filter. Signal was low-pass filtered at 200 Hz and 100Hz and subsequently digitalized at 2kHz. CM were voltage-clamped for Ca<sup>2+</sup> recordings for every 5sec from -50 mV to 0 mV to estimate cell membrane potential. Background luminescence was subtracted and signal was normalised, using diastolic fluorescence. The SR Ca<sup>2+</sup> content was estimated by superfusion with 10mM caffeine and CICR gain was calculated according to standard protocols and can be read in more detail in the publication of Rochetti and colleagues<sup>133</sup>. I<sub>NCX</sub> was recorded during caffeine superfusion and quantified, NCX function was analysed using the I<sub>NCX</sub> density during caffeine pulses and by plotting it as a function of Ca<sup>2+</sup>. Diastolic Ca<sup>2+</sup> was assessed at 80 mV, with the resting fluorescence level after caffeine superfusion as reference.

### 3.6 List of Oligonucleotides

Table adapted from Rocchetti *et al.*<sup>133</sup>.

Gene/Name of Oligo	Use	Sequence 5' - 3'	
CALM1	Sequencing	For	TGTATTTAGTAGGTTAGAGGTGGG
		Rev	TTGTGTGTGTGGACAGAAGG
Sendai Virus	RT PCR	For	GGATCACTAGGTGATATCGAGC
		Rev	ACCAGACAAGAGTTTAAGAGATATGTATC
SOX2 trans	RT PCR	For	ATGCACCGCTACGACGTGAGCGC
		Rev	AATGTATCGAAGGTGCTCAA
KLF4 trans	RT PCR	For	TTCCTGCATGCCAGAGGAGCCC
		Rev	AATGTATCGAAGGTGCTCAA
cMYC trans	RT PCR	For	TAAGTACTAGCAGGCTTGTCG
		Rev	AATGTATCGAAGGTGCTCAA
OCT4 trans	RT PCR	For	CCCGAAAGAGAAAGCGAACCAG
		Rev	AATGTATCGAAGGTGCTCAA
GAPDH	qRT PCR	For	TCCTCTGACTTCAACAGCGA
		Rev	GGGTCTTACTCCTTGGAGGC
c-MYC endo	qRT PCR	For	AGAAATGTCCTGAGCAATCACC
		Rev	AAGGTTGTGAGGTTGCATTTGA
KLF4 endo	qRT PCR	For	ATAGCCTAAATGATGGTGCTTGG
		Rev	AACTTTGGCTTCCTTGTGTTGG
OCT4 endo	qRT PCR	For	GACAGGGGGAGGGGAGGAGCTAGG
		Rev	CTTCCCTCCAACCAGTTGCCCAAAC
SOX2 endo	qRT PCR	For	GGGAAATGGGAGGGGTGCAAAGAGG
		Rev	TTGCGTGAGTGTGGATGGGATTGGTG
NANOG	qRT PCR	For	TGCAAGAACTCTCCAACATCCT
		Rev	ATTGCTATTCTTCGGCCAGTT
REX1	qRT PCR	For	ACCAGCACACTAGGCAAACC
		Rev	TTCTGTTACACAGGCTCCA
TDGF1	qRT PCR	For	CCCAAGAAGTGTTCCTGTG
		Rev	ACGTGCAGACGGTGGTAGTT
PDX1	qRT PCR	For	AAGCTCACGCGTGGAAG
		Rev	GGCCGTGAGATGTACTTGTTG

SOX7	qRT PCR	For	TGAACGCCTTCATGGTTTG
		Rev	AGCGCCTTCCACGACTTT
AFP	qRT PCR	For	GTGCCAAGCTCAGGGTGTAG
		Rev	CAGCCTCAAGTTGTTCTCTG
CD31	qRT PCR	For	ATGCCGTGGAAAGCAGATAC
		Rev	CTGTTCTTCTCGGAACATGGA
DES	qRT PCR	For	GTGAAGATGGCCCTGGATGT
		Rev	TGGTTTCTCGGAAGTTGAGG
ACTA2	qRT PCR	For	GTGATCACCATCGGAAATGAA
		Rev	TCATGATGCTGTTGTAGGTGGT
SCL	qRT PCR	For	CCAACAATCGAGTGAAGAGGA
		Rev	CCGGCTGTTGGTGAAGATAC
MYL2	qRT PCR	For	TACGTTCCGGAAATGCTGAC
		Rev	TTCTCCGTGGGTGATGATG
KRT14	qRT PCR	For	CACCTCTCCTCCTCCAGTT
		Rev	ATGACCTTGGTGCGGATTT
NCAM1	qRT PCR	For	CAGATGGGAGAGGATGGAAA
		Rev	CAGACGGGAGCCTGATCTCT
TH	qRT PCR	For	TGTAAGGTTTACGGTGGAGT
		Rev	TCTCAGGCTCCTCAGACAGG
GABRR2	qRT PCR	For	CTGTGCCTGCCAGAGTTTCA
		Rev	ACGGCCTTGACGTAGGAGA
SCN5A	qRT PCR	For	GAGCTCTGTCACGATTTGAGG
		Rev	GAAGATGAGGCAGACGAGGA
KCNQ1	qRT PCR	For	CGCCTGAACCGAGTAGAAGA
		Rev	TGAAGCATGTCCGGTGTGA
CACNA1C	qRT PCR	For	CAATCTCCGAAGAGGGGTTT
		Rev	TCGCTTCAGACATTCCAGGT
RYR2	qRT PCR	For	GCTATTCTGCACACGGTCATT
		Rev	ATTTCCGTGCCACTTCCCTTT
SERCA	qRT PCR	For	ACAATGGCGCTCTCTGTTCT
		Rev	ATCCTCAGCAAGGACTGGTTT
PLN	qRT PCR	For	TCCATAAACTGGGTGACAGA
		Rev	TGATACCAGCAGGACAGGAA
SLC8A1	qRT PCR	For	GAGACCTGGCTTCCCACTTT

		Rev	ATTCCCAGGAAGACATTACC
PMCA4	qRT PCR	For	TTTATCGCCCTGCTGGTGAAG
		Rev	TCACTGAGAAAAGGATGGCTGC
D130G correction gRNA	To clone into #41824	For	TTTCTTGGCTTTATATATCTTGTGGAAAGGACG AAACACCGACGGACAAGTCAACTATGAGTTTT AGAGCTAGAAATAGCAAGTAAAATAAGGCTA GTC
		Rev	GACTAGCCTATTTTAACTTGCTATTTCTAGCT CTAAACTCATAGTTGACTTGTCCGTCGGTGTT TCGTCCTTTCCACAAGATATATAAAGCCAAGA AA
F142L correction gRNA	To clone into #41824	For	TTTCTTGGCTTTATATATCTTGTGGAAAGGACG AAACACCGTATATTTGTCTTTTCAGAATGTTTT AGAGCTAGAAATAGCAAGTAAAATAAGGCTA GTC
		Rev	AAAGAACCGAAATATATAGAACACCTTTCCTG CTTTGTGGCATATAAACAGAAAAGTCTTACAA AATCTCGATCTTTATCGTTCAATTTTATTCCGA TCAG
120 bp ssODN D130G correction	HDR template D130G correction	For	CAAACCTTAGGAGAAAACTAACAGATGAAGA AGTAGATGAAATGATCAGAGAAGCAGATATCG ATGGAGACGGACAAGTCAACTATGAAGGTAA AACTAAATTCTCTGAGCTCAGTGTTT
120 bp ssODN F142L correction	HDR template F142L correction	For	CATTAAAGCTGTTTTCAAAGATAACCAAAGT TACTATTATATTGTCTTTTCAGAATTCGTTCA GATGATGACTGCAAATGAAGACCTACTTCA ACTCCTTTTTCCCCCTCTAGAA
F142L correction gRNA	To clone into #62988	For	CACCGTATATTTGTCTTTTCAGAAT
		Rev	AAACATTCTGAAAAGACAAATATAC
D130G correction gRNA	To clone into #62988	For	CACCGACGGACAAGTCAACTATGA
		Rev	AAACTCATAGTTGACTTGTCCGTCC
CALM KO guide 1	To clone into #62988	For	CACCGCTGACCGAAGAACAGATTG
		Rev	AAACGCAATCTGTTCTTCGGTCAGC
CALM KO guide 2	To clone into #62988	For	CACCGCTTACCAGCAATCTGTTCTT
		Rev	AAACAAGAACAGATTGCTGGTAAGC
MEIS1 KO guide 70	To clone into #62988	For	CACCGTACTTGTACCCCCGCG
		Rev	AAACCGCGGGGGGTACAAGTAC
U6_FW	Sequencing	For	GACTATCATATGCTTACCGT
T3_FW	Sequencing	For	GCAATTAACCCTCACTAAAGG
T7_FW	Sequencing	For	TAATACGACTCACTATAGGG
AfIII_FI/2	Mutagenesis PCR	For	CCTGGATTTTCTAAAGTGCGATGGATTTGCCAA C
AfIII_RI/2		Rev	GTTGGCAAATCCATCGCACTTTAGAAAATCCA GG
AfIII_FII/2	Mutagenesis PCR	For	GGGGTCCCAAATCCTCAAGGAACACCCAG
AfIII_RII/2		Rev	CTGGGTGTTCTTGAGGATTTGGGACCCC
RA_CRISPR_F		For	CTAAGTATGGCTTCTTCCGC

RA_CRISPR_R	Restriction analysis correction	Rev	TGGCCAGCCCAAACAGTGTA
PosCtrD130G_F	Positive ctr restriction analysis correction D130G	For	CCACCATGCCGAGCAAGTAA
PosCtrD130G_R		Rev	ATTTCACTGGCTGGGAGCG
PosCtrF142L_F	Positive ctr restriction analysis correction F142L	For	TGTGTATTGTGACTGGGTTGG
PosCtrF142L_R		Rev	ATGACAGACCGCTATCAGGG
CALM1 Exon2 KO seq FW	Sequencing <i>CALM1</i> Exon 2	For	TTCATTAATGACCGTGCTACAGG
CALM1 Exon2 KO seq RV		Rev	TGCCTAGTTCTGGCCTTCTG
GeneArt_Calm_seq_F	Colony Screening <i>CALM1</i> KO, Cleavage Detection	For	CCCCACACTACATCATTAGCAA
GeneArt_Calm_seq_R		Rev	GTGTGTGTGGACAGAAGGTACT
GeneArt_MEISKO guide1+4_F	Colony Screening <i>MEIS1</i> KO, Cleavage Detection	For	TTTCTCCGGCCAGATACGCTAAAC
GeneArt_MEISKO guide1+4_R		Rev	TAAGGCCGACTACGTGCTG
MEIS KO Off-target FW	Off- target sequencing MEIS KO gRNA1	For	GCCAGCCTGCCTATTCACATCAAG
MEIS KO Off-target RV		Rev	CATGGAGTTTGGTGTCTCG
MEIS KO gRNA 1	To clone into #62988, knock- out	For	CACCGTACTTGTACCCCCGCG
		Rev	AAACCGCGGGGGGTACAAGTAC
MEIS KO gRNA 2	To clone into #62988, knock- out	For	CACCGTACGACGATCTACCCA
		Rev	AAACTGGGGTAGATCGTCGTAC
MEIS KO gRNA 3	To clone into #62988, knock- out	For	CACCGCACAGCTCATACCAACG
		Rev	AAACCGTTGGTATGAGCTGTGC
MEIS KO gRNA 4	To clone into #62988, knock- out	For	CACCGTATAGCCGTGTTCCGCA
		Rev	AAACTGGCGAACACGGCTATAC
Calm1Ex5F	BAC <i>CALM1</i> Exon 5 sequencing	For	GAGGTGGGAAGTAGAGATCA
Calm1Ex5R1		Rev	AAGTCAAAGGCTGTCTAGTG
Calm1Ex5R2		Rev	GTCAAAGGCTGTCTAGTG
Calm1Ex6F1	BAC <i>CALM1</i> Exon 6 sequencing	For	CTCCTTTGGCAGTGACTAGA
Calm1Ex6F2		For	GGATGGTCCTCTTGTACTTC
Calm1Ex6R2		Rev	GAAGTACAAGAGGACCATCC
Calm1Ex6F3		For	CCCACCTTTCTCTCAAGCATG
Calm1Ex6R3		Rev	CATGCTTGAGAGAAAGTGGG

Calm1Ex6F4		For	CAGCCAAATGGGTGCATTCA
Calm1Ex6R4		Rev	TGAATGCACCCATTTGGCTG
Calm1Ex6F5		For	GAGAGGAAATAGCTGGGTGT
Calm1Ex6R5		Rev	ACACCCAGCTATTTCTCTC
Calm1Ex6F6		For	CTCCTTTGGCAGTGA TAGA
Calm1Ex6R6		Rev	TCTAGTCACTGCCAAAGGAG
Calm1Ex6R7		Rev	GTCTACGGTTATTTCTGGCC
inNeoF	Intron 5 sequencing	For	CCATGCATGGCATAACAG
inNeoR1		Rev	GATTCAAGCCCATGGAAG
inNeoR2		Rev	CATCAGTGCCCAGGATAGTA
1st-step-rec-F	Sequencing for recombination event 1	For	AGGCAGAGTGAGACCTGAGTGATTTCCCTAAC TCAGGGATGGCAGTCGGGCACTCAGTGATATC GATGGATGC
1st-step-rec-R		Rev	ATACACCACTCCGCAGGCTGAATCTTCCACTC CGAGGGAAGAAAGCGCCAGCTCGGCGCGCCA TAACTTC
2 nd-step-rec-F	Sequencing for recombination event 2	For	GACTACCTGTTAGATCATAGGGTAAATCTCAA CAACTACTTTAAAAATCCGCGGCCGCGCTCTC CTGAGTAGGACAAAATC
2 nd-step-rec-R		Rev	TCTATTTTAATTGTCAATGGCCCTGGGGCAACC ACAGAAAGGATCTTTCGTCGACTCACAGCTT GTCTGTAAGCGGATG
CALM1T1	qRT PCR	For	TGGCATCCTGCTTTAGCCTG
		Rev	CCATTTGCCTCGCTCAACAC
CALM1T2	qRT PCR	For	GAGAAATCCACGTTAGCTCTCCTT
		Rev	CCTGCATTATTTGGTCTCCACTGA
CALM1T3	qRT PCR	For	ATTGCCAGATGCGACTGTGC
		Rev	AGGCTTCCTTGAATTCAGCAATC
CALM1T4	qRT PCR	For	ATAGCGCACAGCGGCCTT
		Rev	TGATCAGCCTCCGATGCCGCT
CALM2T1	qRT PCR	For	CTCGTTTGGGATGTTCCGTTAT
		Rev	AGCGCCTCATAAACACCTCC
CALM2T2	qRT PCR	For	TGAAGAGCAGATTGCAGACGGA
		Rev	ATGCTACTGCACTCCAGCCT
CALM2T3	qRT PCR	For	GCAGCATGGTTAGCTTTG
		Rev	GAATTCTGCAATCTGCTC
CALM3T1	qRT PCR	For	CCGGGCAATATTGTGTTCA GTT
		Rev	GAGGAGCCAAATCAGGTAGT
CALM3T2	qRT PCR	For	AGGAGGAGGAGGGAAGAACG
		Rev	ACTCTGCAATCTGCTCCTCA

CALM3T3	qRT PCR	For	GAAAAGGGATGGCTGACC
		Rev	TTGGTGGTGATAGTGCCATC
CALM3T4	qRT PCR	For	GCGGCGAGGGAAAGTAGT
		Rev	AGTCAGCTGGTCAGCCTA
CALM3T5	qRT PCR	For	ACAGTGATGAGATCCCTGG
		Rev	GATCATCTCATCCACCTCATT
CALM3T6	qRT PCR	For	TGGAAGCTGCTGCAGCTGCT
		Rev	TTGAAGCTCATGGCGAGGC
CALM3T7	qRT PCR	For	AGGAACCTTGATCCCCGT
		Rev	AGAAGGCCTCCTGCAATCT
ColScrShortFw	Colony Screening HR	For	CCCGTGATATTGCTGAAGAGCT
ColScrNeoRev		Rev	TCATGAGGTCACTGGGTCAGAA
PosCtrHomRecFW	Positive ctr colony screening	For	GACCCAGCAAGTAGAGAATG
PosCtrHomRecRV		Rev	GAAATGTATAGCCTTGGCCG
Nterm MEIS	qRT PCR	For	CGACGATCTACCCATTACG
		Rev	GTATGAGCTGTGTGCGGGTA
Cterm MEIS	qRT PCR	For	ATGACACGGCATCTACTCGTTC
		Rev	TGTCCAAGCCATCACCTTGCT
KO MEIS	qRT PCR	For	ACCCCTCTTCCCTCTCTTA
		Rev	GTTTTTCTGCGGAATCTGT
BRY	qRT PCR	For	TGTTTATCCATGCTGCAATCC
		Rev	CCGTTGCTCACAGACCACAG
MESP1	qRT PCR	For	GTGCTGGCTCTGTTGGAGA
		Rev	CAGAGACGGCGTCAGTTGT
ISL1	qRT PCR	For	AAAGTTACCAGCCACCTTGGA
		Rev	ATTAGAGCCCGGTCCTCCTT
NKX2.5	qRT PCR	For	CAAGTGTGCGTCTGCCTTT
		Rev	TTGTCCGCCTCTGTCTTCTC

Table 8: List of Oligonucleotides

## IV. Results

### 4.1 Generation and characterization of hiPSCs from patients carrying *CALMI* mutations

#### 4.1.1 Generation of *CALMI*- hiPSCs by reprogramming of patient dermal fibroblasts

##### *Reprogramming*

Somatic skin fibroblasts from 2 unrelated infants, carrying mutations in the *CALMI* gene at aa residues 130 and 142 were obtained by biopsy. Fibroblasts were cultured for 2 days in fibroblast growth medium, until approximately 80% confluent and subsequently transduced with the SeV reprogramming kit, as described in 3.2.2. Infected fibroblasts were observed closely with phase contrast (PH) microscope. 3 days after infection, cell death of few cells was observed. Attached cells resembled fibroblast morphologies and continued to proliferate. 5 days post- infection,  $5 \times 10^5$  infected fibroblasts were transferred onto 10 cm MEF- coated cell culture dishes and henceforward kept in hiPS medium with bFGF. From day 8 onwards, cells began to appear in a rounder shape. Small groups of cells were observed, most likely resulting from cell division. Cells continued to grow clonally, with colonies reaching an average diameter of 0.5 mm on day 13 post- infection. Colonies grew in a round shape with clear edges, with cells appearing homogenous and closely attached to another. 23 days post- infection, colonies reached around 2.5 mm diameter in size and were picked manually. Differentiated regions of colonies were removed from undifferentiated areas and discarded. hiPSC clones were propagated further separately from each other on MEF- coated cell culture dishes in hiPS medium.

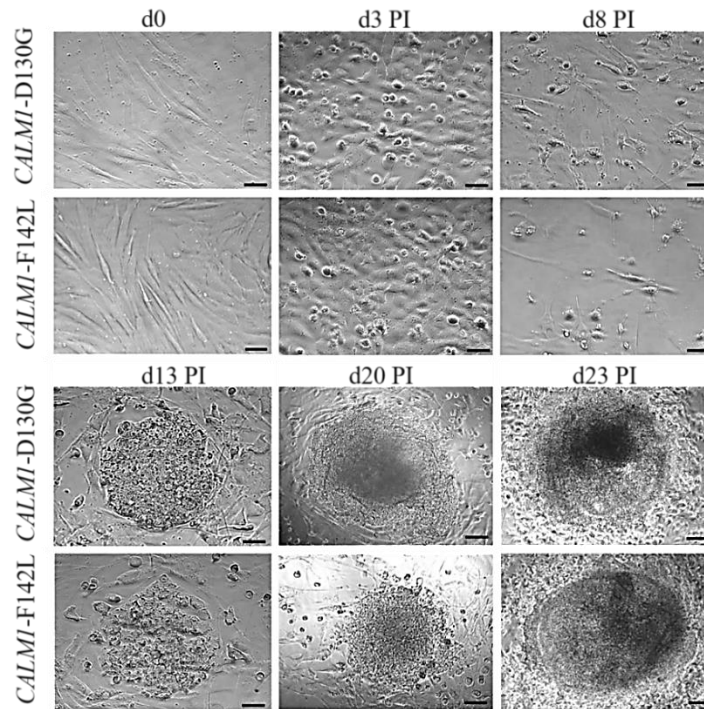


Figure 7: Peripheral skin fibroblasts from day 0 of SeV infection to day 23 post- infection.

Representative PH microscope pictures of hiPSC colonies emerging from transduced skin fibroblasts of patient *CALMI-D130G* and *CALMI-F142L*. d0 to d13 scale bar 50  $\mu\text{m}$ , d20 scale bar 100  $\mu\text{m}$ , d23 scale bar 250  $\mu\text{m}$ .

Expression of Sendai transgenes *SeV* virus, *SeV- OCT3/4*, *SeV- SOX2*, *SeV-KLF4*, *SeV-cMYC* and *GAPDH* was evaluated by RT PCR in uninfected fibroblasts, infected fibroblasts and generated hiPSCs of passage 6. Gene expression of those *SeV* transgenes, also known as Yamanaka factors, is necessary for the reprogramming process of fibroblasts into hiPSCs, as described in Yamanaka's publication<sup>15</sup>. First, total RNA was extracted from cell samples and transcribed into cDNA. Transcripts of interest were amplified by PCR and product was loaded on an agarose gel and visualised with a gel documentation system.

As shown in Figure 8, PSFs of both patients do not show expression of *SeV* transgenes, as expected, indicating no presence of virus or viral genes. Samples from both patients analysed from fibroblasts 10 days after infection show bands for all *SeV* transgene lanes, indicating the presence of *SeV* and expression of viral genes necessary for the reprogramming into hiPSCs. Analysis of gene expression in hiPSCs of passage 10 shows no more detectable level of viral transgene expression in cells. Since the CytoTune Sendai virus is a non- integrating RNA virus, it is expected that no more virus or virus particles are present in the generated hiPSCs after some passages, as shown in Figure 8, lanes 3 and 4.

The housekeeping gene *GAPDH* was detected in all samples at similar levels, demonstrating successful and comparable PCR amplification within all samples.

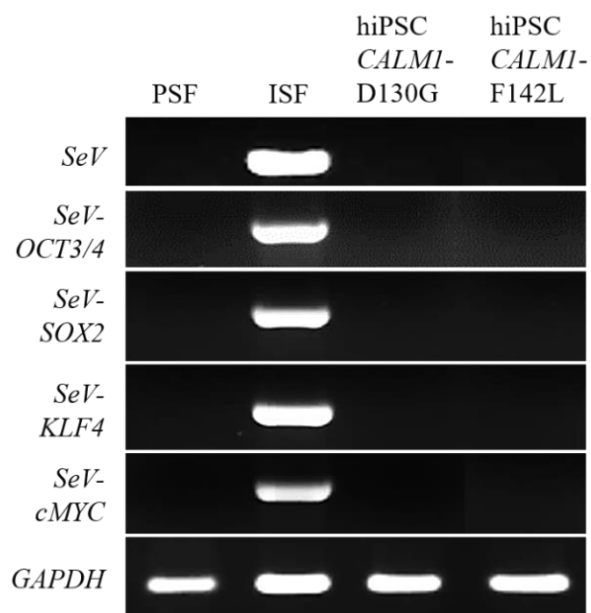


Figure 8: Representative agarose gel of RT PCR transcript expression of *SeV* transgenes in patient cells.

Whole RNA of skin fibroblasts (PSF, lane 1), infected skin fibroblasts (ISF, lane 2) and of hiPSC of passages 6 of patient *CALMI*- D130G (lane 3) and *CALMI*- F142L (lane 4) was extracted and transcribed into cDNA. Transcripts of *SeV* gene, *SeV*- *OCT3/4*, *SeV*. *SOX2*, *SeV*- *KLF4*, *SeV*- *cMYC* and *GAPDH* were amplified in a semi- quantitative manner and analysed on agarose gel.

To assess the presence of SeV HN proteins as a measure of reprogramming stage of hiPSC, immunofluorescence staining of hiPSC colonies of passages 4 and 10 of *CALMI*- D130G and *CALMI*- F142L patient hiPSCs was performed. Colonies of patient lines were grown until approximately 2.5 mm diameter in size and subjected to immunofluorescent staining. Early passages colonies of both patient hiPSC lines show presence of SeV protein, indicating the virus still present in the cells (Figure 9). Patchy distribution of signal may be caused due to single cells not being infected with the virus or to cells that have already lost viral gene expression. The minority of cells within a well- infected colony not undergoing the transition to pluripotency are expected to be lost during the time course of continuous passaging and proliferation. Colonies examined at passage 10 did not show presence any more of SeV proteins. This concludes to the virus not being present in the cells anymore due to passaging and proliferation of the cells. Once colonies were tested negative for SeV protein expression, a selection of clones per patient hiPSC line was selected for further characterizations.

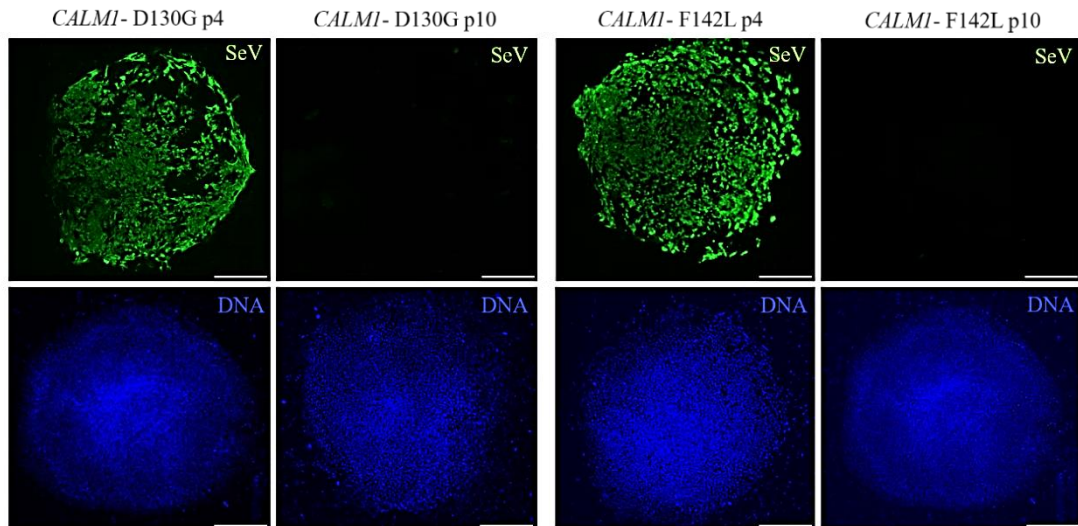


Figure 9: Immunofluorescent staining of SeV HN proteins.

Representative pictures of immunofluorescent staining of *CALMI*- D130G and *CALMI*- F142L hiPSC colonies at passages 4 and 10. Sendai protein (SeV) in green, DNA in blue, scale bar 500  $\mu\text{m}$ . Figure adapted from Rocchetti et al. <sup>133</sup>.

#### 4.1.2 Genetic characterization of generated hiPSC lines

To confirm the derivation of generated patient hiPSCs from their respective patients' skin fibroblasts, the presence of the *CALMI*- D130G and *CALMI*- F142L mutations in the genome of uninfected fibroblasts and resultant generated hiPSCs was confirmed by Sanger sequencing. Fibroblasts and hiPSCs from each line were harvested and genomic DNA was extracted. Genomic sequences around the loci of mutations were amplified by standard PCR, using primer sets listed in the list of oligonucleotides (see 3.6). Retrieved sequencing data was visualized and evaluated using the Chromas Lite MFC software. The first panel of Figure 10 shows the sequencing result of ctr hiPSCs, which harbours an Arginine (A) at c.389, translating together with the Guanine (G) and Thymine (T) into the aa Aspartate (D). The sequence below depicts patient skin fibroblasts. The double read present at c.389, symbolizing an A and G at the same position, results in a Glycine (G) instead of an D on one allele, but translates into the wt D on the other allele. The same heterogeneity is shown in the patient hiPSCs, confirming the lineage of the hiPSC- derived from the patient fibroblasts and the homozygous mutation as previously described by Crotti and colleagues <sup>1</sup>. The D130G mutation is located in exon 5 of the *CALMI* gene.

The same sequence analysis was performed for the *CALMI*- F142L patient cells. The C6 ctr sequence shows a C at c.398 of the *CALMI* gene in exon 6. This nt translates together with two Ts into the aa Phenylalanine (F). *CALMI*- F142L patient fibroblasts carry a C

at position c.426 on one allele and a G on the other allele, as described in the above mentioned publication by Crotti and colleagues. This is confirmed by the double read at this position in the sequencing track. The exchange of nt leads to the translation into the aa Leucine (L), instead of F. The same double read is shown in the sequencing result of *CALMI*- F142L hiPSCs.

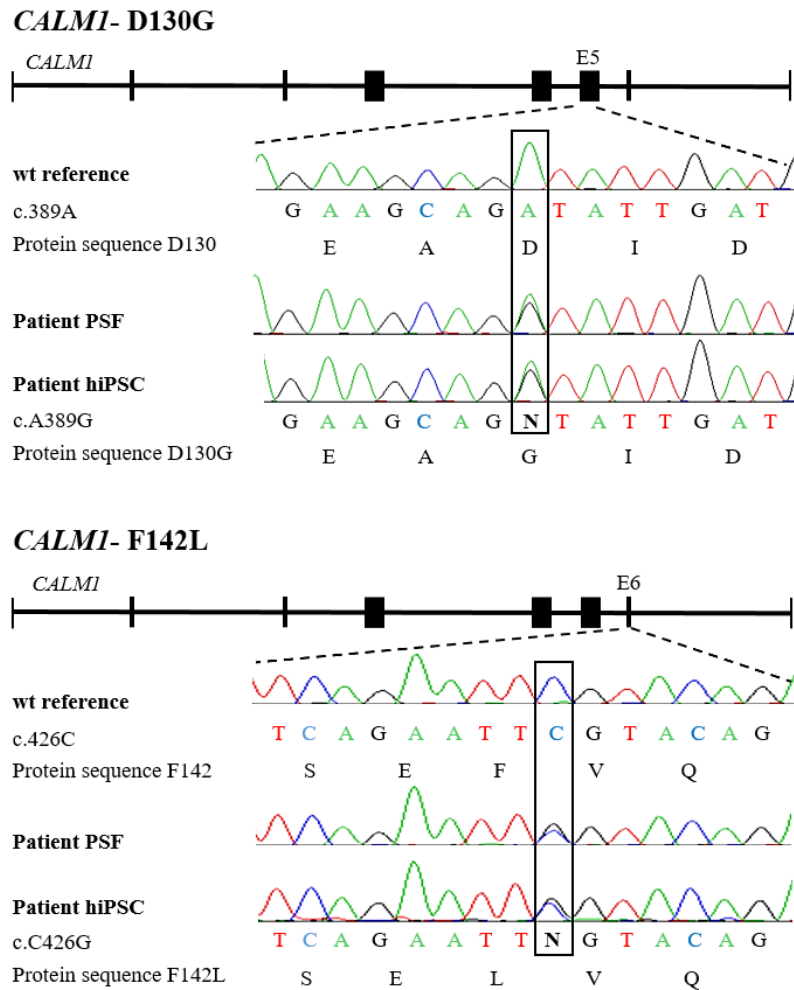


Figure 10: Confirmation of mutations by Sanger sequencing in patient PSFs and patient hiPSCs of both mutant lines.

PSF of *CALMI*- D130G and *CALMI*- F142L patients were analysed with Sanger sequencing and mutations were confirmed. Derived hiPSCs from both patient fibroblast lines were sequenced by Sanger sequencing and mutations were confirmed. hiPSC cells of C6 were analysed as wt reference (wt). Figure adapted from Rocchetti *et al.* <sup>133</sup>.

While culturing hiPSCs, alterations in the karyotype due to chromosomal instability are an observed but unwanted effect, as described in various publications <sup>19,135</sup>. These instabilities can ultimately cause the cell line to behave differently in a variety of experiments and analyses, not reflecting but rather distorting the phenotypical differences due to the patients' mutations when compared to ctr hiPSCs. The karyotype of two clones of the

*CALMI*- F142L hiPSC line and the ctr C6 hiPSC line was examined in collaboration with the institute of human genetics at the Technical University Munich, in the group of Prof. Meitinger. Karyotyping of clones of the *CALMI*- D130G hiPSC was not executed, since the focus of experiments was set on the *CALMI*- F142L hiPSC line.

The karyogram depicted on the left side of Figure 11 shows the chromosomes of one representative *CALMI*- F142L hiPSC clone. The somatic number of  $2n$  of this line is 46, with all autosomal chromosomes present in 2 copies. All other characteristic features of a normal karyotype, like band structure, position of centromeres and their length are present and orderly. Since the donor of the cells is male, X and Y chromosomes are both present. The right side of Figure 11 depicts the karyogram of the ctr hiPSC line C6, which was mainly used as ctr line for later experiments. Chromatic structure, chromosome number and length of chromosomes are normal as well. The somatic number is 46, with no Y chromosome present, since the donor is female. For the duration of the majority of the experiments, hiPSCs were kept in culture on MEF feeders, since it is believed to stabilize the karyotype<sup>135</sup>.

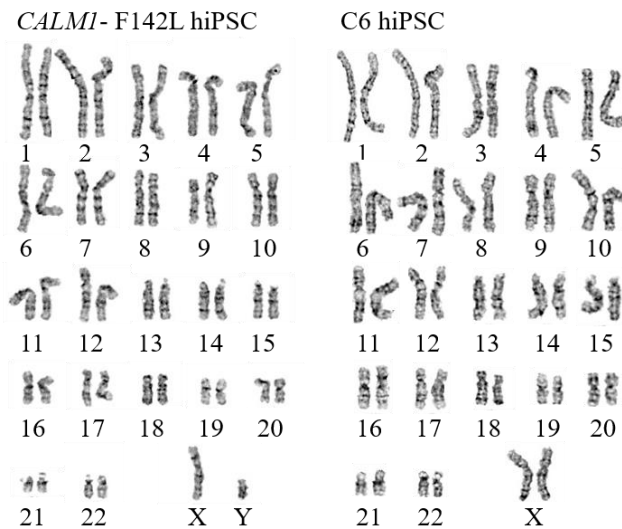


Figure 11: Karyogram of *CALMI*- F142L hiPSCs and C6 hiPSCs.

Representative Karyogram of one clone of the *CALMI*- F142L hiPSC line and of clone 6 of the ctr hiPSC line (C6 hiPSC). Chromosomes are numbered, with chromosomes from 1- 22 and the X and Y chromosome of *CALMI*- F142L on the left side of the panel, and chromosomes 1- 22 and the X chromosome of C6 on the right side of the panel. Figure adapted from Rocchetti *et al.*<sup>133</sup>.

### 4.1.3 Evaluation of pluripotency of generated lines

#### *Alkaline phosphatase activity*

The membrane bound enzyme alkaline phosphatase (AP, EC 3.1.3.1 orthophosphoric-monoesterase, alkaline optimum) is highly expressed in pluripotent stem cells, including ESCs, embryonic germ cells and iPSCs<sup>136</sup>. Whereas the specific role of AP in hiPSCs is still unknown, it is suggested that AP plays an important role in the cascade of neurotransmitter  $\gamma$ -aminobutyric acid synthesis, which is an important factor for the regulation of proliferation and self-renewal in ES cells<sup>137</sup>. AP activity, as a traditional marker for pluripotency, was assessed for different clones of both *CALMI*- hiPSC lines. In Figure 12, the left two panels show colonies of *CALMI*- D130G hiPSC, the right panel shows colonies of *CALMI*- F142L hiPSCs. Colonies of both lines display a round morphology with clear edges. The cells within the colonies appear homogenous and undifferentiated. AP activity is detected in all areas of the colonies, at various levels. Especially the middle areas are darker in colour than the edges, corresponding to highly pluripotent cells. Cells with less AP activity around the edges are considered less pluripotent due to differentiation. Those areas are expected to be lost within further passaging of the hiPSCs. Clones displaying highest level of AP activity, hence pluripotency, were further cultured and pluripotency was assessed more precisely by immunostaining, as described in the next section.

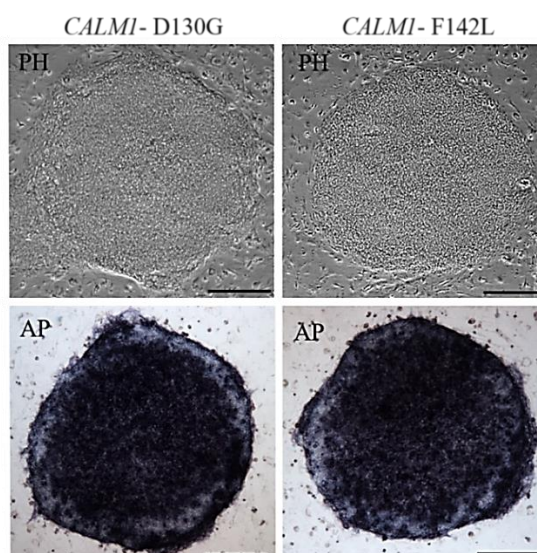


Figure 12: AP staining for pluripotency in *CALMI*- D130G and *CALMI*- F142L hiPSC colonies.

Representative PH microscope images PH (top) and after AP staining (AP) (bottom). Left two panels depicts colonies from the *CALMI*- D130G hiPSC line, right panels from the *CALMI*- F142L line. Scale bars 500  $\mu$ m. Figure adapted from Rocchetti *et al.*<sup>133</sup>.

*Expression of NANOG and TRA1-81 proteins*

Immunofluorescence analysis of pluripotency markers NANOG and TRA1-81 was performed in colonies of *CALMI*- D130G and *CALMI*- F142L hiPSCs (Figure 13). The antibody against TRA1-81 from BD recognizes the keratan sulfate core molecule, also known as podocalyxin, expressed on the cell membrane of hiPSCs. As hiPSCs undergo differentiation, TRA1-81 expression is lost (source BD Bioscience homepage). The anti-NANOG antibody used recognizes the transcription regulator NANOG, which is an important factor for proliferation and self-renewal in pluripotent stem cells (source abcam homepage). TRA1-81 and NANOG immunofluorescence stainings are a well-established measure for assessing pluripotency of hiPSCs, as described before by Takahashi and colleagues<sup>15</sup>. The cells of the colonies of both lines are stained homogeneously in green, with some cells expressing TRA1-81 slightly stronger on the membrane. The MEF feeder cells surrounding the colonies are negative for TRA1-81 expression, acting as a negative ctr for the staining. Overall expression of TRA1-81 in colonies of both hiPSC lines suggests the hiPSCs of both lines being in an undifferentiated state. NANOG is expressed mainly in the nucleus of cells, since it is a transcriptional regulator. The nuclear expression pattern is well visible in colonies of both lines, suggesting an overall expression of the transcription regulator and therefore pluripotency of the cells. Hoechst 22358 is a nucleic acid stain intercalating with dsDNA and emitting blue fluorescence when bound to dsDNA. Hoechst 22358 fluorescent signal is limited to the nuclei of cells, highlighting the specificity of dsDNA staining. Some signal is observed in MEF feeder cells surrounding the colonies, since the staining is not limited to human cells.

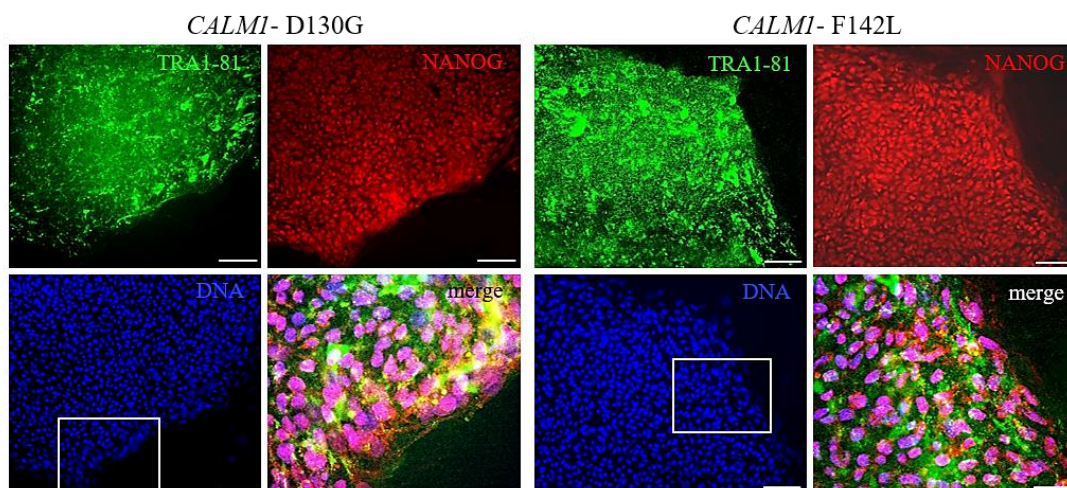


Figure 13: Immunofluorescence analysis of pluripotency markers NANOG (red) and TRA1-81 (green) in representative colonies of the *CALMI*- D130G and *CALMI*- F142L hiPSC lines.

The left side of the figure shows a representative colony of *CALMI*- D130G with anti-TRA1-81 (green), anti-NANOG (red) staining and staining for DNA with DAPI (blue). Scale bar 500  $\mu\text{m}$ . Merged image is the magnification of the framed area. Scale bar 50  $\mu\text{m}$ . The right side of the figure shows the same sequence of stainings and magnifications, on a representative colony of *CALMI*- F142L hiPSC line. Figure adapted from Rocchetti *et al.*<sup>133</sup>.

#### *Activation of endogenous pluripotency genes*

Analysis of expression levels of endogenous pluripotency marker genes is one of the most fast- forward measures to level of pluripotency in hiPSCs and well accepted throughout literature as assay of pluripotency of hiPSCs. Transcription levels of *c-MYC*, *KLF4*, *OCT3/4*, *SOX2*, *NANOG*, *REX1* and *TDGFI* were analysed. *c-MYC* transgene expression is believed to be an initiator for increased proliferation after induction of reprogramming and one of the key reprogramming factors of Yamanaka in generation of hiPSC out of somatic cells<sup>138</sup>. Together with *KLF4*, they are expected to be highly expressed as early as 3 days after induction of reprogramming. Overexpression of those two factors is associated with cancer<sup>139</sup>. Figure 14 shows expected expression values of the genes *c-MYC* and *KLF4* for all hiPSC clones. *OCT3/4* and *SOX2* are the other two reprogramming transgenes previously described by Yamanaka. These two homeodomain transcription factors are understood to “govern[s] pluripotency”<sup>139</sup>, together with NANOG, and are expected to be highly expressed throughout hiPSC culture. Figure 14 shows high expression values for *OCT3/4*, *SOX2* and *NANOG* for all hiPSC clones compared to *GAPDH* expression and relative to corresponding PSFs. These expression values are all within the expected range, as previously described by Moretti and colleagues<sup>129</sup>. As described by literature, *REX1* is a transcription factor crucial in hiPSCs and mouse ESCs to maintain pluripotency<sup>140</sup>. Expression values of *REX1* are for all clones as expected. Expression values of *TDGFI* are slightly lower, but within the expected range for all clones. The

epidermal related growth factor protein *TDGF1* plays an essential role in embryonic development and is among the other described endogenous associated genes for pluripotency a well-recognized marker gene, as described before<sup>129</sup>. Endogenous expression of all analysed pluripotency related genes of *CALMI*- D130G and *CALMI*- F142L hiPSC clones are within the range of expected expression values. The ctr hiPSC clone C6 had been characterized in before in the publication of Pane and colleagues<sup>32</sup> and ranks as well within the expected expression values for all genes.

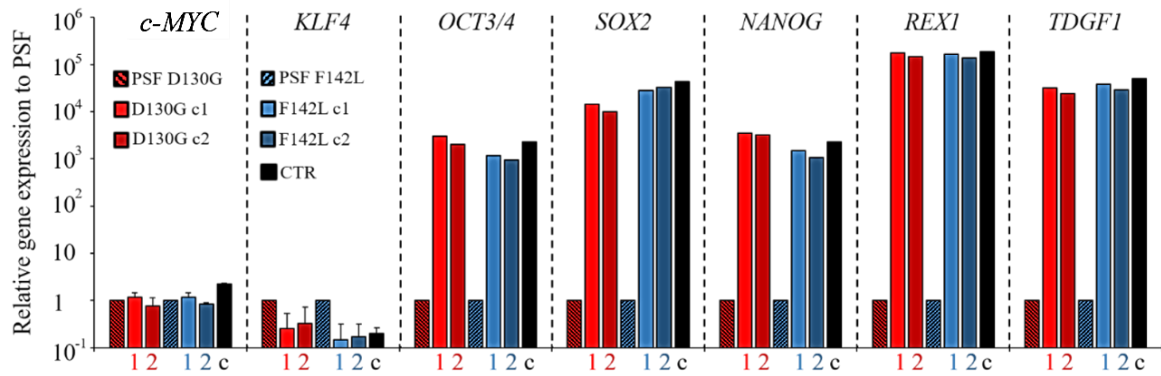


Figure 14: qRT PCR analysis on endogenous pluripotency genes.

qRT PCR analysis of endogenous genes associated with pluripotency (*c-MYC*, *KLF4*, *OCT4*, *SOX2*, *NANOG*, *REX1* and *TDGF1*) in 2 different *CALMI*- D130G hiPSC clones (light red and dark red bars), in 2 different *CALMI*- F142L hiPS clones (light blue and dark blue bars) and ctr hiPSC clone (black bars). Expression values are relative to corresponding primary skin fibroblasts (PSF, red and blue shaded bars), normalized to *GAPDH*, and presented as mean +SEM,  $n=3$ . Figure adapted from Rocchetti *et al.*<sup>133</sup>.

#### Genome- wide expression profile by Pluritest

As another measure of pluripotency, RNA was extracted from hiPSCs of each line and analysed in the PluriTest assay, as described before in methods section 39. This assay was performed by Dr. Parotta at Magna Græcia University, Catanzaro, Italy. RNA was hybridised, loaded on Illumina HT12v4 microarrays and analysed against the ‘Stem Cell Matrix-2’ (SCM2) data set, as described in the appendant publication by Müller and colleagues<sup>130</sup>. PluriTest is described as “a robust open- access bioinformatic assay of pluripotency in human cells based in their gene expression profiles”<sup>130</sup>. Patient hiPSCs were compared against data sets of known pluripotent and non- pluripotent genes and depicted in a graph on a scale from -100 to 50, with -100 being the most non- pluripotent. Gene expression profiles were also compared to data sets of well- characterized pluripotent stem cells to determine the novelty of the sample cells. A novelty score of 4 is marking cells with unknown gene expression profiles, whereas a novelty score of 1 is describing the typical expression patterns of genes of pluripotent stem cells. Figure 15 shows the result of PluriTest analysis. The red cloud defines the expression profile of pluripotent

cells in the SCM2 data set, the blue cloud represents expression profiles of somatic cells, defining a very high novelty score when compared to pluripotent cells. Newly reprogrammed hiPSCs of good pluripotency are expected to be situated within the red cloud. Both lines show pluripotency values of around 40. Both hiPSC lines are well reprogrammed, since they express expected genes of pluripotency and resemble expression patterns of hiPSCs.

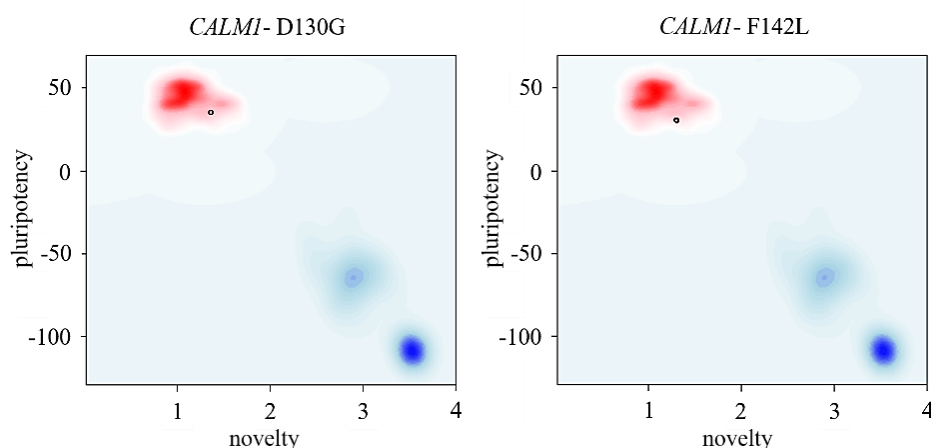


Figure 15: PluriTest analysis of representative clones of *CALMI- D130G* and *CALMI- F142L* hiPSCs.

The left side of the figure shows the *CALMI- D130G* hiPSC sample (black circle) in a graph for pluripotency (y-axis) and novelty (x-axis). The right side shows the analysis of a representative *CALMI- F142L* hiPSC clone. The red cloud symbolises standard pluripotency values, the blue cloud symbolises expected expression patterns for somatic cells. Figure adapted from Rochetti *et al.* <sup>133</sup>.

### *Expression of marker genes specific of all three germ layers upon spontaneous differentiation*

One major characteristic of pluripotent stem cells is the ability to differentiate into cells of all three germ layers. As described in multiple publications before, analysis of upregulation of lineage marker genes of the three germ layers endoderm, mesoderm and ectoderm in embryonic bodies at day 21 after induction of differentiation is a well-established assay to characterize the pluripotent quality of hiPSC lines further <sup>24,32,60</sup>. Endodermal marker genes include *PDX1*, a marker for pancreatic cells, *SOX7*, representing cells of the hemogenic lineage, and *AFP*, marking perinatal liver cells. Mesodermal marker genes analysed were *CD31*, expressed in blood platelets, *DES*, present in muscle-specific filaments, *ACTA2*, also known as gene expressing smooth-muscle protein Actin, *SCL*, a gene involved in hematopoiesis and *MYL2*, expressing the myosin light chain protein. Ectodermal gene expressions evaluated included the marker genes *KRT14*, mostly expressed in keratinocytes of the skin, *NCAM1*, marking neuros, *TH*, encoding for an enzyme ex-

pressed in the central nervous system and *GABRR2*, involved in neuronal activity regulation (source: genecards.org). Depicted in Figure 16 are one analysed clone of each generated hiPSC line out of three clones. Similar results have been obtained for all clones and one clone per hiPSC line was chosen for further experiments. *PDX1*, *SOX7* and *AFP* expression levels are very comparative and within the expected range for all three analysed lines. *CD31*, *ACTA2* and *SCL* marker genes are shown to be at similar levels of all lines. Minor differences are observed at *DES* and *MYL* expression levels. All three lines produce beating CMs upon induction of differentiation, therefore minor differences in expression values are attributed to differences in differentiation efficiencies between biological replicates. *KRT14*, *NCAM1*, *GABRR2* and *TH* are expressed at similar levels for all lines and range within the anticipated fold values. Overall gene expression patterns are comparable to the previously characterized and described C6 hiPSC line.

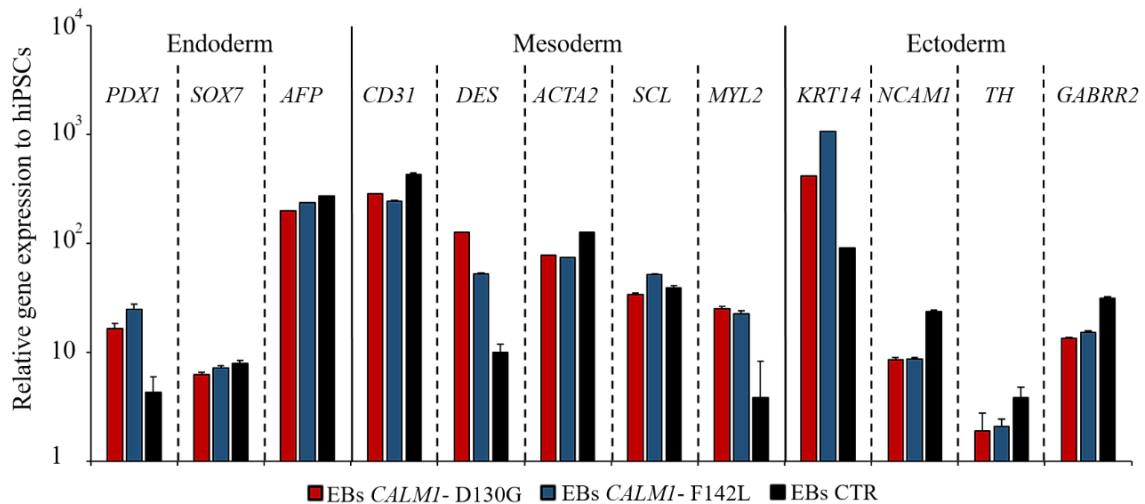


Figure 16: qRT-PCR analysis of markers of the three germ layers in embryonic bodies.

qRT PCR analysis was performed on marker genes of the three germ layers, endoderm (*PDX1*, *SOX7* and *AFP*), mesoderm (*CD31*, *DES*, *ACTA2*, *SCL*, *MYL2*) and ectoderm (*KRT14*, *NCAM1*, *TH* and *GABRR2*) in embryonic bodies (EBs) at day 21 of differentiation from representative *CALMI*- D130G (red bars) and *CALMI*-F142L hiPSC clones (blue bars) and ctr C6 (black bars). Expression values are normalized to *GAPDH* and relative to corresponding undifferentiated hiPSC clones, presented as mean +SEM,  $n=3$ . Figure adapted from Rocchetti *et al.*<sup>133</sup>.

The above mentioned assays and analyses were performed on a subset of clones of each hiPSC line and the two most promising clones were chosen for further analysis and differentiation into CMs.

## 4.2 Differentiation of *CALMI*- hiPSCs into CMs

Differentiation of hiPSCs into CMs was performed as described in methods section 3.2.4. Production of CMs was evaluated as the last and most important characteristic of produced patient's hiPSCs. 2 months after differentiation of hiPSCs into CMs, cells were dissociated and immunofluorescence staining of cardiac muscle proteins cTNT and  $\alpha$ -Actinin was performed. Expression patterns of representative clones of both patients' lines was compared to ctr clone C6. cTNT is the biggest of all three troponin subunits and is encoded by the *TNNT* gene. cTNT is known to bind to the tropomyosin subunit within the troponin complex<sup>141</sup>. The antibody is detecting the localization of the protein on the actin thin filament of cardiac muscles, thereby marking the A- band of the sarcomeres. A striated pattern of immunofluorescent signal is expected (source Thermo Fisher Datasheet for antibody).  $\alpha$ - Actinin is a connecting protein of actin to the Z- lines in cardiac and skeletal muscle cells. This microfilament protein is visible in a striated pattern, when detected by immunofluorescence<sup>142</sup>. Figure 17 depicts immunofluorescence microscopic images of representative 2 months old CMs. The *CALMI*- D130G CM shows the expected striated pattern of cTNT and  $\alpha$ - Actinin, staining the muscle filaments, and the blue coloured nucleus in the centre of the cell. The shape of the CM suggests for a still more fetal state of the muscle cell, since adult CMs present themselves in a more rod-shape. 2 months old hiPSC- derived CMs are however expected to resemble a more fetal phenotype. The same striated patterns are visible with cTNT and  $\alpha$ - Actinin in the *CALMI*- F142L CM. The CM presents itself with 2 nuclei, indicative of a terminally differentiated fetal CM phenotype, or of a cell undergoing cell division. Binucleation is regularly observed in hiPSC- derived CMs<sup>143</sup>. The C6 hiPSC- derived CM, also shows as a binucleated cell. Immunofluorescence staining of cTNT and  $\alpha$ - Actinin are comparable to the other two hiPSC- derived CMs. Magnifications in all three pictures shows the crosslinking of filaments with the adjacent sarcomeres of the red stained  $\alpha$ - Actinin proteins and the green stained troponin complexes within the thin filaments. Nuclei are visible with clear borders by blue staining of the contained DNA.

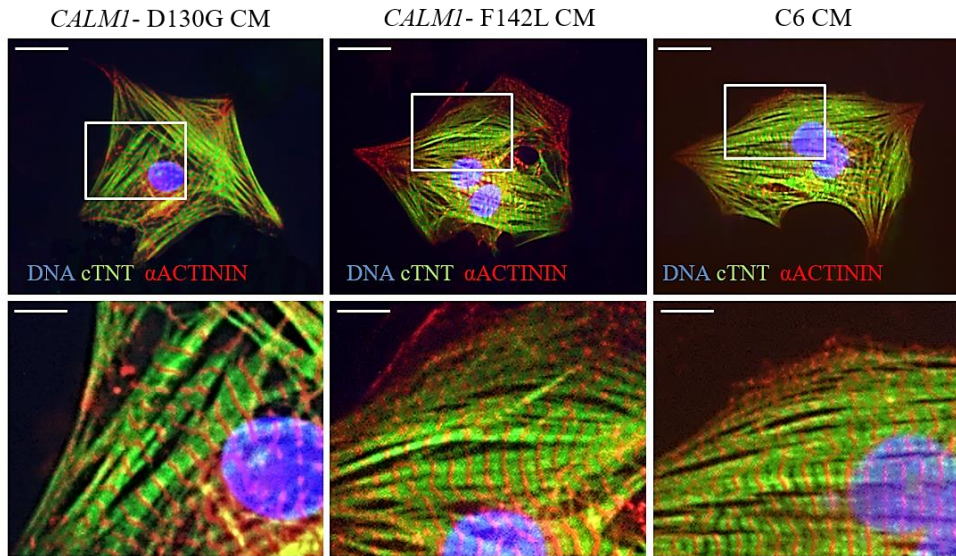


Figure 17: Representative immunofluorescence images of sarcomeric proteins cardiac Troponin T (cTNT, green) and  $\alpha$ -Actinin (red) in CMs.

Nuclei are stained with Hoechst 33528 (blue). Top row images represent from left to right: *CALMI*- D130G CM, *CALMI*- F142L CM and C6 CM. Bottom panels are a magnification of the area framed in the upper images. Scale bars 25  $\mu$ m (top panels) and 10  $\mu$ m (bottom panels). Figure adapted from Rocchetti *et al.*<sup>133</sup>.

### 4.3 Evaluation *CALMI*- CM phenotype

After thorough hiPSC characterizations of both *CALMI*- hiPSC lines and their derived CMs, evaluation of the LQTS phenotype was performed in the *CALMI*- F142L line. The following results are therefore shown on the *CALMI*- F142L hiPSC line and the C6 ctr line, unless stated otherwise.

#### *Ion channel transcript expression*

To evaluate the LQTS phenotype of CMs derived from *CALMI*- F142L hiPSC, expression levels of *CALM* genes, as well as selected CM genes were evaluated in hiPSC- derived CMs of 2.5 months age. Total RNA was extracted from CMs and cDNA was transcribed. Target genes chosen for evaluation were *CALM1*, *CALM2*, *CALM3*, *SCN5A*, *KCNQ1*, *CACNA1C*, *RYR*, *SERCA*, *PLN*, *SLC8A1*, *PMCA4* and *cTNT*. The proteins of these target genes represent a subset of proteins considered important for cardiac AP generation,  $\text{Ca}^{2+}$  handling, and excitation-contraction (EC) coupling. Alterations of gene expression levels of these target genes as a downstream effect of mutant CaM was analysed on CMs from both hiPSC clones of the *CALM1*- F142L lineage and compared to C6 hiPSC- derived CMs of the same age (Figure 18). No differences in transcription of the analysed key genes were observed between patient and ctr line CMs.

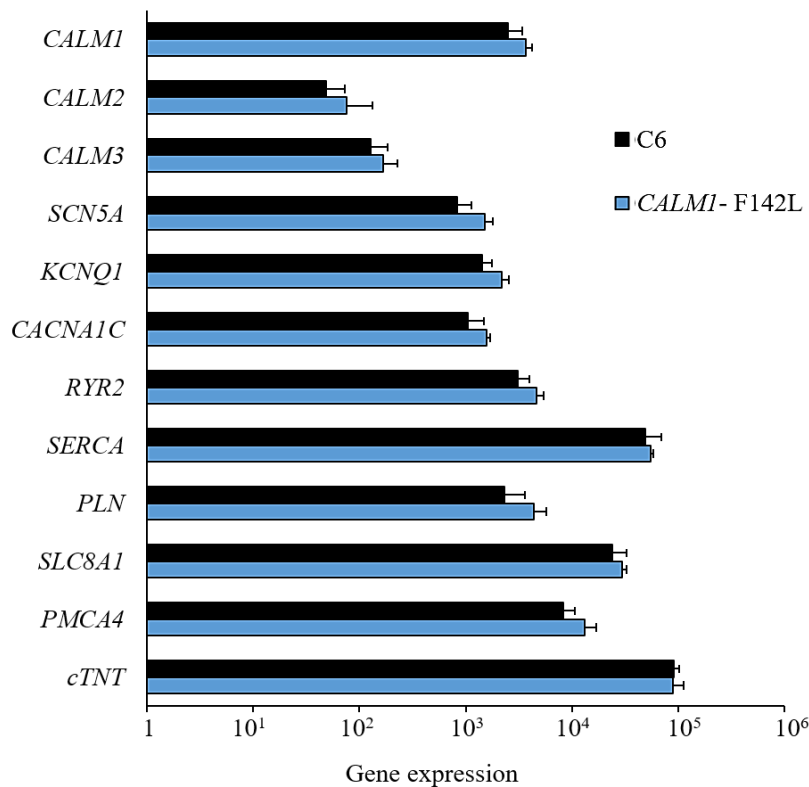


Figure 18: qRT PCR analysis of *CALM* and key myocytic genes in CMs.

qRT PCR analysis of C6 ctr CMs (black bars) and *CALMI*-F142L CMs (blue bars) on *CALMI*, *CALM2*, *CALM3*, *SCN5A*, *KCNQ1*, *CACNA1C*, *RYR*, *SERCA*, *PLN*, *SLC8A1*, *PMCA4* and *cTNT*. Expression values are normalized to *GAPDH*, relative to average *GAPDH* and presented as mean +SEM,  $n=3$ . CMs from both *CALMI*-F142L clones were pooled together. Figure adapted from Rocchetti *et al.*<sup>133</sup>.

The 3 genes *CALMI*, *CALM2* and *CALM3* encode for an identical 149 aa CaM protein in the human organism, with a total of 17 protein coding transcripts and 5 transcripts translating into the 149 aa or 150 aa protein. To investigate possible differences in the transcript expression levels in the *CALMI*-F142L- CMs compared to ctr CMs, primer pairs were designed to specifically amplify the different transcripts encoding the 149 aa or 150 aa CaM protein. Two main transcripts encoded by the *CALMI* gene were investigated. 1 transcript of the *CALM2* gene was included in the analyses and 2 primer pairs were designed to amplify *CALM3* transcript 1 and *CALM3* transcript 3. All transcripts were detected in both lines with fold to *GAPDH* values above 0 (Figure 19). No statistical differences were measured for any of the transcripts between patient and ctr, computed by the 2-sided T-test. Transcript 1 of each of the *CALM* genes had the highest expression level in both lines.

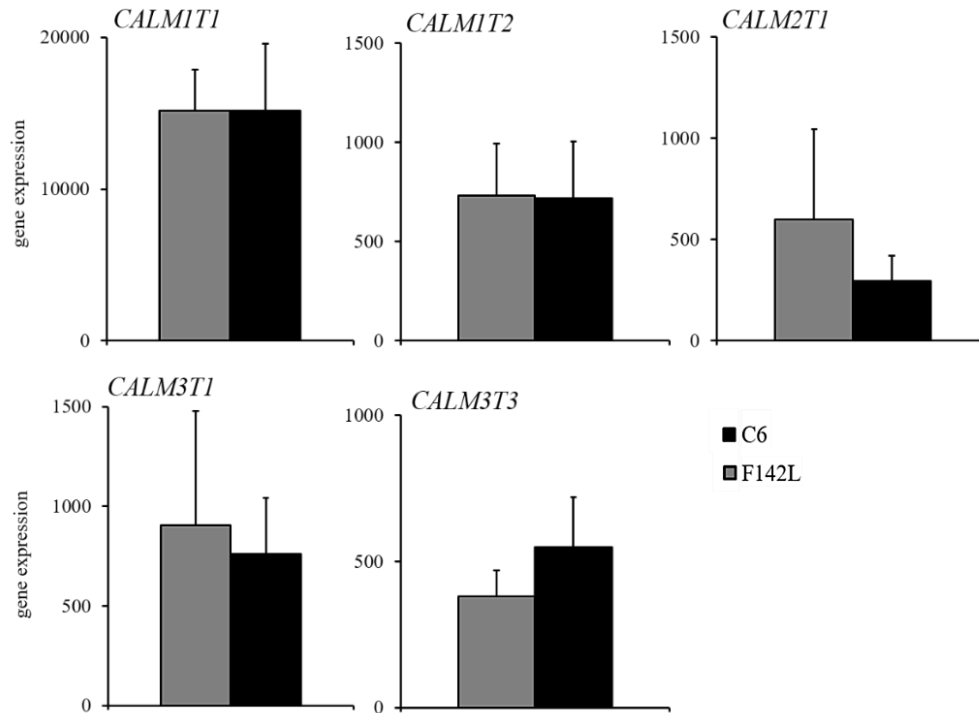


Figure 19: qRT PCR analysis of *CALM* transcripts in CMs.

qRT PCR analysis of C6 ctr CMs (black bars) and *CALMI*-F142L CMs (grey bars) on *CALMI* transcript 1 (*CALMIT1*), *CALMI* transcript 2 (*CALMIT2*), *CALM2* transcript 1 (*CALM2T1*), *CALM3* transcript 1 (*CALM3T1*) and *CALM3* transcript 3 (*CALM3T3*). Expression values are normalized to *GAPDH*, relative to average *GAPDH* and presented as mean +SEM,  $n=3$ .

#### 4.3.1 *CaMKII* activity measurements

The CaM- dependent kinase II (CaMKII) is a CaM- dependent protein kinase. It plays a major role in  $Ca^{2+}$  cycling in CMs and influences  $Ca^{2+}$  uptake and release from the SR during EC coupling<sup>144,145</sup>. To investigate effects of mutated CaM on CaMKII activation, patient hiPSC- derived CMs were transduced with lentivirus encoding Camui- CR, a FRET- based biosensor that allows assessment of dynamic changes in CaMKII $\delta$  activation state<sup>146</sup>. Figure 20 A shows representative fluorescent pseudocolour images of ctr CMs expressing RFP and GFP signals. Working principle of Camui- CR FRET is depicted below. Upon binding of Ca- CaM to FRET- coupled CaMKII, conformational changes result in the loss of the FRET signal. Figure 20 B shows fluorescent ratios of background- corrected RFP to GFP emission in CMs of ctr C6 cells, as well as CMs derived from *CALMI*- F142L hiPSCs. The RFP/ GFP ratio of C6 CMs is higher than for patient CMs. The Mann- Whitney Test was executed to estimate statistical significance between ctr and patient values. Calculated p- value is 0.004 and therefore statistically

significant. This translates to a significantly increased CAMKII $\delta$  activity in *CALMI*-F142L CM compared to ctr CMs.

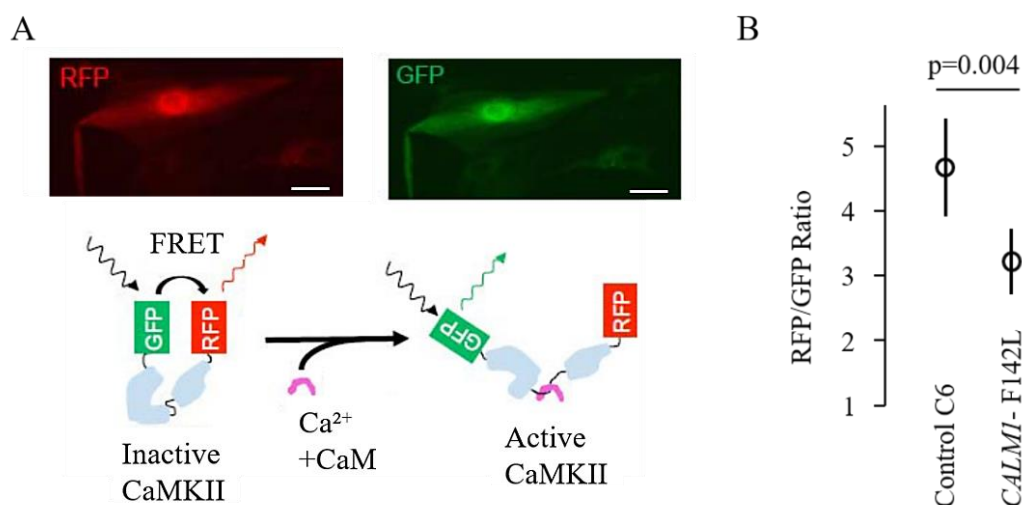


Figure 20: FRET- based CaMKII activity measurement in 2.5 months old hiPSC- derived CMs.

(A) Representative fluorescence images of ctr CMs expressing the CaMKII reporter. Pseudocolour images from RFP and GFP fluorescence signals shown in red and green. Scale bars 25  $\mu$ m. Schematic of Ca- CaM mediated activation of CaMKII, following structural reorganization and loss of FRET signal. (B) 10 hiPSC-derived CMs of the *CALMI*- F142L hiPSC line were analysed for fluorescent RFP to GFP ratio and compared to ctr C6 CMs. Background fluorescence was subtracted and p- values were calculated corresponding to C6 values.  $n= 24$ , from 8 independent experiments. Error bars represent 95% confidence intervals. Figure adapted from Rocchetti *et al.* <sup>133</sup>.

#### 4.3.2 Analysis of electrophysiological phenotype

Electrophysiological analyses were performed by Dr. Rocchetti and colleagues at the department of Biotechnology and Bioscience, University of Milano- Bicocca in Milan, Italy. All work presented in chapter 4.3.2 is in reference of the publication by Rocchetti *et al.* <sup>133</sup>.

Two clones (c1 and c2) of patient's hiPSCs were analysed for  $I_{CaL}$  characterization. Since results were closely comparable, following electrophysiological analyses was performed on CMs pooled from both clones. Ctr values were obtained from C6 healthy ctr hiPSCs.

##### *I<sub>CaL</sub> properties*

Figure 21 shows  $I_{CaL}$  properties for both clones of *CALMI*- F142L patient in 2.5 months old CMs. Panel A shows the steady- state  $I_{CaL}$  I/V relationship. No significant differences in peak  $I_{CaL}$  density were measured between c1, c2 and ctr, however, the sustained  $I_{CaL}$  component was significantly larger <sup>133</sup>. Panel B shows the steady- state dependent  $I_{CaL}$  activation/ inactivation curves for both *CALMI*- F142L clones and ctr C6 CMs. *CALMI*-

F142L c1 and c2 show positively shifted and incomplete  $I_{CaL}$  inactivation compared to ctr CMs. Inactivation of  $I_{CaL}$  was measured slower in mutant clones than in ctr CMs. Sustained  $I_{CaL}$  is therefore longer present in mutant CMs<sup>133</sup>.

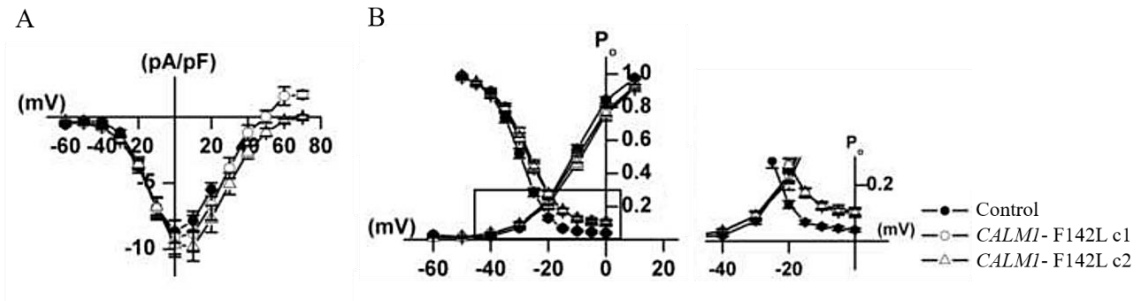


Figure 21:  $I_{CaL}$  I/V relationships and  $I_{CaL}$  steady-state activation and inactivation curves.

$I_{CaL}$  characterization performed on C6 ctr CMs and *CALMI*-F142L CMs of 2.5 months age. Ctr values depicted in filled dots ( $n=11$ ), clone 1 of patient in open dots ( $n=12$ ), clone 2 of patient in open triangles ( $n=13$ ). (A) peak  $I_{CaL}$  I/V relationships. (B)  $I_{CaL}$  steady-state activation and inactivation curves. Right small panel of (B) is the magnification of boxed area of the graph. Figure and figure legend adapted from Rochetti *et al.*<sup>133</sup>.

To evaluate CDI, Calcium/ Barium current density tracings were performed on patient hiPSC-derived CMs from both clones and compared to C6 hiPSC-derived CMs. Figure 22 shows representative  $I_{CaL}$  and  $I_{BaL}$  tracings performed within the same cell and at 0 mV. Dashed area was estimated to determine CDI<sup>133</sup>.

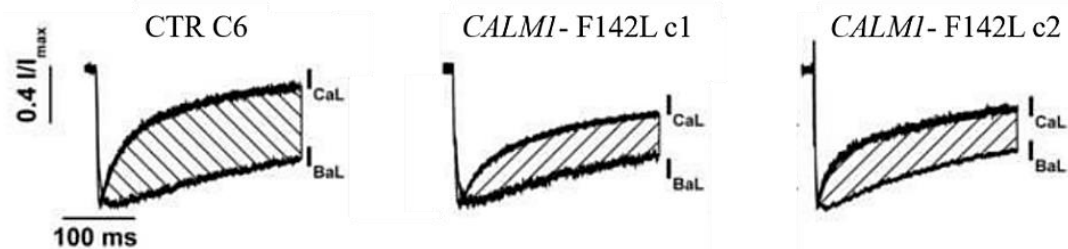


Figure 22:  $I_{CaL}$  and  $I_{BaL}$  tracings.

$I_{CaL}$  and  $I_{BaL}$  tracings of ctr C6 CM, *CALMI*-F142L clone 1 CMs and *CALMI*-F142L clone 2 CMs of 2.5 months age. Tracings for  $I_{CaL}$  and  $I_{BaL}$  were recorded at 0 mV within the same cell. Traces were normalized for their peak value. Dashed area represents CDI and was measured as the difference between  $I_{BaL}$  and  $I_{CaL}$ . Figure and figure legend adapted from Rochetti *et al.*<sup>133</sup>.

$I_{CaL}$  and  $I_{BaL}$  traces were recorded at different test potentials, normalised for their peak value and CDI estimated as dashed area between  $I_{CaL}$  and  $I_{BaL}$  curves. Current remaining at 100 ms ( $r_{100}$ ) and 300 ms ( $r_{300}$ ) was plotted as a function of the test potential (Figure 23). Higher  $r_{100}$  and  $r_{300}$  values for both mutant clones compared to ctr values indicate

slower  $I_{CaL}$  inactivation, due to weaker CDI. The longer sustained  $I_{CaL}$  due to the positively shifted and incomplete inactivation converge to a sustained  $I_{CaL}$  component in mutant hiPSC- derived CMs <sup>133</sup>.

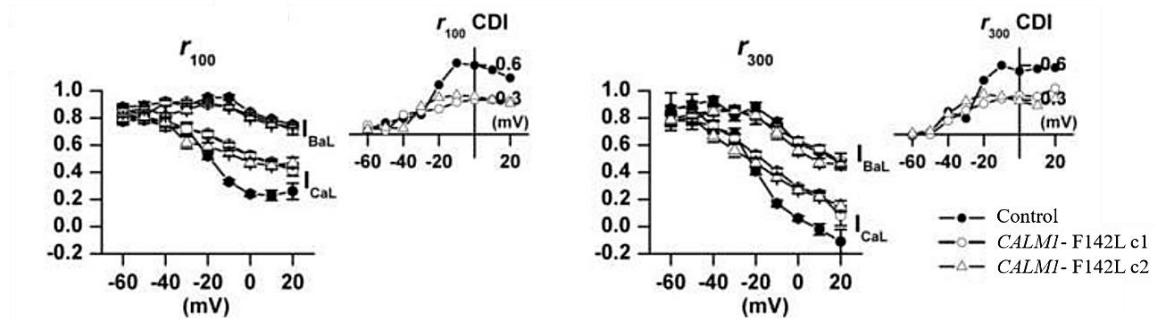


Figure 23: Remaining peaks of  $I_{CaL}$  and  $I_{BaL}$  at 100 ms and 300 ms and their proportions.

“Proportion of peak  $I_{CaL}$  and  $I_{BaL}$  remaining at 100 ms ( $r_{100}$ ) and 300 ms ( $r_{300}$ ), plotted as the function of the test potential. The insets show CDI as a function of test potential” <sup>133</sup>. Figure adapted from Rochetti *et al.* <sup>133</sup>.

Sample tracings at -80 mV and -50 mV interpulse potentials were recorded up to 6000 ms, as depicted in Figure 24 A. Panel B shows the recovery time course for total  $I_{CaL}$  at -80 mV and -50 mV. At short diastolic intervals, a larger proportion of total  $I_{CaL}$  was available in mutant CMs. This stands in concurrence with the observed defective CDI in patients’ hiPSC- derived CMs <sup>133</sup>. Panel C shows the recovery kinetics of the inactivating component alone. Here, no difference in recovery kinetics between ctr C6 and *CALMI-F142L* CMs was detected. At -80 mV, the recovery is observed to be faster and the non-inactivating component is smaller than at -50 mV <sup>133</sup>.

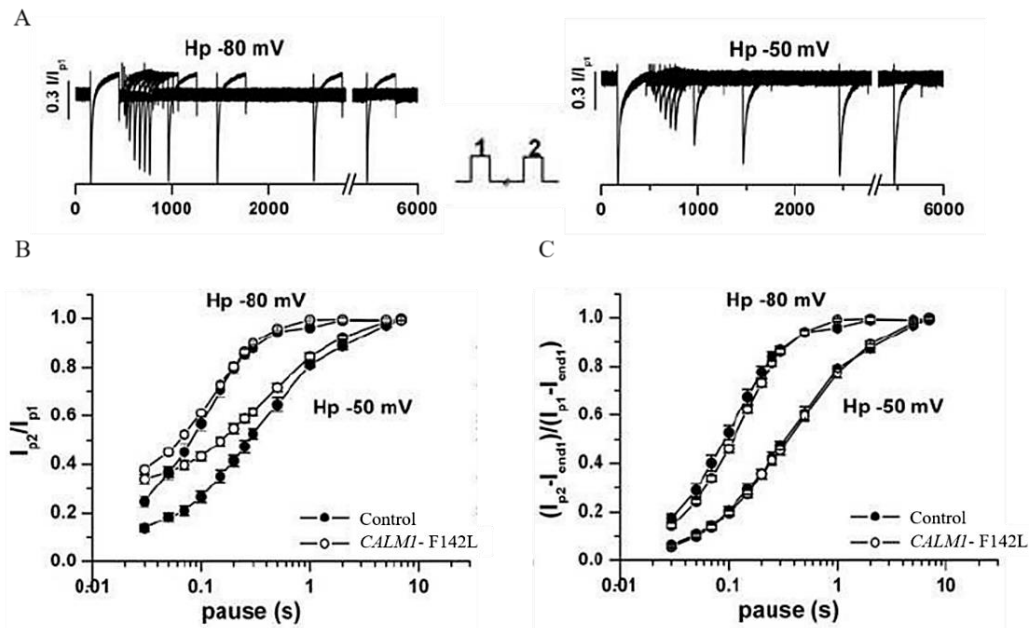


Figure 24:  $I_{CaL}$  inactivation recovery.

Recovery of inactivation was measured at interpulse potentials of -80 and -50 mV. (A) tracings of samples at -80 mV and -50 mV, protocol in the inset. (B) recovery of total  $I_{CaL}$ . (C) analysis of the recovery of the inactivating component. Ctr C6 CMs displayed with filled dots ( $n \geq 9$ ), CALMI-F142L CMs displayed as open dots (clones 1 and 2 pooled) ( $n \geq 10$ ), figure and figure legend adapted from Rochetti *et al.*<sup>133</sup>.

#### *Electrical activity of cardiac bodies*

Field potentials were recorded from spontaneously beating cardiac bodies (CBs) of ctr C6 and CALMI-F142L hiPSCs to mimic tissue environment. Analysis was performed at baseline conditions and under  $\beta$ -adrenergic stimulation by isoproterenol. Effects of Iso were analysed at concentrations ranging from 0.05 to 1.6  $\mu\text{M}$ <sup>133</sup>. Figure 25 A depicts representative field potentials from ctr C6 (top) and CALMI-F142L (bottom) CBs. QT and RR intervals were analysed, statistic shown in Figure 25 B. Clearly visible are the prolonged RR and QT intervals of CBs from CALMI-F142L patient hiPSCs compared to ctr C6. QT was estimated to be at around 1.5 s for mutant CBs and around 0.5 s for ctr CBs. This demonstrates a statistically significant result with  $p < 0.05$ . RR intervals were estimated at around 8 in mutant CBs and at around 2 in C6 ctr CBs, hence also being statistically relevant prolonged<sup>133</sup>.

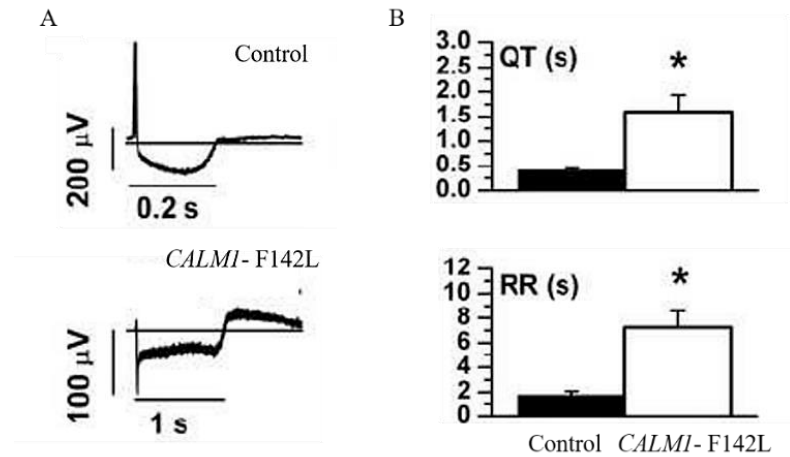


Figure 25: Field potentials and statistics for QT and RR intervals in CBs.

(A) Examples of field potentials from ctr C6 (top) and *CALMI*-F142L 2.5 months old CBs (bottom). (B) Statistics for QT and RR intervals under basal conditions. ctr C6 in black bars ( $n=18$ ), *CALMI*-F142L in white bars ( $n=8$ ). Figure and figure legend adapted from Rochetti *et al.*<sup>133</sup>.

Plotting the relation between RR and QT intervals by linear fitting shows a steeper function for *CALMI*-F142L CBs than for C6 CBs, as depicted in Figure 26 A<sup>133</sup>. The slope for the mutant line is  $0.22 \pm 0.05$  and for C6 CBs  $0.09 \pm 0.02$ . These values are of statistical significance at  $p < 0.05$ , as depicted in panel B<sup>133</sup>.

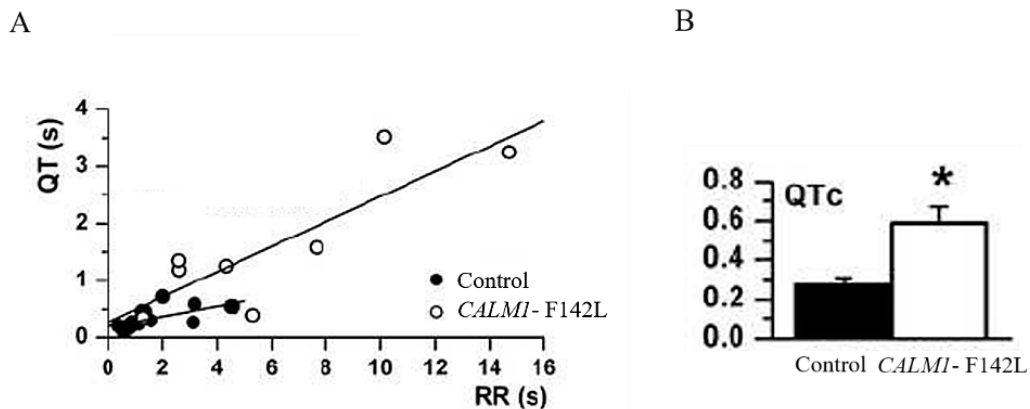


Figure 26: QT- RR relationship.

(A) QT- RR relationship of ctr C6 and *CALMI*-F142L in 2.5 months old CBs. Ctr C6 CM displayed with filled dots, *CALMI*-F142L CM displayed as open dots. (B) QTc statistics,  $*p < 0.05$ . Black bar represents ctr C6, white bar represents *CALMI*-F142L. Figure and figure legend adapted from Rochetti *et al.*<sup>133</sup>.

The effect of the  $\beta$ -adrenoreceptor agonist Isoproterenol on QT and RR intervals in mutant and ctr CBs was evaluated at different concentrations and displayed as function, as shown in Figure 27. Panel A shows effects of Iso on 2.5 months old CBs. Iso concentrations tested range from 0 to  $1.6 \mu\text{M}$ . The effect of Iso on QT and RR reached saturation at  $0.05 \mu\text{M}$ . QT and RR remained larger in mutant CBs than in ctr C6 CBs<sup>133</sup>. The QT-

RR relationship is plotted and displayed in panel B of Figure 27. Clearly visible by plotting QT(s) (y- axis) versus RR(s) (x- axis) is the difference in steepness in *CALMI*- F142L CBs under Iso influence when compared to ctr C6. The QT/RR steepness in mutant CBs was calculated at  $0.49 \pm 0.07$  with  $p < 0.05$  vs -Iso, for C6 CBs at  $0.08 \pm 0.04$  and no statistical significance versus -Iso<sup>133</sup>. QT/RR steepness was therefore significantly increased under influence of Iso in *CALMI*- F142L CBs, but not in ctr C6 CBs.

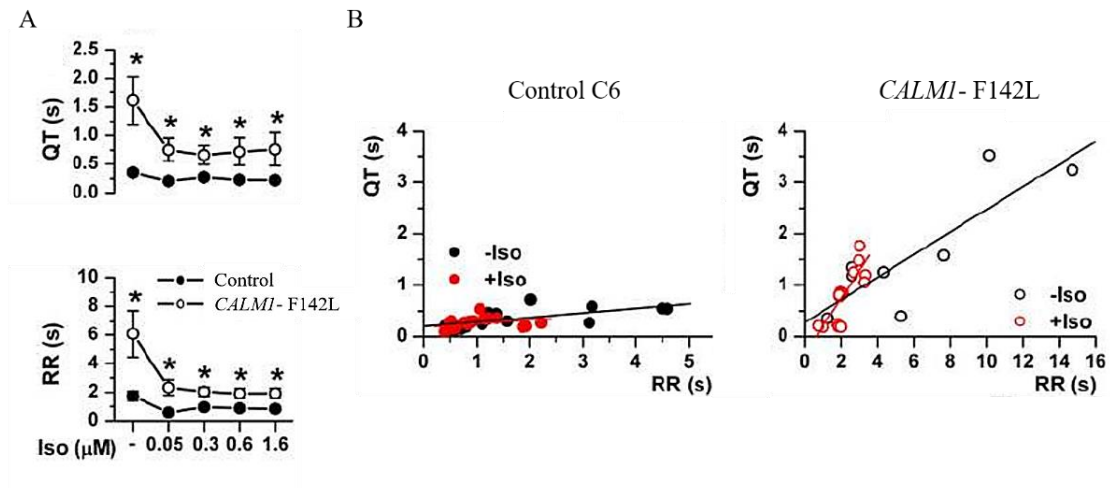


Figure 27: Modulations by isoproterenol.

(A) Effect of isoproterenol (Iso) on QT and RR.  $n = 5$  for all concentrations in both groups. Ctr C6 CMs displayed with filled dots, *CALMI*- F142L CMs displayed as open dots. (B) Plotted QT- RR relationships at increasing Iso concentrations from baseline (-Iso, black symbols) to 1.6  $\mu$ M Iso (+Iso, red symbols), in ctr C6 (left side) and *CALMI*- F142L (right side) 2.5 months old CBs. Figure and figure legend adapted from Rochetti *et al.*<sup>133</sup>.

#### Electrical activity in single hiPSC- derived CMs

APs were recorded in isolated hiPSC- derived CMs at different pacing rates during  $I_{K1}$  injection via Dynamic Clamp (DC), as shown in a representative graph in Figure 28 A<sup>133</sup>. Mature- like, ventricular AP traces were recorded under  $I_{K1}$  injections in *CALMI*- F142L and ctr C6 hiPSC- derived isolated CMs of 2.5 months age. Panel B displays AP duration values, calculated as APD<sub>50</sub> and APD<sub>90</sub>, at different pacing rates. CMs of *CALMI*- F142L hiPSC had significantly longer APDs under DC at all pacing rates below 3 Hz, when compared to ctr C6 CMs<sup>133</sup>. The  $E_{dias}$  values are similar for both lines with no significant differences.

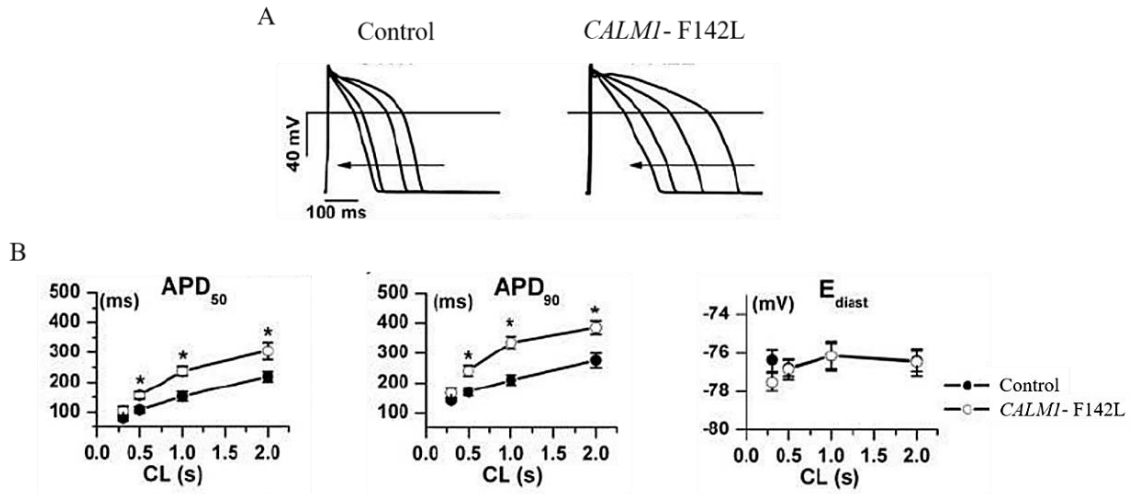


Figure 28: AP and APD statistics in isolated CMs.

(A) Representative APs under DC at different pacing rates. Arrows indicate the direction of rate increase. Left graph ctr C6 CMs, right graph *CALMI*-F142L CMs. (B) Statistics for APD<sub>50</sub> (left), APD<sub>90</sub> (center) and E<sub>diast</sub> (right) in 2.5 months old ctr C6 and *CALMI*-F142L CMs. Filled dots represent ctr values ( $n \geq 6$ ), open dots represent *CALMI*-F142L values ( $n \geq 10$ ). Figure and figure legend adapted from Rochetti *et al.*<sup>133</sup>.

Panel A of Figure 29 represents sequences of APs of ctr C6 (top) and *CALMI*-F142L (bottom) CMs at 3 Hz pacing. Prolongation of APs and failed response to pacing are visible in traces of *CALMI*-F142L CMs only. Statistical analysis of cells failing to follow pacing at 3 Hz is displayed in panel B. 10% of ctr C6 cells and 50% of *CALMI*-F142L cells did not follow pacing at 3 Hz, representing a statistically difference between lines with a p-value of  $p < 0.005$ . This is due to failure of adequate APD shortening<sup>133</sup>.

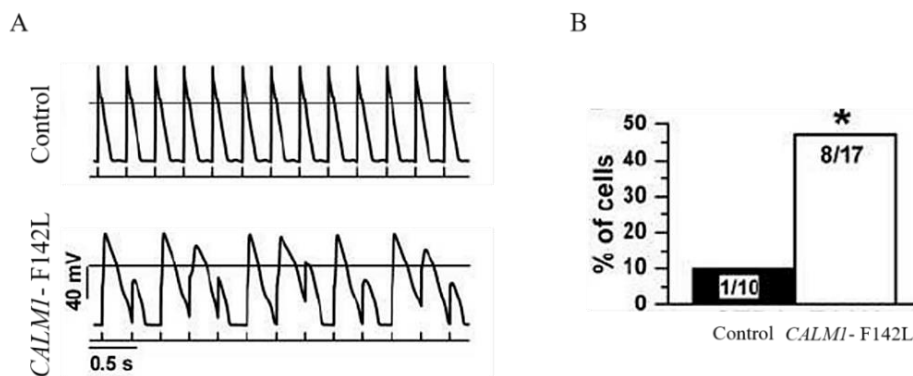


Figure 29: AP sequences and percentage of cells failing to follow pacing.

(A) Representative sequences of APs in 2.5 months old ctr C6 CMs (top) and *CALMI*-F142L CMs (bottom) evoked at 3 Hz. (B) Percentage of cells failing to follow pacing at 3 Hz. \* $p < 0.05$  vs ctr C6. Ctr values depicted in black bar, *CALMI*-F142L values depicted in white bar. Figure and figure legend adapted from Rochetti *et al.*<sup>133</sup>.

### Intracellular $Ca^{2+}$ handling and $Ca^{2+}$ dynamics

Since CaM is influencing  $Ca^{2+}$  dynamics in CMs by participating in intracellular  $Ca^{2+}$  regulation<sup>147</sup>, effects on Calcium handling in mutant CMs was evaluated. Figure 30 depicts analyses of intracellular  $Ca^{2+}$  dynamics. Representative traces of  $I_{CaL}$  (top) and  $Ca^{2+}$  transients (CaT, bottom) of 2.5 months of *CALMI*-F142L CMs versus ctr C6 CMs are shown in Panel A. An increased  $Ca^{2+}$  influx is observed in *CALMI*-F142L CMs, as well as larger  $Ca^{2+}$  transients. This is supported by the statistically relevant difference in CaT amplitude and  $Ca_L$  influx between *CALMI*-F142L CMs and C6 CMs, as depicted in panel B. No statistically relevant difference was detected in excitation- release (ER) gain between the two lines, and therefore no effect on SR  $Ca^{2+}$  content<sup>133</sup>.

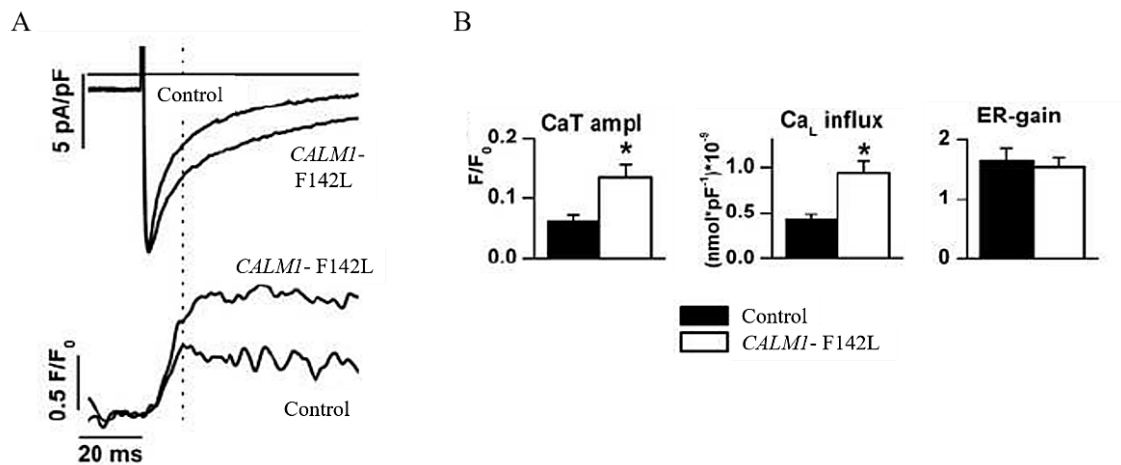


Figure 30:  $I_{CaL}$ ,  $Ca^{2+}$  transients and statistics of  $Ca^{2+}$  dynamics.

(A) Representative traces of  $I_{CaL}$  (top) and  $Ca^{2+}$  transients (CaT, bottom), voltage steps applied from -50 mV to 0 mV. Dotted line represents CaT peak,  $Ca_L$  was measured from  $I_{CaL}$  up to the CaT peak. (B) Amplitude of CaT,  $Ca_L$ , and their ratio in ctr C6 ( $n > 12$ ) and *CALMI*-F142L ( $n > 9$ ). Figure and figure legend adapted from Rochetti *et al.*<sup>133</sup>.

Addition of a caffeine pulse was used to measure SR  $Ca^{2+}$  content and NCX conductance. No differences in  $Ca_{SR}$   $Ca^{2+}$  decay kinetics, and NCX conductance were observed between *CALMI*-F142L CMs and C6 CMs, as shown in Figure 31<sup>133</sup>. Panel A shows representative traces of  $Ca^{2+}$  transients (top) and  $I_{NCX}$  current (bottom) induced by caffeine at -50 mV in ctr and *CALMI*-F142L CMs.  $I_{NCX}$  vs  $Ca^{2+}$  plots are displayed in panel B of this figure. The slope of this function was used to estimate the NCX “conductance”<sup>133</sup>. Results of SR content estimation (left) and slope estimation of  $I_{NCX}/Ca^{2+}$  relations (right) are depicted as bar graph in panel C. No statistical relevance was detected with  $*p < 0.05$  vs ctr C6.

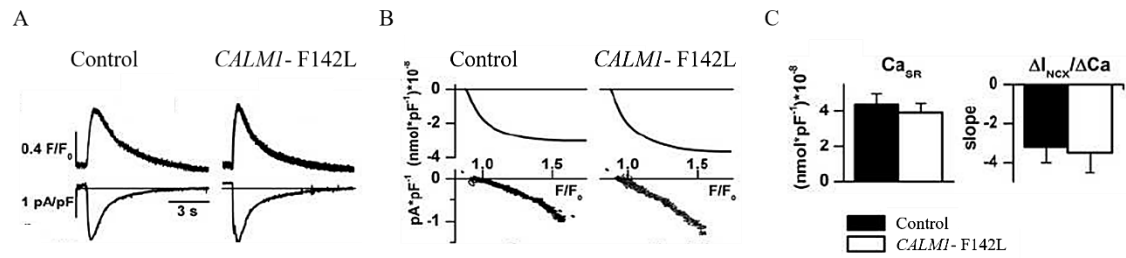


Figure 31:  $I_{NCX}$  measurements.

(A)  $Ca^{2+}$  and current ( $I_{NCX}$ ) transients induced by caffeine at -50 mV. (B) “Cumulative  $I_{NCX}$  integrals (top, used to estimate  $Ca_{SR}$ ) and plots of  $I_{NCX}$  vs  $Ca^{2+}$  (bottom, slope used to estimate NCX “conductance”)”<sup>133</sup>. (C)  $Ca_{SR}$  and  $I_{NCX}/Ca^{2+}$  slope relations in ctr C6 ( $n=12$ ) and *CALMI-F142L* ( $n=13$ ) CMs. \* $p < 0.05$  vs ctr C6. Figure and figure legend adapted from Rochetti *et al.*<sup>133</sup>.

### Rescue of the LQT phenotype with pharmacological measures

Sensitivity to the  $Ca^{2+}$  channel blocker verapamil was assessed in a dose-dependent manner in 2.5 months old *CALMI-F142L* CBs and compared to ctr C6 CBs of the same age by MEA recordings<sup>133</sup>. Sample tracings of *CALMI-F142L* CBs at verapamil concentrations of 150, 100 and 50 nM are depicted aligned on the x-axis in panel A of Figure 32. Effects on the field potential in a dose-dependent manner are visible. Statistical analysis of  $n=8$  measurements for 50 nM verapamil and  $n=4$  measurements for 100 nM verapamil on the QT shortening of *CALMI-F142L* CBs shows statistical relevance with  $p < 0.05$  vs baseline<sup>133</sup>. When compared to effects of verapamil at the same concentrations on ctr C6 CBs, a statistical relevant difference at 50 nM verapamil is detected only in *CALMI-F142L* CBs but not in ctr C6 CBs (Figure 32, panel B), suggesting that the mutation induces a sensitivity to repolarization to verapamil.

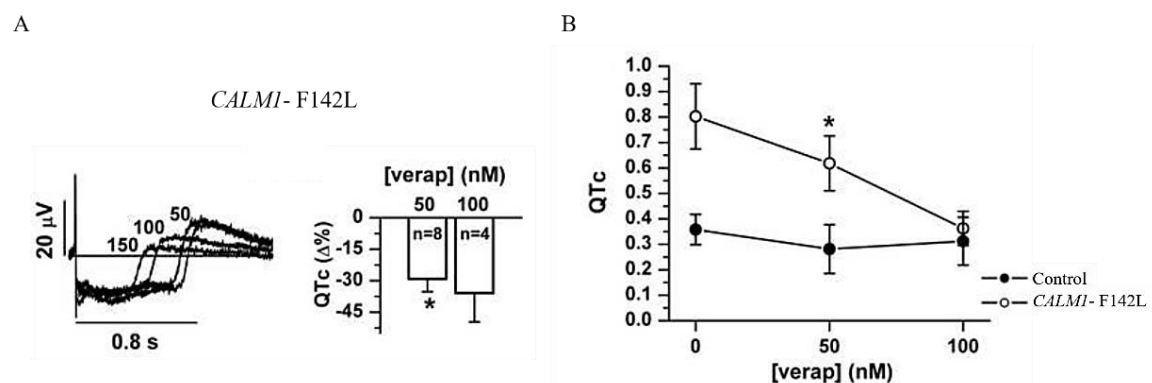


Figure 32: Effect of verapamil on the LQTS phenotype.

(A) Effect of verapamil in a dose-dependent manner on the field potential of a *CALMI-F142L* CBs. Numbers indicate various verapamil concentrations. Tracings are aligned on the time axis (left side). QTc shortening, expressed as  $\Delta\%$  from baseline, by verapamil at 50 and 10 nM (\* $p < 0.05$  vs baseline,  $n \geq 4$ ) (right side). (B) QTc and verapamil dose-dependency in ctr C6 ( $n \geq 5$ ) and *CALMI-F142L* 2.5 months old CBs. \* $p < 0.05$  vs baseline. Figure and figure legend adapted from Rochetti *et al.*<sup>133</sup>.

#### 4.4 Genome- editing of the *CALMI* locus

Differences in genetic background between unrelated ctr lines and the patient- derived hiPSC line can confound disease phenotypes, especially if investigated mutations cause only minor phenotypic alterations. The genome- editing technology enables the generation of isogenic ctr lines by correcting disease- causing mutations in patient hiPSCs. Abolishment of the disease phenotype after correction of the suspected causative mutation furthermore proves the mutation to cause the phenotype.

##### *Single- cell adaptation*

Prior to genome- editing approaches, hiPSCs need to be adapted to single- cell growth in order to be able to perform clonal analysis and expansion of targeted clones. Single- cell adaption was performed on *CALMI*- D130G and *CALMI*- F142L hiPSCs as described in chapter 3.2.3. Figure 33 shows representative images of single- cell adapted *CALMI*- D130G hiPSCs and *CALMI*- F142L hiPSCs on MEF feeders and in feeder free conditions on Geltrex. Single- cell adapted hiPSCs are able to grow colonies out of a single cell in a clonal manner. 1 day after splitting, small clonal colonies are visible. 5 days after splitting, colonies have become bigger and are ready to be split again. General morphology of single- cell adapted hiPSCs is rounder than hiPSCs growing in colonies. Cell- cell borders remain clearly visible even at higher confluency. Cells plated on Geltrex in feeder- free conditions remain growing as monolayer until a higher confluency is reached. Cells on Geltrex tend to become more differentiated and unstable after 15 passages of single- cell splitting. Cells on MEF feeders remain stable for longer passages.

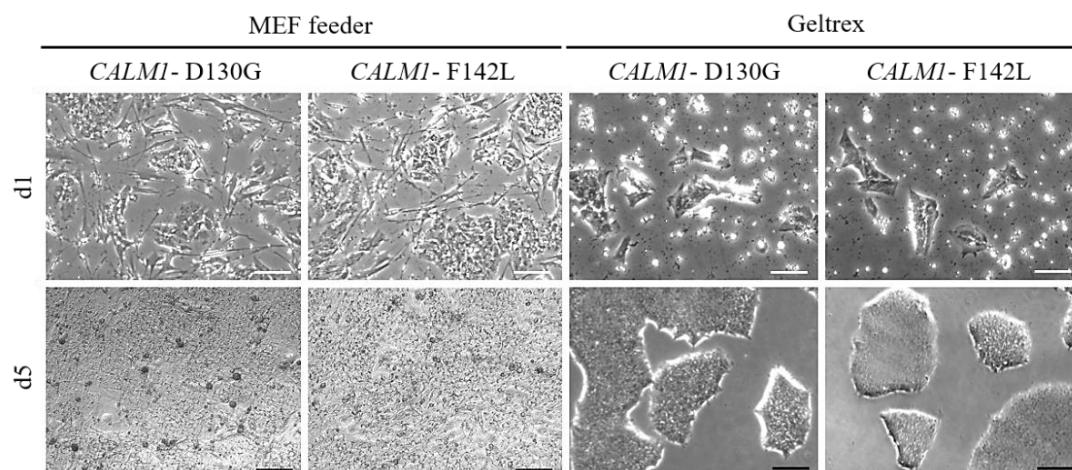


Figure 33: Representative PH images of single- cell adapted hiPSCs on MEF feeders and Geltrex, 1 day and 5 days after splitting.

Top row of images represent hiPSCs 1 day after single- cell splitting (d1), bottom row images of hiPSCs 5 days after single- cell splitting (5d). *CALMI*- D130G hiPSCs labeled as *CALMI*- D130G, *CALMI*- F142L hiPSCs as *CALMI*- F142L. Compared are cells growing on MEF feeders to cells growing on Geltrex. Top row images scale bar 50  $\mu\text{m}$ , bottom row images scale bar 250  $\mu\text{m}$ .

#### 4.4.1 *CALMI* genomic locus targeting by homologous recombination

Correction of the *CALMI*- F142L patient's mutation in hiPSCs *in vitro* was first endeavoured by the classical homologous recombination strategy, using the BAC recombineering approach. Figure 34 shows the strategy for targeted genomic correction of the *CALMI*- F142L mutation and *CALMI*- D130G mutation. A gene targeting vector was designed that included the wt A and C nts at *CALMI* c.A389 and c.C426. Either mutant patient hiPSC line can be targeted with this vector to correct the *CALMI* mutations. The linearized targeting construct was delivered into cells by electroporation. Targeted clones were identified by PCR- screening that amplified a novel junction fragment between the genomic DNA of exon 4 and the integrated targeting vector generated following homologous recombination. Primers a and b of Figure 34 are listed under ColScrShortFW and ColScrNeoRev in the primer list, as well as positive ctr primers c and d (PosCtrHomRecFW, PosCtrHomRecRV). The G418- resistance cassette can be excised by Cre recombinase transfection.

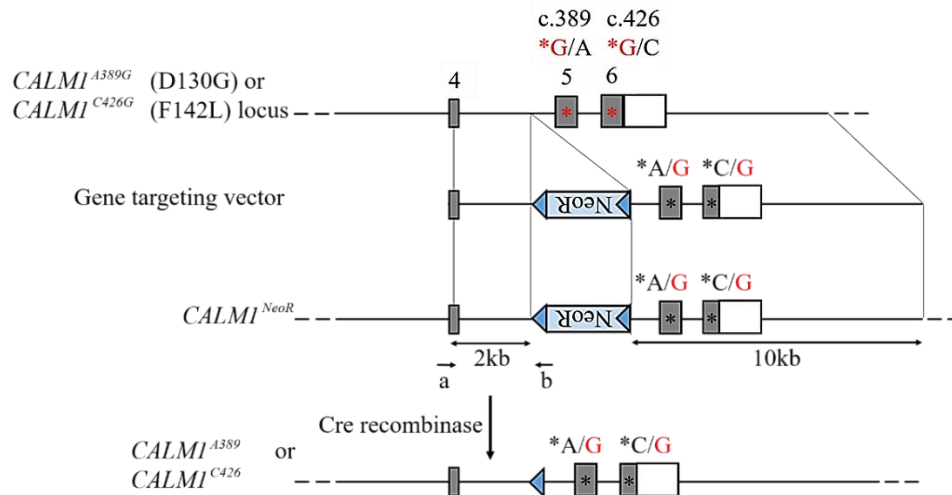


Figure 34: Gene targeting by homologous recombination in *CALMI* mutated hiPSCs.

Strategy for classical homologous recombination using target vector recombination at the *CALMI* locus. Top line, structure of *CALMI* locus. Numbered grey boxes indicate exons 4- 6. Exon 5 is mutated (red star) in *CALMI*- D130G patient hiPSCs by exchange of A to G at position c.389, exon 6 is mutated (red star) in *CALMI*- F142L patient hiPSCs by exchange of C to G at position c.426. Gene targeting vector for correcting both mutations has the wt A and C nts. NeoR, the PGK- Neo cassette encoding G418 resistance flanked by *loxP* sequences (blue triangles), was inserted in the reverse direction. PCR primers (a, b), amplifying a 2.8 kb sequence, were used to identify the targeted clone. PCR primers (c, d) were used as positive ctr. Gene targeting vector has homology arms of 2 kb (3' homology arm) and 10 kb (5' homology arm), indicated as arrows.

The homologous recombination approach was performed in parallel on cells on G418-resistant MEF feeders in hiPS medium and on Geltrex in E8 medium and targeted colonies were selected using G418 antibiotic selection. Figure 35 shows electroporated cells of the *CALMI*- F142L hiPSC lineage from 4 days after electroporation up to 2 days after antibiotic selection. Cells were electroporated in parallel with the targeting construct (*CALMI*- F142L targ.) and with no construct as negative ctr (*CALMI*- F142L mock). Emerging colonies are visible in pictures of all conditions. No colonies of cells electroporated under mock ctr conditions survived after antibiotic selection. Targeted cells on Geltrex grew faster than on MEF feeders. In total, from two experiments of each  $10 \times 10^6$  electroporated cells, 47 colonies emerged on Geltrex. From one experiment with  $10 \times 10^6$  electroporated cells that were plated on MEF feeders, 11 clones emerged. Recovery efficiency of hiPSCs on Geltrex was therefore better than of cells on G418 resistant MEF feeders.

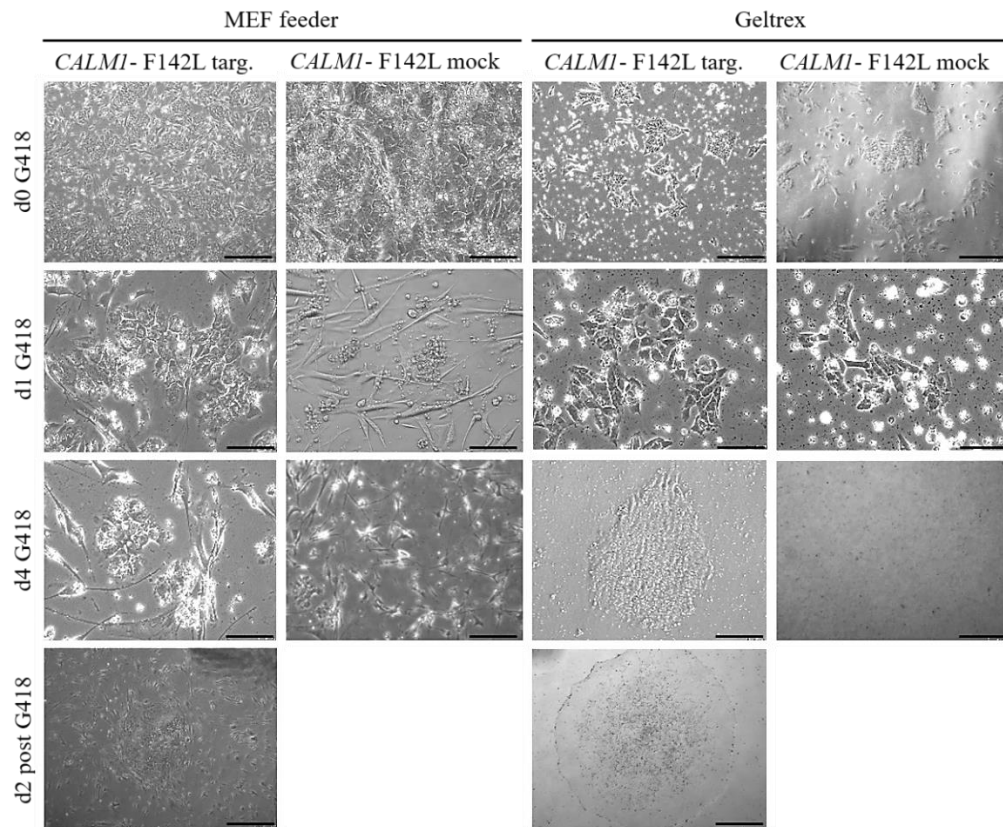


Figure 35: Electroporated *CALMI*- F142L hiPSCs with targeting construct and no construct on MEF feeders and Geltrex from d0 of G418 selection to d2 post- G418 selection.

Representative images of *CALMI*- F142L hiPSCs after electroporation with targeting construct (*CALMI*- F142L targ.) and after mock electroporation (*CALMI*- F142L mock), 2 days after electroporation (d0 G418), scale bars 250  $\mu$ m, 1 day into G418 selection (d1 G418), scale bars 50  $\mu$ m, 4 days into selection (d4 G418), scale bars 250  $\mu$ m, and 2 days post- selection (d2 post G418), scale bars 250 $\mu$ m. Left two lanes of pictures represent cells plated on MEF feeders, with the left side targeting construct- electroporated cells and the right lane negative ctr cells. Right half of the figure shows cells plated on Geltrex, left lane targeting construct electroporated, row of cells on the very left is the according mock electroporated negative ctr.

Picked colonies were split in separate wells and around 20 cells per colony were used for colony screening. PCR for specific amplification of the targeted *CALMI* genomic sequence was performed. Annealing positions of the primers used for identification of targeted clones, as well as positive ctr primers is indicated in Figure 34. PCR products were loaded on an agarose gel and analysed.

Figure 36 depicts a representative agarose gel picture of 2 *CALMI*- F142L clones picked from Geltrex after electroporation with targeting construct and G418 selection. No band of amplified DNA product is detectable on the gel in either of the lane. Since the Colony Screening primer for the homologous recombination approach were designed to only anneal if homologous recombination happened, this result is to be interpreted as negative for both clones. PCR amplification with positive ctr primers shows a band. This positive

ctr serves also as a ctr for DNA content in the lysates used. Lack of a band with negative ctr PCR sample confirms absence of DNA contamination in the PCR reagents. The faint and out of focus signal at around 0.1 kb represent primer dimers.

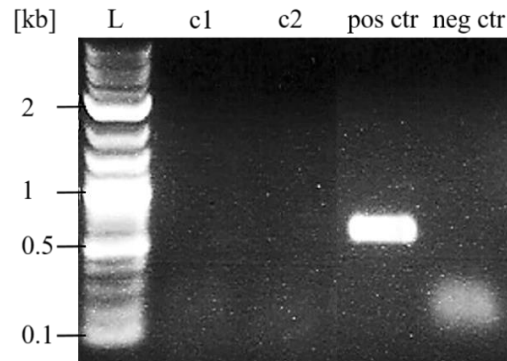


Figure 36: Representative colony screening agarose gel picture of 2 colonies recovered after electroporation and antibiotic selection.

2- log DNA ladder was used as ladder (L) in lane 1. Lane 2 shows PCR amplified lysate DNA of clone 1 (c1), lane 3 shows PCR amplified lysate DNA of clone 2 (c2). Lane 4 shows DNA lysate amplified with positive ctr primer (pos ctr), fifth lane shows negative ctr sample with no DNA input in the PCR reaction (neg ctr).

Three independent experiments were performed, out of which a total of 67 colonies were derived and screened for homologous recombination. All derived clones were tested negative. The promising new gene targeting method CRISPR/ Cas9 was subsequently pursued.

#### 4.4.2 Genome- editing in *CALMI*- hiPSCs using CRISPR/ Cas9

##### 4.4.2.1 *CALMI* mutation correction

Genome- editing by CRISPR/ Cas9 requires the target cell to express the Cas9 endonuclease protein, as well as the gRNA. The gRNA forms a complex with the Cas9 protein and binds to the homologous region, enabling the Cas9 endonuclease to perform a DSB at the point of interest. By providing a homologous repair template, the cell repairs the DSB by HDR using the template. Figure 37 gives an overview of Cas9/ gRNA- mediated gene correction on the *CALMI*- F142L locus. The first panel shows a schematic of the Cas9/ gRNA complex annealing to the target *CALMI*- F142L locus. c.C426G mutation is written in green. The gRNA binds to the DNA target sequence and Cas9 induces the DSB 3 nt upstream of the PAM. The required PAM motif NGG is produced by the c.C426G mutation, therefore the *CALMI*- F142L correction gRNA is allele- specific for the mutated allele and will not bind the target sequence of the healthy allele. Panel B of

the figure displays the HDR repair pathway provoked by DSB and presence of a ssODN repair template. ssODN repair templates can be designed to specific needs. For this mutation- correction approach, the corrections of the point mutations for each patient were included, as well as restriction enzyme cutting sites to enable fast screening of successfully gene edited clones.

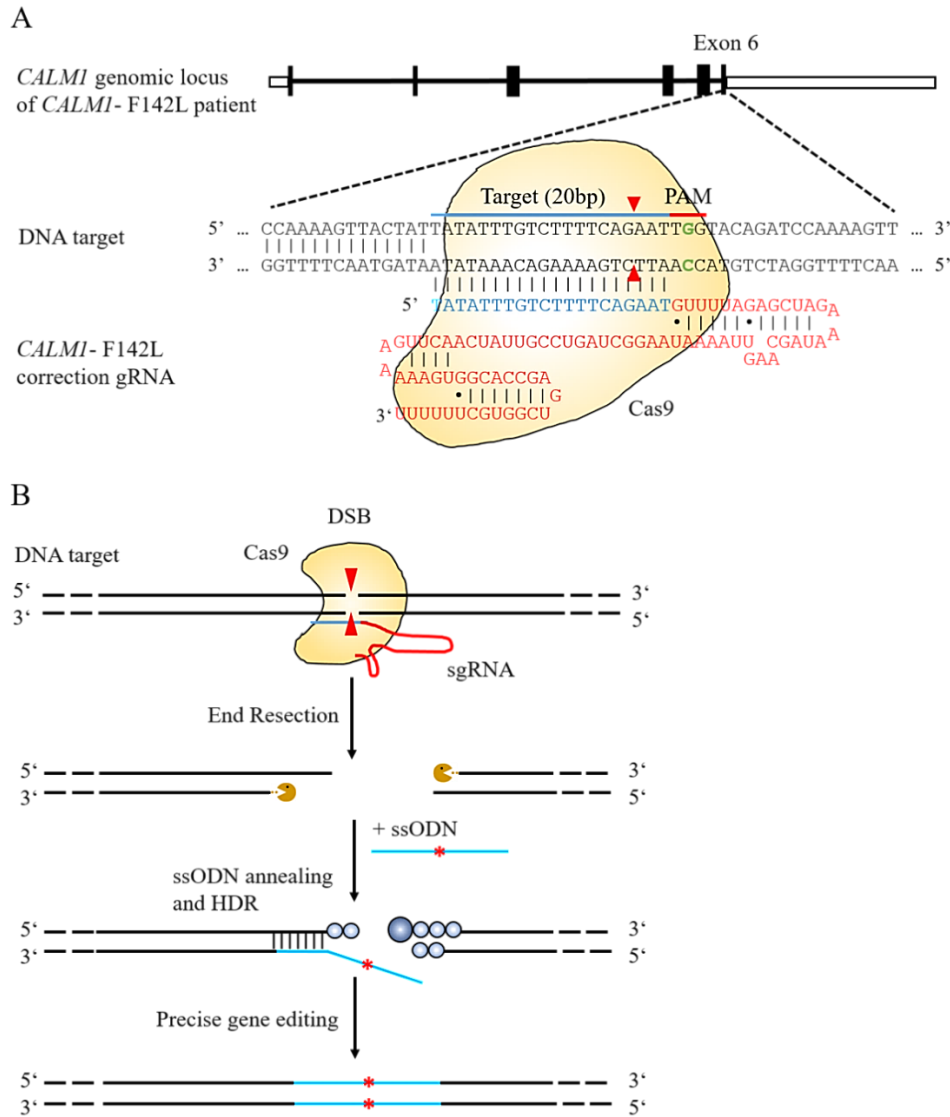


Figure 37: Schematic of Cas9/ gRNA- mediated gene correction of the *CALMI*- F142L mutation.

(A) Schematic of the Cas9/ gRNA complex annealing to the DNA target within *CALMI*, exon 6. 20 nt guide sequence of *CALMI*- F142L correction gRNA displayed in blue, gRNA scaffold in red. Guide sequence binds to DNA target sequence (blue bar on top strand), directly upstream of PAM motif (red bar). Cas9 protein (in yellow) mediates DSB 3 bp upstream of the PAM sequence (red arrows). F142L point mutation depicted in green within the PAM sequence. (B) DSB (red arrows) induced by Cas9 endonuclease (yellow) and guided by gRNA (red and blue) at DNA target sequence. After end resection of cut DNA strands, a supplied ssODN repair template (blue) is used for HDR. Precise gene modifications (red star) can be included by ssODN design, which will then be integrated in the genomic DNA upon DNA repair. Figure adapted from Ran *et al.* <sup>69</sup>.

120 bp sequences of ssODNs were designed for each patient, as depicted in Figure 38. Panel A shows 120 bp ssODN for *CALMI*- D130G correction. The nt exchange to abolish the point mutation is written in red. Green letter marks the alteration made in the sequence, generating the EcoRV restriction cutting site without changing the aa sequence of the gene. Panel B shows the ssODN design for correction of the F142L mutation. Red cytosine marks position of the patient's point mutation. An exchange from A to T was made to generate the XmnI restriction recognition site, this change doesn't alter the aa sequence of the gene.

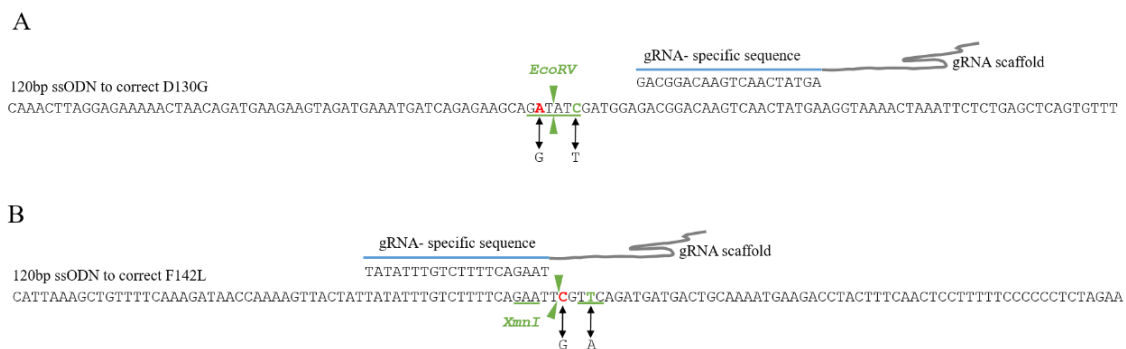


Figure 38: gRNA sequences and ssODN sequences for *CALMI*- D130G and *CALMI*- F142L corrections.

(A) 120 bp ssODN for correction of D130G mutation. c.A389G mutation in red. Change of nt from T to C, generating the EcoRV restriction enzyme cutting site written in green. EcoRV restriction recognition sequence (GATATC) underlined in green. (B) 120 bp ssODN for correction of F142L mutation. c.C426G mutation in red. Change of nt from A to T, generating the XmnI restriction enzyme cutting site written in green. XmnI restriction recognition sequence (GAANNNTTC) underlined in green.

gRNAs need to be tested for efficient guidance and induction of DSBs by Cas9 at the point of interest, since online design tools only provide computational predictions of efficiency. Chromatin structure and secondary structure of gRNAs can also greatly influence accessibility of the DNA by the CRISPR/ Cas9 complex. Delivery methods of plasmids encoding Cas9 and gRNAs need to be optimised for every hiPSC line separately, as well. Cell cycle length, level of pluripotency and passage number of hiPSCs influence delivery efficiency, cleavage efficiency and cell survival.

### Testing of gRNA efficiencies

gRNAs to target genomic locus c.A39G in *CALMI*- D130G patient hiPSCs and gRNAs to target genomic locus c.C426G in *CALMI*- F142L patient hiPSCs were designed as described in methods section 3.3.6 and the most promising gRNA was each cloned into the Addgene gRNA delivery vector backbone. Sequences of designed and cloned gRNAs are listed under 3.6. To test gRNA efficiency and functionality, the gRNA expression

plasmid was co- transfected together with the Cas9 nuclease plasmid (2- plasmid system) in hiPSCs. Cells were harvested 24h later and cleavage detection analysis was performed.

100 ng of input DNA of each sample was digested using the detection enzyme and analysed on a 1.5% agarose gel, as shown in Figure 39. Cleavage detection primers for *CALMI* correction guides were designed to amplify a 542 bp stretch of genomic DNA around the point of indels. Primers are used for both mutant lines, with expected cleaved bands at 149 bp and 393 bp for *CALMI*- D130G gRNA and at 183 bp and 360 bp for *CALMI*- F142L gRNA. Analysis of cleaved band intensities was performed using ImageJ, according to the manufacturer's manual. Estimated cleavage efficiency (CE) of *CALMI*- D130G gRNA is 88%, of *CALMI*- F142L gRNA 37% and the ctr hybrid DNA included in the Genomic Cleavage Detection Kit is cleaved with an efficiency of 83%. Both gRNAs designed are working in appropriate efficiencies and were used subsequently in genome- editing experiments.

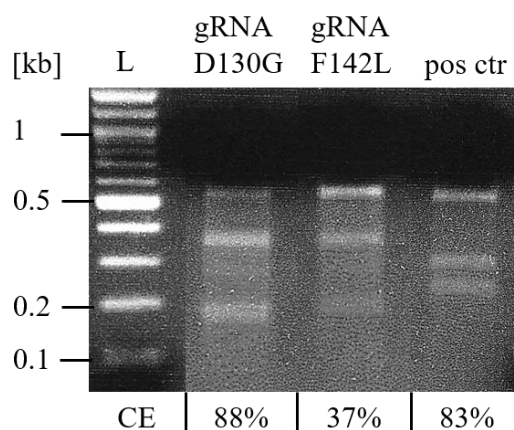


Figure 39: Cleavage detection analysis of correction gRNAs in mutant hiPSCs.

1.5% Agarose Gel detecting cleaved bands by Genomic Cleavage Detection Kit of Cas9 nuclease plasmid and correction gRNA plasmids for *CALMI*- D130G (gRNA D130G) and *CALMI*- F142L (gRNA F142L). From left to right: 2- log DNA ladder (L), *CALMI*- D130G hiPSCs incubated with correction gRNA D130G (gRNA D130G), *CALMI*- F142L hiPSCs incubated with correction gRNA F142L (gRNA F142L), positive ctr sample (pos ctr). Cleavage efficiencies (CE) in percent of each Cas9/ gRNA complex listed below.

#### *Double plasmid approach versus all- in one plasmid approach*

DNA load, and therefore also number of plasmids that need to be delivered into cell nuclei, is an important aspect to consider for successful genome- editing. High DNA concentrations have toxic effects on hiPSCs and are to be averted. Delivery efficiency drops significantly by increasing numbers of plasmids needed to be brought into cell nuclei. The gRNA cloning vector #41824 from Addgene was cloned into the CRISPR/ Cas9 plasmid #44719 from Addgene. Genomic Cleavage detection analysis was performed

subsequently and cleavage efficiencies were evaluated for all- in one plasmids for each patient's gRNAs. Calculated cleavage efficiency (CE) is 61% using the all- in one Cas9 correction gRNA D130G plasmid. This is a decrease in cleavage efficiency compared to the 2 plasmids approach, shown in Figure 39. *CALMI*- F142L hiPSCs targeted by all- in one Cas9 correction gRNA F142L plasmid shows cleavage efficiency of 53%. Here, the all- in one plasmid to target the F142L mutation is more efficient than the 2 plasmids with the same gRNA. The same ctr was used as in Figure 39. Since cleavage efficiencies for both all- in one plasmids were calculated to be over 50%, the following genome- editing experiments performed were done using the CRISPR/ Cas9 all- in one plasmids.

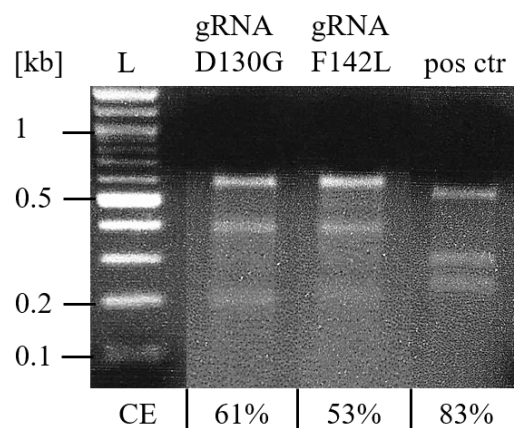


Figure 40: Cleavage detection analysis of correction gRNAs in all- in one Cas9 plasmids.

1.5% Agarose Gel detecting cleaved bands by Genomic Cleavage Detection Kit of Cas9 all- in one nuclease plasmids for *CALMI*- D130G (gRNA D130G) and *CALMI*- F142L (gRNA F142L). From left to right: 2-log DNA ladder (L), *CALMI*- D130G hiPSCs incubated with correction gRNA D130G (gRNA D130G), *CALMI*- F142L hiPSCs incubated with correction gRNA F142L (gRNA F142L), positive ctr sample (pos ctr). Cleavage efficiencies (CE) in percent of each Cas9/ gRNA complex listed below.

#### *Delivery of Cas9/ gRNA plasmid by electroporation and selection of transduced cells by FACS sorting*

Delivery of Cas9/ gRNA plasmids was first performed by electroporation, as described in methods section 3.2.7. Cas9/ gRNA plasmids used for *CALMI* mutation correction are carrying a GFP encoding gene, therefore, successful delivery of plasmids into hiPSCs can be analysed by FACS.

Amount of hiPSCs expressing the Cas9/ gRNA GFP plasmid was assessed 24h and 48h after electroporation, to determine the optimal time point for FACS sorting. To further validate functionality of all- in one Cas9 gRNA plasmids, the identical electroporation experiments were performed in parallel with all- in one Cas9 plasmids, as well as with the separate plasmids encoding Cas9 and gRNAs. Figure 41 shows representative FACS blots of *CALMI*- D130G hiPSCs 24h after electroporation. Shown are cells electroporated

with a negative ctr plasmid, versus D130G- patient hiPSCs electroporated with the *CALMI*- D130G all- in one plasmid and F142L- patient hiPSCs electroporated with the *CALMI*- F142L all- in one plasmid. Cell populations were first gated for size and single-cell status. Cells emitting auto- fluorescence measured in the FL10 channel were disregarded, as they represent dead cells. Cells within gate C were considered true GFP+.

The mock electroporated sample does not include GFP+ cells. GFP+ *CALMI*- D130G cells and GFP+ *CALMI*- F142L cells make up approximately 5.99% and 1.09% of all gated cells. Identical experiments were performed for *CALMI*- D130G and *CALMI*- F142L with 2 separate plasmids encoding the Cas9 and the gRNA. GFP+ populations were determined each 24h of post- electroporation, as well as 48h post electroporation.

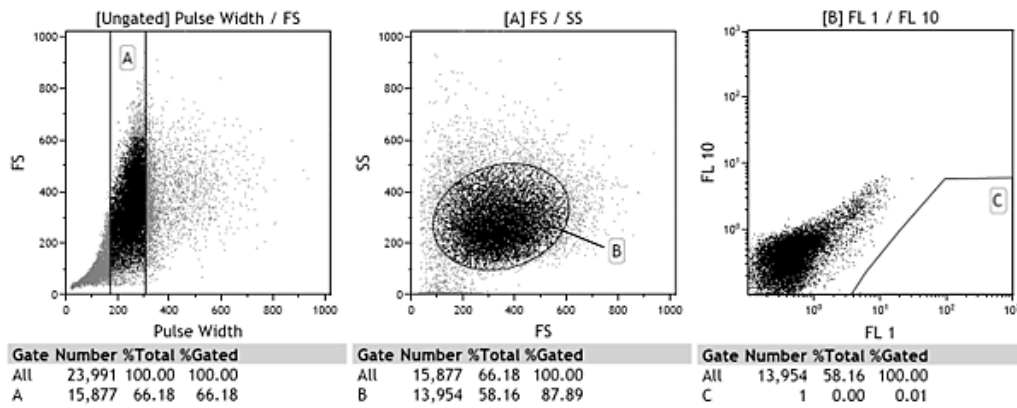
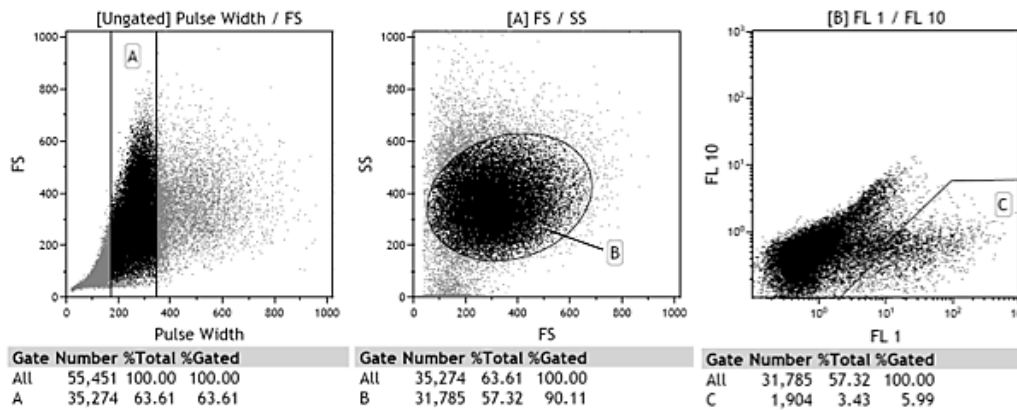
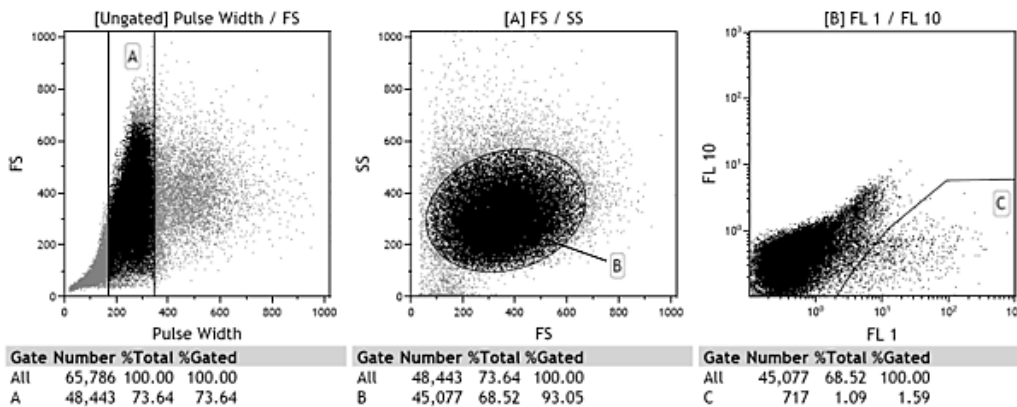
*CALMI*- D130G hiPSC negative control 24 hours*CALMI*- D130G all- in one Cas9 nuklease 24 hours*CALMI*- F142L all- in one Cas9 nuklease 24 hours

Figure 41: Representative FACS analysis of *CALMI*- D130G hiPSCs and *CALMI*- F142L hiPSCs 24h after electroporation with Cas9 all- in one plasmids.

First gating shows selection of cells by their size in forward scatter (FS) and pulse width (gate A). Second gating was set within the size- selected cells measured in the forward scatter (FS) and sideward scatter (SS) on a linear scale (gate B). Following gate C was set for FL1 positive cells, translating to GFP+ cells at 488 nm emission, versus FL10 positive cells, for auto- fluorescent cells appearing in the PE channel. GFP+/PE- cells from gate C were sorted and plated for further analysis. Upper row of plots depicts *CALMI*- D130G hiPSCs negative ctr after 24h, middle row depicts *CALMI*- D130G hiPSCs treated with Cas9 all- in one nuclease plasmid 24h after electroporation, last row depicts *CALMI*- F142L hiPSCs treated with Cas9 all- in one nuclease plasmid 24h after electroporation.

Figure 42 compares the percentage of GFP+ cell populations in both mutant lines 24h and 48h after electroporation, using Cas9/ gRNA all- in one plasmids and the 2 plasmid- system. After 24h, 3.5% of the total cell population was detected GFP+ after treatment with the Cas9/ gRNA *CALMI*- D130G all- in one plasmid. 6.1% of cells were detected GFP+ with both separate plasmids penetrated. After 48h, 8.1% of cells showed GFP+ signal, expressing the all- in one plasmid. 6.9% were estimated to GFP+ 48h after electroporation with both separate plasmids. The biggest GFP+ population of cells is therefore achieved, when electroporated with the all- in one plasmid and sorted 48h after electroporation for the *CALMI*- D130G cell line. 3% of total cells were measured GFP+ 24h after electroporation when targeted with the Cas9/ gRNA *CALMI*- F142L all- in one plasmid. Due to cell quality issues, the analysis of *CALMI*- F142L hiPSCs 24h after electroporation with both separate plasmids was not feasible. 48h after electroporation, 4.9% of cells electroporated with the all- in one plasmid was detected GFP+, 0.7% of cells electroporated with both separate plasmids were counted. Most promising conditions for *CALMI*- F142L hiPSC were therefore determined to be electroporation with *CALMI*- F142L all- in one plasmid and subsequent sorting 48h after delivery of the plasmid.

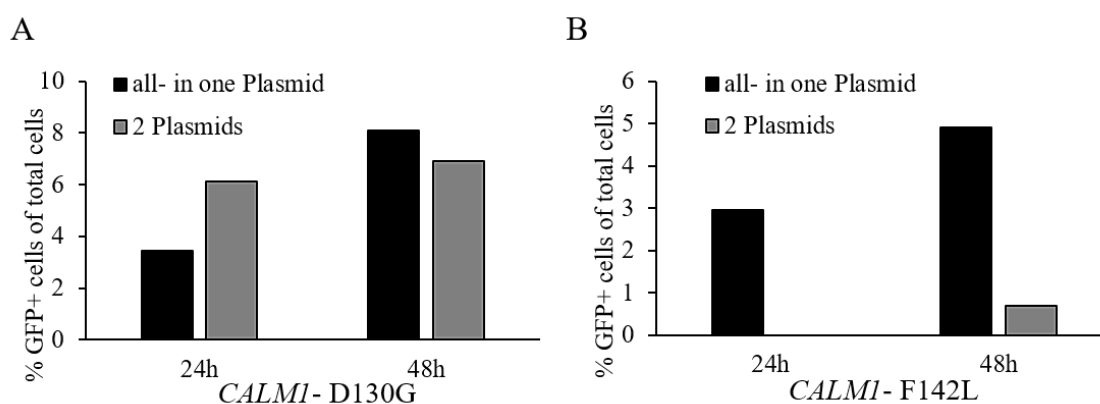


Figure 42: Percentage of GFP+ cells 24h and 48h after electroporation under different conditions.

*CALMI*- D130G hiPSCs electroporated with Cas9/ gRNA all- in one plasmid (black bars) and separate Cas9 and gRNA expressing plasmids (grey bars). Left side represents % of total cells 24h after electroporation, right side 48h after electroporation. (B) *CALMI*- F142L hiPSCs electroporated with Cas9/ gRNA all- in one plasmid (black bars) and separate Cas9 and gRNA expressing plasmids (grey bars). Left side represents % of total cells 24h after electroporation, right side 48h after electroporation.  $n= 1$  for all experiments.

Recovery of hiPSCs after FACS sorting is an important aspect when optimising the genome- editing efficiency. Different plating conditions were evaluated and compared to each other by calculating the recovery efficiency. Recovery efficiency was calculated by counting the number of single- cell emerged colonies in relation to total number of GFP+

single cells plated after FACS sorting. Recovery efficiency is displayed as % of amount of plated cells. Figure 43 shows recovery efficiencies of patient hiPSC lines, when plated as single cells per well into 96- well plates coated with MEF feeders in comparison to 6 cm cell culture plates coated with MEF feeders. *CALMI*- D130G cells showed a recovery efficiency of 4.4% when plated on 96- well plates and of 2.5% when plated on 6 cm plates. These results are not statistically significant. *CALMI*- F142L hiPSCs plated on 96- well MEF plates after FACS sorting showed an average recovery efficiency of 8.8%. Recovery efficiency on 6 cm MEF plates was determined at 0.1%. Due to the higher deviation of experiments, there is no statistical significance of recovery efficiency between the plating types for *CALMI*- F142L. Both mutant cell lines show better recovery efficiencies when plated on 96- well MEF plates after FACS sorting.

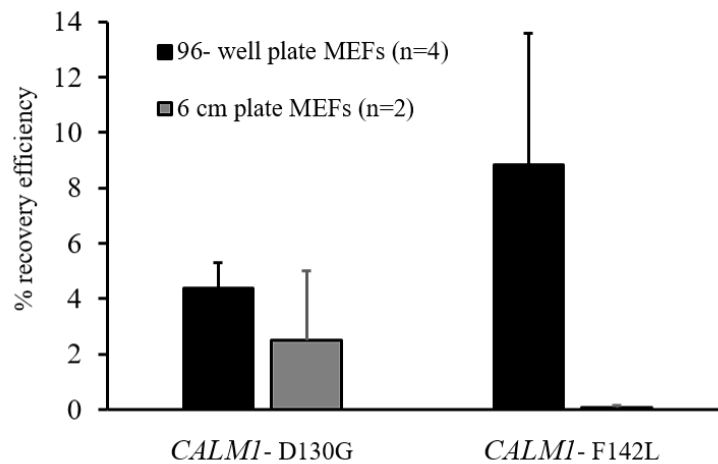


Figure 43: Percentage of recovery efficiency after FACS sorting on 96- well MEF vs 6 cm MEF cell culture plates.

% recovery efficiency counted as number of colonies emerging in relation to number of single cells plated after FACS sorting on 96- well plates with MEF feeders (black bars) versus 6 cm cell culture dishes with MEF feeders (grey bars) for *CALMI*- D130G and *CALMI*- F142L cell lines.  $n = 4$  for FACS sorting on 96- well MEF plates,  $n = 2$  for FACS sorting on 6 cm MEF plates. 2- sided T-test showed no statistical significance.

To elucidate possible positive effects on recovery efficiency further, efficiencies were analysed when plated on Matrigel- coated 96- well cell culture plates. This experiment was only performed with hiPSCs of the *CALMI*- F142L line, since the focus of this study was put on this line. Average recovery efficiency of *CALMI*- F142L hiPSCs plated on 96- well Matrigel plates of 2 independent experiments was 5.8%. Therefore, plating single cell hiPSCs on 96- well MEF coated plates is the most efficient, at 8.8%, as shown in the previous paragraph. No statistical significance was calculated between the two plating conditions.

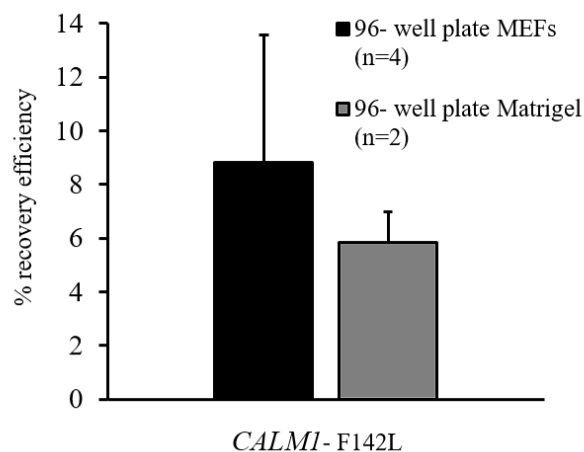


Figure 44: Percentage of recovery efficiency after FACS sorting on 96-well MEF vs 96-well Geltrex plates.

% recovery efficiency counted as number of colonies emerging in relation to number of single cells plated after FACS sorting on 96-well plates with MEF feeders (black bar) versus 96-well plates coated with Matrigel (grey bar) for *CALMI*-F142L hiPSCs.  $n=4$  for FACS sorting on 96-well MEF plates,  $n=2$  for FACS sorting on 96-well Matrigel plates. 2-sided T-test shows no statistical significance.

*CALMI* correction approaches by CRISPR/ Cas9 was performed under optimised conditions. Experiments were performed with single-cell adapted cells that underwent electroporation with all-in-one plasmids including tested gRNAs and 120 bp ssODN repair templates. 48h after electroporation, cells were sorted for GFP positivity and plated on 96-well plates coated with MEFs. Cell lysates were generated according to corresponding methods section 3.3.7. Genomic DNA was amplified using the RA\_CRISPR\_F and RA\_CRISPR\_R primer and products were digested with either EcoRV or XmnI restriction enzymes for clones derived from *CALMI*-D130G and *CALMI*-F142L targeted hiPSCs. Correction of mutations by HDR would incorporate designed enzyme restriction sites into the targeted loci, as well as the exchange of nt to correct the mutations. By digestion of amplified genomic loci with restriction enzymes, a cleaved band is visible if HDR occurred. Positive identified clones are then further analysed by Sanger sequencing. Positive ctr samples are amplified genomic DNA within the *CALMI* gene, naturally containing EcoRV or XmnI restriction cutting sites. This ctr serves as an enzymatic digestion ctr. Primers are listed under 3.6. Figure 45 shows representative screened clones of *CALMI*-D130G hiPSCs and *CALMI*-F142L hiPSCs. Expected bands after EcoRV digestion in corrected *CALMI*-D130G clones would show at 539 bp and 486 bp. Corrected *CALMI*-F142L clones would show bands at 695 bp and 330 bp in XmnI-digested samples. Positive ctr samples of *CALMI*-D130G and *CALMI*-F142L show expected bands at 592 bp and 580 bp, and 702 bp and 392 bp.

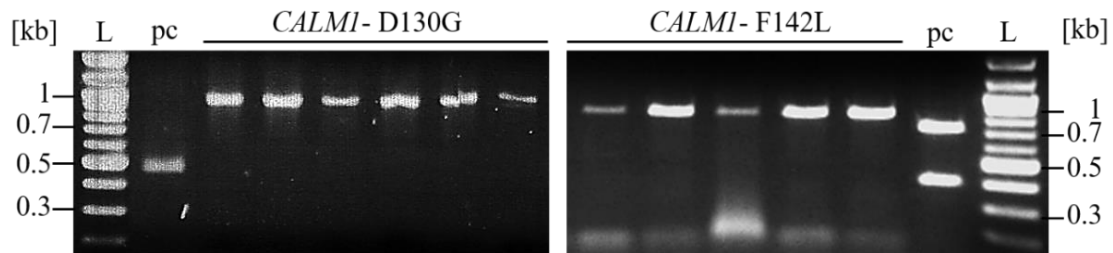


Figure 45: Representative colony screening agarose gel of *CALMI- D130G* and *CALMI- F142L* clones.

Colony screening agarose gel image of representative clones picked after targeting with either Cas9/ gRNA and ssODN template for mutation correction of the *CALMI- D130G* (left) and *CALMI- F142L* (right) hiPSC lines. L: 2- log DNA ladder, pc: according positive ctr sample for each line.

For correction of the *CALMI- D130G* mutation, a total of 4 independent experiments were performed. Overall were 228 single- cell- derived clones screened, but tested negative for correction of the mutation. These numbers conclude to a calculated average of 57 clones retrieved per experiment performed. 14 independent experiments were performed to correct the *CALMI- F142L* mutation. A total of 636 single- cell- derived clones were screened negative for correction. This translates to an average of 45.4 clones recovered per experiment. These numbers clearly indicate the inefficiency of correction experiments by electroporation and FACS sorting in hiPSCs. To further optimise conditions for genome- editing on hiPSCs, nucleofection as delivery method and puromycin selection as single- cell selection method was evaluated.

#### *Delivery of Cas9/ gRNA plasmid by nucleofection and selection of transduced cells by puromycin resistance*

Delivering Cas9/ gRNA plasmids into hiPSCs by electroporation showed a maximum of 8.1% GFP+ cells. After FACS sorting of GFP+ cells, recovery efficiencies of up to 8.8% were reached. To further optimise delivery and recovery efficiencies, nucleofection settings and selection of cells by antibiotic resistance was elucidated. A subset of buffers was first analysed for best delivery and recovery efficiency using a GFP ctr plasmid.

$0.8 \times 10^6$  *CALMI- F142L* hiPSCs were nucleofected in Buffer 1 or Buffer 2 of the Human Stem Cell Nucleofector Kit from Lonza and plated each into 2 wells of a Geltrex- coated 4- well plate. PH images were taken 24h later, as shown in Figure 46. Mutant hiPSCs nucleofected in buffer 1 are attached after 24h. Cell shape is elongated and cells are gathered loosely in groups of cells. Many dead cells are floating and dying cells show granulous cytoplasm. Cell morphology and distribution of cells nucleofected with Buffer 2 is similar to Buffer 1. Slightly more cells are attached and viable, less are dead and floating

than in the left image. The overall appearance of cells nucleofected with Buffer 2 is more positive than cells nucleofected with Buffer 1.

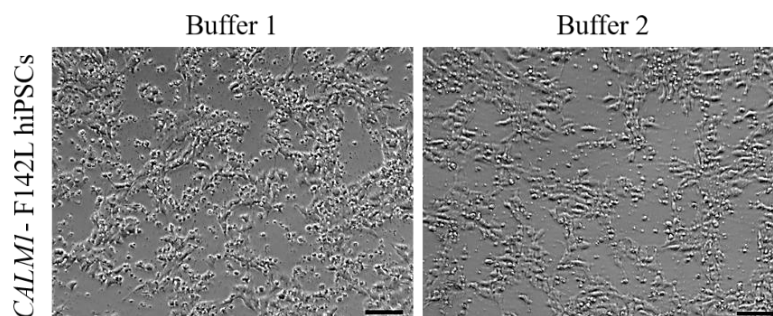


Figure 46: Representative PH images of *CALMI*- F142L hiPSCs nucleofected in Buffer 1 and Buffer 2. Images of single- cell adapted *CALMI*- F142L hiPSCs nucleofected in Buffer 1 (left) and Buffer 2 (right) 24h after nucleofection. Scale bars represent 100  $\mu$ m.

Number of GFP+ cells was analysed after 24h of nucleofection, using a flow cytometer. 24h after nucleofection of GFP ctr plasmid with Buffer 1, 7% of cells were measured GFP+. When nucleofected with Buffer 2, 41% of total cells were expressing GFP. Delivery efficiency in *CALMI*- F142L hiPSCs nucleofected with program B16 of the Amaxa Nucleofector II in combination with Buffer 2 was therefore most efficient. The following

Table 10 summarises delivery efficiencies in tested buffers:

Human Stem Cell Nucleofector Kit Buffer	GFP+ cells out of total [%]
1	7
2	41

Table 9: Delivery efficiency of nucleofection buffer combinations in *CALMI*- F142L hiPSCs.

Same amount of *CALMI*- F142L hiPSCs was nucleofected with either buffer and a ctr GFP plasmid and % of GFP expressing cells was measured after 24h by FACS. Left column lists the two buffers tested, right column lists the percentage of GFP expressing cells out of total cells analysed (GFP+ cells out of total [%]).

For further experiments, *CALMI*- F142L hiPSCs were nucleofected in Buffer 2 with program B16 in the Amaxa 2D Nucleofector from Lonza.

The Addgene Cas9 plasmid pSpCas9(BB)-2A-Puro (PX459) V2.0 (Addgene, #62988) used for delivery with nucleofection carries a puromycin resistance gene. In order to estimate the concentration most suitable for selecting hiPSCs carrying the plasmid and expressing puromycin resistance, a kill- curve was analysed. Single- cell adapted *CALMI*-

F142L hiPSCs were nucleoporated with the Cas9- puro plasmid and with no plasmid as negative ctr and plated as described before. Figure 47 shows many cells attached after nucleofection, but floating dead cells are visible in both conditions. After 12h of incubation with puromycin, more cells are still attached that were treated with the plasmid, than in the ctr condition. After 48h of antibiotic treatment, no more live cells survived the puromycin treatment under ctr conditions. Some cells treated with plasmid are still attached, many dead cells are floating. A slowed cell- division rate in surviving cells was noted even after removal of puromycin. For further CRISPR experiments with the Cas9- puro plasmid, antibiotic selection for 24h with 0.2  $\mu\text{g}/\text{ml}$  was performed.

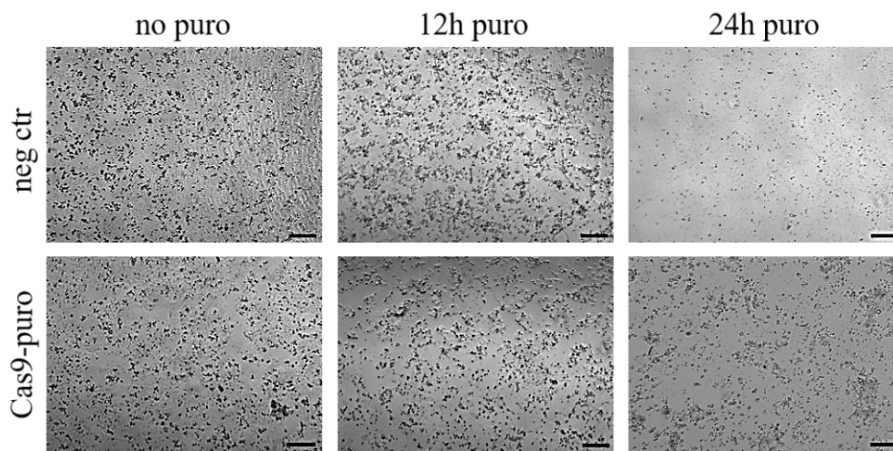


Figure 47: Representative puromycin kill- curve of *CALMI*- F142L hiPSCs ranging from no puromycin to 24h of puromycin incubation.

PH microscopic images of *CALMI*- F142L hiPSCs nucleofected with no plasmid (neg ctr; top row) and with CRISPR/ Cas9 puro plasmid (Cas9- puro; bottom row). First column shows images of cells before puromycin treatment (no puro), second column after 12h of incubation (12h puro) and third column after 24h puromycin incubation (24h puro). Scale bars 250  $\mu\text{m}$ .

#### *Effects of SCR7 on HDR*

The chemical compound SCR7 is described in literature to inhibit NHEJ by targeting the DNA ligase IV<sup>148</sup>. HR by HDR is therefore favoured during the DNA repair process, increasing the efficiency of correcting mutations by CRISPR/ Cas9 together with an oligo repair template. This positive effect was investigated on *CALMI*- F142L hiPSCs with the corresponding Cas9/ gRNA puro correction plasmid and the 120 bp ssODN template DNA. Nucleofection and puromycin selection was performed as described in the methods section 3.2.7 and 3.2.8. SCR7 was purchased from Tocris Bioscience (Cat No. 14892-97-8) and diluted to 1  $\mu\text{M}$  working concentration. After nucleofection and plating of the cells in 4- well plates, 1  $\mu\text{M}$  of SCR7 was added to the culture medium for 24h, as described in the publication by Maruyama and colleagues<sup>148</sup>. 4 nucleofections were performed out of which 302 single- cell colonies emerged and were analysed for mutation correction.

---

All screened colonies were tested negative for correction of the *CALMI*- F142L mutation. Therefore, no conclusion can be drawn about the effect of SCR7.

After all optimisations established for correcting the *CALMI* mutations in the mutant hiPSC lines with no success, the approach to knock -out the mutated *CALMI* gene in patient hiPSCs was elucidated.

#### 4.4.2.2 Generation of *CALMI* knock- out line

Gene knock- outs can be achieved by causing erroneous DNA repair due to NHEJ within the first exons of a gene. Resulting insertions or deletions often cause a frameshift, leading to different aa orders of the protein and premature stop codons. These alterations in nt sequence and aa order often cause the cell to dissipate the mRNA even before translation into mutated proteins can occur. Knocking out *CALMI* by provoking indels within the first exons of the gene was attempted. The Addgene plasmid #62988, pSpCas9(BB)-2A-Puro (PX459) V2.0 was delivered by nucleofection. Figure 48 displays schematic of Cas9/ gRNA- mediated gene knock- out of the *CALMI* gene.

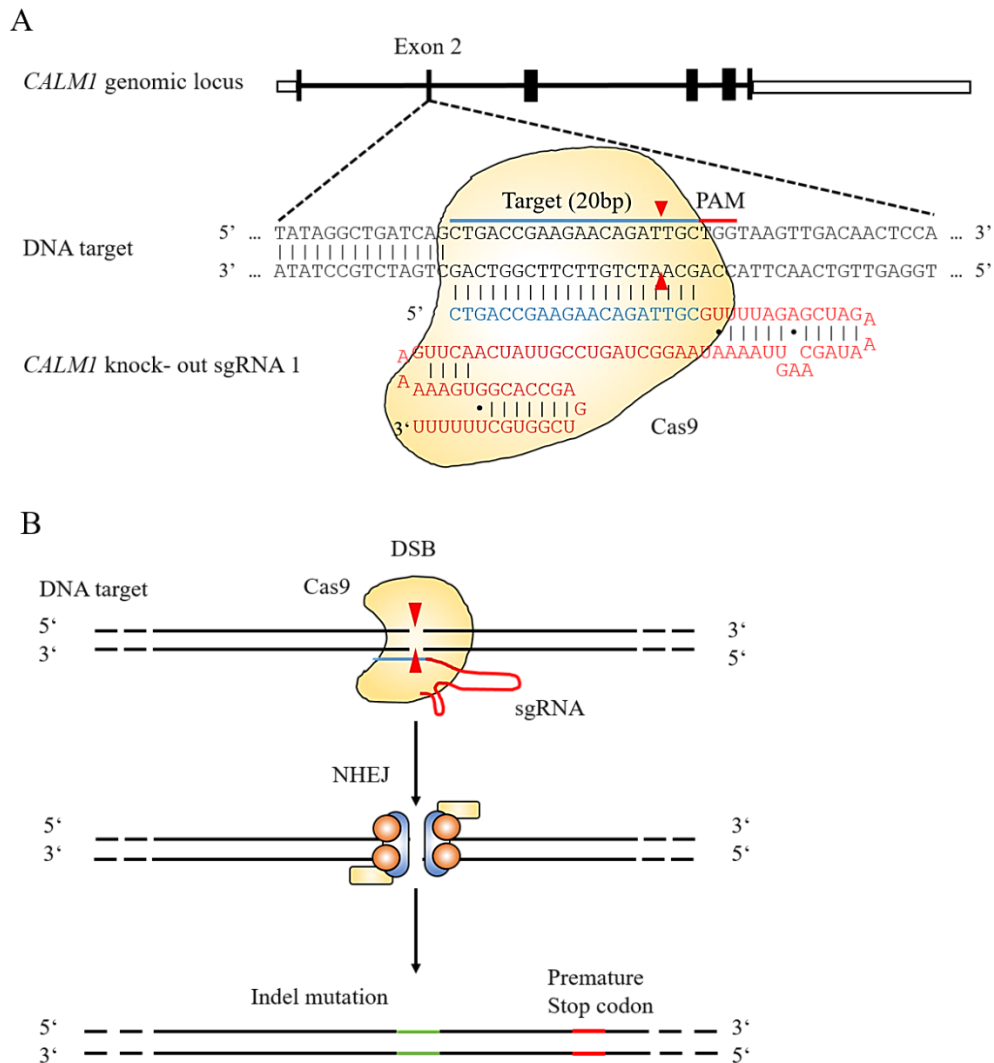


Figure 48: Schematic of Cas9/ gRNA- mediated gene knock- out of the *CALMI* gene.

(A) Schematic of the Cas9/ gRNA complex annealing to the DNA target within *CALMI*, exon 2. 20 nt guide sequence of *CALMI*- KO gRNA 1 displayed in blue, gRNA scaffold in red. Guide sequence binds to DNA target sequence (blue bar on top strand), directly upstream of PAM motif (red bar). Cas9 protein (in yellow) mediates DSB 3 bp upstream of the PAM sequence (red arrows). (B) DSB (red arrows) induced by Cas9 endonuclease (yellow) and guided by gRNA (red and blue) at DNA target sequence. Cellular repair pathway NHEJ is executed, which can result in random indel mutations (green) at the site of DNA repair. Indels can result in frameshifts, creating premature stop codons (red) in the coding region of genes and therefore resulting in gene knock- outs. Figure adapted from Ran *et al.* <sup>69</sup>.

Two independent gRNAs were designed to achieve *CALMI* knock- outs, as shown in Figure 49. *CALMI*- KO sgRNA1 anneals on negative genomic DNA strand, *CALMI*- KO sgRNA 2 anneals on positive strand of the *CALMI* locus. Both target sequences lie within exon 2. Sequences of these gRNAs are listed under 3.6. Cleavage Detection analysis was performed, as described before, and cleaving efficiencies for both guides were determined to be sufficient to commence with attempting the knock- out.

*CALMI* genomic locus

Figure 49: *CALMI*- KO sgRNA 1 and *CALMI*- KO sgRNA 2 annealing schematic.

Both gRNAs anneal for the most part within exon 2 of the *CALMI* genomic locus. Introns are depicted in small grey letters, exon 2 is depicted in capital letters and framed in blue. *CALMI*- KO sgRNA 1 anneals on the negative strand, *CALMI*- sgRNA 2 on the positive strand. Target- specific nt sequences of the gRNAs are depicted, sgRNA scaffolds depicted as dashed lines.

Nucleofection was performed with Buffer 2 and program B16, as tested best for *CALMI*-F142L hiPSCs before. Puromycin selection was conducted with 0.2  $\mu\text{g}/\text{ml}$  for 24h and colony screening was executed on emerging colonies.

*Colony screening*

5 independent *CALMI* KO experiments were performed. The Cas9 plasmid carrying KO gRNA 1 was used in 2 experiments, the KO gRNA 2 plasmid was used in 3 experiments. A total number of 98 single- cell- derived colonies emerged from those experiments, translating to an average of 19.6 colonies per experiment. 9 colony screened clones targeted with Cas9 and gRNA 1 were found to be edited in exon 2. 5 colonies targeted with Cas9 and gRNA 2 showed indels in exon 2. Figure 50 shows the average editing efficiency as percentage of edited clones in relation to number of single- cell- derived clones per gRNA. 16.3% of screened clones targeted with Cas9 and gRNA 1 were edited. 33.3% of colonies targeted with the Cas9 plasmid carrying gRNA 2 showed to carry indels in exon 2. Concluding this analysis, *CALMI*- KO gRNA 2 was better in producing indels in exon 2 in *CALMI*- F142L hiPSCs, however not with statistical significance.

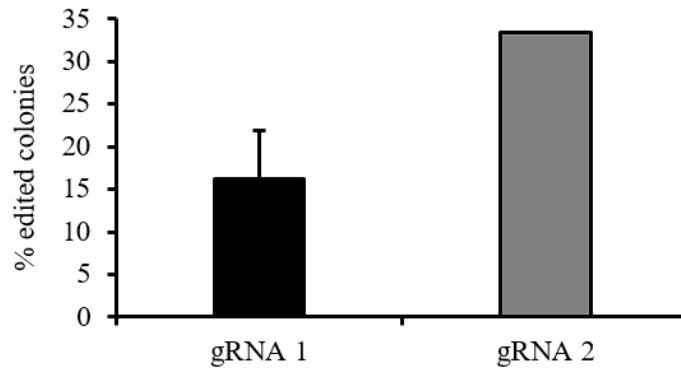


Figure 50: Editing efficiency as percentage of edited clones for *CALMI*- KO gRNA 1 and 2.

Graph representing % of edited clones retrieved from nucleofection and puromycin selection with Cas9 *CALMI*- KO gRNA 1 plasmid (gRNA1, black bar,  $n=3$ ) and Cas9 *CALMI*- KO gRNA 2 plasmid (gRNA 2, grey bar,  $n=2$ ). 2- sided T-test shows no statistical significance.

#### 4.4.2.3 TIDE analysis

After sequencing of retrieved clones, indels were analysed using the TIDE software, as described before in section 3.3.8. Figure 51 depicts a representative sequencing result of a single- cell- derived clone from CRISPR/ Cas9 editing using the *CALMI*- KO gRNA 1. The predicted point of indel was calculated to be between c.29T and c.30T, as indicated with a red arrow. Underlying double peaks are visible in targeted clone sample from c.29 onwards. The original wt nt string is written out below, with no double peaks. The sequence string written out below the wt sequence illustrates a predicted frame shift (red arrow) on one allele, caused by insertion of an A (red boxed green A) at position c.29. An insertion (c.29\_30insA) of the nt A at this position causes all following nts to move one position further downstream. Resulting double peaks are visible from position of insertion onwards. Double peaks are approximately one- third of the height of the wt sequence peaks, suggesting a still more prominent wt population of cells instead of a homogenous heterozygous population of edited cells.

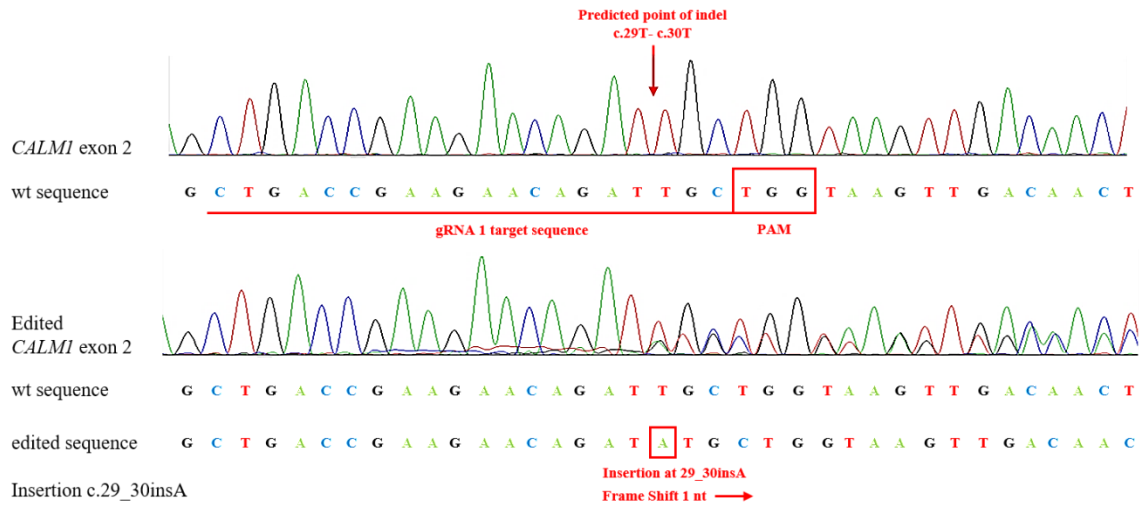


Figure 51: Representative sequencing result of wt clone and edited *CALMI*- KO clone.

*CALMI* exon 2 sequence around expected indel. Wt nt sequence written out below the corresponding sequencing reads. gRNA target sequence labelled in red (gRNA 1 target sequence). Predicted point of indel between c.28T and c.30T, indicated by a red arrow. PAM sequence marked with red box. Sequence string below depicts *CALMI* exon 2 edited sequence (Edited *CALMI* exon 2). Wt and edited nt sequence are listed below. Red boxed A depicts insertion of an A at position c.30 and a resulting frame shift of 1 nt (Insertion at 29\_30insA, Frame Shift 1 nt; red arrow).

By loading a negative ctr sequencing track of an untargeted clone and the sequence of a potentially targeted single- cell- derived clone into the TIDE software, genome- editing can be assessed in a quantitative manner. Figure 52 depicts the sequence decomposition of the representative sequence shown in Figure 51. TIDE analysis of this representative *CALMI*- KO clone estimated a 37.5% efficiency of targeting, labelled as total eff.= 37.5. 35.4% of the sequences are predicted to harbour a frameshift caused by insertion of 1 nt (red bar). Statistical significance with  $p < 0.001$  was estimated for the insertion with an  $R^2$  value of 0.97. 59.7% of sequences were not edited, as depicted by the pink bar. Analysis of the +1 insertion is depicted in the upper right inset. The probability of a T insertion was estimated at 5.4% (red segment of bar). Insertion of a G happened with 36.3% probability (black segment of bar), C is estimated at 2.3% (blue segment) and 56.0% probability was calculated for an insertion of A (green segment of bar). The most likely insertion of an A concurs with the sequence comparison of Figure 51, where an insertion of an A at c.29\_30insA would cause a frameshift of 1 nt and can be followed by resulting double peaks. Statistically insignificant deletions of 2 nts and 3 nts are depicted by low black bars, with significance of  $p \geq 0.001$ .

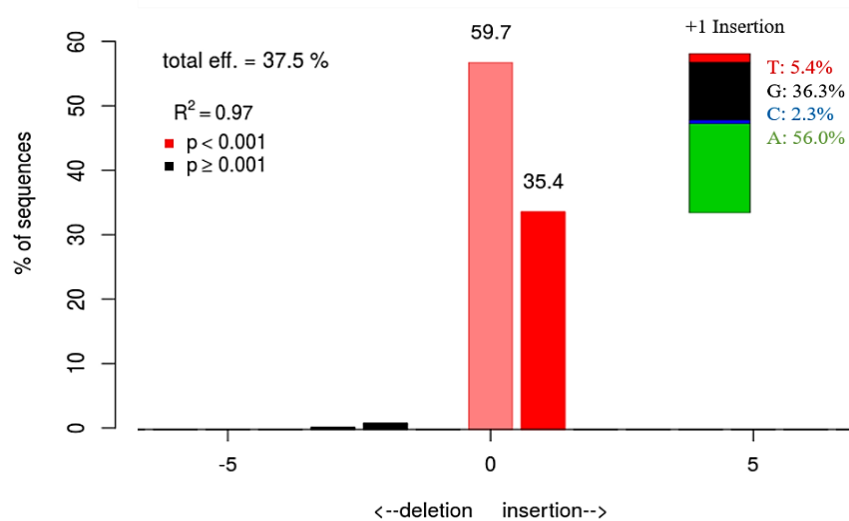


Figure 52: Output of TIDE analysis of a representative *CALMI*- KO clone.

X-axis depicting number of nts inserted or deleted. Y- axis depicting % of sequences edited. Red bar representing 35.5% of sequences with an insertion of 1 nt with  $p < 0.001$  significance. Black bars representing insignificant deletions. Inset in right upper corner depicts probability of nts inserted. Red bar stands for T, black for G, blue bar for C, green bar A.

TIDE analysis of edited *CALMI*- KO clones showed a range of editing efficiencies from 6.6% up to 45.3% with different distributions of insertions and deletions. The maximum percentage of editing reached by one insertion itself was 35.4%. None of the clones edited with 20% efficiency or higher remained stable in culture and could be propagated by standard hiPSC culturing methods. Neither culturing the edited clones on Geltrex in E8 medium, nor culturing them on MEF feeders in hiPSC medium were successful. Further culturing of less edited clones and repeated sequencing after several passages showed the loss of % of edited cells within hybrid colonies.

## 4.5 Genome- editing of the *MEIS1* locus

### 4.5.1 Generating *MEIS1* knock- out line

Due to the difficulties to successfully manipulate patient- specific hiPSCs at the *CALMI* locus, CRISPR/ Cas9 editing was investigated in healthy ctr cell lines with the aim to knock- out the *MEIS1* gene. Healthy ctr hiPSC lines available within the work group were C6, Nu1, Nu3, HAK and Ctr25. All lines were adapted to feeder free culture and single-cell growth. Nu1 and Nu3 hiPSCs were not stably culturable as single cells. Nucleofection protocols were tested on all cell lines and lines were evaluated for delivery efficiency and

recovery efficiency. Only the ctr cell line HAK grew stably on Geltrex in E8 medium and showed a high delivery efficiency and recovery when nucleofected with a ctr GFP plasmid.

### *Single- cell adaptation*

Single- cell adaptation of HAK ctr hiPSCs was performed under feeder- free conditions, as described in methods section 3.2.3. Figure 53 depicts representative HAK cells before and after single- cell adaptation captured by phase contrast microscopy. 4 days after colony splitting, cells grow in round colonies with cells gathering closely to each other. Clear edges of the colony are visible. Morphology of colonies closely resemble appearance of colonies of *CALMI*- D130G and *CALMI*- F142L hiPSCs on Geltrex in E8, as shown in Figure 33. Cells adapted to single- cell growth grow in a monolayer. Cells appear more rod- shaped with some spikes connecting smaller groups of cells with each other. The HAK ctr hiPSC line is stably kept in culture as single cells for more than 20 passages. However, for further experiments, cells not exceeding single- cell passage 15 were used to exclude accumulation of karyotype abnormalities and acquired mutations due to longer feeder- free and single- cell culturing.

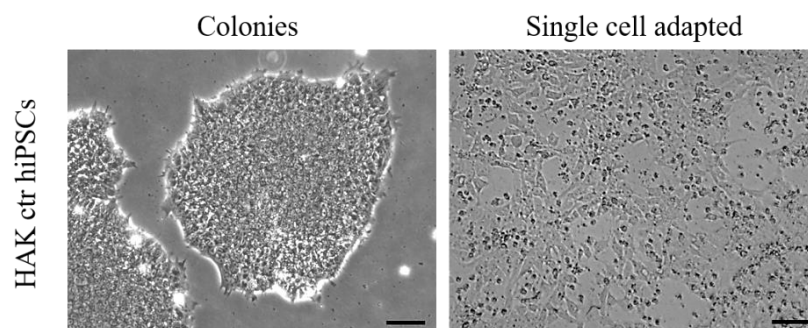


Figure 53: Representative PH images of HAK ctr cells grown on Geltrex in E8 medium as colonies and as single cells.

Left image depicts a HAK ctr hiPSC colony 4 days post- splitting (Colonies). Right image depicts single- cell adapted HAK ctr hiPSCs 4 days post- splitting (Single- cell adapted). Scale bar 100  $\mu$ m.

### *Testing gRNA efficiencies*

The attempt to knock- out the *MEIS1* gene in the HAK ctr hiPSC line was pursued by ordering a gRNA knock- out library from Addgene. This library was kindly deposited by the group of Prof. Zhang and described previously in their publication by Shalem et. al<sup>149</sup>. Targeting efficiencies of *MEIS1*- KO gRNAs HGLibA\_28870, HGLibA\_28871, HGLibA\_28872 and HGLibB\_28829 were tested after cloning into Addgene's Cas9 plasmid #62988, pSpCas9(BB)-2A-Puro (PX459) V2.0, carrying the puromycin resistance

cassette. Plasmids were named Cas9 *MEIS1*- KO gRNA1, carrying HGLibA\_28870 gRNA, Cas9 *MEIS1*- KO gRNA2, carrying HGLibA\_28871 gRNA, Cas9 *MEIS1*- KO gRNA3, carrying HGLibB\_28872 gRNA and Cas9 *MEIS1*- KO gRNA4, carrying HGLibB\_28829 gRNA. Figure 54 depicts annealing positions of *MEIS1*-KO gRNAs 1-4. gRNAs 2 and 3 target within exon 2, gRNAs 1 and 4 target within exon 3 of the *MEIS1* gene.

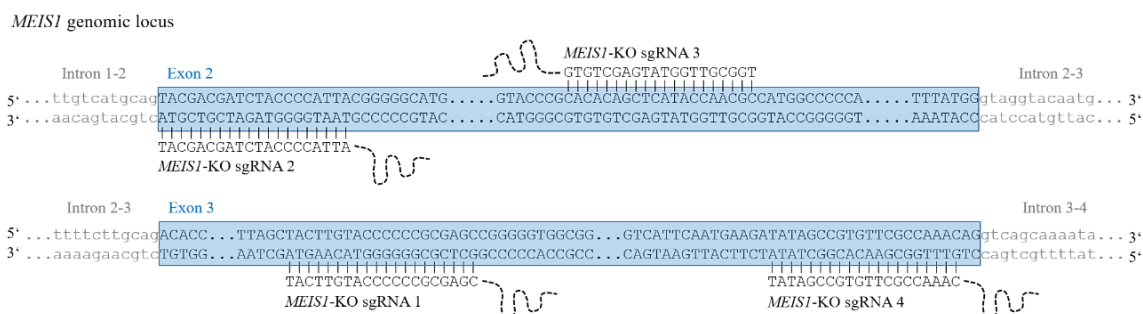


Figure 54: *MEIS1*- KO sgRNAs annealing schematic.

Shown are the *MEIS1*- KO gRNAs 1- 4 annealing to each target sequence within exon2 or 3 of the *MEIS1* locus. gRNA 2 and 3 target exon 2 (blue framed), gRNAs 1 and 4 target exon 3 (blue framed). Introns are depicted in small grey letters. *MEIS1*- KO sgRNA 1, 2 and 4 anneal 5'-3' on negative strand, gRNA 1 on positive strand. Target- specific nt sequences of the gRNAs are depicted, sgRNA scaffolds depicted as dashed lines.

Targeting efficiencies were tested by Genomic Cleavage Detection Kit, as described under methods section 3.3.8 and analysed using the ImageJ software to determine cleavage efficiencies in percent. The following

Table 10 summarises cleavage efficiencies of the four tested *MEIS1*- KO gRNAs determined by cleavage detection analysis:

Cas9 <i>MEIS1</i> - KO gRNA	Cleavage efficiency [%]
gRNA1	61
gRNA2	35
gRNA3	23
gRNA4	59

Table 10: *MEIS1*- KO gRNA cleavage efficiencies in HAK ctr hiPSCs.

Analysed were cleavage efficiencies of gRNA1, gRNA2, gRNA3 and gRNA4 for the *MEIS1*- KO approach. Left column lists gRNAs used for cleavage detection testing, right column lists calculated cleavage efficiency in percentage when compared to overall DNA loaded (Cleavage efficiency [%]).

The Cas9 construct carrying *MEIS1*- KO gRNA1 was used for gene knock- out experiments, since it achieved the best cleavage efficiency.

### *Optimising recovery and delivery efficiency after Nucleofection*

Nucleofection protocol was optimised for HAK ctr hiPSCs for optimal delivery and recovery efficiency. HAK hiPSCs were nucleofected with a GFP expressing ctr plasmid in order to analyse percentage of cells carrying the plasmid, as described before.  $0.8 \times 10^6$  HAK ctr hiPSCs were nucleofected in each buffer and plated into 2 wells of a Geltrex-coated 4- well plate. 24h after nucleofection, PH microscopic images were taken of wells to compare amount of cells attached. hiPSCs nucleofected in either buffer attached well with only some dead cells floating in the wells. Cell death due to nucleofection is expected to some degree. There are no significant differences visible concerning recovery efficiency between the two conditions.

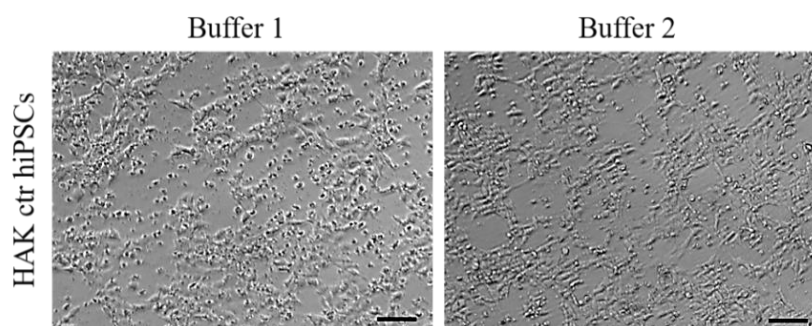


Figure 55: Representative phase contract images of HAK ctr hiPSCs nucleofected in Buffer 1 and Buffer 2.

PH images of single- cell adapted HAK ctr hiPSCs nucleofected in Buffer 1 (left) and Buffer 2 (right) and a GFP ctr plasmid. Pictures taken 24h after nucleofection. Scale bars represent 100  $\mu$ m.

HAK ctr hiPSCs were nucleofected with a GFP ctr plasmid, to analyse delivery efficiency of plasmids into the hiPSCs by FACS. Nucleofection and FACS analysis was performed as described before. Nucleofection protocol B16 was assessed in combination with Buffer 1 or Buffer 2 of the Human Stem Cell Nucleofection Kit from Lonza. The following table lists percentages of GFP+ cells compared to total cell numbers. 21% of analysed HAK ctr hiPSCs were detected GFP+ when nucleofected in Buffer 1. 40% of total cells nucleofected in Buffer 2 were detected to be GFP+. The nucleofection protocol for HAK ctr hiPSCs was set to program B16 in combination with Buffer 2 for further experiments.

Human Stem Cell Nucleofection Kit Buffer	GFP+ cells out of total [%]
Buffer 1	21
Buffer 2	40

Table 11: Delivery efficiencies using nucleofection Buffers 1 or 2 in HAK ctr hiPSCs.

Same amount of HAK ctr hiPSCs were nucleofected with either buffer and a GFP ctr plasmid. % of GFP expressing cells was measured after 24h. Left column lists the two buffers tested, right column lists the percentage of GFP expressing cells out of total cells analysed (GFP+ cells out of total [%]).

### *Puromycin selection*

A puromycin kill- curve was conducted to estimate the optimal puromycin concentration for selecting HAK ctr hiPSCs 24h after nucleofection for 48h. Kill- curve was executed as described before and optimal puromycin concentration for selection was set to be 0.4  $\mu\text{g}/\text{ml}$ .

### *Colony screening*

To achieve a *MEIS1* knock- out in HAK ctr hiPSCs, one nucleofection experiment was performed with Cas9 *MEIS1*- KO gRNA1, which gave rise to 16 colonies after puromycin selection. Colony screening of those 16 colonies by Sanger sequencing revealed indels at the expected point of editing in 9 out of 16 clones. This translates to an editing efficiency of 56.3%.

*TIDE analysis*

TIDE analysis was performed as described before on all edited clones. The following Table 12 lists editing efficiencies and percentages of efficiencies of single events per clone.

Clone number	total efficiency [%]	efficiency single event [%]
1	56.4	32.2 (- 4 nt)
2	35	15.7 (- 4 nt)
3	33.5	7.1 (- 9 nt)
4	22.9	5.9 (- 4 nt)
5	37	15 (- 10 nt)
6	62.6	22.2 (- 7 nt)
7	64.2	35.2 (- 7 nt)
8	47.7	37.2 (- 7 nt)
9	63.8	31 (- 1 nt)

Table 12: Total gene editing efficiencies and single event editing efficiencies in HAK ctr hiPSCs targeted with Cas9 *MEIS1*- KO gRNA1 construct.

Left column lists clone number (clone number), middle column lists total gene editing efficiencies at investigated genomic locus (total efficiency [%]), right column lists gene editing efficiencies of most single event at targeted locus (efficiency single event [%]). Efficiencies are stated as % of all analysed sequencing tracks. Right column also states type of editing of most common editing, with negative number indicating a deletion event and number of nts deleted.

Clones 7, 8 and 9 showed most efficient editing with highest % of single editing events. Deletions of 4 nts (- 4 nt) and 7 nts (- 7 nt) are most abundant among all clones analysed. For further analysis, clones 1, 6, 7, 8 and 9 were kept in culture and propagated for more passages. Only clones 7, 8 and 9 were stable enough to propagate as undifferentiated hiPSCs further, clones 1 and 6 were lost in the course of passaging due to ungovernable differentiation and apoptosis. After 4 passages, clones 7, 8 and 9 were investigated for homogeneity by taking 2- 3 random cell samples per clone from 80% confluent 3.5 cm dishes. PCR amplified genomic DNA was sequenced by Sanger sequencing again and TIDE analysis was performed once more to monitor changes in total editing efficiencies. Clone number 7 showed in both independent samples a total editing efficiency of over 96%. This was mainly ascribable to a single editing event of a 6 nt deletion of around 90% in both samples. Figure 56 displays the TIDE analysis result of one of the two random samples analysed from clone 7. The total editing efficiency is calculated with 96.3%, with 91.5% contribution of the 6 nt deletion editing event. The  $R^2$  value for this sample

was estimated at 96.3%. The 6 nt deletion is statistically relevant with a p value of  $p < 0.001$ . These results suggest a homogenous knock-out of 6 nts on both alleles.

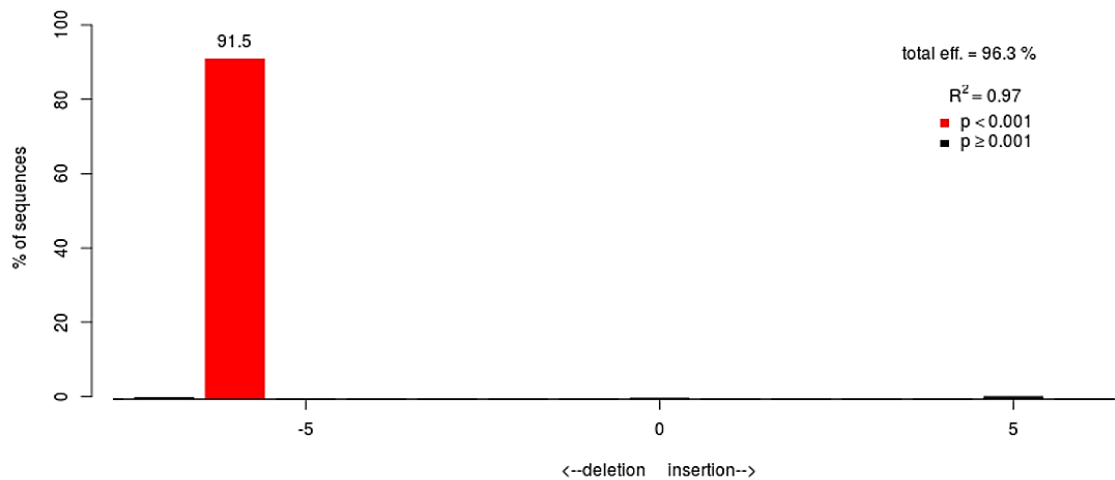


Figure 56: Representative TIDE analysis of *MEIS1*- KO clone 7.

X-axis depicting number of nts inserted or deleted. y- axis depicting % of sequences edited. Red bar representing 91.5% of sequences with a deletion of 6 nts with  $p < 0.001$  significance. Black bars representing insignificant deletions.

3 randomly taken cell samples of a dish from clone 8 were equally sequenced and analysed. TIDE analysis revealed total editing efficiencies ranging from 8.8% to 23.3%. Most promising single editing event of a deletion of 8 nts was estimated at only 7.9% efficiency. Single editing events among the three samples were not concordant. These results suggest a very heterogeneous clone, losing the fraction of edited cells in the course of passaging. 3 randomly taken cell samples were likewise taken and analysed from clone 9, which was previously estimated at 63.8% total edited efficiency. After 4 passages, this clone did not show any editing anymore in the three independent samples analysed. Total editing efficiency of all three was measured at 0%. This concludes, that the clone lost all edited cells in the course of propagation. The focus for further analysis was therefore put on clone number 7. This clone is subsequently named *MEIS1*- KO clone.

By comparing the edited nt sequence of the *MEIS1*- KO clone with the corresponding wt nt sequence, information on changes in nt and therein changes in protein sequence were gathered. Figure 57 depicts the sequence comparison of wt and edited clone 7. Predicted point of indel is c.G306- c.A307. There are no double peaks visible in the sequencing track following that point, indicating the editing to be homogenous on both alleles. The

wt nt sequence listed below is marked by red boxes at the positions where editing was predicted. A deletion of 6 nts was predicted by the TIDE analysis. The analysis tool does not distinguish between deletions of connected 6 nts or a total of 6 nts that can be distributed along the analysed sequence. By comparison of the edited sequence with the wt sequence, a deletion of the 4 nts AGCC from c.A307- c.C310 is apparent. This deletion is marked in the wt nt sequence by a red box. In the edited nt sequence below, the position of deletion is marked by a red cross. The missing nts are listed below under a red parenthesis, labelled Del 4 nt. 2 more deletions at positions c.G20 and c.C23, translating to a G and C, are visible by comparing the sequences. Those single nt deletions are boxed in red in the wt sequence and marked by red crosses at the respective positions and red arrows in the edited sequence. Taken together, a total of 6 nts were deleted in clone 7, as predicted by the TIDE program. Exchanges of nts are not detectable by the TIDE logarithm. However, comparing the sequences with each other, an exchange of GT to TA at c.G15 and c.T16 is apparent, as indicated by a red box in the wt and mutated sequence and red arrows. Taken together, 8 nts were altered either by deletions or exchanges in clone 7.

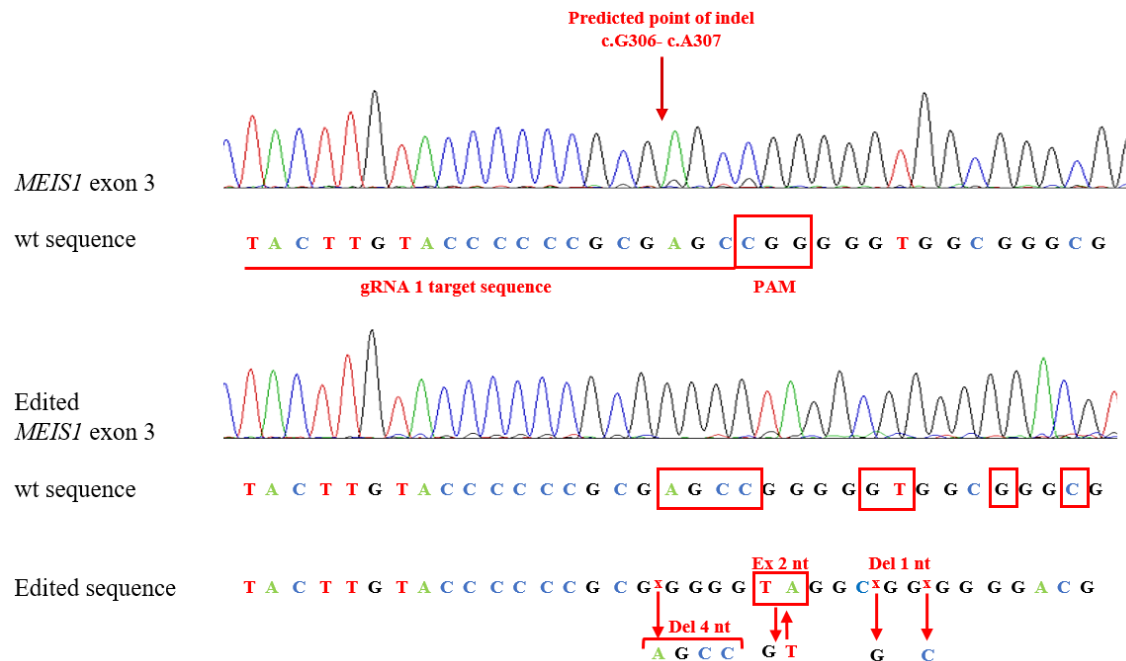


Figure 57: Representative sequencing result of wt clone and edited *MEIS1*- KO clone.

*MEIS1* exon 3 sequence. wt nt sequence written out below the corresponding sequencing reads (wt sequence). gRNA target sequence labeled in red (gRNA 1 target sequence). Predicted point of indel between c.G306- c.A307 indicated by a red arrow. PAM sequence marked with red box. Sequence string below depicts *MEIS1* exon 3 edited sequence (Edited *MEIS1* exon 3). wt and edited nt sequence are listed below (wt sequence; edited sequence). Red boxed nts depicts edited nts. Deletion of 4 nts marked by red arrow and parenthesis (Del 4 nt), exchange of 2 nts marked by red box and arrows (Ex 2 nt), deletions of twice 1 nts marked by arrows, labelled Del 1 nt.

These analysed alterations in nt sequence translate to altered aa sequences. The following Figure 58 compares the wt aa sequence to the resulting aa sequence of edited clone 7. The red nts display the missing or exchanges nts, red aas stand for altered aas. Those changes in nt sequence cause a premature stop codon at protein position 105. The resulting *MEIS1*-KO protein is therefore predicted to be 104 aa in size instead of the wt *MEIS1* protein of 390 aa.

<i>MEIS1</i> exon 3														p.G105 c.G313- c.G314	
aa	...	P	R	E	P	G	V	A	G	G	D	V	C	...	
wt	...	CCC	CGC	GAG	CCG	GGG	GTG	GCG	GGC	GGG	GAC	GTC	TGC	...	
KO	...	CCC	CGC	G - -	- - G	GGG	TAG	GC -	GG -	GGG	GAC	GTC	TGC	...	

Edited <i>MEIS1</i> exon 3														p.G105Stop c.G313T- c.G314	
aa shift	...	P	R	G	G	STOP									
KO shift	...	CCC	CGC	GGG	GGT	TAG									

Figure 58: Comparison of nt and aa sequence of wt *MEIS1* exon 3 to edited *MEIS1*- KO clone.

Top panel lists aa sequence from p.P101 to p.C112. According nt sequence below labelled as wt. Edited sequence written out below with alterations marked in red (KO). Panel 2 shows resulting aa sequence and nt sequence including changes (Edited *MEIS1* exon 3). Altered and shifted aa sequence (aa shift), altered and shifted nt sequence (KO shift). Resulting aberrant aas and nts marked in red.

### *Off- target analysis*

Genomic regions that show high similarity to the target sequence might become edited due to gRNAs guiding the Cas9 protein mistakenly to those highly similar regions. The online CRISPR design tool (crispr.mit.edu) used for designing gRNAs for the *CALMI* correction and knock- out approach was also utilised to find predicted off- targets to *MEIS1*- KO gRNA1. In order to rule out unwanted editing events in the DNA, regions spanning predicted exonic off- targets were sequenced. The CRISPR design tool identified one potential exonic off- target region targeted by the *MEIS1*- KO gRNA on chromosome 5, position -140856454. The predicted off- target sequence was namely GACTT-GTACCACGCGCGTGCCGG. This off- target sequence contains 4 mismatching nts at positions 1, 11, 13 and 18 compared to the *MEIS1*- KO gRNA1 target sequence. Region spanning predicted off- target was sequenced using primers listed under 3.6. TIDE analysis was performed as described before. Figure 59 depicts TIDE analysis of off- target region with an estimated total efficiency of editing of 3.5%. No deletions or insertions with statistical significance were found. 92.8% of all sequences analysed are predicted to be wt. The not covered 3.7% and statistically insignificant deletion and insertion of 1 nt each can be accounted to background noise of sequencing. This results concludes the predicted off- target not being affected.

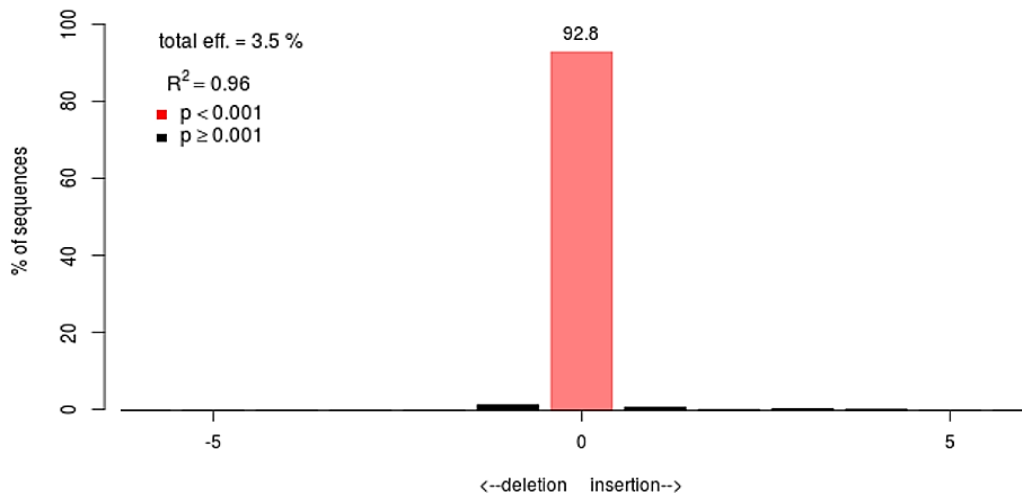


Figure 59: TIDE analysis of *MEIS1*- KO off- target sequence.

X-axis depicting number of nts inserted or deleted. Y- axis depicting % of sequences edited. Red bar representing 92.8% of sequences with no editing with  $p < 0.001$  significance. Black bars representing insignificant deletions.  $R^2$  value at 0.96. Total editing efficiency estimated at 3.5%.

#### *qRT PCR analysis of MEIS1 transcript expression*

TIDE analysis and sequence comparison with wt sequences revealed the editing to result in a premature stop codon and a shortened MEIS1 protein. Since *MEIS1* expression peaks at 48h of cardiac differentiation of hiPSCs (see 4.5.2), qRT PCR analysis on *MEIS1* transcript expression in 48h differentiated *MEIS1*- KO hiPSCs was performed with primers covering the region before the mutation (Nterm MEIS), after the mutation (Cterm MEIS) and one primer pair spanning the region with the point of indel in the middle of the amplified sequence (KO MEIS). Cardiac differentiation was performed using the PSC CM Differentiation Kit. Sequences of designed primers are listed under 3.6. Figure 60 depicts measured expression values in HAK ctr hiPSCs (HAK CTR) and *MEIS1*- KO hiPSCs (MEIS KO). Statistical differences were calculated for all three primer pairs between ctr and KO hiPSCs *MEIS1* expression. These results suggest a degradation of the edited *MEIS1* transcript in the *MEIS1*- KO hiPSCs line. To further characterise the *MEIS1*- KO hiPSC line, protein levels are investigated and compared to ctr HAK samples.

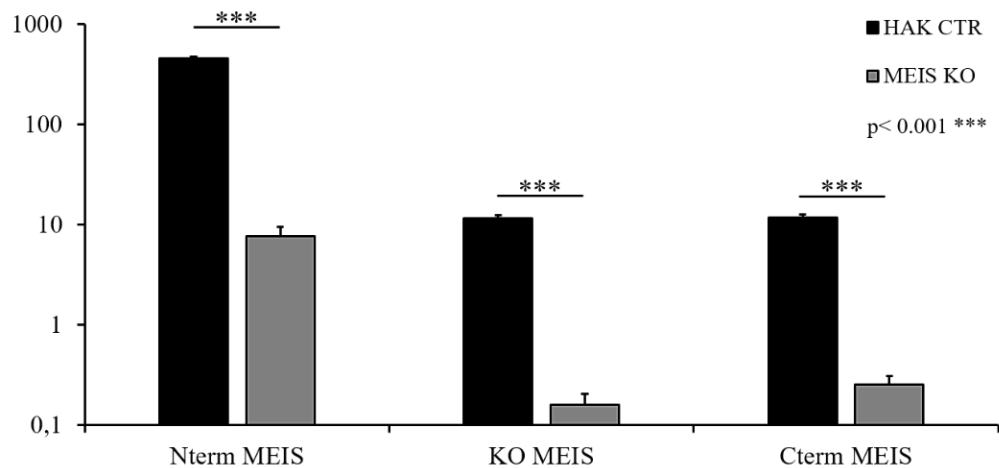


Figure 60: qRT PCR analysis of *MEIS1* transcript expression in HAK ctr hiPSCs and *MEIS1*- KO hiPSCs differentiated for 48 h.

Nterm MEIS representing expression of the N- terminal region of *MEIS1* transcript, KO MEIS amplified region spanning the region of genome- editing, Cterm MEIS representing expression of the C- terminal region of *MEIS1* transcript. Values of HAK ctr hiPSCs illustrated in black bars, *MEIS1*- KO hiPSCs in grey bars. Values normalized to *GAPDH*, and presented as mean +SEM,  $n=3$ .

#### *WB analysis*

Homeobox protein Meis1 expression was analysed in wt HAK hiPSCs and *MEIS1*- KO hiPSCs 48h after induction of cardiac differentiation using the PSC CM Differentiation Kit. After induction of differentiation, cells were harvested and protein content was estimated, as described in the methods section 3.3.3. Samples were separated by protein size on a SDS PAGE gel and transferred to nitrocellulose membrane, as described before. Antibodies specific for the N-terminal region of the human MEIS1 protein and specific for the human C- terminal MEIS1 protein were probed with the blotted samples and bands were detected by HRP reaction and development on film. Figure 61 shows a representative WB of human MEIS1 protein detection in the wt HAK and *MEIS1*- KO line. First two lanes depict probing of samples with MEIS1 antibody against the C-terminal part of the MEIS1 protein. A band at the expected size of 40 kDa is visible in the wt HAK sample (HAK CTR). No band is visible in the *MEIS1*- KO sample (MEIS KO). Lane 3 and 4 from the left show a representative probing in lysate of both lines with the N-terminal MEIS1 antibody. A band at 40kDa is visible in the HAK ctr sample, no band is detected in the MEIS1 KO sample lysate. The antibody detecting the N-terminal part of the MEIS1 protein is more sensitive. The same amount of protein was loaded for all samples and lanes. Last two lanes represent the loading ctr probed with HSP90 antibody. The band detected in samples of wt HAK lysate is more faint than for the *MEIS1*- KO samples,

enhancing the statement of absence of MEIS1 protein expression in the *MEIS1*- KO hiPSC line. This Blot is a representative WB performed in 3 biological replicates.

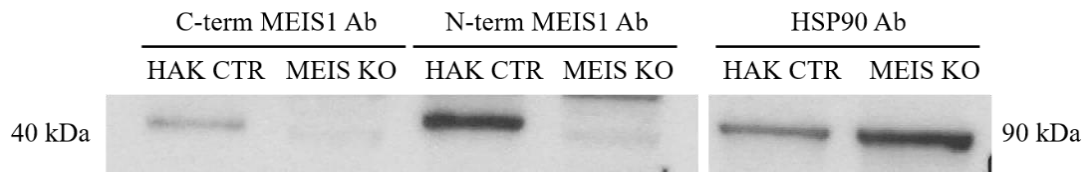


Figure 61: Representative WB of C-terminal MEIS1, N-terminal MEIS1 and HSP90 protein in HAK ctr and *MEIS1*- KO hiPSCs.

Whole cell lysates of 48h differentiated hiPSC of wt HAK and *MEIS1*- KO hiPSCs were probed with antibodies specific for human c-terminal MEIS1 protein (C-term MEIS Ab) and N- terminal MEIS1 protein (N-term MEIS Ab). Detected MEIS1 protein is visible at 40 kDa, loading ctr HSP90 is visible at 90 kDa.

Expression intensities of human MEIS1 protein detected with antibodies directed against the C- terminal and N- terminal part of the protein was examined in 3 biological replicates with samples of wt HAK hiPSCs and *MEIS1* KO hiPSCs differentiated for 48h. Semi-quantitative protein expression analysis was performed using the Image J software. A statistically significant difference in N-terminal MEIS1 protein level and in C- terminal protein level was calculated between wt HAK and *MEIS1* KO samples. These results stay in concordance with the previously shown *MEIS1* transcript expression levels shown in Figure 60. *MEIS1* gene transcript levels are degraded in *MEIS1* KO hiPSCs and translate to an absence of MEIS1 protein expression in these lines.

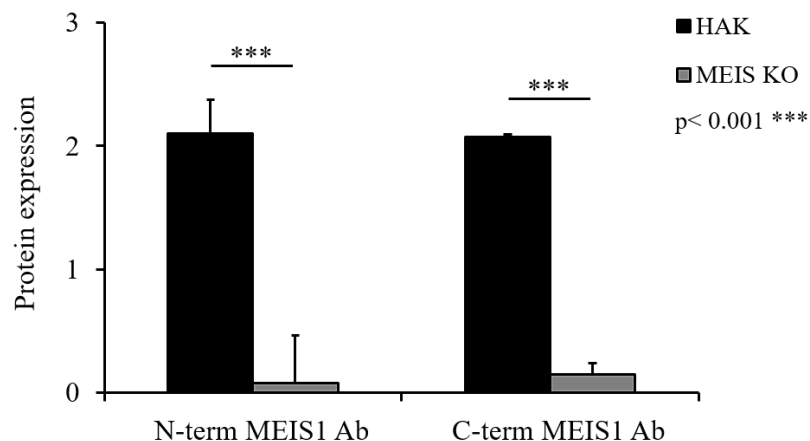


Figure 62: Semi- quantitative WB evaluation of N-terminal and C-terminal MEIS1 protein expression in HAK and *MEIS1*- KO hiPSCs after 48h differentiation.

Three biological replicates of MEIS1 protein detection by WB was evaluated using Image J. Black bars represent HAK ctr hiPSC protein samples, grey bars depict values for *MEIS1*- KO hiPSC line. Protein was probed with antibodies for N-terminal MEIS1 protein detection (N-term MEIS1 Ab) and C-terminal MEIS1 protein detection (C-term MEIS1 Ab). Values were normalized to HSP90 detection levels. Standard error presented as mean +SEM,  $n=3$ .

#### 4.5.2 Investigating the role of *MEIS1* during human cardiogenesis *in vitro*

In order to investigate the role of *MEIS1* during human cardiogenesis *in vitro*, hiPSCs of the HAK ctr line and of the generated isogenic *MEIS1*- KO cell line were differentiated using the PSC Cardiomyocyte Differentiation Kit for 9 days and cardiac progenitors as well as CMs were analysed.

##### *MEIS1* expression profile in HAK ctr line

Firstly, *MEIS1* expression during human cardiogenesis *in vitro* was analysed using the HAK ctr hiPSC line. Cells were differentiated and total RNA was extracted on d0, d1, d2, d3, d4, d6, d8 and d12 of cardiac induction. cDNA was transcribed from each sample. The *MEIS1* transcript expression was analysed for each time point. Figure 63 depicts *MEIS1* transcript expression profile from d0 to d12 of cardiac differentiation. No *MEIS1* transcript was measured at d0 and d1 of differentiation compared to *GAPDH* expression levels. An increase of 0.24- fold to *GAPDH* is observed at d2 of differentiation. Another peak is visible at d4, with 0.11- fold expression of the transcript. d3 and d5 show almost no fold increase in expression. A slow increase from d6 to d12 is measured subsequently. Prominent errors bars indicate the high heterogeneity between biological replicates impacting *MEIS1* transcript expression levels.

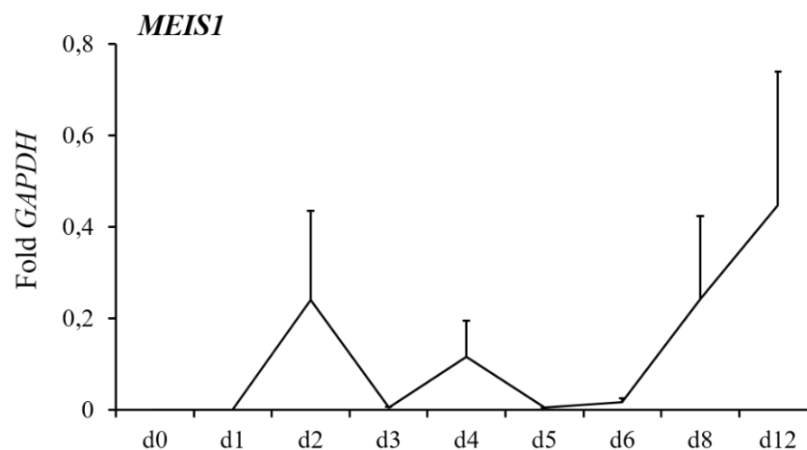


Figure 63: qRT PCR analysis of *MEIS1* expression in HAK ctr hiPSCs during differentiation.

qRT PCR analysis of wt ctr cells at d0, d1, d2, d3, d4, d5, d6, d8 and d12 of cardiac induction (black line). Expression values are normalized to *GAPDH*, fold to *GAPDH* and presented as mean +SEM,  $n=3$ .

*Gene expression profile in MEIS1- KO line*

Secondly, changes in transcript expression patterns during induction of cardiac differentiation in *MEIS1*- KO hiPSC line compared to isogenic wt ctr line (HAK CTR) was investigated by performing qRT PCR on samples taken at d0, d1, d2, d3, d4, d5, d6, d8 and d12 of cardiac differentiation, shown in Figure 64. *BRY* expression patterns between the KO and ctr lines is concordant. *BRY* is a marker for early mesodermal formation and greatly influencing cardiac progenitor cell formation<sup>87</sup>. *MESPI* expression patterns are mostly concordant, however increase and decrease of transcript expression are less steep in the KO line. Differences at the peak on d3 are not significant. *MESPI* plays a central role in cardiac precursor migration out of the primitive streak and cardiovascular progenitor specification<sup>150</sup>. *ISLI* expression pattern seems to be shifted 24h earlier in KO than in ctr lines. Peaking already at d5 in KO line, but at d6 in the ctr line. Fold expression is similar again by d12. Overall, no significance is determined at either time point for *ISLI* expression. *ISLI* marks SHF cardiac progenitor cells and contribute to formation of the primitive heart tube, atria and ventricles in the developing human heart<sup>90</sup>. *Nkx2.5* is a secondary master regulator, driving myocardial differentiation<sup>91</sup>. Expression values for *NKX2.5* are similar between the lines. Only day 12 of differentiation shows a higher value in *MEIS1*- KO samples, however with high error bars, marking the difference statistically not significant. By qRT PCR evaluation, overall no statistically significant differences were detected for the examined gene transcripts between the two lines. High error bars throughout experiments conclude a high variability between differentiations. A higher number of biological replicates is necessary.

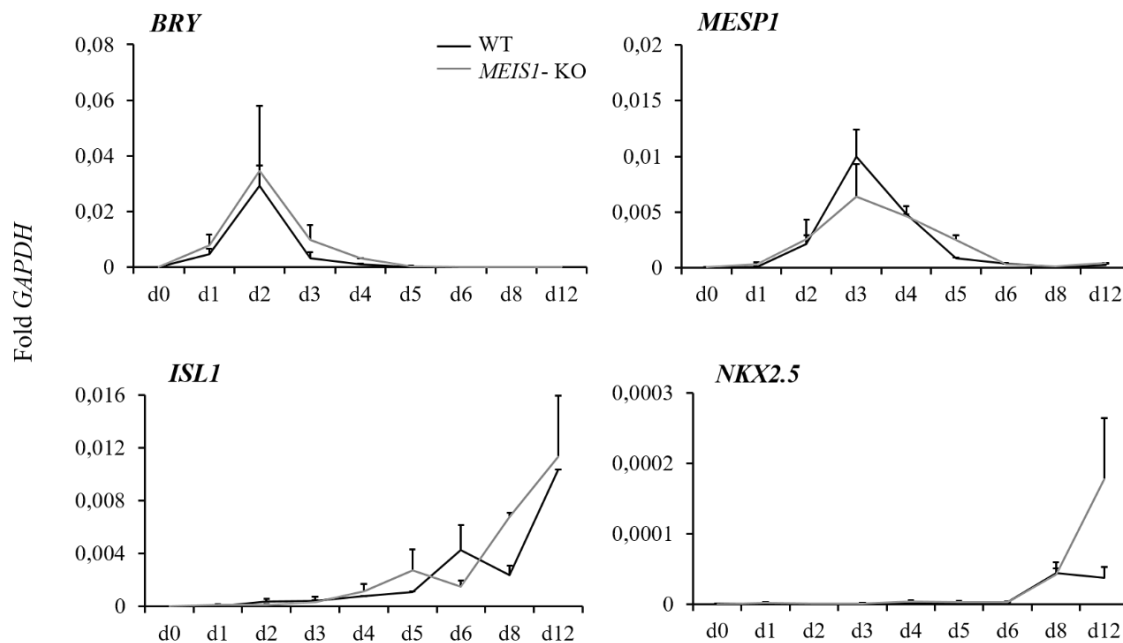


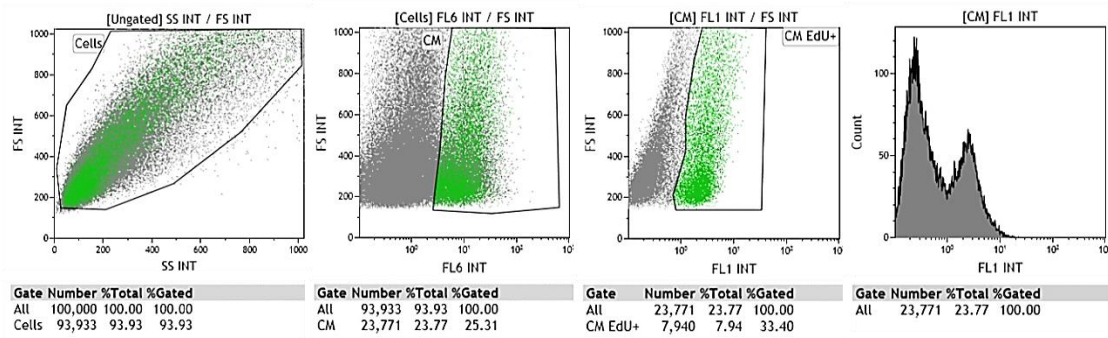
Figure 64: qRT PCR analysis of *BRY*, *MESP1*, *ISL1* and *NKX2.5* expressions in *MEIS1*- KO hiPSC and wt ctr hiPSCs during differentiation.

qRT PCR analysis of *MEIS1*- KO cells at d0, d1, d2, d3, d4, d5, d6, d8 and d12 of cardiac induction (grey line) and wt ctr hiPSCs (black line). Expression values are normalized to *GAPDH*, fold to *GAPDH* and presented as mean +SEM,  $n=3$ .

#### *Differentiation potential of MEIS1- KO hiPSC line into CMs and proliferative capacity of CMs*

Since *MEIS1* has been reported to play an important role in the cell- cycle exit of adult CMs<sup>100</sup>, differentiation potential of *MEIS1*- KO hiPSCs into CMs and proliferative capacity of CMs were investigated first. Beating loci were observed in all samples starting from day 7 of differentiation. Cells were harvested and stained for cTNT and EdU using the Click-iT EdU Alexa Fluor 488 Flow Cytometry Assay Kit. Stained cell populations were measured in a Flow Cytometer from Beckman Coulter and analysed using the Kaluza Flow Cytometry Analysis software. Figure 65 depicts a representative FACS analysis. 25.31% of cells were analysed cTNT+ and are considered CMs in the ctr sample. 33.4% of gated CMs were EdU+, categorizing them as proliferative CMs. Out of all gated cells, 23.77% were measured cTNT+/ EdU+. 33.12% of *MEIS1*- KO cells were measured cTNT+. Out of this CM population, 10.17% of cells were EdU+ and therefore considered proliferative CMs at the moment of fixation. In the *MEIS1*- KO sample, more cells were gated as CMs, but less within this group were measured as EdU+, when compared to the isogenic HAK ctr cell population. This analysis represents one of multiple executed FACS analysis performed on HAK ctr and *MEIS1*- KO 9d CMs.

## HAK CTR CM



## MEIS1 KO CM

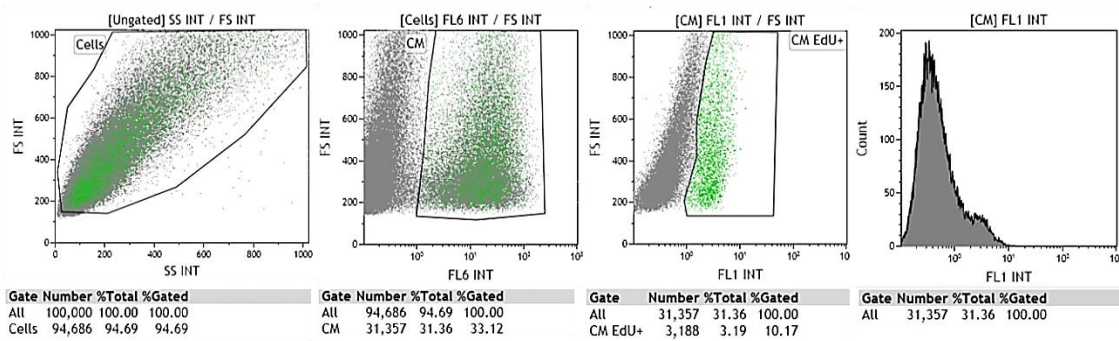


Figure 65: Representative FACS analysis of cTNT+ and EDU+ CMs of HAK ctr and *MEIS1*- KO line 9 days after induction of differentiation.

First gating shows selection of cells by their size in forward scatter (FS) and sideward scatter (SS). Second gating was set with cells measured in the FL6 channel (FL6) for 647 nm emission for cTNT+ stained populations (CM). Following gate was set for FL1 positive cells, translating to EdU+ cells (CM EdU+). Last plot shows fluorescent intensity of 488 nm emitting cells (FL1) versus cell number (count). Upper row of plots depicts 9d CM of HAK ctr line, lower panel of *MEIS1* KO CM.

FACS analysis of 9d CMs of both lineages was performed in 4 independent experiments for the HAK ctr line and in 6 independent experiments for the *MEIS1*- KO line. Figure 66 depicts %Total mean values of percentage of cTNT+ cells of each line in panel A, as well as percentage of cTNT+/EdU+ cells of each line in panel B. 33.5% cells of the isogenic HAK ctr lineage were measured cTNT+, 27.7% of the *MEIS1*- KO lineage were measured cTNT+. This difference is not statistically significant. Mean percentage of double- positive CMs in the isogenic HAK ctr CMs was calculated at 23.5%. Double- positive *MEIS1*- KO cell population represent 14.1% of cells analysed. This difference is also not statistically significant. Some variation between experiments was noted and is represented by the error bars. These differences are referring to variations within differentiations.

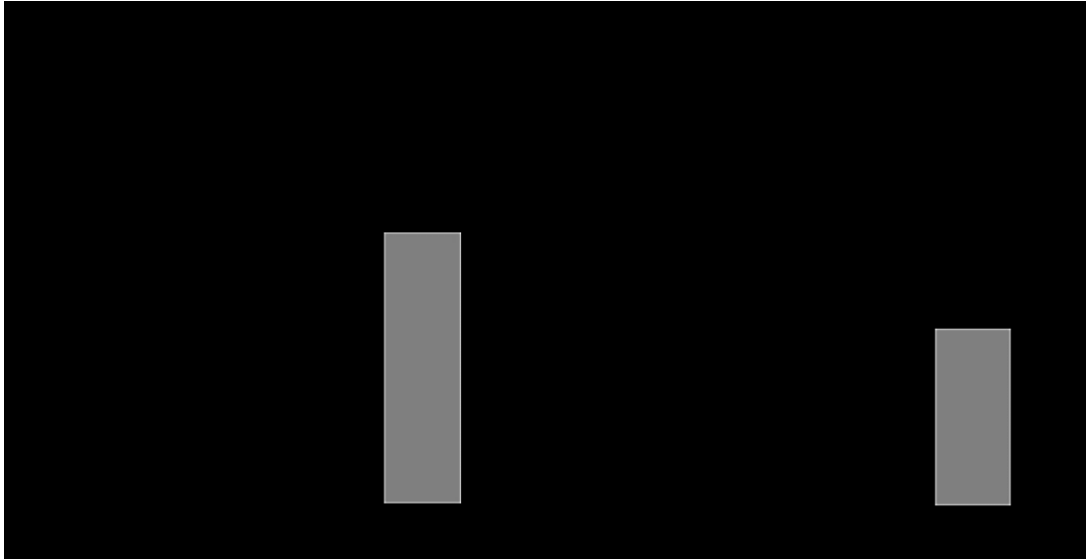


Figure 66: Evaluation of differentiation and proliferation capacity of *MEIS1*-KO hiPSC into CMs compared to HAK wt line.

Black bars represent HAK ctr CMs (HAK CTR) of 9 days age of 4 independent experiments. Grey bars represent *MEIS1*-KO CMs (MEIS KO) of 9 days age of 6 independent experiments. Error bars presented as mean +SEM. (A) Percentage of cells measured cTNT+. (B) Percentage of cells measured double-positive for cTNT and EdU.

## V. Discussion

### 5.1 Importance of disease modelling in *CALMI*- hiPSC lines

LQTS is a congenital genetic disorder, causing life- threatening arrhythmias and posing a high risk of sudden cardiac death <sup>118</sup>. Without therapy, 21% of symptomatic patients die within one year of the first syncope, defining LQTS as one of the leading causes of early and sudden death in infants <sup>118</sup>. Lia Crotti and her colleagues first identified mutations of the *CALMI* gene to be associated with LQTS and cardiac arrest in children <sup>1</sup>. Two young patients carrying mutations in proximity within the *CALMI* gene were chosen as donors of somatic cells to generate patient- specific hiPSCs for disease modelling. The technology to reprogram somatic cells into patient- specific hiPSCs and to further differentiate them into hiPSC- derived CMs is creating the opportunity to investigate mechanisms of cardiovascular disease pathogenesis *in vitro* in the diseased cell type without the need to obtain those cells directly from the patients. Not only can altered molecular mechanisms be revealed, but new treatment options and drug screenings can be explored and made of use to tailor medical therapy for each patient individually.

hiPSC lines of LQTS patients carrying the D130G and F142L mutation were successfully generated (Figure 10). hiPSC lines were tested positive for pluripotency by different approaches (Figure 14, Figure 12, Figure 13, Figure 15 and Figure 16), and generated CMs were shown to meet all criteria to be categorized as hiPSC- derived CMs (Figure 17, Figure 18). Patient- specific hiPSC- derived CMs carrying the F142L mutation recapitulate the disease phenotype *in vitro*. CaM acts in CMs directly on RyR2 receptor channels, the Ca<sub>v</sub>1.2 channel, and influences CaMKII activation, among many other targets <sup>147</sup>. We demonstrated in Figure 30 and Figure 31, that mutated CaM in hiPSC- derived CMs did not cause RyR2 instability, even though expected. Compensation of wt CaM is suggested to secure normal RyR2 function. Findings by heterologous expression studies support this proposal, since diastolic RyR2 stabilisation is performed by Ca<sup>2+</sup> bound CaM and dependent on high affinity Ca<sup>2+</sup> binding to the C- lobe of CaM <sup>110</sup>. Ca<sup>2+</sup> binding was shown to be impaired by the F142L mutation, further supporting the idea of compensation to stabilise RyR2 <sup>1</sup>. CDI is a mechanism mediated by Ca<sub>v</sub>1.2 channels under apoCaM pre-association <sup>151</sup>. apoCaM possesses an increased affinity for binding Ca<sub>v</sub>1.2, affecting directly AP duration and influencing the balance between Ca<sup>2+</sup> influx and K<sup>+</sup> efflux <sup>101</sup>. CDI

is shown to be strongly impaired in patient hiPSC- derived CMs (Figure 22). Considering only 1/6 of CaM- encoding alleles to produce mutant CaM protein, a strong dominant negative effect is obvious. It is suggested that mutant apoCaM is predominant in the pre-bound apoCaM pool due to its weaker Ca<sup>2+</sup> binding affinity and strong Cav1.2 binding affinity, by which Cav1.2 modulation is mediated<sup>133</sup>. The observed lack of negative effect on CaMKII activation in mutant CMs further supports the theory of compensation by upregulation of wt CaM, even resulting in an increase of wt CaM- CaMKII complexes. A gain in Ca<sup>2+</sup> influx by impaired CDI triggers the small raise in CaMKII activation<sup>133</sup>. An unchanged NCX “conductance” (Figure 31), unaffected SR Ca<sup>2+</sup> content (Figure 31), but yet a defective CDI (Figure 22) imply the functional reserve of existing NCX sufficient to balance higher Ca<sup>2+</sup> influx. Enhanced recruitment of NCX is likely attributed to the higher Ca<sup>2+</sup> influx itself. Other ion channels were not upregulated on the transcriptional level (Figure 18). Overall “[...] CDI may not be essential for homeostasis of Ca<sup>2+</sup> content in hiPSC- CMs.”<sup>133</sup>.

Characterization of the LQT phenotype in hiPSC- derived CMs showed prolonged QTc (Figure 25), a steeper QT/ RR relation (Figure 26) and a higher sensitivity to isoproterenol. These features recapitulate the phenotype of the F142L patient<sup>1</sup>. The failure to shorten APD at high rates (Figure 29 B) and the abnormal constancy of I<sub>CaL</sub> availability shown in isolated hiPSC- CMs point to an abnormality in repolarization in mutant CMs. Figure 29 A depicts resulting effects of these abnormalities, causing irregularities and failure in AP sequences. Contradictory results shown in Figure 25 are explained by a limitation of spontaneous beating rate due to delayed repolarisation in CBs<sup>133</sup>. Another inconsistency in results was the steeper QT/ RR and APD/ CL relations, as displayed in Figure 25- Figure 29. It is known that pro- arrhythmic risk is brought about by a strong rate- dependency of repolarization<sup>152</sup>, yet steeper APD rate dependency is provoked itself by APD prolongation<sup>153</sup>. However, “[...] defective CDI might contribute to enhance sensitivity to β-adrenergic stimulation.”<sup>133</sup>.

Taken together, the acquired results from patient- specific hiPSC- derived CMs conclude that the patient’s arrhythmogenesis is solemnly caused by excess I<sub>CaL</sub> and its effect on repolarization. Due to those conclusions, the effect of the calcium channel blocker verapamil was tested. Indeed, a reversal of the mutation phenotype was observed (Figure 32).

In previous studies on LQTS, fetal murine cells harbouring the D130G mutation in the *CALMI* gene failed to follow pacing at slow rates. β- adrenergic stimulation showed a

reversion of this potential arrhythmogenic feature, concluding  $\beta$ -adrenergic stimulation to be the suggested therapeutic approach<sup>115</sup>. The same study however showed murine cells harbouring the F142L mutation to behave only limited in that way, just like the F142L hiPSC-derived CMs. Since  $\beta$ -adrenergic stimulation involves an increase in pro-arrhythmic risk<sup>152</sup>, this therapeutic approach is not suggested for the patient carrying the F142L *CALMI* mutation. A heterologous study in guinea pig ventricular CMs overexpressing CaM with F142L mutation resulted in prolonged APD and increased  $\text{Ca}^{2+}$  current<sup>116</sup>, which lies in conformity with our findings. However, they also describe an increased SR  $\text{Ca}^{2+}$  load, which is not the case in our hiPSC-derived CMs. It becomes clear, that heterologous systems have their limitations in accuracy of unveiling underlying pathogenic mechanisms. Using overexpression plasmids to imitate mutated protein expression can never achieve intracellular mutant protein concentrations and subcellular localisation comparable to the patient's system<sup>133</sup>. Gene and protein expression profiles in human CMs are unique and differ from all other established model systems<sup>154</sup>.

Greatly divergent results highlight the importance of disease modelling in patient-derived hiPSC-CMs to tailor therapeutic appliances. It furthermore proves limitations and inaccuracy of heterologous systems to investigate disease mechanisms. Especially when affected cells are not easily available, such as CMs, taking advantage of patient-derived hiPSC generation and differentiation into patient-specific target cells displays state-of-the-art science.

#### 5.1.1 Optimal control lines: knock-out and correction of the mutated allele

The newly discovered gene editing technology CRISPR/Cas9 opens up uncountable possibilities from disease modelling, over functional analyses and drug screening platforms up to therapeutic treatment options. Disease modelling in patient-derived hiPSCs is a potent technology to investigate pathogenic mechanisms within the genomic background of the patient. Many complex disease phenotypes underlie the impact of not only one single genetic mutation, but are presumably a composite of many genetic and epigenetic aspects<sup>155</sup>. However, discrimination between disease related variations and background related variations in the appearance of the phenotype can be challenging with hiPSCs, above all when the genetic variant under study has a subtle effect<sup>60</sup>. Choosing several unrelated, healthy ctr hiPSC lines as reference would only help to a limited degree. The discovery of technologies to enhance efficiency of HR in hiPSCs, ZFN, TALEN and

CRISPR/ Cas9 opened up the possibility to not only create corrected hiPSC lines and providing therewith the ideal isogenic ctr for disease modelling in hiPSCs, but to rescue the disease phenotype. Previous publications demonstrated successful cardiac disease modelling by comparing mutated hiPSC- derived CMs with their isogenic ctrs on LQTS<sup>60</sup> and familial cardiomyopathy<sup>156</sup>. Efforts have been made to generate isogenic hiPSC lines to characterize cardiac disease for mitochondrial cardiomyopathy<sup>157</sup>, dilated cardiomyopathy due to titin mutations<sup>158</sup> and phospholamban mutations causing cardiomyopathy<sup>159</sup>. Gene- correction as a means of disease modelling was also shown for other diseases, for example for characterizing gyrate atrophy<sup>160</sup>, Duchenne muscular dystrophy<sup>161</sup> and sickle cell disease<sup>162</sup>. However, it has to be emphasized, that genome- editing in hiPSCs has been proven a challenging task due to low HDR efficiencies and the fragile nature of hiPSCs. The low number of publications on successfully generated isogenic hiPSC lines and corrected patient hiPSC lines since the advent of the CRISPR/ Cas9 technology impressively reflects these challenges. While CRISPR/ Cas9 has become a highly effective tool for generation of mouse knock- out and disease models, efficient and precise genome- editing in hiPSCs still remains a labour- intensive and demanding task. Protocols are still being improved and refined methods are needed to improve efficiencies in hiPSCs further.

To correct the *CALMI* F142L mutation in patient- derived hiPSCs, different approaches were endeavoured including classical homologous recombination and CRISPR/Cas9. It was observed, that F142L hiPSCs were only stable in culture for 10 to 15 passages as single cells, limiting the time window to perform correction experiments significantly. F142L hiPSCs were noted to be more sensitive and would react by uncontrollable differentiation compared to ctr hiPSC lines, regardless of culturing on MEF feeders or in feeder- free conditions on Geltrex. Attempts to correct the mutation by classical homologous recombination were unsuccessful. This is primarily believed to be due to sensitivity of cells against electrical current induced pore formations and the inability to tolerate being electroporated with great amounts of DNA. Transfection of DNA is stressful to cells and can trigger cyclic GMP-AMP cyclase activation<sup>163</sup>. Reduced cell survival is a known disadvantage of electroporation and has been described to be difficult to use for high- throughput usage<sup>164</sup>. Only 67 colonies were derived out of 3 experiments (see page 91 and following). The CRISPR technology is described as a faster and more efficient method to edit genomes compared to the classical homologous recombination approach

<sup>69,165,166</sup>. It was therefore refrained from further optimising the classical homologous recombination technology. The CRISPR genome-editing approach was first carried out by electroporation of hiPSCs with Cas9 expressing plasmids encoding a GFP signal and a separate gRNA expression plasmid (section 4.4.2), in dependence on publications of Ran *et al.* <sup>69</sup> and Davis *et al.* <sup>131</sup>. Upon optimisations by using all-in-one plasmids encoding both the Cas9 protein and the gRNA sequence on one plasmid, delivery efficiencies of up to 6.9% were reached (Figure 42), with recovery efficiencies of up to 8.8% (Figure 43 and Figure 44). However, all screened colonies did not show correction of the F142L mutation in the patient's hiPSCs. In other publications, gene correction efficiencies using CRISPR in hiPSCs were reported ranging only from 0.5- 10% <sup>148,155,167</sup>, strongly depending on the genomic locus to be targeted, cell quality and equipment provided to perform experiments in a high throughput manner. Especially cell sorting by FACS is believed to cause high incidence of cell death, resulting in a low recovery efficiency. Taking together the low delivery and recovery efficiencies reached in hiPSCs carrying the F142L mutation and the low reported efficiencies of successful gene mutation corrections in literature, finding no corrected clone among 636 screened clones is ascribable to limitations in performing experiments at a larger scale. In order to increase clone numbers to be screened, an upscaling of experimental setup is necessary, but very challenging. The very fragile nature of the *CALMI*- F142L hiPSC line further complicated experiments.

A cruder and yet more efficient way of studying the impact of a genetic mutation within a certain genetic background are loss-of-function studies, by knocking-out the gene of interest. In our specific case of a heterozygous mutation in one of the 3 genes encoding CaM, which is clearly acting in a dominant-negative way, knock-out of the mutated *CALMI* allele or both would be very informative. While gene correction by the CRISPR/Cas9 system requires the presence of an exogenous DNA template for repairing DSB by HDR, knocking-out a gene with CRISPR/Cas9 uses the NHEJ pathway, which will often lead to indels and therefore evoking premature stop codons by frameshifts and exchanges of nts <sup>168</sup>. Previous publications report knock-out efficiencies between 15% and 64% in hiPSCs, using different CRISPR/Cas9 systems <sup>148,155,169,170</sup>.

Figure 50 displays editing efficiencies in the *CALMI*- F142L hiPSC line of up to 33%. By knocking-out the mutated *CALMI* gene and examining the resulting phenotypic and molecular pathway changes, conclusions can be drawn on the negative dominant effect of the mutation. After eliminating the expression of mutated CaM in hiPSC-derived CMs,

a rescue of the disease phenotype would be expected, if the cells react by compensating CaM concentrations from other gene transcripts. If the cell is not able to compensate for the loss of transcript from the mutated *CALMI* gene, an even greater electrophysiological imbalance is expected. Many electrophysiological processes, such as CDI, CDF, AP propagation, but also changes in transcriptional regulation are influenced by CaM<sup>101</sup> and would be heavily disturbed. It might be well possible that hiPSCs not being able to compensate for the loss of one allele expressing *CALMI* become instable and won't be cultivable as hiPSCs or as CMs. In a total of 14 colonies genomic alterations were detected, which are assumed to have led to a *CALMI* knock-out on one or even both alleles. The fact, that none of the edited clones of the *CALMI* knock-out approach remained stable in culture, but underwent apoptosis or differentiation, supports the theory, that all three *CALM* genes are crucial for cell survival. The strongly conserved identity of CaM across species<sup>171</sup> and discovery of severe disease phenotypes provoked by mono-allelic point mutations within *CALM* genes<sup>1,110,115,172-174</sup> further support this theory.

Since the discovery of CRISPR/ Cas9 potential in precise genome- editing, many great publications showed gene modifications in different cell types. However, the majority of genome- editing in human cells is performed in HEK293 cells or human neonatal fibroblasts, since those cells are easily manipulated and transfected<sup>155</sup>. The paucity of publications describing genome- editing in hiPSCs mirrors the difficulties one faces in targeting hiPSCs genomes. hiPSCs are difficult to culture as single cells and selection methods are harsh on fragile hiPSCs. Single- cell clonal expansion, that is necessary in order to isolate targeted clones, is very labour intensive and not always successful. Many edited clones might not be stable enough to succeed in clonal expansion<sup>175</sup>.

### 5.1.2 Off- target analysis

Other aspects of CRISPR/ Cas9 genome- editing approaches in hiPSCs that need to be considered include unwanted off- target gene editing events. Since the discovery of the potential of CRISPR/ Cas9, several research groups investigated the incidence of unwanted DSBs in the DNA caused by misguidance of Cas9<sup>176-180</sup>. Off- target events are provoked by binding of the Cas9 nuclease to genomic sites that share homology with the target sequence due to misguidance of the designed gRNA. Off- target cleavage of the DNA will cause the cell to initiate DNA repair mechanisms, which can cause gene mutations and chromosomal dislocations<sup>177</sup>. Even though incidence of off- target effects in

hiPSCs have been reported to be very low <sup>180</sup>, efforts have been made to most accurately screen for those events. *In silico* online software tools perform bioinformatics- based off-target side prediction <sup>181,182</sup>, however do not take *in vivo* situations like accessibility of the genetic locations into account. Epigenetic status of the locus affects performance of the Cas9 endonuclease <sup>182-184</sup>. Many other strategies were developed to detect off- target events, including IDLV <sup>185</sup>, GUIDE- seq. <sup>179</sup>, HTGTS <sup>186</sup>, or BLESS <sup>187</sup>, just to name a few. It becomes clear by the amount of research put into the matter of detecting off- target events, that generated off- target events represent a drawback in the potential of CRISPR in basic research, but even more so in clinical applications.

Since genome- editing approaches in *CALMI*- F142L hiPSCs did not result in stable corrected or knock- out hiPSC clones, no conclusion can be drawn on the off- target potential when targeting the *CALMI* locus. Designing the gRNAs for correction and knock- out approaches using the crispr.mit.edu online software, potential exonic off- target loci were carefully noted and would have been investigated appropriately. Primers were designed to sequence predicted off- target locations and screen for unwanted editing events. Genome wide sequencing would also be considered necessary.

### 5.1.3 New CRISPR versions

Since the advent of CRISPR/ Cas9 as editing tool, many studies have investigated editing efficiencies and off- target effects in different model systems. Variants of Cas9 have been developed to further refine this tool. One of the first alterations on the Cas9 protein was the development of the mutant Cas9n nickase by Zhang and colleagues <sup>188</sup>. By producing single strand DNA breaks instead of DSBs, unwanted off- target effects are being reduced and HDR is promoted. Another refined Cas9 model makes use of a high fidelity version of Cas9 (SpCas9- HF1), described to target the genome with the same efficiency but reducing off- target events to a minimum <sup>189</sup>. If no classical PAM sequence is available close enough to the targeting point, Cas9 proteins originating from other host organisms can be made of use. SaCas9 originates from *Staphylococcus aureus*, is over 1kb shorter and recognizes a PAM of NNAGAAW, nevertheless has been shown to reach editing efficiencies close to SpCas9 <sup>190</sup>. Another variation of this SaCas9, namely KKH SaCas9, recognizes NNNRRT as PAM, increasing its targeting range 2- to 4- fold <sup>191</sup>. Increased specificity in human cell systems has been reported by using truncated gRNAs and di-

meric RNA-guided FokI nucleases<sup>192</sup>. CRISPR- Cpf1 is one of the most recent developments in gene targeting tools. This endonuclease produces cohesive double- strand breaks and is guided by a single- RNA (crRNA)<sup>193</sup>. All above mentioned nuclease adaptations are just a selection of developments in this rapidly forward moving field of research. Considering Cas9 genome- editing in hiPSCs for disease modelling is however mostly limited by the difficulty of reaching a high editing efficiency in hiPSCs, rather than the concern of off- target events. While knocking- out genes is achieved with higher efficiency by using paired gRNA approaches<sup>194</sup>, knocking- in or correcting genomes in hiPSC still poses a bigger challenge.

One of the most recent advances in CRISPR/ Cas9 genome engineering described is the delivery of Cas9 mRNA/ gRNA or pre- complexed Cas9 protein/ gRNA ribonucleoprotein complexes (Cas9 RNPs) through liposome-mediated transfection or electroporation<sup>195</sup>. This method is described in producing indels at 79% efficiency, with less off- target events. It is supposed to be especially suitable for human cell lines and sensitive cells like hiPSCs. 2- fold more colonies were recovered in hESCs using this method<sup>196</sup>. Since *CALMI*- F142L hiPSCs were observed to be more sensitive to DNA delivery via electroporation, delivery of Cas9 RNPs might be a more favourable approach.

## 5.2 Applications of CRISPR/ Cas9 to investigate genes of cardiogenesis in vitro

CRISPR/ Cas9 was applied in the healthy ctr hiPSC line HAK, that remained stable in culture after adaption to single- cell growth (Figure 53). The *MEIS1* gene was chosen for a knocking- out approach by CRISPR/ Cas9 in hiPSCs to shed light on the role of *MEIS1* during cardiogenesis. KO gRNA sequences were chosen from the KO gRNA library and cloned into the Addgene CRISPR backbone #62988. Nucleofection delivery efficiencies of 40% were reached (

Table 11) under optimised conditions, editing efficiencies of 56.3% were shown. TIDE analysis of a selected clone revealed this KO clone to be edited on both alleles. Both alleles harbour the same editing, a deletion of 4 nts, an exchange of 2 nts, followed by deletions of twice 1 nt (Figure 57). Sequencing results without underlying double reads clarify identical editing on both alleles (Figure 57). When translating the edited sequence

into corresponding aa sequences, the changes result into a premature stop codon, as depicted in Figure 58. This was further confirmed by qRT PCR. Significantly less transcript of *MEIS1* was present in KO cells compared to untargeted HAK hiPSCs (Figure 60). Remaining transcript levels are interpreted as alternate splice variants missing the targeted region and therefore not being affected by the KO. According to the genome browser ensembl.org, 5 transcripts encode for an orthologue MEIS1 protein in the human organism. 9 additional transcripts are described as processed, however they don't possess an ORF and are therefore most likely not transcribed. Those variants are made accountable for insignificant transcript detection in the qRT PCR. Most importantly it is shown by WB analysis, that no more MEIS1 protein is present in *MEIS1*- KO CMs derived from *MEIS1*- KO hiPSCs, affirming the sequencing and qRT PCR results (Figure 62). Further effects of knocking- out *MEIS1* were elucidated by qRT PCR.

### 5.2.1 The role of *MEIS1* in cardiogenesis

*MEIS1* is described in literature as a member of HOX genes, encoding a TALE homeo-domain transcription factor protein<sup>95</sup>. This family of transcription factor proteins is known to act as key regulators of cardiac development during embryogenesis<sup>97</sup>. Before *MEIS1* was attributed to heart development, it was described to be involved in hematopoietic stem cell quiescence, activation of oncogenic genes and cellular hyper-proliferation in myeloid leukaemia cells<sup>96</sup>. Global *Meis1* knock-out studies in mice revealed *Meis1* contributing to embryonic haematopoiesis and heart development<sup>99, 98</sup>. Mahmoud and colleagues identified “[...] *Meis1* as a potential transcriptional regulator of neonatal heart regeneration.”<sup>100</sup>. Following studies identified the role of *Meis1* in CM cell cycle post-natal in KO mice. *Meis1* expression is reported from day 1 to day 7 postnatal by qRT PCR, as well as by immunostaining starting from d4 after birth and throughout adulthood<sup>100</sup>. *Meis1* deletion in KO mice resulted in an increase in CM proliferation, measured by staining and quantification of pH3+ TnnT2+ cells as a marker for mitosis. An increase in sarcomere disassembly as indication of proliferation, the cytokinesis marker Aurora B kinase and an increase in BrdU+ cells were found as well<sup>100</sup>. While total number of CMs stayed the same, the percentage of mononucleated cells increased compared to binucleated cells<sup>100</sup>. This was interpreted as proliferative mononucleated CMs population<sup>197-199</sup>.

Investigating the transcriptomic influence of *MEIS1* on CM proliferation revealed a large proportion of cardiac enhancers binding to NKX2.5 also sharing binding sites with

MEIS1<sup>200</sup>. Dupays and colleagues further speculate NKX2.5 and MEIS1 to share a common set of gene targets in mouse and in the human system. During the transition from cardiac progenitors to differentiated CMs many changes in gene expression and cell cycle have been documented<sup>97,201-203</sup>. The reported changes coincide with a switch from MEIS1 to NKX2.5 expressions and their shift in binding to common enhancer regions. It is speculated, that therefore the subgroup of MEIS1 regulated genes is associated with the transition of proliferation to differentiation of CMs during cardiogenesis<sup>200</sup>. Another publication supporting this theory suggested cardiac development being co-regulated by Meis/Hox and Gata factors in mouse embryonic stem cell-derived CMs due to an overlap of TF binding sites at enhancer regions<sup>97</sup>. Tbx20 overexpression studies in adult mouse CMs showed that Tbx20 binds and represses *Meis1* expression, contributing to Tbx20-induced CM proliferation<sup>204</sup>.

Taken together, it becomes eminent that MEIS1 is a transcription factor playing a crucial role in cardiogenesis. Even though most studies were performed in mice as model systems, an equally important role of MEIS1 in the human organism during cardiogenesis is to be expected. Knock-out studies in hiPSCs represent an opportunity to investigate the role of this transcription factor during differentiation stages from pluripotent stem cell via cardiac progenitor cells up to CMs in the human system.

### 5.2.2 Effects of *MEIS1* knock-out on hiPSC cardiac differentiation

*MEIS1*-KO hiPSCs were differentiated into CMs for 9 days and harvested to analyse the number of cTNT+ and proliferating cells. Cell populations were gated for cell size, cTNT positivity and EdU positivity, representing proliferative CMs at the time point of analysis (Figure 65). No statistically significant difference was noted regarding cTNT/EdU double positive cell number between wt ctr and isogenic *MEIS1*-KO CMs (Figure 66). Mahmoud and colleagues report a decrease in CM cell size in mice *MEIS1*-KO CMs 14 days postnatal, as well as an increase in proliferation in those CMs in mice<sup>100</sup>. This observation was not made in hiPSC-derived CMs after 9 days of differentiation. As shown in Figure 65, on average 23.5% of HAK CMs and 14.1% of *MEIS1* KO CMs were detected cTNT/EdU double positive. However, hiPSC-derived CMs 9 days after induction to cardiac differentiation are considered to be in an early embryonic state, rather than a postnatal CM state and proliferate at a similar pace to embryonic or fetal CMs<sup>205-207</sup>. hiPSC-derived CMs are described to possess 10% proliferative capacity even after 4 weeks in

culture<sup>206,208</sup>. Therefore, no direct comparison in proliferative capacity due to *MEIS1* gene KO can be made between the *Meis1*-KO mice CMs at d14 after birth<sup>100</sup> and the hiPSC-derived CMs analysed in this study. The same accounts for the difference noted in cell size between wt and KO post-natal mouse CMs. No difference in cell size was noted between the ctr versus KO hiPSC CMs. Further investigation using wt and *MEIS1*-KO hiPSC-derived CMs at several months of differentiation (which resemble more closely late-embryonic/ post-natal CMs) will be necessary to draw conclusions on the proliferative effects provoked by *MEIS1* gene knock-out in human CMs.

One conclusion that can be drawn from the experimental results presented in this study is that *MEIS1* is dispensable for hiPSC cardiac differentiation. *MEIS1*-KO hiPSCs were able to generate CMs upon cardiac induction and specify progressively to mesoderm, cardiac mesoderm, and cardiac progenitor cells.

Specifically, no differences in transcript expression level of the early mesoderm marker *BRY* was noted between wt control and isogenic *MEIS1*-KO hiPSCs at the beginning of cardiac induction (Figure 64). Differences in expression levels of *MESPI* transcript, as marker of early cardiac mesoderm, are not significant. However, the increase in *MESPI* transcript expression in KO cells was less steep and does not reach the same maximum value as in the wt ctr line. Decline of fold change is also slower in the KO hiPSCs than in wt control. The measured difference in expression between ctr and *MEIS1* KO line might be the result of knocking-out *MEIS1*. *Mesp1* is described as activator of *Meis1* expression in mouse ESC-derived endothelial cells<sup>209</sup>. Furthermore, *MESP1* is a marker for early cardiovascular progenitors<sup>210</sup>, promotor for cardiovascular development during embryogenesis and cardiac differentiation of stem cells<sup>150</sup>. It is believed, that “[...] *Mesp1* resides at the top of the cellular and transcriptional hierarchy that orchestrates MCP (multipotent cardiovascular progenitor) specification.”<sup>150</sup>. Disturbance of expression of this key regulator in the *MEIS1*-KO lines is easily believed to majorly influence cardiac differentiation. Understanding the underlying mechanisms, by which a lack of *MEIS1* expression would negatively influence *MESP1* expression demands a more detailed investigation.

*ISL1* expression, marking a specific population of cardiovascular progenitor cells known as second heart field (SHF) progenitors<sup>211</sup>, shows a steady increase in both lines over the time course analysed. Expression patterns between the two lines are shifted, however, no significant difference is measured between the lines. To further elucidate, if differences

are due to the effects of *MEIS1*-KO or rather due to variabilities between biological replicates, a more detailed investigation is necessary. Insignificance of differences point towards *MEIS1*-KO neither influencing specification of ISL1 expressing cardiac progenitors, nor to regulate *ISL1* transcription itself.

The same is true for *NKX2.5*, a key regulator of both cardiac progenitor cells and cardiomyocytes. The steady increase in *NKX2.5* transcript expression is similar in both wt and *MEIS1*-KO line. Differences at d12 of differentiation between the control and KO line are not significant due to prominent error bars.

The steady increase of expression of *MEIS1* from day 4 post-induction of cardiac differentiation of hiPSCs proposes a role of MEIS1 at a cardiac progenitor stage and during the transition from cardiac progenitor to differentiated CMs. Further experiments are warranted to exploit the function of MEIS1 in this context. Reports by Dupays and colleagues on the impact of Meis1 on cardiac differentiation<sup>200</sup>, as well as findings of Mahmoud and colleagues support a role of Meis1 in regulating postnatal cell cycle arrest<sup>100</sup>. Another interesting finding promoting the theory of Meis1 playing an important role in cardiac differentiation is the statement by Paige and colleagues<sup>95</sup>. They identified MEIS2 to harbour histone modification patterns identified as cardiac regulatory genes by ChiP-seq of hESC undergoing cardiac differentiation<sup>95</sup>. Belonging to the same MEIS class protein family of TALE homeobox genes, they are highly conserved throughout species and share a high sequence homology<sup>212</sup>. A common profile in cardiac development can be assumed and is worth examining further.

### 5.2.3 Multiple and conditional gene targeting as analysis tool for cardiogenesis

Deciphering transcriptional processes that drive human cardiogenesis is a difficult task, taken the limiting accessibility of human fetal material. The combination of hiPSCs and CRISPR/Cas9 technologies can be made of use to precisely investigate gene interplay during human organogenesis. Not only preventing transcription by gene knock-out, but activation of transcription can be controlled by the endonuclease Cas9. Different Cas9-gRNA systems have been developed to influence activation of transcription, namely Cas9 using SAM as guide RNA, scRNA or epitope based Cas9-gRNA systems like SUPernova or SunTag<sup>213-215</sup>. By fusing activation domains to Cas9 variants without endonuclease activity (dCas9), several genes important for neurogenesis in hiPSCs were specifically activated. A significantly increased neuronal differentiation capacity was observed as a

result<sup>216</sup>. Protocols on how to clone up to 4 gRNAs into expression vectors for activation of transcription studies in hiPSC lines are readily available<sup>217</sup>. This system allows induction of transcriptional activation of up to 4 different genes in human cells<sup>217</sup>. Even simultaneous activation and repression of transcription was shown in HEK293 cells<sup>215</sup>. The group by J. Zalatan developed CRISPR-associated modular scaffold RNAs that enable to influence multigene transcriptional programs. By using orthogonal Cas9 proteins, that use different gRNA sequences for recognition<sup>72</sup>, in combination with RNA binding modules, multiple genes can be activated and repressed simultaneously<sup>215</sup>. They demonstrate this advance in yeast model organisms and propose optimisation of metabolic engineering, but also suggest applications for genetic reprogramming to influence cell fates<sup>215</sup>. Combining these newly advanced methods to influence master regulators with inducible Cas9 systems would provide the possibility to control pathways on multiple genes in a temporal manner. Different groups have published work about chemically inducible Cas9 systems. Liu and colleagues developed an inducible Cas9 by fusion with the hormone binding domain of the ERT2 receptor<sup>218</sup>. Others make use of doxycycline-inducible Cas9 vectors<sup>219</sup>. A great advantage of inducible Cas9 systems is the very low off-target efficiency due to a limited active time span of the endonuclease protein<sup>219</sup>.

The potential of temporally controlled, multi-gene targeting pathway stimulation by CRISPR/Cas9 opens up great new experimental opportunities. Cardiac differentiation could be optimised, as described for neural differentiation in Chavez's publication<sup>216</sup>, by enhancing transcription of cardiac genes like *ISL1* or *NKX2.5*. To promote differentiation into a specific cardiac subtype, one can imagine to enhance expression of *HAND*, *NKX2.5* and *IRX4* to promote ventricular cell differentiation, or to investigate pro-atrial differentiation effects when stimulating *COUP-TFII* expression<sup>220</sup>. Effects on cardiogenesis by influencing gene pathways and expression profiles could be studied more precisely by influencing gene expression in a temporal manner. Up to date, over 40 cardiovascular disorders have been identified as monogenetic disorders, however many diseases display a clinical or phenotypical heterogeneity, mainly accounted to secondary genetic factors<sup>221</sup>. Gene variants and polymorphisms may act on gene promotor regions, influencing gene expression or enzymatic processes, disturbing cardiogenesis<sup>222</sup>. Inducible scaffold CRISPR/Cas9 systems acting simultaneously on causal genes and suspected modifier genes of the genetic background would greatly facilitate the understanding of many cardiovascular disorders.

### 5.3 Future outlook of CRISPR/ Cas9

The fast pace of advancement of the CRISPR/ Cas9 technology throughout many research areas reflects the high potential that is yet to be taken advantage of. As demonstrated impressively by Barrangou and Doudna in their publication by a bar graph (Figure 67), the number of manuscripts published since 2002, including CRISPR, ZFN or TALEN as keywords, has been increasing exponentially<sup>223</sup>. While many researchers focus on eliminating off-target effects by optimising the endonuclease activity of Cas9 or altered PAM recognition, the greatest hurdle to efficiently use this system in disease modelling in hiPSCs is the low efficiency of HDR. Great differences in HDR efficiencies are noted between lines and differ pivotal between genomic loci to be targeted. Protocols have to be adapted for every hiPSCs line. The sensitive nature of hiPSCs challenges delivery and selection methods. Analysis of targeted clones through clonal expansion is very work intensive and difficult with fragile hiPSCs. These objections in CRISPR/ Cas9 genome-editing in hiPSCs have also become eminent for this study.

Future use of CRISPR/ Cas9 for hiPSC disease modelling will involve improving efficiency of delivery methods, which will subsequently cancel out the necessity for selection of targeted cell populations. Using Cas9- gRNA protein complexes is believed to have a high potential of increasing delivery and therefore also targeting efficiency in hiPSCs. Transfection as a means of DNA or protein delivery into hiPSCs is a much more sensitive approach when compared to nucleofection or electroporation, a higher cell survival after treatment is expected<sup>195</sup>. Recent research already provides new nanoparticle- creating reagents to deliver Cas9 protein- mRNA complexes (Cas9 RNPs) and show high success rates of genome- editing<sup>224</sup>. Increasing delivery efficiencies will contribute greatly to multiple- gene targeting approaches using CRISPR/ Cas9 to investigate transcriptional influences and pathways during differentiation processes. The commercial availability of hiPSC lines stably expressing an inducible Cas9 by integration of the endonuclease encoding gene into safe- loci further simplifies protocols using CRISPR on hiPSCs<sup>225</sup>. Generation of reporter hiPSC lines by knocking- in long donor DNA templates encoding fluorescent proteins or protein tags is still challenging, but by embracing more efficient delivery methods of gRNAs within nanoparticles and usage of iCRISPR platforms, efficient generation of reporter lines is possible. Possibilities of CRISPR/ Cas9 applications in hiPSC and cardiac disease modelling are innumerable considering these recent technological progresses.

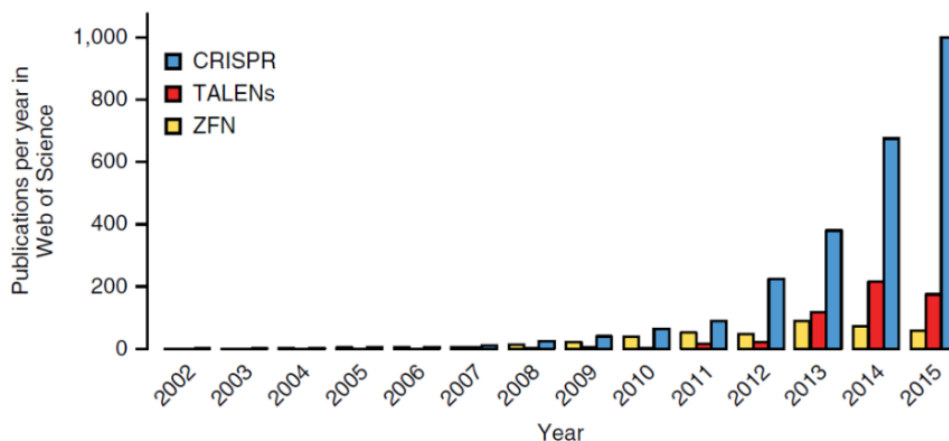


Figure 67: Number of manuscripts published including CRISPR, ZFN or TALEN as keywords since 2002. Manuscripts per year published about CRISPR (blue bars), ZFN (yellow bars) and TALENs (red bars), from 2002 until 2015. Figure published by Barragou *et al.* <sup>223</sup>.

Apart from mentioned application ranges of CRISPR/ Cas9 in hiPSC disease modelling, this promising tool is utilized in many other research and development areas, as illustrated by Barragou and colleagues <sup>223</sup>. Large gRNA libraries are used for genome-wide screenings in loss-of function, transcriptional repression and activation studies <sup>149,226-228</sup>. Loss-of function screens successfully identified genes involved in tumor growth <sup>229</sup>, impressively highlighting the great potential of this technology. By expansion of this library generation into lentiviral delivery methods, many other model platforms can implement this research technique. Many great discoveries are to be expected in the future by CRISPR-based screenings of the non-coding genome. Acting modalities of regulatory sequences and enhancer elements will be deciphered <sup>230,231</sup>.

Moving from *in vitro* to *in vivo* disease modelling with CRISPR/ Cas9 is a challenging but very promising development. CRISPR/ Cas9 genome-editing has been established fast in creating mouse models, whereas applications in larger animal models are demanding. A high potential for disease modelling in pigs and primate models is offered by the combination of CRISPR with somatic cell nuclear transfer <sup>232</sup>. Other application models range from xenograft studies to development of therapeutic strategies and drug safety research <sup>233-235</sup>. Moving this technology further into the clinic for therapeutic appliances remains a great challenge. The most recent approved clinical trials include genetic alterations of patients' immune cells to render them effective against cancer <sup>236</sup>. Main concerns towards off-target effects, DNA-based toxicity and eventual unforeseen side-effects of edited human cells re-introduced into the patient need to be very carefully discussed and precluded. It is to be expected that more clinical trials will be approved in the coming

years, however likely including cells and tissues that are more easily targeted with current targeting methods, like blood cells, muscles or the eye <sup>223</sup>. Further development of the CRISPR/ Cas9 technology will most likely include reducing off- target effects, increasing HDR rates and involving strictly spatio- temporal acting mechanisms to control the action radius of this editing tool further.

Outside of medical research applications, the gene editing tool has been employed to increase livestock efficiency by e.g. making them less susceptible to viruses or remove horns <sup>237,238</sup>. Crops are improved in yield, draught tolerance, nutritional value and other traits to meet higher agricultural aims <sup>239,240</sup>. Genome edited bacteria, yeast and fungi are harnessed to produce products ranging from biofuel to probiotic cultures <sup>241,242</sup>. Even potential data storage by capturing DNA sequences in bacterial genomes has been demonstrated by electroporating bacteria with Cas proteins <sup>243</sup>.

The capability of naturally occurring CRISPR/ Cas variants for use in multidisciplinary research and development is by far not fully capitalized. What started with an “ [...] odd genomic feature [...] ” <sup>67</sup> in prokaryotic cells, that happened to be identified as prokaryotic adaptive immune system, quickly turned into a “ [...] fundamental component of the biologist’s toolkit [...] ” <sup>223</sup> with the potential to have an unforeseen impact on everybody’s life.

## VI. References

- 1 Crotti, L. *et al.* Calmodulin mutations associated with recurrent cardiac arrest in infants. *Circulation* **127**, 1009-1017, doi:10.1161/CIRCULATIONAHA.112.001216 (2013).
- 2 de Wert, G. & Mummery, C. Human embryonic stem cells: research, ethics and policy. *Hum Reprod* **18**, 672-682 (2003).
- 3 Thomson, J. A. *et al.* Embryonic stem cell lines derived from human blastocysts. *Science (New York, N.Y.)* **282**, 1145-1147 (1998).
- 4 Shambloott, M. J. *et al.* Derivation of pluripotent stem cells from cultured human primordial germ cells. *Proc Natl Acad Sci U S A* **95**, 13726-13731 (1998).
- 5 Rumman, M., Dhawan, J. & Kassem, M. Concise Review: Quiescence in Adult Stem Cells: Biological Significance and Relevance to Tissue Regeneration. *Stem Cells* **33**, 2903-2912, doi:10.1002/stem.2056 (2015).
- 6 Fuchs, E. & Segre, J. A. Stem cells: a new lease on life. *Cell* **100**, 143-155 (2000).
- 7 Weissman, I. L. Stem cells: units of development, units of regeneration, and units in evolution. *Cell* **100**, 157-168 (2000).
- 8 Anderson, D. J., Gage, F. H. & Weissman, I. L. Can stem cells cross lineage boundaries? *Nat Med* **7**, 393-395, doi:10.1038/86439 (2001).
- 9 Clarke, D. L. *et al.* Generalized potential of adult neural stem cells. *Science (New York, N.Y.)* **288**, 1660-1663 (2000).
- 10 Pittenger, M. F. *et al.* Multilineage potential of adult human mesenchymal stem cells. *Science (New York, N.Y.)* **284**, 143-147 (1999).
- 11 Jiang, Y. *et al.* Pluripotency of mesenchymal stem cells derived from adult marrow. *Nature* **418**, 41-49, doi:10.1038/nature00870 (2002).
- 12 Reyes, M. & Verfaillie, C. M. Characterization of multipotent adult progenitor cells, a subpopulation of mesenchymal stem cells. *Ann N Y Acad Sci* **938**, 231-233; discussion 233-235 (2001).
- 13 Verfaillie, C. M. Hematopoietic stem cells for transplantation. *Nat Immunol* **3**, 314-317, doi:10.1038/ni0402-314 (2002).
- 14 Jung, K. W. Perspectives on human stem cell research. *J Cell Physiol* **220**, 535-537, doi:10.1002/jcp.21786 (2009).
- 15 Takahashi, K. *et al.* Induction of pluripotent stem cells from adult human fibroblasts by defined factors. *Cell* **131**, 861-872, doi:10.1016/j.cell.2007.11.019 (2007).
- 16 Takahashi, K. & Yamanaka, S. Induction of pluripotent stem cells from mouse embryonic and adult fibroblast cultures by defined factors. *Cell* **126**, 663-676, doi:10.1016/j.cell.2006.07.024 (2006).
- 17 Bellin, M., Marchetto, M. C., Gage, F. H. & Mummery, C. L. Induced pluripotent stem cells: the new patient? *Nat Rev Mol Cell Biol* **13**, 713-726, doi:10.1038/nrm3448 (2012).
- 18 Chari, S. & Mao, S. Timeline: iPSCs--The First Decade. *Cell Stem Cell* **18**, 294, doi:10.1016/j.stem.2016.01.005 (2016).
- 19 Rebuzzini, P., Zuccotti, M., Redi, C. A. & Garagna, S. Achilles' heel of pluripotent stem cells: genetic, genomic and epigenetic variations during prolonged culture. *Cell Mol Life Sci*, doi:10.1007/s00018-016-2171-8 (2016).

- 20 Gonzalez, F., Boue, S. & Izpisua Belmonte, J. C. Methods for making induced pluripotent stem cells: reprogramming a la carte. *Nat Rev Genet* **12**, 231-242, doi:10.1038/nrg2937 (2011).
- 21 Avior, Y., Sagi, I. & Benvenisty, N. Pluripotent stem cells in disease modelling and drug discovery. *Nat Rev Mol Cell Biol* **17**, 170-182, doi:10.1038/nrm.2015.27 (2016).
- 22 Peters, J. The role of genomic imprinting in biology and disease: an expanding view. *Nat Rev Genet* **15**, 517-530, doi:10.1038/nrg3766 (2014).
- 23 Matsa, E. *et al.* Drug evaluation in cardiomyocytes derived from human induced pluripotent stem cells carrying a long QT syndrome type 2 mutation. *Eur Heart J* **32**, 952-962, doi:10.1093/eurheartj/ehr073 (2011).
- 24 Moretti, A. *et al.* Patient-specific induced pluripotent stem-cell models for long-QT syndrome. *N Engl J Med* **363**, 1397-1409, doi:10.1056/NEJMoa0908679 (2010).
- 25 Itzhaki, I. *et al.* Modelling the long QT syndrome with induced pluripotent stem cells. *Nature* **471**, 225-229, doi:10.1038/nature09747 (2011).
- 26 Lahti, A. L. *et al.* Model for long QT syndrome type 2 using human iPS cells demonstrates arrhythmogenic characteristics in cell culture. *Dis Model Mech* **5**, 220-230, doi:10.1242/dmm.008409 (2012).
- 27 Cerrone, M. *et al.* Missense mutations in plakophilin-2 cause sodium current deficit and associate with a Brugada syndrome phenotype. *Circulation* **129**, 1092-1103, doi:10.1161/CIRCULATIONAHA.113.003077 (2014).
- 28 Yazawa, M. *et al.* Using induced pluripotent stem cells to investigate cardiac phenotypes in Timothy syndrome. *Nature* **471**, 230-234, doi:10.1038/nature09855 (2011).
- 29 Lin, B. *et al.* High-purity enrichment of functional cardiovascular cells from human iPS cells. *Cardiovasc Res* **95**, 327-335, doi:10.1093/cvr/cvs185 (2012).
- 30 Jung, C. B. *et al.* Dantrolene rescues arrhythmogenic RYR2 defect in a patient-specific stem cell model of catecholaminergic polymorphic ventricular tachycardia. *EMBO Mol Med* **4**, 180-191, doi:10.1002/emmm.201100194 (2012).
- 31 Fatima, A. *et al.* In vitro modeling of ryanodine receptor 2 dysfunction using human induced pluripotent stem cells. *Cell Physiol Biochem* **28**, 579-592, doi:10.1159/000335753 (2011).
- 32 Gramlich, M. *et al.* Antisense-mediated exon skipping: a therapeutic strategy for titin-based dilated cardiomyopathy. *EMBO Mol Med* **7**, 562-576, doi:10.15252/emmm.201505047 (2015).
- 33 Lee, G. *et al.* Modelling pathogenesis and treatment of familial dysautonomia using patient-specific iPSCs. *Nature* **461**, 402-406, doi:10.1038/nature08320 (2009).
- 34 Marchetto, M. C. *et al.* A model for neural development and treatment of Rett syndrome using human induced pluripotent stem cells. *Cell* **143**, 527-539, doi:10.1016/j.cell.2010.10.016 (2010).
- 35 Devine, M. J. *et al.* Parkinson's disease induced pluripotent stem cells with triplication of the alpha-synuclein locus. *Nat Commun* **2**, 440, doi:10.1038/ncomms1453 (2011).
- 36 Brennand, K. J. *et al.* Modelling schizophrenia using human induced pluripotent stem cells. *Nature* **473**, 221-225, doi:10.1038/nature09915 (2011).
- 37 Lu, S. *et al.* A calcium-dependent protease as a potential therapeutic target for Wolfram syndrome. *Proc Natl Acad Sci U S A* **111**, E5292-5301, doi:10.1073/pnas.1421055111 (2014).

- 38 Madison, J. M. *et al.* Characterization of bipolar disorder patient-specific induced pluripotent stem cells from a family reveals neurodevelopmental and mRNA expression abnormalities. *Mol Psychiatry* **20**, 703-717, doi:10.1038/mp.2015.7 (2015).
- 39 Engle, S. J. & Vincent, F. Small molecule screening in human induced pluripotent stem cell-derived terminal cell types. *J Biol Chem* **289**, 4562-4570, doi:10.1074/jbc.R113.529156 (2014).
- 40 Barmada, S. J. *et al.* Autophagy induction enhances TDP43 turnover and survival in neuronal ALS models. *Nat Chem Biol* **10**, 677-685, doi:10.1038/nchembio.1563 (2014).
- 41 Mummery, C. Induced pluripotent stem cells--a cautionary note. *N Engl J Med* **364**, 2160-2162, doi:10.1056/NEJMcibr1103052 (2011).
- 42 Lister, R. *et al.* Hotspots of aberrant epigenomic reprogramming in human induced pluripotent stem cells. *Nature* **471**, 68-73, doi:10.1038/nature09798 (2011).
- 43 Toupet, K. *et al.* Long-term detection of human adipose-derived mesenchymal stem cells after intraarticular injection in SCID mice. *Arthritis Rheum* **65**, 1786-1794, doi:10.1002/art.37960 (2013).
- 44 Laflamme, M. A. *et al.* Cardiomyocytes derived from human embryonic stem cells in pro-survival factors enhance function of infarcted rat hearts. *Nat Biotechnol* **25**, 1015-1024, doi:10.1038/nbt1327 (2007).
- 45 Kooreman, N. G., Ransohoff, J. D. & Wu, J. C. Tracking gene and cell fate for therapeutic gain. *Nat Mater* **13**, 106-109, doi:10.1038/nmat3868 (2014).
- 46 Cao, F. *et al.* In vivo visualization of embryonic stem cell survival, proliferation, and migration after cardiac delivery. *Circulation* **113**, 1005-1014, doi:10.1161/CIRCULATIONAHA.105.588954 (2006).
- 47 Ben-David, U. *et al.* Selective elimination of human pluripotent stem cells by an oleate synthesis inhibitor discovered in a high-throughput screen. *Cell Stem Cell* **12**, 167-179, doi:10.1016/j.stem.2012.11.015 (2013).
- 48 Pearl, J. I., Kean, L. S., Davis, M. M. & Wu, J. C. Pluripotent stem cells: immune to the immune system? *Sci Transl Med* **4**, 164ps125, doi:10.1126/scitranslmed.3005090 (2012).
- 49 Schwartz, S. D. *et al.* Human embryonic stem cell-derived retinal pigment epithelium in patients with age-related macular degeneration and Stargardt's macular dystrophy: follow-up of two open-label phase 1/2 studies. *Lancet* **385**, 509-516, doi:10.1016/S0140-6736(14)61376-3 (2015).
- 50 Golpanian, S. *et al.* Concise Review: Review and Perspective of Cell Dosage and Routes of Administration From Preclinical and Clinical Studies of Stem Cell Therapy for Heart Disease. *Stem Cells Transl Med* **5**, 186-191, doi:10.5966/sctm.2015-0101 (2016).
- 51 Lebkowski, J. GRNOPC1: the world's first embryonic stem cell-derived therapy. Interview with Jane Lebkowski. *Regen Med* **6**, 11-13, doi:10.2217/rme.11.77 (2011).
- 52 Menasche, P. *et al.* Towards a clinical use of human embryonic stem cell-derived cardiac progenitors: a translational experience. *Eur Heart J* **36**, 743-750, doi:10.1093/eurheartj/ehu192 (2015).
- 53 Watanabe, K. *et al.* A ROCK inhibitor permits survival of dissociated human embryonic stem cells. *Nat Biotechnol* **25**, 681-686, doi:10.1038/nbt1310 (2007).
- 54 Li, H. L., Gee, P., Ishida, K. & Hotta, A. Efficient genomic correction methods in human iPS cells using CRISPR-Cas9 system. *Methods*, doi:10.1016/j.ymeth.2015.10.015 (2015).

- 55 Hoeijmakers, J. H. DNA damage, aging, and cancer. *N Engl J Med* **361**, 1475-1485, doi:10.1056/NEJMra0804615 (2009).
- 56 Zwaka, T. P. & Thomson, J. A. Homologous recombination in human embryonic stem cells. *Nat Biotechnol* **21**, 319-321, doi:10.1038/nbt788 (2003).
- 57 Kawasaki, T. *et al.* Introduction of a foreign gene into zebrafish and medaka cells using adenoviral vectors. *Zebrafish* **6**, 253-258, doi:10.1089/zeb.2009.0596 (2009).
- 58 Merkert, S. *et al.* Efficient ZFN-based gene inactivation in transgenic human iPS cells as a model for gene editing in patient-specific cells. *J Stem Cells Regen Med* **6**, 118 (2010).
- 59 Song, H. & Xu, Y. Disease research and drug development models based on genetically altered human embryonic stem cells. *Discov Med* **9**, 500-503 (2010).
- 60 Bellin, M. *et al.* Isogenic human pluripotent stem cell pairs reveal the role of a KCNH2 mutation in long-QT syndrome. *EMBO J* **32**, 3161-3175, doi:10.1038/emboj.2013.240 (2013).
- 61 Yusa, K. *et al.* Targeted gene correction of alpha1-antitrypsin deficiency in induced pluripotent stem cells. *Nature* **478**, 391-394, doi:10.1038/nature10424 (2011).
- 62 Delacote, F. & Lopez, B. S. Importance of the cell cycle phase for the choice of the appropriate DSB repair pathway, for genome stability maintenance: the trans-S double-strand break repair model. *Cell Cycle* **7**, 33-38, doi:10.4161/cc.7.1.5149 (2008).
- 63 Symington, L. S. & Gautier, J. Double-strand break end resection and repair pathway choice. *Annu Rev Genet* **45**, 247-271, doi:10.1146/annurev-genet-110410-132435 (2011).
- 64 Sander, J. D. & Joung, J. K. CRISPR-Cas systems for editing, regulating and targeting genomes. *Nat Biotechnol* **32**, 347-355, doi:10.1038/nbt.2842 (2014).
- 65 Gaj, T., Gersbach, C. A. & Barbas, C. F., 3rd. ZFN, TALEN, and CRISPR/Cas-based methods for genome engineering. *Trends Biotechnol* **31**, 397-405, doi:10.1016/j.tibtech.2013.04.004 (2013).
- 66 Bogdanove, A. J. & Voytas, D. F. TAL effectors: customizable proteins for DNA targeting. *Science (New York, N.Y.)* **333**, 1843-1846, doi:10.1126/science.1204094 (2011).
- 67 Mojica, F. J. & Rodriguez-Valera, F. The discovery of CRISPR in archaea and bacteria. *FEBS J* **283**, 3162-3169, doi:10.1111/febs.13766 (2016).
- 68 Mohanraju, P. *et al.* Diverse evolutionary roots and mechanistic variations of the CRISPR-Cas systems. *Science (New York, N.Y.)* **353**, aad5147, doi:10.1126/science.aad5147 (2016).
- 69 Ran, F. A. *et al.* Genome engineering using the CRISPR-Cas9 system. *Nat Protoc* **8**, 2281-2308, doi:10.1038/nprot.2013.143 (2013).
- 70 Jinek, M. *et al.* A programmable dual-RNA-guided DNA endonuclease in adaptive bacterial immunity. *Science (New York, N.Y.)* **337**, 816-821, doi:10.1126/science.1225829 (2012).
- 71 Haeussler, M. & Concordet, J. P. Genome Editing with CRISPR-Cas9: Can It Get Any Better? *J Genet Genomics* **43**, 239-250, doi:10.1016/j.jgg.2016.04.008 (2016).
- 72 Esvelt, K. M. *et al.* Orthogonal Cas9 proteins for RNA-guided gene regulation and editing. *Nat Methods* **10**, 1116-1121, doi:10.1038/nmeth.2681 (2013).
- 73 Richardson, C. D., Ray, G. J., DeWitt, M. A., Curie, G. L. & Corn, J. E. Enhancing homology-directed genome editing by catalytically active and

- inactive CRISPR-Cas9 using asymmetric donor DNA. *Nat Biotechnol* **34**, 339-344, doi:10.1038/nbt.3481 (2016).
- 74 Yang, L. *et al.* Optimization of scarless human stem cell genome editing. *Nucleic Acids Res* **41**, 9049-9061, doi:10.1093/nar/gkt555 (2013).
- 75 Yang, H. *et al.* One-step generation of mice carrying reporter and conditional alleles by CRISPR/Cas-mediated genome engineering. *Cell* **154**, 1370-1379, doi:10.1016/j.cell.2013.08.022 (2013).
- 76 Li, S. *et al.* Human Induced Pluripotent Stem Cell NEUROG2 Dual Knockin Reporter Lines Generated by the CRISPR/Cas9 System. *Stem Cells Dev* **24**, 2925-2942, doi:10.1089/scd.2015.0131 (2015).
- 77 Gonzalez, F. *et al.* An iCRISPR platform for rapid, multiplexable, and inducible genome editing in human pluripotent stem cells. *Cell Stem Cell* **15**, 215-226, doi:10.1016/j.stem.2014.05.018 (2014).
- 78 Merkle, F. T. *et al.* Efficient CRISPR-Cas9-mediated generation of knockin human pluripotent stem cells lacking undesired mutations at the targeted locus. *Cell Rep* **11**, 875-883, doi:10.1016/j.celrep.2015.04.007 (2015).
- 79 Kan, Y., Ruis, B., Lin, S. & Hendrickson, E. A. The mechanism of gene targeting in human somatic cells. *PLoS Genet* **10**, e1004251, doi:10.1371/journal.pgen.1004251 (2014).
- 80 Ousterout, D. G. *et al.* Multiplex CRISPR/Cas9-based genome editing for correction of dystrophin mutations that cause Duchenne muscular dystrophy. *Nat Commun* **6**, 6244, doi:10.1038/ncomms7244 (2015).
- 81 Soldner, F. *et al.* Generation of isogenic pluripotent stem cells differing exclusively at two early onset Parkinson point mutations. *Cell* **146**, 318-331, doi:10.1016/j.cell.2011.06.019 (2011).
- 82 Firth, A. L. *et al.* Functional Gene Correction for Cystic Fibrosis in Lung Epithelial Cells Generated from Patient iPSCs. *Cell Rep* **12**, 1385-1390, doi:10.1016/j.celrep.2015.07.062 (2015).
- 83 Horii, T., Tamura, D., Morita, S., Kimura, M. & Hatada, I. Generation of an ICF syndrome model by efficient genome editing of human induced pluripotent stem cells using the CRISPR system. *Int J Mol Sci* **14**, 19774-19781, doi:10.3390/ijms141019774 (2013).
- 84 Mummery, C. L. *et al.* Differentiation of human embryonic stem cells and induced pluripotent stem cells to cardiomyocytes: a methods overview. *Circ Res* **111**, 344-358, doi:10.1161/CIRCRESAHA.110.227512 (2012).
- 85 Yamashita, J. K. ES and iPSC cell research for cardiovascular regeneration. *Exp Cell Res* **316**, 2555-2559, doi:10.1016/j.yexcr.2010.04.004 (2010).
- 86 Brade, T., Pane, L. S., Moretti, A., Chien, K. R. & Laugwitz, K. L. Embryonic heart progenitors and cardiogenesis. *Cold Spring Harb Perspect Med* **3**, a013847, doi:10.1101/cshperspect.a013847 (2013).
- 87 Burridge, P. W., Sharma, A. & Wu, J. C. Genetic and Epigenetic Regulation of Human Cardiac Reprogramming and Differentiation in Regenerative Medicine. *Annu Rev Genet* **49**, 461-484, doi:10.1146/annurev-genet-112414-054911 (2015).
- 88 Bondue, A. *et al.* Mesp1 acts as a master regulator of multipotent cardiovascular progenitor specification. *Cell Stem Cell* **3**, 69-84, doi:10.1016/j.stem.2008.06.009 (2008).
- 89 Spater, D. *et al.* A HCN4+ cardiomyogenic progenitor derived from the first heart field and human pluripotent stem cells. *Nat Cell Biol* **15**, 1098-1106, doi:10.1038/ncb2824 (2013).

- 90 Moretti, A. *et al.* Multipotent embryonic *Isl1*<sup>+</sup> progenitor cells lead to cardiac, smooth muscle, and endothelial cell diversification. *Cell* **127**, 1151-1165, doi:10.1016/j.cell.2006.10.029 (2006).
- 91 Srivastava, D. Genetic regulation of cardiogenesis and congenital heart disease. *Annu Rev Pathol* **1**, 199-213, doi:10.1146/annurev.pathol.1.110304.100039 (2006).
- 92 Cai, C. L. *et al.* *Isl1* identifies a cardiac progenitor population that proliferates prior to differentiation and contributes a majority of cells to the heart. *Dev Cell* **5**, 877-889 (2003).
- 93 Lyons, I. *et al.* Myogenic and morphogenetic defects in the heart tubes of murine embryos lacking the homeo box gene *Nkx2-5*. *Genes Dev* **9**, 1654-1666 (1995).
- 94 Krishnan, A. *et al.* A detailed comparison of mouse and human cardiac development. *Pediatr Res* **76**, 500-507, doi:10.1038/pr.2014.128 (2014).
- 95 Paige, S. L. *et al.* A temporal chromatin signature in human embryonic stem cells identifies regulators of cardiac development. *Cell* **151**, 221-232, doi:10.1016/j.cell.2012.08.027 (2012).
- 96 Yuan, X. & Braun, T. An unexpected switch: regulation of cardiomyocyte proliferation by the homeobox gene *meis1*. *Circ Res* **113**, 245-248, doi:10.1161/CIRCRESAHA.113.302023 (2013).
- 97 Wamstad, J. A. *et al.* Dynamic and coordinated epigenetic regulation of developmental transitions in the cardiac lineage. *Cell* **151**, 206-220, doi:10.1016/j.cell.2012.07.035 (2012).
- 98 Hisa, T. *et al.* Hematopoietic, angiogenic and eye defects in *Meis1* mutant animals. *EMBO J* **23**, 450-459, doi:10.1038/sj.emboj.7600038 (2004).
- 99 Azcoitia, V., Aracil, M., Martinez, A. C. & Torres, M. The homeodomain protein *Meis1* is essential for definitive hematopoiesis and vascular patterning in the mouse embryo. *Dev Biol* **280**, 307-320, doi:10.1016/j.ydbio.2005.01.004 (2005).
- 100 Mahmoud, A. I. *et al.* *Meis1* regulates postnatal cardiomyocyte cell cycle arrest. *Nature* **497**, 249-253, doi:10.1038/nature12054 (2013).
- 101 Sorensen, A. B., Sondergaard, M. T. & Overgaard, M. T. Calmodulin in a heartbeat. *FEBS J* **280**, 5511-5532, doi:10.1111/febs.12337 (2013).
- 102 Kortvely, E. & Gulya, K. Calmodulin, and various ways to regulate its activity. *Life Sciences* **74**, 1065-1070, doi:10.1016/j.lfs.2003.07.026 (2004).
- 103 Maier, L. B., D. Calcium, Calmodulin and Calcium- Calmodulin Kinase II: Heartbeat to Heartbeat and Beyond. *Journal of Molecular and Cellular Cardiology* **34**, 919-939 (2002).
- 104 Chin, D. & Means, A. R. Calmodulin: a prototypical calcium sensor. *Trends Cell Biol* **10**, 322-328 (2000).
- 105 Zuhlke, R. D., Pitt, G. S., Deisseroth, K., Tsien, R. W. & Reuter, H. Calmodulin supports both inactivation and facilitation of L-type calcium channels. *Nature* **399**, 159-162, doi:10.1038/20200 (1999).
- 106 Shamgar, L. *et al.* Calmodulin is essential for cardiac IKS channel gating and assembly: impaired function in long-QT mutations. *Circ Res* **98**, 1055-1063, doi:10.1161/01.RES.0000218979.40770.69 (2006).
- 107 Vassilakopoulou, V. *et al.* Distinctive malfunctions of calmodulin mutations associated with heart RyR2-mediated arrhythmic disease. *Biochim Biophys Acta* **1850**, 2168-2176, doi:10.1016/j.bbagen.2015.07.001 (2015).

- 108 Gomez-Hurtado, N. *et al.* Novel CPVT-Associated Calmodulin Mutation in CALM3 (CALM3-A103V) Activates Arrhythmogenic Ca Waves and Sparks. *Circ Arrhythm Electrophysiol* **9**, doi:10.1161/CIRCEP.116.004161 (2016).
- 109 Pipilas, D. C. *et al.* Novel calmodulin mutations associated with congenital long QT syndrome affect calcium current in human cardiomyocytes. *Heart Rhythm* **13**, 2012-2019, doi:10.1016/j.hrthm.2016.06.038 (2016).
- 110 Sondergaard, M. T. *et al.* Arrhythmogenic Calmodulin Mutations Affect the Activation and Termination of Cardiac Ryanodine Receptor-mediated Ca<sup>2+</sup> Release. *J Biol Chem* **290**, 26151-26162, doi:10.1074/jbc.M115.676627 (2015).
- 111 Hwang, H. S. *et al.* Divergent regulation of ryanodine receptor 2 calcium release channels by arrhythmogenic human calmodulin missense mutants. *Circ Res* **114**, 1114-1124, doi:10.1161/CIRCRESAHA.114.303391 (2014).
- 112 Xu, X. *et al.* Defective calmodulin binding to the cardiac ryanodine receptor plays a key role in CPVT-associated channel dysfunction. *Biochem Biophys Res Commun* **394**, 660-666, doi:10.1016/j.bbrc.2010.03.046 (2010).
- 113 Tian, X., Tang, Y., Liu, Y., Wang, R. & Chen, S. R. Calmodulin modulates the termination threshold for cardiac ryanodine receptor-mediated Ca<sup>2+</sup> release. *Biochem J* **455**, 367-375, doi:10.1042/BJ20130805 (2013).
- 114 Boczek, N. J. *et al.* Spectrum and Prevalence of CALM1-, CALM2-, and CALM3-Encoded Calmodulin Variants in Long QT Syndrome and Functional Characterization of a Novel Long QT Syndrome-Associated Calmodulin Missense Variant, E141G. *Circ Cardiovasc Genet* **9**, 136-146, doi:10.1161/CIRCGENETICS.115.001323 (2016).
- 115 Yin, G. *et al.* Arrhythmogenic calmodulin mutations disrupt intracellular cardiomyocyte Ca<sup>2+</sup> regulation by distinct mechanisms. *J Am Heart Assoc* **3**, e000996, doi:10.1161/JAHA.114.000996 (2014).
- 116 Limpitikul, W. B. *et al.* Calmodulin mutations associated with long QT syndrome prevent inactivation of cardiac L-type Ca(2+) currents and promote proarrhythmic behavior in ventricular myocytes. *J Mol Cell Cardiol* **74**, 115-124, doi:10.1016/j.yjmcc.2014.04.022 (2014).
- 117 Schwartz, P. J. *et al.* Prevalence of the congenital long-QT syndrome. *Circulation* **120**, 1761-1767, doi:10.1161/CIRCULATIONAHA.109.863209 (2009).
- 118 Schwartz, P. J., Crotti, L. & Insolia, R. Long-QT syndrome: from genetics to management. *Circ Arrhythm Electrophysiol* **5**, 868-877, doi:10.1161/CIRCEP.111.962019 (2012).
- 119 Tester, D. J. & Ackerman, M. J. Genetics of long QT syndrome. *Methodist Debakey Cardiovasc J* **10**, 29-33 (2014).
- 120 Nakano, Y. & Shimizu, W. Genetics of long-QT syndrome. *J Hum Genet* **61**, 51-55, doi:10.1038/jhg.2015.74 (2016).
- 121 Derangeon, M., Montnach, J., Baro, I. & Charpentier, F. Mouse Models of SCN5A-Related Cardiac Arrhythmias. *Front Physiol* **3**, 210, doi:10.3389/fphys.2012.00210 (2012).
- 122 Nuyens, D. *et al.* Abrupt rate accelerations or premature beats cause life-threatening arrhythmias in mice with long-QT3 syndrome. *Nat Med* **7**, 1021-1027, doi:10.1038/nm0901-1021 (2001).
- 123 Davis, R. P., van den Berg, C. W., Casini, S., Braam, S. R. & Mummery, C. L. Pluripotent stem cell models of cardiac disease and their implication for drug discovery and development. *Trends Mol Med* **17**, 475-484, doi:10.1016/j.molmed.2011.05.001 (2011).

- 124 Moretti, A. B., M.; Welling, A.; Jung, C.; Lam, J.; Bott-Flügel, L.; Dorn, T.;  
Goedel, A.; Höhnke, C.; Hofmann, F.; Seyfarth, M.; Sinnecker, D.; Schömig,  
A.; Laugwitz, K.-L. Patient-specific Induced Pluripotent Stem-Cell Models for  
Long-QT Syndrome. *New England Journal of Medicine* **363** (2010).
- 125 Malan, D., Friedrichs, S., Fleischmann, B. K. & Sasse, P. Cardiomyocytes  
obtained from induced pluripotent stem cells with long-QT syndrome 3  
recapitulate typical disease-specific features in vitro. *Circ Res* **109**, 841-847,  
doi:10.1161/CIRCRESAHA.111.243139 (2011).
- 126 Awe, J. P., Vega-Crespo, A. & Byrne, J. A. Derivation and characterization of a  
transgene-free human induced pluripotent stem cell line and conversion into  
defined clinical-grade conditions. *J Vis Exp*, e52158, doi:10.3791/52158 (2014).
- 127 Matsa, E. *et al.* Allele-specific RNA interference rescues the long-QT syndrome  
phenotype in human-induced pluripotency stem cell cardiomyocytes. *Eur Heart  
J* **35**, 1078-1087, doi:10.1093/eurheartj/eht067 (2014).
- 128 Mummery, C. *et al.* Differentiation of human embryonic stem cells to  
cardiomyocytes: role of coculture with visceral endoderm-like cells. *Circulation*  
**107**, 2733-2740, doi:10.1161/01.CIR.0000068356.38592.68 (2003).
- 129 Moretti, A. *et al.* Mouse and human induced pluripotent stem cells as a source  
for multipotent Isl1+ cardiovascular progenitors. *FASEB J* **24**, 700-711,  
doi:10.1096/fj.09-139477 (2010).
- 130 Muller, F. J. *et al.* A bioinformatic assay for pluripotency in human cells. *Nat  
Methods* **8**, 315-317, doi:10.1038/nmeth.1580 (2011).
- 131 Davis, R. P. *et al.* Generation of human embryonic stem cell reporter knock-in  
lines by homologous recombination. *Curr Protoc Stem Cell Biol* **Chapter 5**,  
Unit 5B 1 1 1-34, doi:10.1002/9780470151808.sc05b01s11 (2009).
- 132 Peters, D. Genome editing in human pluripotent stem cells. *StemBook*,  
doi:10.3824/stembook.1.94.1 (2014).
- 133 Rocchetti, M. *et al.* Elucidating the arrhythmogenic mechanism of long QT  
syndrome caused by the CALM1-F142L mutation using patient-specific induced  
pluripotent stem cell-derived cardiomyocytes. *Cardiovasc Res*,  
doi:10.1093/cvr/cvx006. (2017).
- 134 Rizzetto, R. *et al.* Late sodium current (INaL) in pancreatic beta-cells. *Pflugers  
Arch* **467**, 1757-1768, doi:10.1007/s00424-014-1613-0 (2015).
- 135 Nguyen, H. T., Geens, M. & Spits, C. Genetic and epigenetic instability in  
human pluripotent stem cells. *Hum Reprod Update* **19**, 187-205,  
doi:10.1093/humupd/dms048 (2013).
- 136 Stefkova, K., Prochazkova, J. & Pachernik, J. Alkaline phosphatase in stem  
cells. *Stem Cells Int* **2015**, 628368, doi:10.1155/2015/628368 (2015).
- 137 Andang, M. *et al.* Histone H2AX-dependent GABA(A) receptor regulation of  
stem cell proliferation. *Nature* **451**, 460-464, doi:10.1038/nature06488 (2008).
- 138 Hawkins, K., Joy, S. & McKay, T. Cell signalling pathways underlying induced  
pluripotent stem cell reprogramming. *World J Stem Cells* **6**, 620-628,  
doi:10.4252/wjsc.v6.i5.620 (2014).
- 139 Ruff, D. & Lieu, P. T. Profiling stem cells using quantitative PCR protein  
assays. *Methods Mol Biol* **997**, 225-236, doi:10.1007/978-1-62703-348-0\_18  
(2013).
- 140 Son, M. Y., Choi, H., Han, Y. M. & Cho, Y. S. Unveiling the critical role of  
REX1 in the regulation of human stem cell pluripotency. *Stem Cells* **31**, 2374-  
2387, doi:10.1002/stem.1509 (2013).

- 141 Adamcova, M. *et al.* Cardiac troponins-Translational biomarkers in cardiology: Theory and practice of cardiac troponin high-sensitivity assays. *Biofactors* **42**, 133-148, doi:10.1002/biof.1261 (2016).
- 142 Ribeiro Ede, A., Jr. *et al.* The structure and regulation of human muscle alpha-actinin. *Cell* **159**, 1447-1460, doi:10.1016/j.cell.2014.10.056 (2014).
- 143 Paradis, A. N., Gay, M. S. & Zhang, L. Binucleation of cardiomyocytes: the transition from a proliferative to a terminally differentiated state. *Drug Discov Today* **19**, 602-609, doi:10.1016/j.drudis.2013.10.019 (2014).
- 144 Fischer, T. H., Neef, S. & Maier, L. S. The Ca-calmodulin dependent kinase II: a promising target for future antiarrhythmic therapies? *J Mol Cell Cardiol* **58**, 182-187, doi:10.1016/j.yjmcc.2012.11.003 (2013).
- 145 Bers, D. M. & Morotti, S. Ca(2+) current facilitation is CaMKII-dependent and has arrhythmogenic consequences. *Front Pharmacol* **5**, 144, doi:10.3389/fphar.2014.00144 (2014).
- 146 Erickson, J. R., Patel, R., Ferguson, A., Bossuyt, J. & Bers, D. M. Fluorescence resonance energy transfer-based sensor Camui provides new insight into mechanisms of calcium/calmodulin-dependent protein kinase II activation in intact cardiomyocytes. *Circ Res* **109**, 729-738, doi:10.1161/CIRCRESAHA.111.247148 (2011).
- 147 Saucerman, J. J. & Bers, D. M. Calmodulin binding proteins provide domains of local Ca<sup>2+</sup> signaling in cardiac myocytes. *J Mol Cell Cardiol* **52**, 312-316, doi:10.1016/j.yjmcc.2011.06.005 (2012).
- 148 Maruyama, T. *et al.* Increasing the efficiency of precise genome editing with CRISPR-Cas9 by inhibition of nonhomologous end joining. *Nat Biotechnol* **33**, 538-542, doi:10.1038/nbt.3190 (2015).
- 149 Shalem, O., Sanjana, N. E. & Zhang, F. High-throughput functional genomics using CRISPR-Cas9. *Nat Rev Genet* **16**, 299-311, doi:10.1038/nrg3899 (2015).
- 150 Bondue, A. & Blanpain, C. Mesp1: a key regulator of cardiovascular lineage commitment. *Circ Res* **107**, 1414-1427, doi:10.1161/CIRCRESAHA.110.227058 (2010).
- 151 Erickson, M. G., Liang, H., Mori, M. X. & Yue, D. T. FRET two-hybrid mapping reveals function and location of L-type Ca<sup>2+</sup> channel CaM preassociation. *Neuron* **39**, 97-107 (2003).
- 152 Gilmour, R. F., Jr. A novel approach to identifying antiarrhythmic drug targets. *Drug Discov Today* **8**, 162-167 (2003).
- 153 Zaza, A. Control of the cardiac action potential: The role of repolarization dynamics. *J Mol Cell Cardiol* **48**, 106-111, doi:10.1016/j.yjmcc.2009.07.027 (2010).
- 154 Davis, R. P. *et al.* Cardiomyocytes derived from pluripotent stem cells recapitulate electrophysiological characteristics of an overlap syndrome of cardiac sodium channel disease. *Circulation* **125**, 3079-3091, doi:10.1161/CIRCULATIONAHA.111.066092 (2012).
- 155 Grobarczyk, B., Franco, B., Hanon, K. & Malgrange, B. Generation of Isogenic Human iPS Cell Line Precisely Corrected by Genome Editing Using the CRISPR/Cas9 System. *Stem Cell Rev* **11**, 774-787, doi:10.1007/s12015-015-9600-1 (2015).
- 156 Stillitano, F. *et al.* Genomic correction of familial cardiomyopathy in human engineered cardiac tissues. *Eur Heart J*, doi:10.1093/eurheartj/ehw307 (2016).
- 157 Wang, G. *et al.* Modeling the mitochondrial cardiomyopathy of Barth syndrome with induced pluripotent stem cell and heart-on-chip technologies. *Nat Med* **20**, 616-623, doi:10.1038/nm.3545 (2014).

- 158 Hinson, J. T. *et al.* HEART DISEASE. Titin mutations in iPS cells define sarcomere insufficiency as a cause of dilated cardiomyopathy. *Science (New York, N.Y.)* **349**, 982-986, doi:10.1126/science.aaa5458 (2015).
- 159 Karakikes, I. *et al.* Correction of human phospholamban R14del mutation associated with cardiomyopathy using targeted nucleases and combination therapy. *Nat Commun* **6**, 6955, doi:10.1038/ncomms7955 (2015).
- 160 Howden, S. E. *et al.* Genetic correction and analysis of induced pluripotent stem cells from a patient with gyrate atrophy. *Proc Natl Acad Sci U S A* **108**, 6537-6542, doi:10.1073/pnas.1103388108 (2011).
- 161 Li, H. L. *et al.* Precise correction of the dystrophin gene in duchenne muscular dystrophy patient induced pluripotent stem cells by TALEN and CRISPR-Cas9. *Stem Cell Reports* **4**, 143-154, doi:10.1016/j.stemcr.2014.10.013 (2015).
- 162 Hoban, M. D. *et al.* CRISPR/Cas9-Mediated Correction of the Sicklet Mutation in Human CD34+ cells. *Mol Ther*, doi:10.1038/mt.2016.148 (2016).
- 163 Sun, L., Wu, J., Du, F., Chen, X. & Chen, Z. J. Cyclic GMP-AMP synthase is a cytosolic DNA sensor that activates the type I interferon pathway. *Science (New York, N.Y.)* **339**, 786-791, doi:10.1126/science.1232458 (2013).
- 164 Moore, J. C. *et al.* Efficient, high-throughput transfection of human embryonic stem cells. *Stem Cell Res Ther* **1**, 23, doi:10.1186/scrt23 (2010).
- 165 Gerlai, R. Gene Targeting Using Homologous Recombination in Embryonic Stem Cells: The Future for Behavior Genetics? *Front Genet* **7**, 43, doi:10.3389/fgene.2016.00043 (2016).
- 166 Biet, E., Larue, L. & Dutreix, M. [Homologous recombination and gene targeting]. *C R Biol* **326**, 51-64 (2003).
- 167 Byrne, S. M., Mali, P. & Church, G. M. Genome editing in human stem cells. *Methods Enzymol* **546**, 119-138, doi:10.1016/B978-0-12-801185-0.00006-4 (2014).
- 168 Peng, R., Lin, G. & Li, J. Potential pitfalls of CRISPR/Cas9-mediated genome editing. *FEBS J* **283**, 1218-1231, doi:10.1111/febs.13586 (2016).
- 169 Shalem, O. *et al.* Genome-scale CRISPR-Cas9 knockout screening in human cells. *Science (New York, N.Y.)* **343**, 84-87, doi:10.1126/science.1247005 (2014).
- 170 Chen, Y. *et al.* Engineering Human Stem Cell Lines with Inducible Gene Knockout using CRISPR/Cas9. *Cell Stem Cell* **17**, 233-244, doi:10.1016/j.stem.2015.06.001 (2015).
- 171 Toutenhoofd, S. L. & Strehler, E. E. The calmodulin multigene family as a unique case of genetic redundancy: multiple levels of regulation to provide spatial and temporal control of calmodulin pools? *Cell Calcium* **28**, 83-96, doi:10.1054/ceca.2000.0136 (2000).
- 172 Makita, N. *et al.* Novel calmodulin mutations associated with congenital arrhythmia susceptibility. *Circ Cardiovasc Genet* **7**, 466-474, doi:10.1161/CIRCGENETICS.113.000459 (2014).
- 173 Nyegaard, M. *et al.* Mutations in calmodulin cause ventricular tachycardia and sudden cardiac death. *Am J Hum Genet* **91**, 703-712, doi:10.1016/j.ajhg.2012.08.015 (2012).
- 174 Sondergaard, M. T. *et al.* Calmodulin mutations causing catecholaminergic polymorphic ventricular tachycardia confer opposing functional and biophysical molecular changes. *FEBS J* **282**, 803-816, doi:10.1111/febs.13184 (2015).
- 175 Doench, J. G. CRISPR/Cas9 gene editing special issue. *FEBS J* **283**, 3160-3161, doi:10.1111/febs.13823 (2016).

- 176 Tan, E. P., Li, Y., Velasco-Herrera Mdel, C., Yusa, K. & Bradley, A. Off-target assessment of CRISPR-Cas9 guiding RNAs in human iPS and mouse ES cells. *Genesis* **53**, 225-236, doi:10.1002/dvg.22835 (2015).
- 177 Yee, J. K. Off-target effects of engineered nucleases. *FEBS J* **283**, 3239-3248, doi:10.1111/febs.13760 (2016).
- 178 Kim, D., Kim, S., Kim, S., Park, J. & Kim, J. S. Genome-wide target specificities of CRISPR-Cas9 nucleases revealed by multiplex Digenome-seq. *Genome Res* **26**, 406-415, doi:10.1101/gr.199588.115 (2016).
- 179 Tsai, S. Q. *et al.* GUIDE-seq enables genome-wide profiling of off-target cleavage by CRISPR-Cas nucleases. *Nat Biotechnol* **33**, 187-197, doi:10.1038/nbt.3117 (2015).
- 180 Veres, A. *et al.* Low incidence of off-target mutations in individual CRISPR-Cas9 and TALEN targeted human stem cell clones detected by whole-genome sequencing. *Cell Stem Cell* **15**, 27-30, doi:10.1016/j.stem.2014.04.020 (2014).
- 181 Fine, E. J., Cradick, T. J., Zhao, C. L., Lin, Y. & Bao, G. An online bioinformatics tool predicts zinc finger and TALE nuclease off-target cleavage. *Nucleic Acids Res* **42**, e42, doi:10.1093/nar/gkt1326 (2014).
- 182 Hsu, P. D. *et al.* DNA targeting specificity of RNA-guided Cas9 nucleases. *Nat Biotechnol* **31**, 827-832, doi:10.1038/nbt.2647 (2013).
- 183 Fu, Y. *et al.* High-frequency off-target mutagenesis induced by CRISPR-Cas nucleases in human cells. *Nat Biotechnol* **31**, 822-826, doi:10.1038/nbt.2623 (2013).
- 184 Cho, S. W. *et al.* Analysis of off-target effects of CRISPR/Cas-derived RNA-guided endonucleases and nickases. *Genome Res* **24**, 132-141, doi:10.1101/gr.162339.113 (2014).
- 185 Gabriel, R. *et al.* An unbiased genome-wide analysis of zinc-finger nuclease specificity. *Nat Biotechnol* **29**, 816-823, doi:10.1038/nbt.1948 (2011).
- 186 Frock, R. L. *et al.* Genome-wide detection of DNA double-stranded breaks induced by engineered nucleases. *Nat Biotechnol* **33**, 179-186, doi:10.1038/nbt.3101 (2015).
- 187 Crosetto, N. *et al.* Nucleotide-resolution DNA double-strand break mapping by next-generation sequencing. *Nat Methods* **10**, 361-365, doi:10.1038/nmeth.2408 (2013).
- 188 Cong, L. *et al.* Multiplex genome engineering using CRISPR/Cas systems. *Science (New York, N.Y.)* **339**, 819-823, doi:10.1126/science.1231143 (2013).
- 189 Kleinstiver, B. P. *et al.* High-fidelity CRISPR-Cas9 nucleases with no detectable genome-wide off-target effects. *Nature* **529**, 490-495, doi:10.1038/nature16526 (2016).
- 190 Garneau, J. E. *et al.* The CRISPR/Cas bacterial immune system cleaves bacteriophage and plasmid DNA. *Nature* **468**, 67-71, doi:10.1038/nature09523 (2010).
- 191 Kleinstiver, B. P. *et al.* Broadening the targeting range of *Staphylococcus aureus* CRISPR-Cas9 by modifying PAM recognition. *Nat Biotechnol* **33**, 1293-1298, doi:10.1038/nbt.3404 (2015).
- 192 Wyvekens, N., Tsai, S. Q. & Joung, J. K. Genome Editing in Human Cells Using CRISPR/Cas Nucleases. *Curr Protoc Mol Biol* **112**, 31 33 31-18, doi:10.1002/0471142727.mb3103s112 (2015).
- 193 Kim, D. *et al.* Genome-wide analysis reveals specificities of Cpf1 endonucleases in human cells. *Nat Biotechnol* **34**, 863-868, doi:10.1038/nbt.3609 (2016).

- 194 Liu, Z. *et al.* Efficient CRISPR/Cas9-Mediated Versatile, Predictable, and Donor-Free Gene Knockout in Human Pluripotent Stem Cells. *Stem Cell Reports*, doi:10.1016/j.stemcr.2016.07.021 (2016).
- 195 Liang, X. *et al.* Rapid and highly efficient mammalian cell engineering via Cas9 protein transfection. *J Biotechnol* **208**, 44-53, doi:10.1016/j.jbiotec.2015.04.024 (2015).
- 196 Kim, S., Kim, D., Cho, S. W., Kim, J. & Kim, J. S. Highly efficient RNA-guided genome editing in human cells via delivery of purified Cas9 ribonucleoproteins. *Genome Res* **24**, 1012-1019, doi:10.1101/gr.171322.113 (2014).
- 197 Bersell, K., Arab, S., Haring, B. & Kuhn, B. Neuregulin1/ErbB4 signaling induces cardiomyocyte proliferation and repair of heart injury. *Cell* **138**, 257-270, doi:10.1016/j.cell.2009.04.060 (2009).
- 198 Pasumarthi, K. B., Nakajima, H., Nakajima, H. O., Soonpaa, M. H. & Field, L. J. Targeted expression of cyclin D2 results in cardiomyocyte DNA synthesis and infarct regression in transgenic mice. *Circ Res* **96**, 110-118, doi:10.1161/01.RES.0000152326.91223.4F (2005).
- 199 Gude, N. *et al.* Akt promotes increased cardiomyocyte cycling and expansion of the cardiac progenitor cell population. *Circ Res* **99**, 381-388, doi:10.1161/01.RES.0000236754.21499.1c (2006).
- 200 Dupays, L. *et al.* Sequential Binding of MEIS1 and NKX2-5 on the Popdc2 Gene: A Mechanism for Spatiotemporal Regulation of Enhancers during Cardiogenesis. *Cell Rep* **13**, 183-195, doi:10.1016/j.celrep.2015.08.065 (2015).
- 201 Domian, I. J. *et al.* Generation of functional ventricular heart muscle from mouse ventricular progenitor cells. *Science (New York, N.Y.)* **326**, 426-429, doi:10.1126/science.1177350 (2009).
- 202 Cai, C. L. *et al.* T-box genes coordinate regional rates of proliferation and regional specification during cardiogenesis. *Development* **132**, 2475-2487, doi:10.1242/dev.01832 (2005).
- 203 van den Berg, G. *et al.* A caudal proliferating growth center contributes to both poles of the forming heart tube. *Circ Res* **104**, 179-188, doi:10.1161/CIRCRESAHA.108.185843 (2009).
- 204 Xiang, F. L., Guo, M. & Yutzey, K. E. Overexpression of Tbx20 in Adult Cardiomyocytes Promotes Proliferation and Improves Cardiac Function After Myocardial Infarction. *Circulation* **133**, 1081-1092, doi:10.1161/CIRCULATIONAHA.115.019357 (2016).
- 205 Snir, M. *et al.* Assessment of the ultrastructural and proliferative properties of human embryonic stem cell-derived cardiomyocytes. *Am J Physiol Heart Circ Physiol* **285**, H2355-2363, doi:10.1152/ajpheart.00020.2003 (2003).
- 206 McDevitt, T. C., Laflamme, M. A. & Murry, C. E. Proliferation of cardiomyocytes derived from human embryonic stem cells is mediated via the IGF/PI 3-kinase/Akt signaling pathway. *J Mol Cell Cardiol* **39**, 865-873, doi:10.1016/j.yjmcc.2005.09.007 (2005).
- 207 Cui, L., Johkura, K., Takei, S., Ogiwara, N. & Sasaki, K. Structural differentiation, proliferation, and association of human embryonic stem cell-derived cardiomyocytes in vitro and in their extracardiac tissues. *J Struct Biol* **158**, 307-317, doi:10.1016/j.jsb.2006.11.009 (2007).
- 208 Robertson, C., Tran, D. D. & George, S. C. Concise review: maturation phases of human pluripotent stem cell-derived cardiomyocytes. *Stem Cells* **31**, 829-837, doi:10.1002/stem.1331 (2013).

- 209 Cai, M. *et al.* Dual actions of Meis1 inhibit erythroid progenitor development and sustain general hematopoietic cell proliferation. *Blood* **120**, 335-346, doi:10.1182/blood-2012-01-403139 (2012).
- 210 Chiapparo, G. *et al.* Mesp1 controls the speed, polarity, and directionality of cardiovascular progenitor migration. *J Cell Biol* **213**, 463-477, doi:10.1083/jcb.201505082 (2016).
- 211 Laugwitz, K. L., Moretti, A., Caron, L., Nakano, A. & Chien, K. R. Islet1 cardiovascular progenitors: a single source for heart lineages? *Development* **135**, 193-205, doi:10.1242/dev.001883 (2008).
- 212 Mukherjee, K. & Burglin, T. R. Comprehensive analysis of animal TALE homeobox genes: new conserved motifs and cases of accelerated evolution. *J Mol Evol* **65**, 137-153, doi:10.1007/s00239-006-0023-0 (2007).
- 213 Konermann, S. *et al.* Genome-scale transcriptional activation by an engineered CRISPR-Cas9 complex. *Nature* **517**, 583-588, doi:10.1038/nature14136 (2015).
- 214 Tanenbaum, M. E., Gilbert, L. A., Qi, L. S., Weissman, J. S. & Vale, R. D. A protein-tagging system for signal amplification in gene expression and fluorescence imaging. *Cell* **159**, 635-646, doi:10.1016/j.cell.2014.09.039 (2014).
- 215 Zalatan, J. G. *et al.* Engineering complex synthetic transcriptional programs with CRISPR RNA scaffolds. *Cell* **160**, 339-350, doi:10.1016/j.cell.2014.11.052 (2015).
- 216 Chavez, A. *et al.* Highly efficient Cas9-mediated transcriptional programming. *Nat Methods* **12**, 326-328, doi:10.1038/nmeth.3312 (2015).
- 217 Kabadi, A. M., Ousterout, D. G., Hilton, I. B. & Gersbach, C. A. Multiplex CRISPR/Cas9-based genome engineering from a single lentiviral vector. *Nucleic Acids Res* **42**, e147, doi:10.1093/nar/gku749 (2014).
- 218 Liu, K. I. *et al.* A chemical-inducible CRISPR-Cas9 system for rapid control of genome editing. *Nat Chem Biol*, doi:10.1038/nchembio.2179 (2016).
- 219 Cao, J. *et al.* An easy and efficient inducible CRISPR/Cas9 platform with improved specificity for multiple gene targeting. *Nucleic Acids Res*, doi:10.1093/nar/gkw660 (2016).
- 220 Srivastava, D. & Olson, E. N. A genetic blueprint for cardiac development. *Nature* **407**, 221-226, doi:10.1038/35025190 (2000).
- 221 Kelly, M. & Semsarian, C. Multiple mutations in genetic cardiovascular disease: a marker of disease severity? *Circ Cardiovasc Genet* **2**, 182-190, doi:10.1161/CIRCGENETICS.108.836478 (2009).
- 222 Marian, A. J. Modifier genes for hypertrophic cardiomyopathy. *Curr Opin Cardiol* **17**, 242-252 (2002).
- 223 Barrangou, R. & Doudna, J. A. Applications of CRISPR technologies in research and beyond. *Nat Biotechnol* **34**, 933-941, doi:10.1038/nbt.3659 (2016).
- 224 Yu, X. *et al.* Improved delivery of Cas9 protein/gRNA complexes using lipofectamine CRISPRMAX. *Biotechnol Lett* **38**, 919-929, doi:10.1007/s10529-016-2064-9 (2016).
- 225 Zhu, Z., Gonzalez, F. & Huangfu, D. The iCRISPR platform for rapid genome editing in human pluripotent stem cells. *Methods Enzymol* **546**, 215-250, doi:10.1016/B978-0-12-801185-0.00011-8 (2014).
- 226 Gilbert, L. A. *et al.* Genome-Scale CRISPR-Mediated Control of Gene Repression and Activation. *Cell* **159**, 647-661, doi:10.1016/j.cell.2014.09.029 (2014).
- 227 Kampmann, M. *et al.* Next-generation libraries for robust RNA interference-based genome-wide screens. *Proc Natl Acad Sci U S A* **112**, E3384-3391, doi:10.1073/pnas.1508821112 (2015).

- 228 Kampmann, M., Bassik, M. C. & Weissman, J. S. Functional genomics platform for pooled screening and generation of mammalian genetic interaction maps. *Nat Protoc* **9**, 1825-1847, doi:10.1038/nprot.2014.103 (2014).
- 229 Chen, S. *et al.* Genome-wide CRISPR screen in a mouse model of tumor growth and metastasis. *Cell* **160**, 1246-1260, doi:10.1016/j.cell.2015.02.038 (2015).
- 230 Korkmaz, G. *et al.* Functional genetic screens for enhancer elements in the human genome using CRISPR-Cas9. *Nat Biotechnol* **34**, 192-198, doi:10.1038/nbt.3450 (2016).
- 231 Rajagopal, N. *et al.* High-throughput mapping of regulatory DNA. *Nat Biotechnol* **34**, 167-174, doi:10.1038/nbt.3468 (2016).
- 232 Klymiuk, N. *et al.* Tailored Pig Models for Preclinical Efficacy and Safety Testing of Targeted Therapies. *Toxicol Pathol* **44**, 346-357, doi:10.1177/0192623315609688 (2016).
- 233 Yang, L. *et al.* Genome-wide inactivation of porcine endogenous retroviruses (PERVs). *Science (New York, N.Y.)* **350**, 1101-1104, doi:10.1126/science.aad1191 (2015).
- 234 Niu, Y. *et al.* Generation of gene-modified cynomolgus monkey via Cas9/RNA-mediated gene targeting in one-cell embryos. *Cell* **156**, 836-843, doi:10.1016/j.cell.2014.01.027 (2014).
- 235 Barrangou, R. & May, A. P. Unraveling the potential of CRISPR-Cas9 for gene therapy. *Expert Opin Biol Ther* **15**, 311-314, doi:10.1517/14712598.2015.994501 (2015).
- 236 Cyranoski, D. Chinese scientists to pioneer first human CRISPR trial. *Nature* **535**, 476-477, doi:10.1038/nature.2016.20302 (2016).
- 237 Whitworth, K. M. *et al.* Gene-edited pigs are protected from porcine reproductive and respiratory syndrome virus. *Nat Biotechnol* **34**, 20-22, doi:10.1038/nbt.3434 (2016).
- 238 Carlson, D. F. *et al.* Production of hornless dairy cattle from genome-edited cell lines. *Nat Biotechnol* **34**, 479-481, doi:10.1038/nbt.3560 (2016).
- 239 Belhaj, K., Chaparro-Garcia, A., Kamoun, S., Patron, N. J. & Nekrasov, V. Editing plant genomes with CRISPR/Cas9. *Curr Opin Biotechnol* **32**, 76-84, doi:10.1016/j.copbio.2014.11.007 (2015).
- 240 Riccroch, A. E. & Henard-Damave, M. C. Next biotech plants: new traits, crops, developers and technologies for addressing global challenges. *Crit Rev Biotechnol* **36**, 675-690, doi:10.3109/07388551.2015.1004521 (2016).
- 241 Barrangou, R. & van Pijkeren, J. P. Exploiting CRISPR-Cas immune systems for genome editing in bacteria. *Curr Opin Biotechnol* **37**, 61-68, doi:10.1016/j.copbio.2015.10.003 (2016).
- 242 van Pijkeren, J. P. & Britton, R. A. Precision genome engineering in lactic acid bacteria. *Microb Cell Fact* **13 Suppl 1**, S10, doi:10.1186/1475-2859-13-S1-S10 (2014).
- 243 Shipman, S. L., Nivala, J., Macklis, J. D. & Church, G. M. Molecular recordings by directed CRISPR spacer acquisition. *Science (New York, N.Y.)* **353**, aaf1175, doi:10.1126/science.aaf1175 (2016).

## VII. Appendix

### 7.1 List of Abbreviations

AP	Action potential	DSB	Double- strand break	PAM	protospacer-adjacent motif
aa	Amino acid	EB	Embryoid body	PCR	polymerase chain reaction
AAV	Adeno- associated virus	ECG	Electrocardiogram	pH	potential hydrogen
Ab	Antibody	F	force	PH	phase contrast
APD	Action potential duration	FACS	Fluorescent-activated cell sorting	PSF	peripheral skin fibroblats
ASC	Adult stem cell	FHF	First heart field	qRT PCR	quantitative real- time PCR
BAC	Bacterial artificial chromosome	FRET	Fluorescent resonance energy transfer	RNA	ribonucleic acid
bp	base pair	FS	Forward scatter	rpm	rounds per minute
CaM	Calmodulin	g	gravity	RR	inter- beat
CaMKII	CaM-dependent kinase II	hESC	human embryonic stem cell	RT	room temperature
CB	Cardiac body	HiFi	High Fidelity	SCD	sudden cardiac death
CDF	Calcium- dependent facilitation	hiPSC	human induced pluripotent stem cell	SD	standard deviation
CDI	Calcium- dependent inactivation	HR	homologous recombination	SEM	standard error of the mean
cDNA	copy DANN	HTS	high- throughput sequencing	SeV	Sendai virus
CDS	coding sequence	Hz	Hertz	sgRNA	single guide RNA
CICR	Calcium- induced Calcium release	Indel	Insertion or Deletion	SHF	second heart field
CIV	Cell infection units	kb	kilo base	SpCas9	Cas9 from <i>S.pyogenes</i>
CM	Cardiomyocyte	kDa	kilo Dalton	SS	sideward scatter
CPVT	Catecholaminergic polymorphic ventricular tachycardia	KO	knock- out	ssODN	single- strand oligonucleotide

CRISPR	Clustered regularly interspaced palindromic repeats	LQTS	Long QT syndrome	TALEN	Transcription activator-like effector nucleases
crRNA	CRISPR RNA	LTCC	L- type Calcium channel	TdP	Torsade de pointes
ctr	control	M	Molar	tracrRNA	trans-activating crRNA
DC	Dynamic clamp	MEF	mouse embryonic fibroblast	V	Volt
DNA	Deoxyribonucleic acid	NHEJ	non- homologous end-joining	wt	wild- type
dNTP	Desoxyribonucleosid-triphosphate	nt	nucleotide	ZFN	Zinc finger nuclease

## 7.2 List of figures and tables

### List of figures

Figure 1: Generation of hiPSCs, their differentiated cells and applications. ....	8
Figure 2: Cellular repair mechanism pathways induced by double strand breaks. ....	12
Figure 3: Schematic of the Cas9-sgRNA complex.....	14
Figure 4: Map of pRRL.sin-18.PPT.PGK.MCS.Camui-CR.pre. ....	42
Figure 5: Map of CALM1-pGK-Neo-MinimalVector construct.....	45
Figure 6: Map of pCas9_GFP-AflII mut/mut-U6-gRNA.....	50
Figure 7: Peripheral skin fibroblasts from day 0 of SeV infection to day 23 post-infection.....	67
Figure 8: Representative agarose gel of RT PCR transcript expression of SeV transgenes in patient cells.....	68
Figure 9: Immunofluorescent staining of SeV HN proteins.....	69
Figure 10: Confirmation of mutations by Sanger sequencing in patient PSFs and patient hiPSCs of both mutant lines.....	70
Figure 11: Karyogram of CALM1- F142L hiPSCs and C6 hiPSCs. ....	71
Figure 12: AP staining for pluripotency in CALM1- D130G and CALM1- F142L hiPSC colonies. ....	72
Figure 13: Immunofluorescence analysis of pluripotency markers NANOG (red) and TRA1-81 (green) in representative colonies of the CALM1- D130G and CALM1- F142L hiPSC lines. ....	74
Figure 14: qRT PCR analysis on endogenous pluripotency genes.....	75
Figure 15: PluriTest analysis of representative clones of CALM1- D130G and CALM1- F142L hiPSCs. ....	76

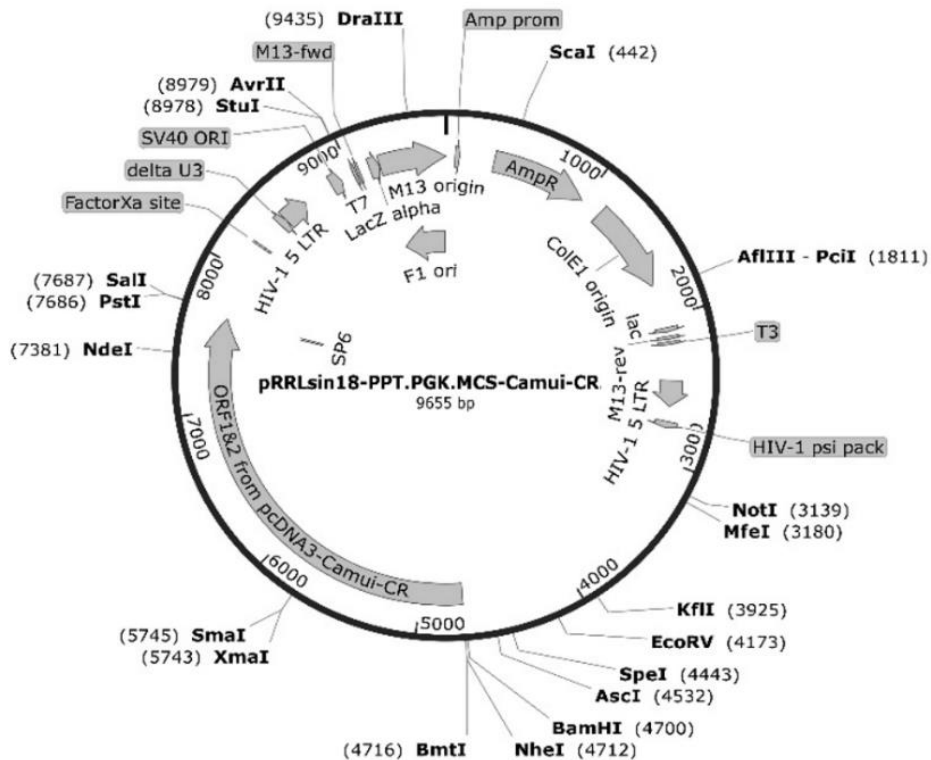
Figure 16: qRT- PCR analysis of markers of the three germ layers in embryonic bodies.	77
Figure 17: Representative immunofluorescence images of sarcomeric proteins cardiac Troponin T (cTNT, green) and $\alpha$ -Actinin (red) in CMs.	79
Figure 18: qRT PCR analysis of CALM and key myocytic genes in CMs.	80
Figure 19: qRT PCR analysis of CALM transcripts in CMs.	81
Figure 20: FRET- based CaMKII activity measurement in 2.5 months old hiPSC- derived CMs.	82
Figure 21: $I_{CaL}$ I/V relationships and $I_{CaL}$ steady- state activation and inactivation curves.	83
Figure 22: $I_{CaL}$ and $I_{BaL}$ tracings.	83
Figure 23: Remaining peaks of $I_{CaL}$ and $I_{BaL}$ at 100 ms and 300 ms and their proportions.	84
Figure 24: $I_{CaL}$ inactivation recovery.	85
Figure 25: Field potentials and statistics for QT and RR intervals in CBs.	86
Figure 26: QT- RR relationship.	86
Figure 27: Modulations by isoproterenol.	87
Figure 28: AP and APD statistics in isolated CMs.	88
Figure 29: AP sequences and percentage of cells failing to follow pacing.	88
Figure 30: $I_{CaL}$ , $Ca^{2+}$ transients and statistics of $Ca^{2+}$ dynamics.	89
Figure 31: $I_{NCX}$ measurements.	90
Figure 32: Effect of verapamil on the LQTS phenotype.	90
Figure 33: Representative PH images of single- cell adapted hiPSCs on MEF feeders and Geltrex, 1 day and 5 days after splitting.	92
Figure 34: Gene targeting by homologous recombination in CALM1 mutated hiPSCs.	93
Figure 35: Electroporated CALM1- F142L hiPSCs with targeting construct and no construct on MEF feeders and Geltrex from d0 of G418 selection to d2 post- G418 selection.	94
Figure 36: Representative colony screening agarose gel picture of 2 colonies recovered after electroporation and antibiotic selection.	95
Figure 37: Schematic of Cas9/ gRNA- mediated gene correction of the CALM1- F142L mutation.	96
Figure 38: gRNA sequences and ssODN sequences for CALM1- D130G and CALM1- F142L corrections.	97
Figure 39: Cleavage detection analysis of correction gRNAs in mutant hiPSCs.	98
Figure 40: Cleavage detection analysis of correction gRNAs in all- in one Cas9 plasmids.	99
Figure 41: Representative FACS analysis of CALM1- D130G hiPSCs and CALM1- F142L hiPSCs 24h after electroporation with Cas9 all- in one plasmids.	101
Figure 42: Percentage of GFP+ cells 24h and 48h after electroporation under different conditions.	102
Figure 43: Percentage of recovery efficiency after FACS sorting on 96- well MEF vs 6 cm MEF cell culture plates.	103

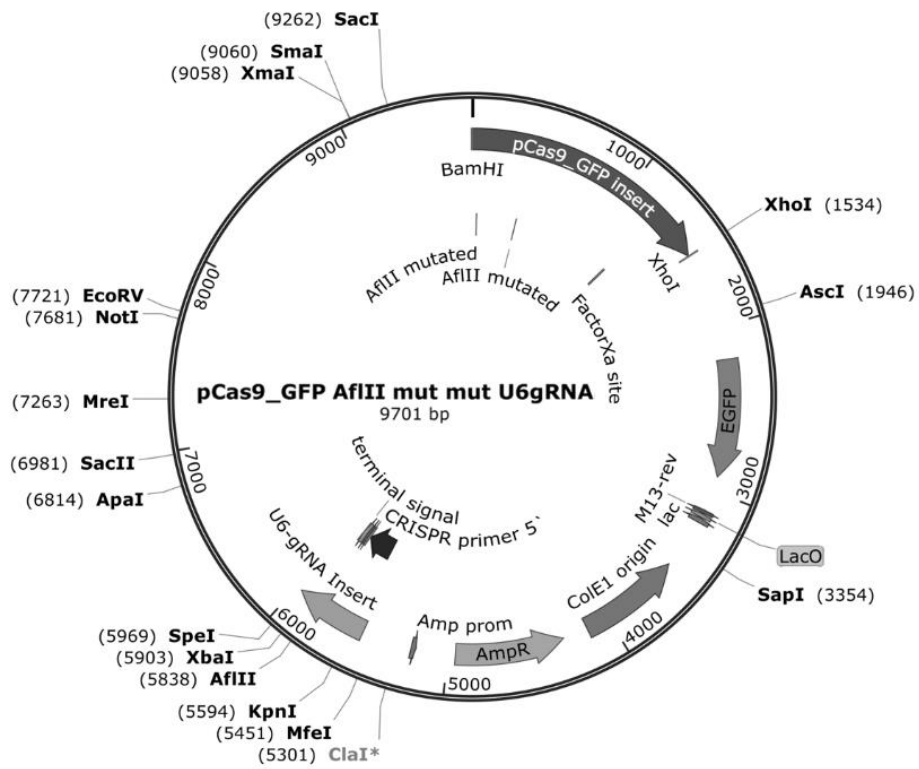
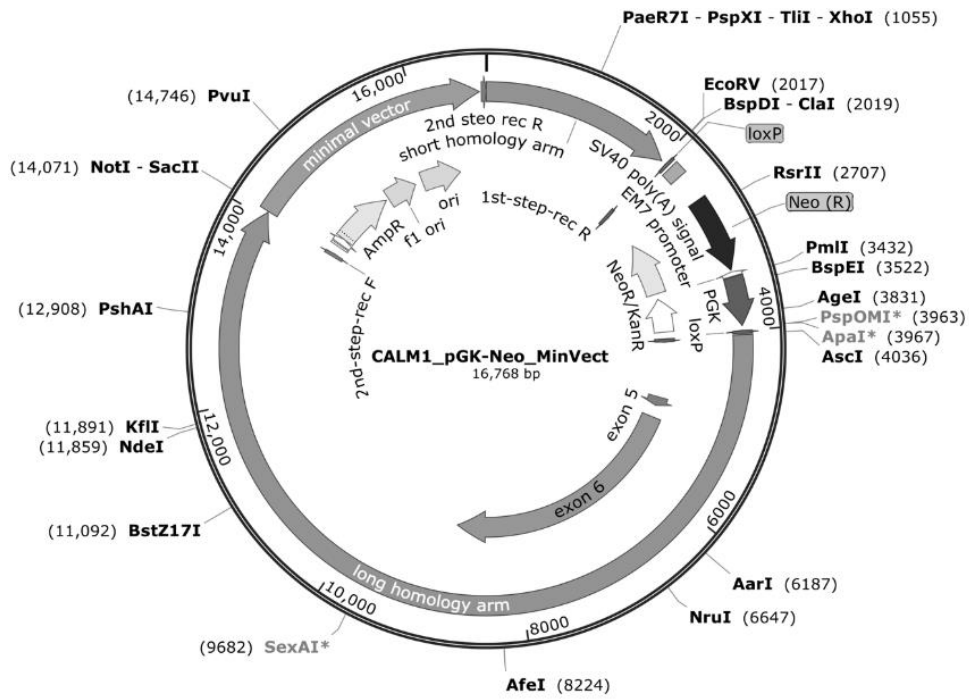
Figure 44: Percentage of recovery efficiency after FACS sorting on 96- well MEF vs 96- well Geltrex plates. ....	104
Figure 45: Representative colony screening agarose gel of CALM1- D130G and CALM1- F142L clones. ....	105
Figure 46: Representative PH images of CALM1- F142L hiPSCs nucleoporated in Buffer 1 and Buffer 2. ....	106
Figure 47: Representative puromycin kill- curve of CALM1- F142L hiPSCs ranging from no puromycin to 24h of puromycin incubation. ....	107
Figure 48: Schematic of Cas9/ gRNA- mediated gene knock- out of the CALM1 gene. ....	109
Figure 49: CALM1- KO sgRNA 1 and CALM1- KO sgRNA 2 annealing schematic. ....	110
Figure 50: Editing efficiency as percentage of edited clones for CALM1- KO gRNA 1 and 2. ....	111
Figure 51: Representative sequencing result of wt clone and edited CALM1- KO clone. ....	112
Figure 52: Output of TIDE analysis of a representative CALM1- KO clone. ....	113
Figure 53: Representative PH images of HAK ctr cells grown on Geltrex in E8 medium as colonies and as single cells. ....	114
Figure 54: MEIS1- KO sgRNAs annealing schematic. ....	115
Figure 55: Representative phase contract images of HAK ctr hiPSCs nucleoporated in Buffer 1 and Buffer 2. ....	116
Figure 56: Representative TIDE analysis of MEIS1- KO clone 7. ....	119
Figure 57: Representative sequencing result of wt clone and edited MEIS1- KO clone. ....	121
Figure 58: Comparison of nt and aa sequence of wt MEIS1 exon 3 to edited MEIS1- KO clone. ....	122
Figure 59: TIDE analysis of MEIS1- KO off- target sequence. ....	123
Figure 60: qRT PCR analysis of MEIS1 transcript expression in HAK ctr hiPSCs and MEIS1- KO hiPSCs differentiated for 48 h. ....	124
Figure 61: Representative WB of C-terminal MEIS1, N-terminal MEIS1 and HSP90 protein in HAK ctr and MEIS1- KO hiPSCs. ....	125
Figure 62: Semi- quantitative WB evaluation of N-terminal and C-terminal MEIS1 protein expression in HAK and MEIS1- KO hiPSCs after 48h differentiation. .	125
Figure 63: qRT PCR analysis of MEIS1 expression in HAK ctr hiPSCs during differentiation. ....	126
Figure 64: qRT PCR analysis of BRY, MESP1, ISL1 and NKX2.5 expressions in MEIS1- KO hiPSC and wt ctr hiPSCs during differentiation. ....	128
Figure 65: Representative FACS analysis of cTNT+ and EDU+ CMs of HAK ctr and MEIS1- KO line 9 days after induction of differentiation. ....	129
Figure 66: Evaluation of differentiation and proliferation capacity of MEIS1- KO hiPSC into CMs compared to HAK wt line. ....	130
Figure 67: Number of manuscripts published including CRISPR, ZFN or TALEN as keywords since 2002. ....	145

List of tables

Table 1: List of genes associated with LQTS..... 21  
 Table 2: qRT PCR Reaction master mix ..... 37  
 Table 3: qRT PCR program..... 37  
 Table 4: Sendai RT PCR program..... 39  
 Table 5: gRNA sequences for mutation correction approach..... 47  
 Table 6: Colony PCR master mix..... 52  
 Table 7: Colony PCR program ..... 53  
 Table 8: List of Oligonucleotides ..... 65  
 Table 9: Delivery efficiency of nucleofection buffer combinations in CALM1- F142L hiPSCs..... 106  
 Table 10: MEIS1- KO gRNA cleavage efficiencies in HAK ctr hiPSCs..... 115  
 Table 11: Delivery efficiencies using nucleofection Buffers 1 or 2 in HAK ctr hiPSCs. .... 117  
 Table 12: Total gene editing efficiencies and single event editing efficiencies in HAK ctr hiPSCs targeted with Cas9 MEIS1- KO gRNA1 construct..... 118

7.3 Plasmid maps





## 7.4 List of publications

- Rocchetti M.\*, Sala L.\*, **Dreizehnter L.\***, Crotti L., Sinnecker D., Mura M., Pane L.S., Altomare C., Mostacciolo G., Severi S., Porta A., George A.L., Schwartz P.J., Gnechi M., Moretti A., Zaza A.; \* equal contribution

Elucidating the arrhythmogenic mechanism of long QT syndrome caused by the CALM1-F142L mutation using patient-specific induced pluripotent stem cell-derived cardiomyocytes; *Cardiovascular Research*; in revision

- Chen Z., Xian W., Bellin M., Dorn T., Tian Q., Goedel A., **Dreizehnter L.**, Schneider C.M., Ward-van Oostwaard D., Ng J.K., Hinkel R., Pane L.S., Mummery C.L., Lipp P., Moretti A., Laugwitz K.L., Sinnecker D.;

Subtype-specific promoter-driven action potential imaging for precise disease modelling and drug testing in hiPSC-derived cardiomyocytes; *European Heart Journal*, published 16 June 2016, DOI: 10.1093/eurheartj/ehw189

- Schweitzer M.K., Wilting F., Sedej S., **Dreizehnter L.**, Dupper N.J., Moretti A., My I., Kwon O., Priori S.G., Laugwitz K.L., Breit A., Mederos y Schnitzler M., Gudermann T., Schredelseker J.;

Suppression of arrhythmia by enhancing mitochondrial Ca<sup>2+</sup> uptake in models for catecholaminergic ventricular tachycardia; *Circulation Research*; Manuscript submitted October 2016

## VIII. Acknowledgements

I would like to thank Prof. Dr. Laugwitz and Prof. Dr. Moretti for providing me the opportunity to pursue my PhD studies under their supervision and guidance. Thank you for your support and help throughout the years. Many thanks to Dr. Lia Crotti for her feedback as member of my PhD Committee, as well as making the collaboration of the CALM1 project possible. Acknowledgements also go to Dr. Antonio Zaza and his colleagues at the University of Milano- Bicocca for the collaboration and performance of the electrophysiological experiments.

Many thanks to Dr. Tatjana Dorn and Christina Scherb for support, guidance and technical assistance in the lab, as well as to everybody in the molecular cardiology lab and former lab members, Birgit Campbell, Zhifen Chen, Alexander Goedel, Diana Grewe, Jessica Haas, Svenja Laue, Ilaria My and Luna Simona Pane.

To the Crazy Scientists, Fly Bunnies, Th'm girls Nina and Anuja, to Eva, Elena, Sina and Philipp: Thank you very much for the laughs, coffee breaks, lunchtimes, the parties, BBQs, Isar pick nicks, movie nights, dinners and drinks and making sure work- life balance doesn't completely fail. Thanks to Dominic for support and encouragement through good and bad times. Thanks to all the chocolate and magazine donors, supporters over phone calls, postcards and text messages for the encouragement and thanks to 9gag.

Most importantly, the biggest thank you to my family Hermann, Birgit and Felix for always supporting me and always having an open ear and a strong shoulder, no matter the distance between us or which time of day and night. You are the best family one can wish for!